frontiers | Research Topics

Community series in inflammation in respiratory and neurological diseases and the immune-interaction of the lung-brain axis, volume II

Edited by
Jialin C. Zheng, Ping Yuan, Xiaohuan Xia, Wen-Hui Wu, Danchen Wu and Yi Yan

Published in
Frontiers in Immunology

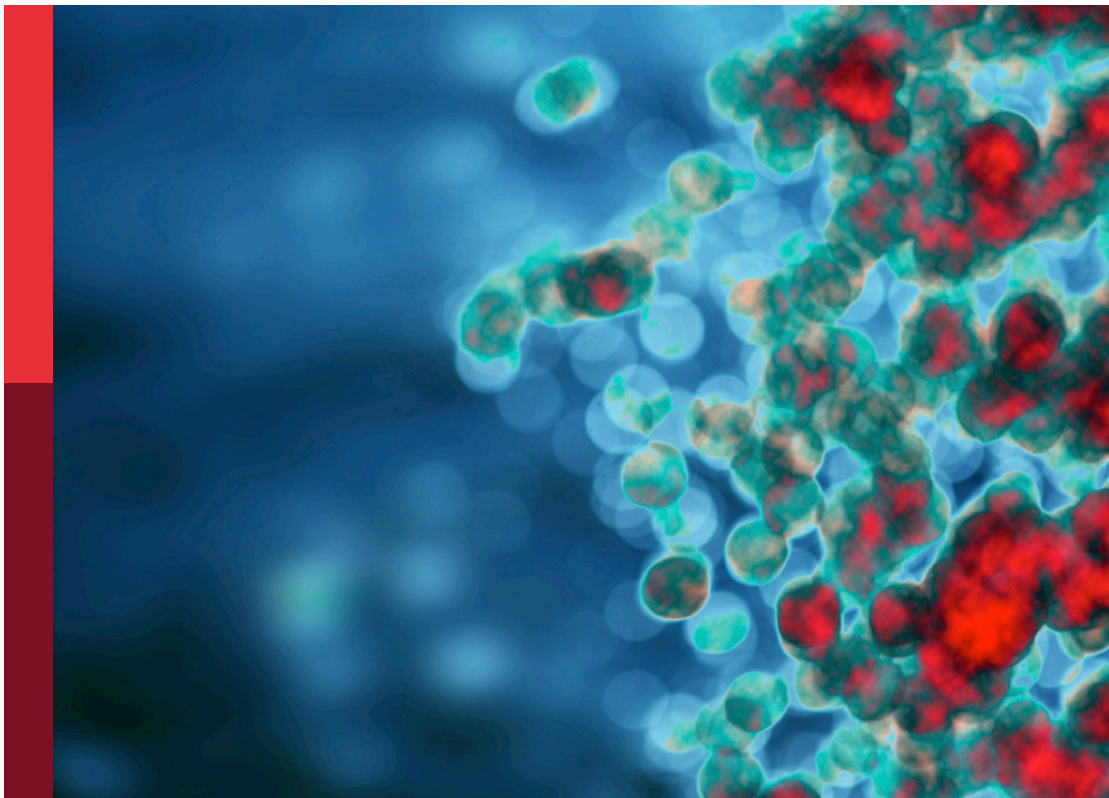

ISSN 1664-8714
ISBN 978-2-8325-6501-8
DOI 10.3389/978-2-8325-6501-8

Generative AI statement
Any alternative text (Alt text) provided alongside figures in the articles in this ebook has been generated by Frontiers with the support of artificial intelligence and reasonable efforts have been made to ensure accuracy, including review by the authors wherever possible. If you identify any issues, please contact us.

About Frontiers

Frontiers is more than just an open access publisher of scholarly articles: it is a pioneering approach to the world of academia, radically improving the way scholarly research is managed. The grand vision of Frontiers is a world where all people have an equal opportunity to seek, share and generate knowledge. Frontiers provides immediate and permanent online open access to all its publications, but this alone is not enough to realize our grand goals.

Frontiers journal series

The Frontiers journal series is a multi-tier and interdisciplinary set of open-access, online journals, promising a paradigm shift from the current review, selection and dissemination processes in academic publishing. All Frontiers journals are driven by researchers for researchers; therefore, they constitute a service to the scholarly community. At the same time, the *Frontiers journal series* operates on a revolutionary invention, the tiered publishing system, initially addressing specific communities of scholars, and gradually climbing up to broader public understanding, thus serving the interests of the lay society, too.

Dedication to quality

Each Frontiers article is a landmark of the highest quality, thanks to genuinely collaborative interactions between authors and review editors, who include some of the world's best academicians. Research must be certified by peers before entering a stream of knowledge that may eventually reach the public - and shape society; therefore, Frontiers only applies the most rigorous and unbiased reviews. Frontiers revolutionizes research publishing by freely delivering the most outstanding research, evaluated with no bias from both the academic and social point of view. By applying the most advanced information technologies, Frontiers is catapulting scholarly publishing into a new generation.

What are Frontiers Research Topics?

Frontiers Research Topics are very popular trademarks of the *Frontiers journals series*: they are collections of at least ten articles, all centered on a particular subject. With their unique mix of varied contributions from Original Research to Review Articles, Frontiers Research Topics unify the most influential researchers, the latest key findings and historical advances in a hot research area.

Find out more on how to host your own Frontiers Research Topic or contribute to one as an author by contacting the Frontiers editorial office: frontiersin.org/about/contact

Community series in inflammation in respiratory and neurological diseases and the immune-interaction of the lung-brain axis, volume II

Topic editors

Jialin C. Zheng — Tongji University, China
Ping Yuan — Tongji University, China
Xiaohuan Xia — Tongji Hospital Affiliated to Tongji University, China
Wen-Hui Wu — Tongji University, China
Danchen Wu — Queen's University, Canada
Yi Yan — Shanghai Jiaotong University School of Medicine, China

Citation

Zheng, J. C., Yuan, P., Xia, X., Wu, W.-H., Wu, D., Yan, Y., eds. (2025). *Community series in inflammation in respiratory and neurological diseases and the immune-interaction of the lung-brain axis, volume II*. Lausanne: Frontiers Media SA. doi: 10.3389/978-2-8325-6501-8

Table of contents

frontiers | Frontiers in Immunology

TYPE Editorial
PUBLISHED 12 June 2025
DOI 10.3389/fimmu.2025.1634921

OPEN ACCESS

EDITED AND REVIEWED BY
Pietro Ghezzi,
Brighton and Sussex Medical School,
United Kingdom

*CORRESPONDENCE
Ping Yuan
pandyyuan@tongji.edu.cn
Xuejing Wang
kfwxj@wfmc.edu.cn

RECEIVED 25 May 2025
ACCEPTED 29 May 2025
PUBLISHED 12 June 2025

CITATION
Liu Y, Zhang C, Wu W, Wang X and Yuan P (2025) Editorial: Community series in inflammation in respiratory and neurological diseases and the immune-interaction of the lung-brain axis, volume II.
Front. Immunol. 16:1634921.
doi: 10.3389/fimmu.2025.1634921

Editorial: Community series in inflammation in respiratory and neurological diseases and the immune-interaction of the lung-brain axis, volume II

Yuyan Liu[1,2], Caicai Zhang[3], Wenhui Wu[1], Xuejing Wang[1]* and Ping Yuan[1,2]*

[1]Rehabilitation Medicine College, Shandong Second Medical University, Weifang, Shandong, China, [2]Department of Cardio-Pulmonary Circulation, Shanghai Pulmonary Hospital, School of Medicine, Tongji University, Shanghai, China, [3]Department of Physiology, Hainan Medical University, Haikou, Hainan, China

KEYWORDS

lung-brain axis, inflammation, respiratory disease, neurological disease, pulmonary hypertension

Editorial on the Research Topic
Community series in inflammation in respiratory and neurological diseases and the immune-interaction of the lung-brain axis, volume II

The inflammatory response has emerged as a critical determinant in the pathogenesis of a wide range of respiratory and neurological disorders, a recognition that has progressed alongside advances in immunological research. Immune cell activation and the subsequent inflammatory cascades are now widely recognized as key drivers of disease progression in both systems. Notably, pulmonary inflammation extends beyond localized vascular remodeling, exerting systemic effects—particularly on the central nervous system—through complex immune-mediated mechanisms. Growing evidence supports the existence of a lung-brain axis that facilitates this crosstalk, indicating that inflammation within the respiratory tract can influence neurological function and pathology. These findings underscore the central role of inflammation not only in shaping disease trajectories in the lungs and brain but also in mediating their interconnection. A deeper understanding of these immunoregulatory mechanisms may offer valuable insights for developing targeted therapies that address both respiratory and neurological dysfunction. In this editorial, we highlight emerging insights and key advancements that are shaping this rapidly evolving field.

Pulmonary hypertension and the immune-inflammatory response

In recent years, there has been a growing focus on the role of immunity and inflammation in the pathogenesis of pulmonary hypertension (PH) (1). This involves

various immune-related changes, such as increased activation of monocytes and macrophages, infiltration of T and B cells around blood vessels, and the formation of lymphoid-like structures near pulmonary arteries. In addition, impaired regulatory T cell function, overactive dendritic cells, and neutrophil-driven inflammation further contribute to disease progression by promoting abnormal blood vessel remodeling and damaging the lung environment (2). Zhao et al. reviewed that inflammatory cells and their chemokines and cytokines (such as IL-1β and TNF-α, and IL-6) affect pulmonary vascular system. And expounded the potential relationship of vascular cells or bone morphogenetic protein receptor 2 (BMPR2) in immune regulation. Ferrian S et al. identified TIM-3$^+$ T cells and IDO-1$^+$ TIM-3$^+$ SAMHD1$^+$ DCs as novel contributors to immune dysregulation that drives the driving progression of PAH. Notably, monocyte-derived dendritic cells (mo-DCs), along with neutrophils, play a significant role in promoting vascular remodeling and endothelial dysfunction, thereby representing promising targets for therapeutic intervention (2).

DCs exacerbate disease progression through pleiotropic cytokine secretion, particularly interleukin-6 (IL-6)—a multifunctional mediator independently associated with the pathogenesis of PH (3). B cells are involved in the development of PH by producing antibodies and pro-inflammatory cytokines. These antibodies prompt immune cells to accumulate in the vessel wall, leading to vascular inflammation, fibrosis, and vascular remodeling. Regulatory T cells (Tregs) play a balancing role in maintaining immune tolerance, and in patients with systemic sclerosis-associated pulmonary arterial hypertension (SSc-PAH), loss of Tregs function exacerbates immune dysfunction and vascular injury. Endothelial cells are stimulated by the deposition of immune complexes and cytokines, and dysfunction occurs, these changes further exacerbate the development of PH.

The development of PAH in patients with autoimmune connective tissue diseases (CTDs)—termed CTD-associated pulmonary arterial hypertension (CTD-PAH)—serves as compelling clinical evidence for the central role of maladaptive immunophenotypic changes in PAH pathophysiology, particularly through dysregulated immune cell activation and sustained inflammatory cascades. van Uden D et al. reviewed that the dendritic cell (DC) compartment comprises distinct subsets under steady-state conditions: conventional DCs, plasmacytoid DCs, and specialized AXL+Siglec6+ DCs. During inflammation, monocytes differentiate into mo-DCs. DC subset dynamics critically influence autoimmune pathogenesis and likely drive pulmonary hypertension development (idiopathic PAH/CTD-PAH) through T-cell activation and pathogenic B-cell antibody production (4).

Immune-related biomarkers have also demonstrated predictive value in PH. In chronic thromboembolic pulmonary hypertension (CTEPH), serum levels of asialoglycoprotein receptor 2 (ASGR2) correlate significantly with various immune cell parameters, particularly in relation to balloon pulmonary angioplasty (BPA). Patients with CTEPH exhibited significantly elevated ASGR2 levels prior to BPA, which decreased notably following the procedure (Xu et al.).

Beyond PH, immune dysregulation is also evident in other pulmonary conditions such as community-acquired pneumonia (CAP). Qin et al. analyzed CAP patients using machine learning and identified three immunophenotypes. Among these, Type C is significantly associated with a more severe inflammatory state and poor prognosis.

Immune-mediated mechanisms in the fibrotic process

Immune cells and mediators are key drivers of fibrosis during tissue injury and repair, with macrophages playing a central role in both initiation and progression. Macrophage-myofibroblast transformation (MMT) has become a Research Topic in a variety of fibrosis diseases. Li et al. reviewed that macrophages are mainly activated through the TGF-β mediated Smad3 signaling pathway, which drives their differentiation to myofibroblasts expressing α-smooth muscle actin (α-SMA) and synthesizing extracellular matrix (ECM) components such as collagen. In addition to transforming growth factor (TGF-β), Notch signaling pathway and Wnt/β-catenin signaling pathway also play important regulatory roles in the MMT process (5). Fibroblasts, once seen as passive structural cells, are now recognized as immune sentinels that actively shape inflammatory responses (6). These insights highlight the dynamic crosstalk between immunity and fibrosis.

The lung-brain axis: bidirectional interaction of immune responses between the respiratory and nervous systems

Under normal physiological conditions, the lungs and brain communicate via complex signaling pathways that help maintain systemic homeostasis. However, lung infections can disrupt this balance, leading to functional or structural changes in the brain. COVID-19 infection increases the risk of optic nerve and visual pathway disorders, potentially through viral neuroinvasion, heightened inflammation, and immune overactivation (Cao et al.).

Air pollution has emerged as a global public health concern, with growing evidence linking respiratory exposure to neurobehavioral impairments. This suggests that the lung–brain axis may be a critical conduit by which microbiome dysbiosis and environmental factors affect brain health (7). Notably, Threatt et al. reported that organic dust exposure not only intensified pulmonary inflammation but also induced neuroinflammatory responses in the murine brain.

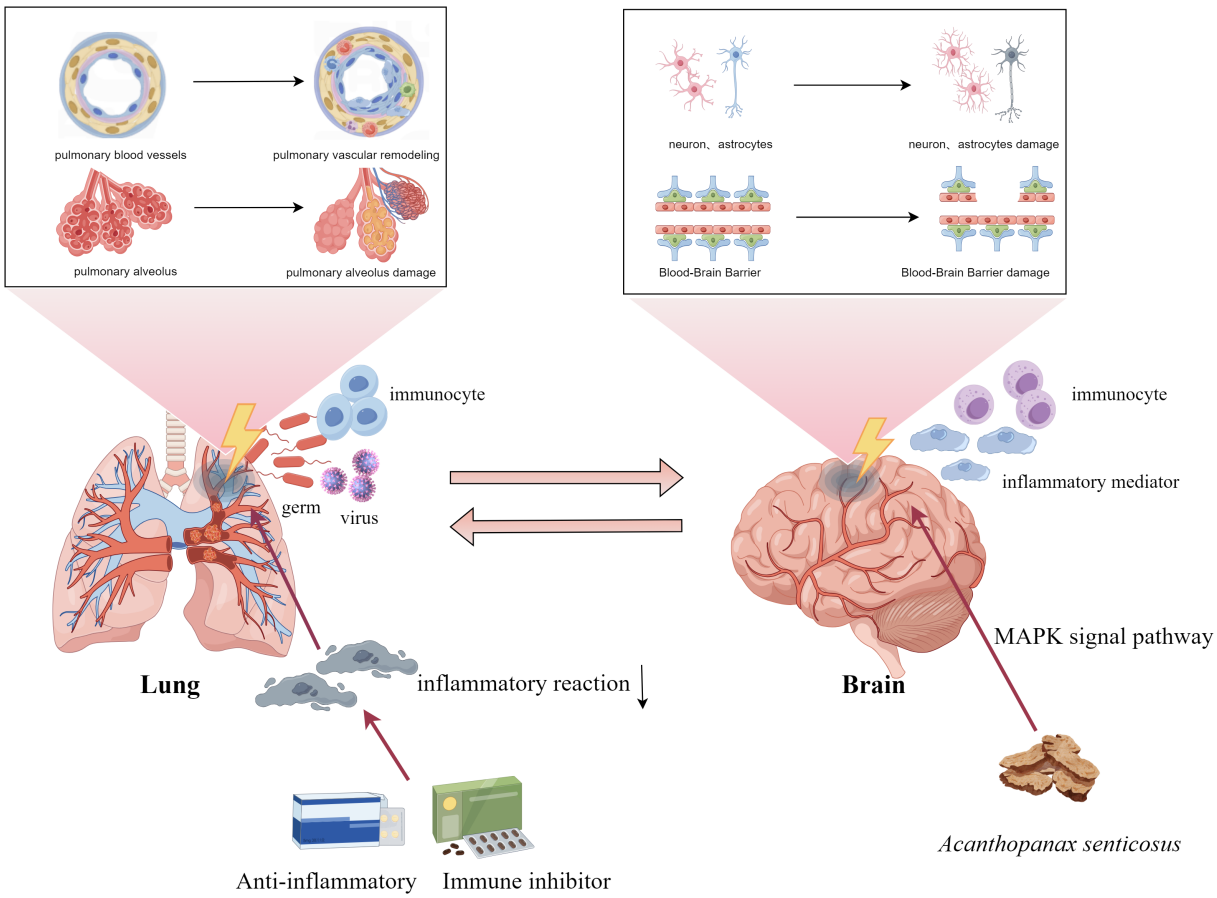

FIGURE 1
Lung-brain axis and immune response.

Targeting immune-inflammatory regulation

Zhang et al. demonstrated that *Acanthopanax senticosus* can significantly improve cognitive deficits in Alzheimer's disease mice by promoting phosphorylation of mitogen-activated protein kinase (MAPK) signaling pathway and inhibiting the production of inflammatory factors. ATP/GTP-binding protein like 4 gene (AGBL4) promotes malignant progression of glioblastoma (GBM) by regulating matrix metalloproteinase-1 (MMP-1). Zhang et al. demonstrated that knockdown of AGBL4 inhibited the proliferation, migration, and invasive ability of GBM cells, while overexpression had the opposite effect.

Inflammation also plays a critical role in pulmonary vascular remodeling in PH (8). Li et al. highlighted the therapeutic potential of immunosuppression in treating CTD-PAH by dampening immune dysregulation. Immunosuppression strategies have reversed PH in preclinical models, suggesting their value as adjunctive treatments.

In summary, this study underscores the immune-inflammatory connection between respiratory and neurological diseases, highlighting shared mechanisms involving immune cells, cytokines, and signaling pathways—particularly those mediated by the lung—brain axis (Figure 1). While current findings point toward the promise of immunosuppression therapy, challenges remain. Future efforts should aim to precisely target immune pathways to enhance treatment specificity, and improve clinical safety.

Author contributions

YL: Writing – original draft. CZ: Writing – original draft, Writing – review & editing. WW: Writing – review & editing. XW: Writing – review & editing. PY: Writing – original draft, Writing – review & editing.

Funding

The author(s) declare that financial support was received for the research and/or publication of this article. This work was supported

by y the Program of Key Research and Development projects in Hainan Province (ZDYF2024SHFZ057), Joint Research Development Project between Shenkang and United Imaging on Clinical Research and Translation (No. SKLY2022CRT202 to J.S.), Program of National Natural Science Foundation of China (82370057), the Program of Natural Science Foundation of Shanghai (22ZR1452400).

Conflict of interest

The authors declare that the research was conducted in the absence of any commercial or financial relationships that could be construed as a potential conflict of interest.

Generative AI statement

The author(s) declare that no Generative AI was used in the creation of this manuscript.

Publisher's note

All claims expressed in this article are solely those of the authors and do not necessarily represent those of their affiliated organizations, or those of the publisher, the editors and the reviewers. Any product that may be evaluated in this article, or claim that may be made by its manufacturer, is not guaranteed or endorsed by the publisher.

References

1. Humbert M, Kovacs G, Hoeper MM, Badagliacca R, Berger RMF, Brida M, et al. 2022 ESC/ERS Guidelines for the diagnosis and treatment of pulmonary hypertension. *Eur Respir J.* (2022) 43(38):3618-731. doi: 10.1093/eurheartj/ehad005

2. Ferrian S, Cao A, McCaffrey EF, Saito T, Greenwald NF, Nicolls MR, et al. Single-cell imaging maps inflammatory cell subsets to pulmonary arterial hypertension vasculopathy. *Am J Respir Crit Care Med.* (2024) 209:206–18. doi: 10.1164/rccm.202209-1761OC

3. Su X, Sun Y, Dai A. New insights into pulmonary arterial hypertension: interaction between PANoptosis and perivascular inflammatory responses. *Apoptosis.* (2025). doi: 10.1007/s10495-025-02086-0

4. van Uden D, Boomars K, Kool M. Dendritic cell subsets and effector function in idiopathic and connective tissue disease-associated pulmonary arterial hypertension. *Front Immunol.* (2019) 10:11. doi: 10.3389/fimmu.2019.00011

5. Logan CY, Nusse R. The Wnt signaling pathway in development and disease. *Annu Rev Cell Dev Biol.* (2004) 20:781–810. doi: 10.1146/annurev.cellbio.20.010403.113126

6. Di X, Chen J, Li Y, Wang M, Wei J, Li T, et al. Crosstalk between fibroblasts and immunocytes in fibrosis: From molecular mechanisms to clinical trials. *Clin Transl Med.* (2024) 14:e1545. doi: 10.1002/ctm2.v14.1

7. Wu T, Liu K, Chen S, Ye Z, Xia J, He J, et al. Pulmonary microbiota disruption by respiratory exposure to carbon quantum dots induces neuronal damages in mice. *J Hazard Mater.* (2025) 487:137255. doi: 10.1016/j.jhazmat.2025.137255

8. Cohen-Kaminsky S, Hautefort A, Price L, Humbert M, Perros F. Inflammation in pulmonary hypertension: what we know and what we could logically and safely target first. *Drug Discov Today.* (2014) 19:1251–6. doi: 10.1016/j.drudis.2014.04.007

frontiers | Frontiers in Immunology

TYPE Review
PUBLISHED 11 March 2024
DOI 10.3389/fimmu.2024.1374506

OPEN ACCESS

EDITED BY
Danchen Wu,
Queen's University, Canada

REVIEWED BY
Yonglei Wu,
First Hospital of Jiaxing, China
Dong Liu,
Shanghai Jiao Tong University, China
Xiaojian Liu,
The First Hospital of Tongxiang, China

*CORRESPONDENCE
Xuguang Wang
wxg888662024@163.com
Dapeng Wang
wangdapeng1053@163.com
Yuqing Miao
yqmiao@usst.edu.cn

†These authors have contributed equally to this work and share first authorship

RECEIVED 22 January 2024
ACCEPTED 26 February 2024
PUBLISHED 11 March 2024

CITATION
Zhao H, Song J, Li X, Xia Z, Wang Q, Fu J, Miao Y, Wang D and Wang X (2024) The role of immune cells and inflammation in pulmonary hypertension: mechanisms and implications.
Front. Immunol. 15:1374506.
doi: 10.3389/fimmu.2024.1374506

The role of immune cells and inflammation in pulmonary hypertension: mechanisms and implications

Hui Zhao[1†], Jialin Song[2†], Xiujun Li[3], Zhaoyi Xia[4,5], Qian Wang[1], Jiaqi Fu[1], Yuqing Miao[1*], Dapeng Wang[6*] and Xuguang Wang[2*]

[1]School of Materials and Chemistry, Institute of Bismuth and Rhenium, University of Shanghai for Science and Technology, Shanghai, China, [2]Department of Limb Trauma, Wendeng Orthopaedic Hospital of Shandong Province, Weihai, Shandong, China, [3]Department of Medicine, Chifeng University, Chifeng, China, [4]Department of Library, Children's Hospital Affiliated to Shandong University, Jinan, Shandong, China, [5]Department of Library, Jinan Children's Hospital, Shandong, Jinan, Shandong, China, [6]Department of Intensive Medicine, Wuxi People's Hospital Affiliated to Nanjing Medical University, Wuxi, Jiangsu, China

Pulmonary hypertension (PH) is a malignant disease with progressive increase of pulmonary vascular pressure, which eventually leads to right heart failure. More and more evidences show that immune cells and inflammation play an important role in the occurrence and development of PH. In the context of pulmonary vascular diseases, immune cells migrate into the walls of the pulmonary vascular system. This leads to an increase in the levels of cytokines and chemokines in both the bloodstream and the surrounding tissues of the pulmonary vessels. As a result, new approaches such as immunotherapy and anti-inflammatory treatments are being considered as potential strategies to halt or potentially reverse the progression of PH. We reviewed the potential mechanisms of immune cells, cytokines and chemokines in PH development. The potential relationship of vascular cells or bone morphogenetic protein receptor 2 (BMPR2) in immune regulation was also expounded. The clinical application and future prospect of immunotherapy were further discussed.

KEYWORDS

inflammation, immunity, cytokines, chemokines, pulmonary hypertension, immunosuppressive therapy

1 Introduction

Pulmonary hypertension (PH) is a condition characterized by changes in the structure and function of the pulmonary vasculature, resulting in an increase in pulmonary vascular resistance and arterial pressure (1, 2). If left untreated, PH can progress to a severe form of right heart failure or even death. The underlying pathophysiology of PH is complex and not

yet fully understood. However, it is widely accepted that the development and progression of PH are closely associated with vascular remodeling (3). In physiological state, the contraction and relaxation of blood vessels maintain a balanced state (4, 5). When immune inflammatory reaction occurs, various inflammatory factors and oxygen free radicals are produced to damage endothelium, leading to its dysfunction (6). The balance between vasodilating substances such as NO and vasoconstricting substances such as endothelin (ET) is broken, and the contractility of pulmonary blood vessels is abnormally increased (7–9). It is reported that the thickness of intima, media and adventitia and the average pulmonary artery pressure are correlated with the average perivascular inflammation score, which supports the role of perivascular inflammation in pulmonary vascular remodeling (10). In addition, the study also showed that the inflammatory pathology is more advanced when the bone morphogenetic protein type 2 receptor (BMPR2) is mutated. In the experimental PH, the fact that inflammation precedes vascular remodeling indicates that immune changes are the cause of vascular diseases rather than the result (11).

Further analysis of immune function in patients with PH proved that immune response exists in the process of PH occurrence and development (12). This can explain the accumulation of inflammatory cells around vessels and the excess of cytokines and chemokines (13, 14). In reality, maintaining a delicate balance between immunity and tolerance is crucial. Any disruption to this balance can result in chronic inflammation or even autoimmune disorders (15, 16). This review summarized the evidence and potential mechanism of immune cells and inflammation in PH in recent years. In addition, the potential relationship between vascular cells or BMPR2 in immune regulation was expounded. It is suggested that immunity and inflammation may be the key factors and promising therapeutic targets for PH development in Figure 1.

2 Immune cells and PH

Pulmonary vascular remodeling in pulmonary arterial hypertension (PAH) patients and PH animal models is often accompanied by different degrees of perivascular inflammatory infiltration, including T cells, B cells, macrophages, dendritic cells (DC), mast cells and neutrophils. This suggested that these immune cells may play an important role in the process of pulmonary vascular remodeling.

2.1 T cell

T cells are an important part of adaptive immune response and play an important role in the pathogenesis of PH, mainly helper T cells (Th cells) and regulatory T cells (Tregs) (17). Different types of T cells have specific functions and reactions in the inflammatory cascade reaction. Th cells produce pro-inflammatory response, while Tregs play a balanced response to achieve self-tolerance and prevent autoimmune (18). Studies have confirmed that the balance and homeostasis of T cells and their cytokines can prevent the loss of self-tolerance, and then affect the development of inflammation and PAH.

Based on the pro-inflammatory substances they release, Th cells can be categorized into different subsets, including Th1, Th2, and Th17 cells. Th1 and Th17 cells are capable of promoting inflammation through the production of various cytokines such as interleukin-6 (IL-6), IL-2, IL-21, interferon-gamma (IFN-γ), and tumor necrosis factor-alpha (TNF-α) (19, 20). The levels of peripheral Th17 cells, cytokines, and mRNA in patients with connective tissue diseases-associated PAH (CTD-PAH) were elevated (21). More importantly, the Th17/Tregs ratio was significantly related to the severity and prognosis of CTD-PAH (21). Moreover, the expression of T cell activation markers CD86

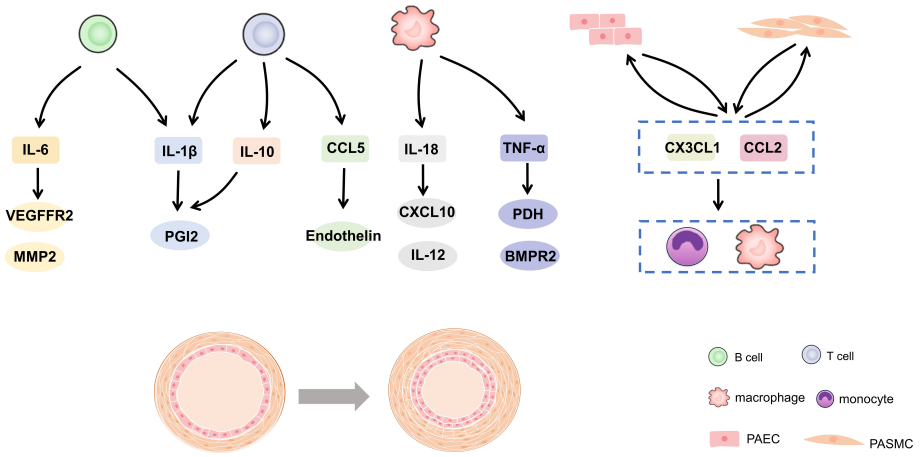

FIGURE 1
Cytokines and chemokines in pulmonary hypertension. IL, interleukin; CCL, C-C motif chemokine ligand; TNF, tumor necrosis factor-alpha; PGI2, prostacyclin; VEGFR2, vascular endothelial growth factor receptor 2; MMP, matrix metalloprotein; CXCL, C-X-C motif chemokine ligand; PDH, pyruvate dehydrogenase; BMPR2, bone morphogenetic protein type 2 receptor.

and CD40 was higher in idiopathic PAH (IPAH) patients following pretreatment with dexamethasone (22). Both with and without dexamethasone, PAH monocyte-derived DCs induced a higher activation and proliferation of CD4+ T cells, associated with a reduced expression of IL-4 (Th2 cells response) and a higher expression of IL-17 (Th17 cells response) (22). Animal studies have demonstrated that depleting CD4 cells or using SR1001, a Th17 cells development inhibitor, prevented the elevation of pressure and remodeling responses to chronic hypoxia (23). Furthermore, in a mice model of hypoxia-induced PH (HPH), the use of the receptor antibody MR16-1 to block IL-6 showed promising results. This treatment not only improved the condition of PH but also hindered the accumulation of macrophages and Th17 cells in the lungs (24).

And Th2 cells produce IL-4 and IL-13, which are described as antagonists of autoimmune pathological development. Researchers identified that Th2 CD4 T cells were necessary for Schistosoma-induced PH, given that deletion of CD4 T cells or inhibiting their Th2 cells function protected against type 2 inflammation and PH following Schistosoma exposure (25). They also observed that adoptive transfer of Schistosoma-sensitized CD4 Th2 cells was sufficient to drive type 2 inflammation and PH (25). Besides, it found that chemoattractant receptor homologous molecule expressed on Th2 cell (CRTH2) expression was up-regulated in circulating CD3CD4 T cells in patients with IPAH and in rodent PAH models (26). CRTH2 deficiency suppressed Th2 cells activation, including IL-4 and IL-13 secretion. CRTH2 disruption dramatically ameliorated pulmonary artery remodeling and PH in different PAH mice models (26).

Tregs play an important role in regulating the inflammatory response of Th cells to their own and foreign antigens. Tregs not only controls other T cells, but also regulates monocytes, macrophages, DCs, natural killer cells and B cells. In thymus-free rats with T cell immunodeficiency, pulmonary arterioles were blocked by proliferating endothelial cells. Blood vessels were surrounded by mast cells, B cells and macrophages, similar to human PAH (27). In addition, Tregs can regulate the proliferation of human pulmonary artery smooth muscle cells (HPASMCs). Tregs treatment significantly reduced the increase of right ventricular systolic pressure (RVSP) and Fulton index induced by hypoxia, decreased the expression of pro-inflammatory cytokines, and increased the level of IL-10 *in vivo*. This was attributed to the fact that Tregs treatment decreased the proliferation of HPASMCs and the expression of cyclin D1, cyclin-dependent kinase 4, p-Akt and p-ERK, and increased the expression of p27 *in vitro* (28). Furthermore, Tregs can inhibit the accumulation of collagen by inhibiting the secretion of transforming growth factor (TGF)-β1 and fibroblast growth factor 9 (29). Tregs also down-regulated cardiac fibroblasts by secreting IL-10, which helped to control the development of right ventricular hypertrophy (RVH) in PAH (30).

2.2 Macrophage

Macrophages play a crucial role as a key component of the innate immune system, and the produced antigen is presented to T cells to differentiate and activate adaptive immune system. Studies have shown that pulmonary inflammation mediated by peripulmonary macrophages is the key factor of pulmonary vascular remodeling. In PAH rat model and patients with left heart disease-related PH (LHD-PH), compared with the control group, macrophages increased, accompanied by an increase in lung IL-6 (31). At the same time, in the mice model of chronic thromboembolic PH (CTEPH), F4/80 positive monocytes/macrophages obviously accumulated in high-flow arteries (32). In human and animal models with PH, it has been reported that the level of monocyte recruitment chemokines in the lung is increased, and the number of peripheral blood monocytes is increased. Upon migration to the pulmonary vascular system, monocytes had the potential to differentiate into perivascular macrophages. This process was facilitated by the activation of chemokines chemokine ligand 2 (CCL2) and C-X3-C motif chemokine ligand 1 (CX3CL1) (33). Moreover, the recruitment and activation of macrophages around pulmonary vessels have an impact on the function of pulmonary vascular cells. SU5416 induced PH in athymic rats, and macrophages gathered around pulmonary arterioles and synthesize excessive leukotriene B4 (LTB4). LTB4 can damage endothelial cells (ECs) of nearby blood vessels, cause apoptosis, and cause abnormal proliferation of SMCs. Blocking macrophage-derived LTB4 biosynthesis or signal transduction can reverse the experimental PH, while depletion of CD68+ macrophages can prevent the occurrence of PH in thymus-free rats treated by sugen (34). Similarly, the development of HPH was related to the significant increase of levels of CX3CR1, CC chemokine receptor 2 (CCR2) and their respective ligands CX3CR1 and CCL2. CX3CR1 deficiency can prevent HPH by regulating monocyte recruitment, macrophage polarization and PASMCs proliferation (35).

2.3 B Cell, DC and neutrophil

B cells have the ability to differentiate into plasma cells, which are responsible for producing autoantibodies. In addition, B cells play a crucial role in immune responses by collaborating with antigen-presenting DCs and lymphoid organs. They achieved this through antigen presentation, the production of various cytokines, and the facilitation of T effector cell differentiation (31, 36). On the one hand, a functional role for B cells in PH was demonstrated in that either blocking B cells by an anti-CD20 antibody or B cells deficiency in JH-KO rats attenuated right ventricular systolic pressure and vascular remodeling in experimental PH (32). On the other hand, B cell depletion therapy was a potentially effective and safe adjuvant treatment for systemic sclerosis-PAH and systemic lupus erythematosus-PAH (37, 38).

In monocrotaline (MCT)-induced rats and hypoxic mice, the accumulation of pulmonary neutrophils increased (39, 40). Although neutrophils have received little attention in the pathogenesis of PAH, it has been found that neutrophil elastase can affect the pathogenesis. Neutrophil elastase isolated from PAH patients, PASMCs and PH rat models was enhanced (41–44). In MCT-induced and Sugen/hypoxic rat models, after treatment with elafin, an inhibitor of neutrophil elastase, the changes of pulmonary intima subsided and the lumen size increased (39).

The study revealed that the number of circulating myeloid DCs in IPAH patients was lower than that in the control group, and the immune deficiency of monocyte-derived DCs was obvious (45). However, the circulating plasma DCs (pDCs) value of IPAH patients did not change, and the pDCs value in lung tissue increased (46). pDCs secretes inflammatory factors and chemokines to promote the activation of immune cells. At the same time, these inflammatory factors and chemokines attracted monocytes to the lungs of patients with IPAH and CTD-PAH, and produced monocyte-derived DCs, which further aggravated inflammation (47).

3 Cytokine and PH

The increase of perivascular immune cell accumulation and intravascular infiltration, accompanied by the abnormal increase of some cytokines, leads to the increase of vascular cell inflammation and the formation of dysfunction. They played crucial roles as regulatory factors in PAH and are closely associated with the disease's severity (48). At the same time, the circulating level of cytokines was an important marker for the diagnosis and treatment of PAH (49). Targeting specific cytokine responses and pathways is considered a promising therapeutic strategy.

Some cytokines and chemokines were related to the poor clinical outcome of PAH patients, and may be used as biomarkers of disease progression. Some, such as IL-1β and TNF-α, were related to the accumulation of extracellular matrix proteins (such as fibronectin), which were found in PAH lesions, while others, such as IL-6, are related to the proliferation of SMCs.

3.1 IL-1β

A study has provided evidence that the levels of IL-1β are significantly elevated in patients with PH. This increase in IL-1β had been found to be associated with a poorer prognosis for individuals with PH (50). The mice model of PH showed the same conclusion, and it has been proved that starting IL-1β receptor antagonist can reduce PH and RVH (51). Furthermore, there existed a correlation between IL-1β and prostacyclin (PGI2) (17, 52). IL-1β increased PGI2 production in a dose-dependent manner (52). Cyclooxygenase-2 (COX-2) was the key enzyme for PGI2 synthesis (52). After treating PASMCs with IL-1β, the level of COX-2 mRNA increased, which induced the expression of PGI2 (52, 53). However, IL-1β has been found to have a negative impact on adenosine cyclase, leading to a decrease in cyclic adenosine monophosphate (cAMP) production. This, in turn, weakened the role of PGI2 (54). Furthermore, IL-1β activated other cytokines and chemokines to play a role. The cleavage of IL-18 by IL-1β invertase resulted in the production of bioactive IL-18. This increase in bioactive IL-18 has been observed in patients with pulmonary vascular diseases. Additionally, the levels of the downstream chemokine CXCL10 were also elevated in these patients (55). The increased expression of IL-18 and CXCL10 may make the inflammatory environment permanent and eventually lead to the vascular occlusion characteristics of PAH (55).

3.2 IL-6

IL-6 is a cytokine secreted by lymphocytes, which has extensive pro-inflammatory properties and participates in the occurrence and development of PH. IL-6 has been found to have prognostic value in patients with PH. The serum level of IL-6 has been shown to be an independent predictor of survival in PH patients and can be used to predict the outcome of these patients (56). Animal model revealed that the RVH of rats injected with recombinant human IL-6 increased, and PH appeared under normal oxygen conditions (57). Similarly, lung-specific IL-6 overexpression mice spontaneously produced PH under chronic hypoxia, and showed muscular distal arterioles and proliferative lesions in vascular cells. The IL-6 receptor knockout rats were not affected by HPH, and the progressive accumulation of PASMCs was reduced (58).

IL-6 may promoted PH in the following ways: (1) IL-6 induced excessive proliferation of pulmonary artery ECs (PAECs) and PASMCs in the distal pulmonary vascular wall by up-regulating vascular endothelial growth factor receptor 2 (VEGFR2) and matrix metalloprotein -2 (20). (2) IL-6 affected many signal pathways, such as BMPR2/Smad, MAPK/P38 and MAPK/JNK (17). (3) IL-6 played a crucial role in regulating the balance between Th17 cells and Treg cells. It can stimulate the immune response of Th17 cells while inhibiting the suppressive function of Treg cells. This imbalance in the immune response, with an increased presence of Th17 cells and reduced Treg cell activity, has been associated with an increased risk of PAH (59).

3.3 IL-10, IL-18 and TNF-α

Abnormal levels of cytokines, including IL-10, IL-18, and TNF-a, have been observed in both human and animal models of PH.

IL-10 is released by T cells, which is negatively correlated with PGI2 therapy. And IL-10 was decreased in patients after cardiopulmonary bypass (60). At the same time, it has been proved that the decrease of IL-10 level is a risk factor for chronic obstructive pulmonary disease (COPD)-PH (61). However, exogenous IL-10 significantly reduced macrophage infiltration and vascular cell proliferation in the remodeled pulmonary artery. It also significantly reduced the lung levels of TGF-β1 and IL-6 (62). Therefore, the effect of IL-10 on the development of PH needs to be studied.

Under the influence of caspase-1, the inactive precursor form of IL-18 is converted into its active form, IL-18, which possesses biological activity (55). IL-18 acted on the cytokine-chemokine cascade reaction of type I immune response, affecting the expression of IL-12, IFN-γ and CXCL10. This promoted the recruitment of more lymphocytes to the vascular wall, which in turn exacerbated the pathological progression of PAH (55). Besides, IL-18 affected SMCs in an autocrine or paracrine way. IL-18 could

thicken the smooth muscle layer by up-regulating the chemotaxis of metalloproteins and cells that constitute the vascular skeleton (63).

TNF-α is an important proinflammatory factor, which is significantly increased in the medial layer of pulmonary artery in COPD-PH patients (64). It is reported that transgenic mice that overexpress TNF-α will have severe PH value and right ventricular hypertrophy (65). Similarly, injection of TNF-a into the rat model led to increased vascular activity and remodeling (66). TNF-α may drove the proliferation of PAECs and PASMCs in HPH by inhibiting pyruvate dehydrogenase (PDH) activity, inhibiting BMPR2 and changing NOTCH signal transduction (63).

4 Chemokine and PH

4.1 CCL2

CCL2 is secreted by vascular ECs and SMCs, and its role is mediated by CCR2. CCL2 is an effective medium for the activation of monocytes and macrophages, which induces the secretion of cytokines and the expression of adhesion molecules (17, 67). It is reported that CCL2 induces the proliferation and migration of PAECs and SMCs in patients with PH, which leads to vascular remodeling and blood pressure increase (68). This may be because the increase of CCL2 produced by pulmonary vascular cells contributes to the increase of chemotactic activity of monocytes/macrophages. So that adventitial fibroblasts are activated (69, 70), the migration and proliferation of PASMCs increased, and pathological vascular remodeling was induced. In the presence of pulmonary ECs, the mobility of monocytes decreased significantly, while the blocking antibody of CCL2 increased significantly. The migration and proliferation of PASMCs in patients with PAH increased in response to CCL2 stimulation (71).

4.2 CCL5

CCL5 is expressed and secreted by T cells (17). Studies have confirmed that CCL5 can promote the proliferation of ECs. ET-converting enzyme-1 and ET promoted mitosis and vasoconstriction, and accelerated the pathological process of PH (72). In fact, compared with the control group, the expression of CCL5 mRNA in lung samples of PAH patients was increased, which may be derived from ECs (73). Moreover, the crosstalk between CCR5 and CCR2 mediated the synergy between macrophages and PASMCs, thus promoting inflammatory cell infiltration and PASMCs migration and proliferation during the development of PAH (74).

4.3 CX3CL1

CX3CL1 exists as a cell adhesion molecule on ECs or as a chemotactic protein, and its function is mediated by CX3CR1 (67). Under the pathological condition of PH, CX3CL1 led to the adhesion of macrophages expressing CX3CR1 to PAECs, which led to PAECs dysfunction and trigger perivascular inflammatory reaction (75). In addition, CX3CL1 promoted the proliferation of pericytes and PASMCs, which further aggravated the remodeling of pulmonary small vessels, leading to further aggravation of PH (76). CX3CR1 deficiency protected against HPH by modulating monocyte recruitment, macrophage polarization, and PAMCs proliferation (35).

5 Vascular cells and BMPR2

5.1 Vascular cells

ECs play a key role in maintaining vascular homeostasis under various stimuli, and regulate inflammation through mediators such as NO, ET, cell adhesion molecules, cytokines and chemokines. Under pathological conditions such as inflammation and hypoxia, PAECs can reduce the production of vasodilators (such as NO) and vascular growth factors, which is beneficial to the vasoconstriction of the distal pulmonary artery (77). Circulating ECs may be involved in the process of vascular injury, tumorigenesis or interaction with immune cells. In addition, endothelial progenitor cells were bone marrow-derived cells involved in homeostasis, and they were also physiological and pathological angiogenesis cells. The increase of proinflammatory cytokines was also beneficial to the activation of platelet adhesion and coagulation cascade reaction, which led to further occlusion of arterioles (78).

It has been suggested that inflammation can recruit SMCs population and enhance their contribution to pulmonary vascular remodeling. Because excessive proliferation of SMCs was observed in locally occluded blood vessels. Some studies also showed that continuous hypoxia can induce the recruitment of mesenchymal progenitor cells around blood vessels. The recruitment of these cells was very important for the occurrence of PAH (79) [142,143]. The changes of inflammatory vascular system may be caused by these migrating cells and resident SMCs, which restore the ability needed for vascular remodeling.

5.2 BMPR2 and immune

On the one hand, BMPR2 gene mutation has been identified as the main genetic cause of PAH. On the other hand, BMPR2 plays an important role in maintaining the immune system (80, 81). The disruption of BMPR2 signaling pathway causes an increased degree of inflammation and decreases the ability of the immune system to resolve it. Inhibition of BMPR2 gene expression led to unregulated proliferation and survival of endothelial cells through disordered TGF-β signaling, thus promoting vascular remodeling (82). In order to cope with the decrease of BMPR2 function in ECs, it is assumed that the integrity of ECs dysfunction may be damaged, which may lead to apoptosis, the release of TGF-β and the development of anti-apoptotic clones (83). On the contrary, SMCs proliferate due to TGF-β signaling, and undergo excessive growth reaction, leading to vascular remodeling (84).

Loss of BMPR2 expression enhanced ECs inflammatory response through various mechanisms mediated by ROS,

nicotinamide adenine dinucleotide phosphate oxidase and NF-κB activity (85, 86). In innate immune response, BMPR2 deficiency increased the recruitment of macrophages to the perivascular area of pulmonary vascular. Mutated BMPR2 can also increase the production of granulocyte macrophage colony-stimulating factor, thus activating macrophages (87, 88). Activated macrophages secreted proinflammatory cytokines, such as IL-6 and IL-8 (86). In addition, the imbalance of BMPR2 in adaptive cellular immunity will destroy the development of T cells and lead to the increase of ECs apoptosis. The decrease of BMPR2 expression was also related to CD4 T cells depletion. Lack of T cells population led to inflammation around the artery, which was dominated by macrophage and B cells activity, thus aggravating PAH (11, 46).

6 Immunosuppression therapy in PH

At present, it is generally believed that there is a connection between inflammation and PH, but there are still several problems. Firstly, it is not clear whether inflammation is enough to promote the development of PH. Secondly, what are the causes of immune and inflammatory changes in PH lung tissues? Finally, does this have pathological or clinical significance? It is necessary to better understand the mechanism of immune cells, cytokines and chemokines in PH affecting abnormal angiogenesis and pulmonary artery remodeling. Although it is necessary to understand the immune/inflammatory components of PH more clearly, recent studies have shown promising results in animal models regarding the efficacy of anti-inflammatory therapies in reducing or even reversing the effects of PH. Currently, therapeutic drugs targeting the three pathological pathways of PH primarily focus on vasodilation. However, it is worth noting that these drugs also exhibit immunomodulatory properties (89). At present, there is no approved treatment specifically targeting the inflammatory process associated with pulmonary vascular diseases.

Tacrolimus is a calcineurin inhibitor, which can regulate immunity and has anti-inflammatory activity. Low-dose tacrolimus has been proved to reverse the disease progression of PAH rats induced by mc and hypoxia, restore the normal function of pulmonary artery endothelial cells, and activate other functions of BMPR2 receptor signal transduction by removing FKBP12 from BMPR 1 type co-receptor (90).Based on B cell depletion therapy, patients who received rituximab (an anti-CD20 monoclonal antibody) showed a decrease in rheumatoid factor, IL-12 and IL-17 (37). Hydroxymethylglutaryl coenzyme A (statins) have been proved to have anti-inflammatory and immunomodulatory functions (91, 92). Patients with IPAH, HPAH and CTD-PAH were treated with simvastatin, which inhibited lymphocyte function and improved right ventricular remodeling (93, 94). In addition, compared with the control group, the level of circulating inflammatory markers in patients with chronic embolic PH and PAH increased (95). After treatment with corticosteroids or immunosuppressants, the clinical symptoms of some patients improved (96). The above evidence reveals that suppressing immunity and inflammation can be used as a potential strategy for PH treatment. However, immunosuppressants are a kind of drugs that can effectively inhibit immune cell function, reduce immune response and inhibit inflammation. So far, no immunosuppressants have been approved for the treatment of multiple PH. The therapeutic effect of most immunomodulators on PH is still in the clinical trial stage.

7 Conclusion

It is an obvious fact that immune cells and inflammation play an important role in the pathophysiology of PH. There is increasing evidence that PH is not only caused by dynamic vasoconstriction. Inflammatory cells and their chemokines and cytokines affect pulmonary vascular system. However, many molecular and cellular mechanisms remain unsolved. It is significant for immunotherapy and anti-inflammation to better understand how inflammation and immunity participate in the development of polycyclic aromatic hydrocarbons.

Author contributions

HZ: Conceptualization, Writing – original draft. JS: Investigation, Writing – original draft. XL: Investigation, Visualization, Writing – review & editing. ZX: Visualization, Writing – review & editing. QW: Writing – review & editing, Formal Analysis. JF: Writing – review & editing, Methodology. YM: Project administration, Writing – review & editing. DW: Conceptualization, Project administration, Writing – review & editing. XW: Conceptualization, Project administration, Writing – review & editing.

Funding

The author(s) declare that financial support was received for the research, authorship, and/or publication of this article. This work was supported by the Program of Taihu-Talent Project of Wuxi government (2021THRC-TD-ZZYXK-2021).

Conflict of interest

The authors declare that the research was conducted in the absence of any commercial or financial relationships that could be construed as a potential conflict of interest.

Publisher's note

References

1. Humbert M, Kovacs G, Hoeper MM, Badagliacca R, Berger RMF, Brida M, et al. 2022 ESC/ERS Guidelines for the diagnosis and treatment of pulmonary hypertension. *Eur Heart J*. (2022) 43:3618–731. doi: 10.1183/13993003.00879-2022

2. Johnson S, Sommer N, Cox-Flaherty K, Weissmann N, Ventetuolo CE, Maron BA. Pulmonary hypertension: A contemporary review. *Am J Respir Crit Care Med*. (2023) 208:528–48. doi: 10.1164/rccm.202302-0327SO

3. Humbert M, Guignabert C, Bonnet S, Dorfmüller P, Klinger JR, Nicolls MR, et al. Pathology and pathobiology of pulmonary hypertension: state of the art and research perspectives. *Eur Respir J*. (2019) 53:1801887. doi: 10.1183/13993003.01887-2018

4. Thenappan T, Ormiston ML, Ryan JJ, Archer SL. Pulmonary arterial hypertension: pathogenesis and clinical management. *Bmj*. (2018) 360:j5492. doi: 10.1136/bmj.j5492

5. Hu Y, Chi L, Kuebler WM, Goldenberg NM. Perivascular inflammation in pulmonary arterial hypertension. *Cells*. (2020) 9:2338. doi: 10.3390/cells9112338

6. Zheng D, Liu J, Piao H, Zhu Z, Wei R, Liu K. ROS-triggered endothelial cell death mechanisms: Focus on pyroptosis, parthanatos, and ferroptosis. *Front Immunol*. (2022) 13:1039241. doi: 10.3389/fimmu.2022.1039241

7. Krüger-Genge A, Blocki A, Franke RP, Jung F. Vascular endothelial cell biology: an update. *Int J Mol Sci*. (2019) 20:4411. doi: 10.3390/ijms20184411

8. Vanhoutte PM, Shimokawa H, Feletou M, Tang EH. Endothelial dysfunction and vascular disease - a 30th anniversary update. *Acta Physiol (Oxf)*. (2017) 219:22–96. doi: 10.1111/apha.2017.219.issue-1

9. Potente M, Gerhardt H, Carmeliet P. Basic and therapeutic aspects of angiogenesis. *Cell*. (2011) 146:873–87. doi: 10.1016/j.cell.2011.08.039

10. Stacher E, Graham BB, Hunt JM, Gandjeva A, Groshong SD, McLaughlin VV, et al. Modern age pathology of pulmonary arterial hypertension. *Am J Respir Crit Care Med*. (2012) 186:261–72. doi: 10.1164/rccm.201201-0164OC

11. Tamosiuniene R, Tian W, Dhillon G, Wang L, Sung YK, Gera L, et al. Regulatory T cells limit vascular endothelial injury and prevent pulmonary hypertension. *Circ Res*. (2011) 109:867–79. doi: 10.1161/CIRCRESAHA.110.236927

12. Humbert M, Kovacs G, Hoeper MM, Badagliacca R, Berger RMF, Brida M, et al. 2022 ESC/ERS Guidelines for the diagnosis and treatment of pulmonary hypertension. *Eur Respir J*. (2023) 61:2200879. doi: 10.1183/13993003.00879-2022

13. Roy P, Orecchioni M, Ley K. How the immune system shapes atherosclerosis: roles of innate and adaptive immunity. *Nat Rev Immunol*. (2022) 22:251–65. doi: 10.1038/s41577-021-00584-1

14. Wagner DD, Frenette PS. The vessel wall and its interactions. *Blood*. (2008) 111:5271–81. doi: 10.1182/blood-2008-01-078204

15. Amaya-Uribe L, Rojas M, Azizi G, Anaya JM, Gershwin ME. Primary immunodeficiency and autoimmunity: A comprehensive review. *J Autoimmun*. (2019) 99:52–72. doi: 10.1016/j.jaut.2019.01.011

16. Romagnani S. Immunologic influences on allergy and the TH1/TH2 balance. *J Allergy Clin Immunol*. (2004) 113:395–400. doi: 10.1016/j.jaci.2003.11.025

17. Wang RR, Yuan TY, Wang JM, Chen YC, Zhao JL, Li MT, et al. Immunity and inflammation in pulmonary arterial hypertension: From pathophysiology mechanisms to treatment perspective. *Pharmacol Res*. (2022) 180:106238. doi: 10.1016/j.phrs.2022.106238

18. Rabinovitch M, Guignabert C, Humbert M, Nicolls MR. Inflammation and immunity in the pathogenesis of pulmonary arterial hypertension. *Circ Res*. (2014) 115:165–75. doi: 10.1161/CIRCRESAHA.113.301141

19. Luger D, Silver PB, Tang J, Cua D, Chen Z, Iwakura Y, et al. Either a Th17 or a Th1 effector response can drive autoimmunity: conditions of disease induction affect dominant effector category. *J Exp Med*. (2008) 205:799–810. doi: 10.1084/jem.20071258

20. Steiner MK, Syrkina OL, Kolliputi N, Mark EJ, Hales CA, Waxman AB. Interleukin-6 overexpression induces pulmonary hypertension. *Circ Res*. (2009) 104:236–44, 28p following 244. doi: 10.1161/CIRCRESAHA.108.182014

21. Gaowa S, Zhou W, Yu L, Zhou X, Liao K, Yang K, et al. Effect of Th17 and Treg axis disorder on outcomes of pulmonary arterial hypertension in connective tissue diseases. *Mediators Inflammation*. (2014) 2014:247372. doi: 10.1155/2014/247372

22. Hautefort A, Girerd B, Montani D, Cohen-Kaminsky S, Price L, Lambrecht BN, et al. T-helper 17 cell polarization in pulmonary arterial hypertension. *Chest*. (2015) 147:1610–20. doi: 10.1378/chest.14-1678

23. Maston LD, Jones DT, Giermakowska W, Howard TA, Cannon JL, Wang W, et al. Central role of T helper 17 cells in chronic hypoxia-induced pulmonary hypertension. *Am J Physiol Lung Cell Mol Physiol*. (2017) 312:L609–l624. doi: 10.1152/ajplung.00531.2016

24. Hashimoto-Kataoka T, Hosen N, Sonobe T, Arita Y, Yasui T, Masaki T, et al. Interleukin-6/interleukin-21 signaling axis is critical in the pathogenesis of pulmonary arterial hypertension. *Proc Natl Acad Sci U.S.A*. (2015) 112:E2677–86. doi: 10.1073/pnas.1424774112

25. Kumar R, Mickael C, Kassa B, Sanders L, Koyanagi D, Hernandez-Saavedra D, et al. Th2 CD4(+) T cells are necessary and sufficient for schistosoma-pulmonary hypertension. *J Am Heart Assoc*. (2019) 8:e013111. doi: 10.1161/JAHA.119.013111

26. Chen G, Zuo S, Tang J, Zuo C, Jia D, Liu Q, et al. Inhibition of CRTH2-mediated Th2 activation attenuates pulmonary hypertension in mice. *J Exp Med*. (2018) 215:2175–95. doi: 10.1084/jem.20171767

27. Taraseviciene-Stewart L, Nicolls MR, Kraskauskas D, Scerbavicius R, Burns N, Cool C, et al. Absence of T cells confers increased pulmonary arterial hypertension and vascular remodeling. *Am J Respir Crit Care Med*. (2007) 175:1280–9. doi: 10.1164/rccm.200608-1189OC

28. Chu Y, Xiangli X, Xiao W. Regulatory T cells protect against hypoxia-induced pulmonary arterial hypertension in mice. *Mol Med Rep*. (2015) 11:3181–7. doi: 10.3892/mmr.2014.3106

29. Peng X, Moore MW, Peng H, Sun H, Gan Y, Homer RJ, et al. CD4+CD25+FoxP3+ Regulatory Tregs inhibit fibrocyte recruitment and fibrosis via suppression of FGF-9 production in the TGF-β1 exposed murine lung. *Front Pharmacol*. (2014) 5:80. doi: 10.3389/fphar.2014.00080

30. Cao Y, Xu W, Xiong S. Adoptive transfer of regulatory T cells protects against Coxsackievirus B3-induced cardiac fibrosis. *PLoS One*. (2013) 8:e74955. doi: 10.1371/journal.pone.0074955

31. Kherbeck N, Tamby MC, Bussone G, Dib H, Perros F, Humbert M, et al. The role of inflammation and autoimmunity in the pathophysiology of pulmonary arterial hypertension. *Clin Rev Allergy Immunol*. (2013) 44:31–8. doi: 10.1007/s12016-011-8265-z

32. Breitling S, Hui Z, Zabini D, Hu Y, Hoffmann J, Goldenberg NM, et al. The mast cell-B cell axis in lung vascular remodeling and pulmonary hypertension. *Am J Physiol Lung Cell Mol Physiol*. (2017) 312:L710–l721. doi: 10.1152/ajplung.00311.2016

33. Florentin J, Coppin E, Vasamsetti SB, Zhao J, Tai YY, Tang Y, et al. Inflammatory macrophage expansion in pulmonary hypertension depends upon mobilization of blood-borne monocytes. *J Immunol*. (2018) 200:3612–25. doi: 10.4049/jimmunol.1701287

34. Tian W, Jiang X, Tamosiuniene R, Sung YK, Qian J, Dhillon G, et al. Blocking macrophage leukotriene b4 prevents endothelial injury and reverses pulmonary hypertension. *Sci Transl Med*. (2013) 5:200ra117. doi: 10.1126/scitranslmed.3006674

35. Amsellem V, Abid S, Poupel L, Parpaleix A, Rodero M, Gary-Bobo G, et al. Roles for the CX3CL1/CX3CR1 and CCL2/CCR2 chemokine systems in hypoxic pulmonary hypertension. *Am J Respir Cell Mol Biol*. (2017) 56:597–608. doi: 10.1165/rcmb.2016-0201OC

36. Ulrich S, Taraseviciene-Stewart L, Huber LC, Speich R, Voelkel N. Peripheral blood B lymphocytes derived from patients with idiopathic pulmonary arterial hypertension express a different RNA pattern compared with healthy controls: a cross sectional study. *Respir Res*. (2008) 9:20. doi: 10.1186/1465-9921-9-20

37. Zamanian RT, Badesch D, Chung L, Domsic RT, Medsger T, Pinckney A, et al. Safety and efficacy of B-cell depletion with rituximab for the treatment of systemic sclerosis-associated pulmonary arterial hypertension: A multicenter, double-blind, randomized, placebo-controlled trial. *Am J Respir Crit Care Med*. (2021) 204:209–21. doi: 10.1164/rccm.202009-3481OC

38. Hennigan S, Channick RN, Silverman GJ. Rituximab treatment of pulmonary arterial hypertension associated with systemic lupus erythematosus: a case report. *Lupus*. (2008) 17:754–6. doi: 10.1177/0961203307087610

39. Taylor S, Dirir O, Zamanian RT, Rabinovitch M, Thompson AAR. The role of neutrophils and neutrophil elastase in pulmonary arterial hypertension. *Front Med (Lausanne)*. (2018) 5:217. doi: 10.3389/fmed.2018.00217

40. Frid MG, Brunetti JA, Burke DL, Carpenter TC, Davie NJ, Reeves JT, et al. Hypoxia-induced pulmonary vascular remodeling requires recruitment of circulating mesenchymal precursors of a monocyte/macrophage lineage. *Am J Pathol*. (2006) 168:659–69. doi: 10.2353/ajpath.2006.050599

41. Cowan KN, Heilbut A, Humpl T, Lam C, Ito S, Rabinovitch M. Complete reversal of fatal pulmonary hypertension in rats by a serine elastase inhibitor. *Nat Med*. (2000) 6:698–702. doi: 10.1038/76282

42. Spiekerkoetter E, Alvira CM, Kim YM, Bruneau A, Pricola KL, Wang L, et al. Reactivation of gammaHV68 induces neointimal lesions in pulmonary arteries of S100A4/Mts1-overexpressing mice in association with degradation of elastin. *Am J Physiol Lung Cell Mol Physiol*. (2008) 294:L276–89. doi: 10.1152/ajplung.00414.2007

43. Kim YM, Haghighat L, Spiekerkoetter E, Sawada H, Alvira CM, Wang L, et al. Neutrophil elastase is produced by pulmonary artery smooth muscle cells and is linked to neointimal lesions. *Am J Pathol*. (2011) 179:1560–72. doi: 10.1016/j.ajpath.2011.05.051

44. Rose F, Hattar K, Gakisch S, Grimminger F, Olschewski H, Seeger W, et al. Increased neutrophil mediator release in patients with pulmonary hypertension–suppression by inhaled iloprost. *Thromb Haemost*. (2003) 90:1141–9. doi: 10.1160/TH03-03-0173

45. Wang W, Yan H, Zhu W, Cui Y, Chen J, Wang X, et al. Impairment of monocyte-derived dendritic cells in idiopathic pulmonary arterial hypertension. *J Clin Immunol*. (2009) 29:705–13. doi: 10.1007/s10875-009-9322-8

46. Marsh LM, Jandl K, Grünig G, Foris V, Bashir M, Ghanim B, et al. The inflammatory cell landscape in the lungs of patients with idiopathic pulmonary

arterial hypertension. *Eur Respir J*. (2018) 51:1701214. doi: 10.1183/13993003.01214-2017

47. Itoh T, Nagaya N, Ishibashi-Ueda H, Kyotani S, Oya H, Sakamaki F, et al. Increased plasma monocyte chemoattractant protein-1 level in idiopathic pulmonary arterial hypertension. *Respirology*. (2006) 11:158–63. doi: 10.1111/j.1440-1843.2006.00821.x

48. Groth A, Vrugt B, Brock M, Speich R, Ulrich S, Huber LC. Inflammatory cytokines in pulmonary hypertension. *Respir Res*. (2014) 15:47. doi: 10.1186/1465-9921-15-47

49. Soon E, Holmes AM, Treacy CM, Doughty NJ, Southgate L, MaChado RD, et al. Elevated levels of inflammatory cytokines predict survival in idiopathic and familial pulmonary arterial hypertension. *Circulation*. (2010) 122:920–7. doi: 10.1161/CIRCULATIONAHA.109.933762

50. Zhong DX, Zhang Y, Jin Q, Zhang XC, Zhang F, Chen DD, et al. Increased serum PCSK9 in patients with idiopathic pulmonary arterial hypertension: insights from inflammatory cytokines. *Pulm Circ*. (2021) 11:20458940211051292. doi: 10.1177/20458940211051292

51. Voelkel NF, Tuder RM, Bridges J, Arend WP. Interleukin-1 receptor antagonist treatment reduces pulmonary hypertension generated in rats by monocrotaline. *Am J Respir Cell Mol Biol*. (1994) 11:664–75. doi: 10.1165/ajrcmb.11.6.7946395

52. Itoh A, Nishihira J, Makita H, Miyamoto K, Yamaguchi E, Nishimura M. Effects of IL-1beta, TNF-alpha, and macrophage migration inhibitory factor on prostacyclin synthesis in rat pulmonary artery smooth muscle cells. *Respirology*. (2003) 8:467–72. doi: 10.1046/j.1440-1843.2003.00491.x

53. Wen FQ, Watanabe K, Tanaka H, Yoshida M. Cytokines and lipopolysaccharide enhance basal and thrombin-stimulated production of PGI2 by cultured human pulmonary artery smooth muscle cells. *Prostaglandins Leukot Essent Fatty Acids*. (1997) 56:185–92. doi: 10.1016/S0952-3278(97)90532-9

54. El-Haroun H, Clarke DL, Deacon K, Bradbury D, Clayton A, Sutcliffe A, et al. IL-1beta, BK, and TGF-beta1 attenuate PGI2-mediated cAMP formation in human pulmonary artery smooth muscle cells by multiple mechanisms involving p38 MAP kinase and PKA. *Am J Physiol Lung Cell Mol Physiol*. (2008) 294:L553–62. doi: 10.1152/ajplung.00044.2006

55. Ross DJ, Strieter RM, Fishbein MC, Ardehali A, Belperio JA. Type I immune response cytokine-chemokine cascade is associated with pulmonary arterial hypertension. *J Heart Lung Transplant*. (2012) 31:865–73. doi: 10.1016/j.healun.2012.04.008

56. Heresi GA, Aytekin M, Hammel JP, Wang S, Chatterjee S, Dweik RA. Plasma interleukin-6 adds prognostic information in pulmonary arterial hypertension. *Eur Respir J*. (2014) 43:912–4. doi: 10.1183/09031936.00164713

57. Golembeski SM, West J, Tada Y, Fagan KA. Interleukin-6 causes mild pulmonary hypertension and augments hypoxia-induced pulmonary hypertension in mice. *Chest*. (2005) 128:572s–3s. doi: 10.1378/chest.128.6_suppl.572S-a

58. Tamura Y, Phan C, Tu L, Le Hiress M, Thuillet R, Jutant EM, et al. Ectopic upregulation of membrane-bound IL6R drives vascular remodeling in pulmonary arterial hypertension. *J Clin Invest*. (2018) 128:1956–70. doi: 10.1172/JCI96462

59. Kimura A, Kishimoto T. IL-6: regulator of Treg/Th17 balance. *Eur J Immunol*. (2010) 40:1830–5. doi: 10.1002/eji.201040391

60. Lei Y, Zhen J, Ming XL, Jian HK. Induction of higher expression of IL-beta and TNF-alpha, lower expression of IL-10 and cyclic guanosine monophosphate by pulmonary arterial hypertension following cardiopulmonary bypass. *Asian J Surg*. (2002) 25:203–8. doi: 10.1016/S1015-9584(09)60176-7

61. Yang D, Wang L, Jiang P, Kang R, Xie Y. Correlation between hs-CRP, IL-6, IL-10, ET-1, and chronic obstructive pulmonary disease combined with pulmonary hypertension. *J Healthc Eng*. (2022) 2022:3247807. doi: 10.1155/2022/3247807

62. Ito T, Okada T, Miyashita H, Nomoto T, Nonaka-Sarukawa M, Uchibori R, et al. Interleukin-10 expression mediated by an adeno-associated virus vector prevents monocrotaline-induced pulmonary arterial hypertension in rats. *Circ Res*. (2007) 101:734–41. doi: 10.1161/CIRCRESAHA.107.153023

63. Sutendra G, Dromparis P, Bonnet S, Haromy A, McMurtry MS, Bleackley RC, et al. Pyruvate dehydrogenase inhibition by the inflammatory cytokine TNFα contributes to the pathogenesis of pulmonary arterial hypertension. *J Mol Med (Berl)*. (2011) 89:771–83. doi: 10.1007/s00109-011-0762-2

64. Joppa P, Petrasova D, Stancak B, Tkacova R. Systemic inflammation in patients with COPD and pulmonary hypertension. *Chest*. (2006) 130:326–33. doi: 10.1378/chest.130.2.326

65. Fujita M, Mason RJ, Cool C, Shannon JM, Hara N, Fagan KA. Pulmonary hypertension in TNF-alpha-overexpressing mice is associated with decreased VEGF gene expression. *J Appl Physiol (1985)*. (2002) 93:2162–70. doi: 10.1152/japplphysiol.00083.2002

66. Stevens T, Janssen PL, Tucker A. Acute and long-term TNF-alpha administration increases pulmonary vascular reactivity in isolated rat lungs. *J Appl Physiol (1985)*. (1992) 73:708–12. doi: 10.1152/jappl.1992.73.2.708

67. Pullamsetti SS, Savai R, Janssen W, Dahal BK, Seeger W, Grimminger F, et al. Inflammation, immunological reaction and role of infection in pulmonary hypertension. *Clin Microbiol Infect*. (2011) 17:7–14. doi: 10.1111/j.1469-0691.2010.03285.x

68. El Chami H, Hassoun PM. Immune and inflammatory mechanisms in pulmonary arterial hypertension. *Prog Cardiovasc Dis*. (2012) 55:218–28. doi: 10.1016/j.pcad.2012.07.006

69. Li M, Riddle SR, Frid MG, El Kasmi KC, McKinsey TA, Sokol RJ, et al. Emergence of fibroblasts with a proinflammatory epigenetically altered phenotype in severe hypoxic pulmonary hypertension. *J Immunol*. (2011) 187:2711–22. doi: 10.4049/jimmunol.1100479

70. Ye Y, Xu Q, Wuren T. Inflammation and immunity in the pathogenesis of hypoxic pulmonary hypertension. *Front Immunol*. (2023) 14:1162556. doi: 10.3389/fimmu.2023.1162556

71. Sanchez O, Marcos E, Perros F, Fadel E, Tu L, Humbert M, et al. Role of endothelium-derived CC chemokine ligand 2 in idiopathic pulmonary arterial hypertension. *Am J Respir Crit Care Med*. (2007) 176:1041–7. doi: 10.1164/rccm.200610-1559OC

72. Hassoun PM, Mouthon L, Barberà JA, Eddahibi S, Flores SC, Grimminger F, et al. Inflammation, growth factors, and pulmonary vascular remodeling. *J Am Coll Cardiol*. (2009) 54:S10–s19. doi: 10.1016/j.jacc.2009.04.006

73. Dorfmüller P, Zarka V, Durand-Gasselin I, Monti G, Balabanian K, Garcia G, et al. Chemokine RANTES in severe pulmonary arterial hypertension. *Am J Respir Crit Care Med*. (2002) 165:534–9. doi: 10.1164/ajrccm.165.4.2012112

74. Abid S, Marcos E, Parpaleix A, Amsellem V, Breau M, Houssaini A, et al. CCR2/CCR5-mediated macrophage-smooth muscle cell crosstalk in pulmonary hypertension. *Eur Respir J*. (2019) 54:1802308. doi: 10.1183/13993003.02308-2018

75. Zhang J, Hu H, Palma NL, Harrison JK, Mubarak KK, Carrie RD, et al. Hypoxia-induced endothelial CX3CL1 triggers lung smooth muscle cell phenotypic switching and proliferative expansion. *Am J Physiol Lung Cell Mol Physiol*. (2012) 303:L912–22. doi: 10.1152/ajplung.00014.2012

76. Xiang Y, Zheng F, Zhang Q, Zhang R, Pan H, Pang Z, et al. Tanreqing injection regulates cell function of hypoxia-induced human pulmonary artery smooth muscle cells (HPASMCs) through TRPC1/CX3CL1 signaling pathway. *Oxid Med Cell Longev*. (2022) 2022:3235102. doi: 10.1155/2022/3235102

77. Perros F, Ranchoux B, Izikki M, Bentebbal S, Happé C, Antigny F, et al. Nebivolol for improving endothelial dysfunction, pulmonary vascular remodeling, and right heart function in pulmonary hypertension. *J Am Coll Cardiol*. (2015) 65:668–80. doi: 10.1016/j.jacc.2014.11.050

78. Diller GP, Thum T, Wilkins MR, Wharton J. Endothelial progenitor cells in pulmonary arterial hypertension. *Trends Cardiovasc Med*. (2010) 20:22–9. doi: 10.1016/j.tcm.2010.03.003

79. Burke DL, Frid MG, Kunrath CL, Karoor V, Anwar A, Wagner BD, et al. Sustained hypoxia promotes the development of a pulmonary artery-specific chronic inflammatory microenvironment. *Am J Physiol Lung Cell Mol Physiol*. (2009) 297:L238–50. doi: 10.1152/ajplung.90591.2008

80. Tatius B, Wasityastuti W, Astarini FD, Nugrahaningsih DAA. Significance of BMPR2 mutations in pulmonary arterial hypertension. *Respir Investig*. (2021) 59:397–407. doi: 10.1016/j.resinv.2021.03.011

81. Farha S, Asosingh K, Xu W, Sharp J, George D, Comhair S, et al. Hypoxia-inducible factors in human pulmonary arterial hypertension: a link to the intrinsic myeloid abnormalities. *Blood*. (2011) 117:3485–93. doi: 10.1182/blood-2010-09-306357

82. Teichert-Kuliszewska K, Kutryk MJ, Kuliszewski MA, Karoubi G, Courtman DW, Zucco L, et al. Bone morphogenetic protein receptor-2 signaling promotes pulmonary arterial endothelial cell survival: implications for loss-of-function mutations in the pathogenesis of pulmonary hypertension. *Circ Res*. (2006) 98:209–17. doi: 10.1161/01.RES.0000200180.01710.e6

83. McDonald PP, Fadok VA, Bratton D, Henson PM. Transcriptional and translational regulation of inflammatory mediator production by endogenous TGF-beta in macrophages that have ingested apoptotic cells. *J Immunol*. (1999) 163:6164–72. doi: 10.4049/jimmunol.163.11.6164

84. Morrell NW. Pulmonary hypertension due to BMPR2 mutation: a new paradigm for tissue remodeling? *Proc Am Thorac Soc*. (2006) 3:680–6. doi: 10.1513/pats.200605-118SF

85. Kim CW, Song H, Kumar S, Nam D, Kwon HS, Chang KH, et al. Anti-inflammatory and antiatherogenic role of BMP receptor II in endothelial cells. *Arterioscler Thromb Vasc Biol*. (2013) 33:1350–9. doi: 10.1161/ATVBAHA.112.300287

86. Soon E, Crosby A, Southwood M, Yang P, Tajsic T, Toshner M, et al. Bone morphogenetic protein receptor type II deficiency and increased inflammatory cytokine production. A gateway to pulmonary arterial hypertension. *Am J Respir Crit Care Med*. (2015) 192:859–72. doi: 10.1164/rccm.201408-1509OC

87. Andruska A, Spiekerkoetter E. Consequences of BMPR2 deficiency in the pulmonary vasculature and beyond: contributions to pulmonary arterial hypertension. *Int J Mol Sci*. (2018) 19:2499. doi: 10.3390/ijms19092499

88. Sawada H, Saito T, Nickel NP, Alastalo TP, Glotzbach JP, Chan R, et al. Reduced BMPR2 expression induces GM-CSF translation and macrophage recruitment in humans and mice to exacerbate pulmonary hypertension. *J Exp Med*. (2014) 211:263–80. doi: 10.1084/jem.20111741

89. Cohen-Kaminsky S, Hautefort A, Price L, Humbert M, Perros F. Inflammation in pulmonary hypertension: what we know and what we could logically and safely target first. *Drug Discovery Today*. (2014) 19:1251–6. doi: 10.1016/j.drudis.2014.04.007

90. Spiekerkoetter E, Tian X, Cai J, Hopper RK, Sudheendra D, Li CG, et al. FK506 activates BMPR2, rescues endothelial dysfunction, and reverses pulmonary hypertension. *J Clin Invest*. (2013) 123:3600–13. doi: 10.1172/JCI65592

91. Gomberg-Maitland M, Olschewski H. Prostacyclin therapies for the treatment of pulmonary arterial hypertension. *Eur Respir J*. (2008) 31:891–901. doi: 10.1183/09031936.00097107

92. Wilkins MR, Ali O, Bradlow W, Wharton J, Taegtmeyer A, Rhodes CJ, et al. Simvastatin as a treatment for pulmonary hypertension trial. *Am J Respir Crit Care Med*. (2010) 181:1106–13. doi: 10.1164/rccm.200911-1699OC

93. Hillyard DZ, Cameron AJ, McDonald KJ, Thomson J, MacIntyre A, Shiels PG, et al. Simvastatin inhibits lymphocyte function in normal subjects and patients with cardiovascular disease. *Atherosclerosis*. (2004) 175:305–13. doi: 10.1016/j.atherosclerosis.2004.03.018

94. Kao PN. Simvastatin treatment of pulmonary hypertension: an observational case series. *Chest*. (2005) 127:1446–52. doi: 10.1016/S0012-3692(15)34501-3

95. Quarck R, Nawrot T, Meyns B, Delcroix M. C-reactive protein: a new predictor of adverse outcome in pulmonary arterial hypertension. *J Am Coll Cardiol*. (2009) 53:1211–8. doi: 10.1016/j.jacc.2008.12.038

96. Sanchez O, Sitbon O, Jaïs X, Simonneau G, Humbert M. Immunosuppressive therapy in connective tissue diseases-associated pulmonary arterial hypertension. *Chest*. (2006) 130:182–9. doi: 10.1378/chest.130.1.182

frontiers | Frontiers in Immunology

TYPE Original Research
PUBLISHED 13 March 2024
DOI 10.3389/fimmu.2024.1383464

OPEN ACCESS

EDITED BY
Ping Yuan,
Tongji University, China

REVIEWED BY
Kim Cuong Cap,
Houston Methodist Research Institute, United States
Wengong Wang,
Peking University, China
Rong Jiang,
Tongji University, China

*CORRESPONDENCE
Xiao Shi
mdshixiao@163.com
Yan Shen
sheny26@126.com

†These authors have contributed equally to this work

RECEIVED 07 February 2024
ACCEPTED 26 February 2024
PUBLISHED 13 March 2024

CITATION
Zhang Z, Wu Y, Shi D, Jiang C, Cao H, Jiang F, Bao X, Shen Y and Shi X (2024) *Acanthopanax senticosus* improves cognitive impairment in Alzheimer's disease by promoting the phosphorylation of the MAPK signaling pathway. *Front. Immunol.* 15:1383464. doi: 10.3389/fimmu.2024.1383464

Acanthopanax senticosus improves cognitive impairment in Alzheimer's disease by promoting the phosphorylation of the MAPK signaling pathway

Zhichun Zhang[1,2†], Yonghui Wu[2†], Dan Shi[1†], Chanyu Jiang[2], Hengyan Cao[1], Fengyi Jiang[1], Xiaomin Bao[1], Yan Shen[1*] and Xiao Shi[1*]

[1]Department of Gerontology, Yueyang Hospital of Integrated Traditional Chinese and Western Medicine, Shanghai, China, [2]Graduate School of Shanghai University of Traditional Chinese Medicine, Shanghai, China

Background: *Acanthopanax senticosus* (AS) can improve sleep, enhance memory, and reduce fatigue and is considered as an effective drug for Alzheimer's disease (AD). The therapeutic effect and mechanism need to be further investigated.

Methods: To confirm the AS play efficacy in alleviating memory impairment in mice, 5×FAD transgenic mice were subjected to an open-field experiment and a novelty recognition experiment. Network pharmacology technique was used to analyze the information of key compounds and potential key targets of AS for the treatment of AD, molecular docking technique was applied to predict the binding ability of targets and compounds, and Gene Ontology (GO) and Kyoto Encyclopedia of Genes and Genomes (KEGG) analyses were also performed on the targets to derive the possible metabolic processes and pathway mechanisms of AS in treating AD. Quantitative real-time PCR (qRT-PCR) and western blot technique were carried out to validate the candidate genes and pathways.

Results: In the open-field experiment, compared with the wild-type (WT) group, the number of times the mice in the AD group crossed the central zone was significantly reduced ($P< 0.01$). Compared with the AD group, the number of times the mice in the AS group crossed the central zone was significantly increased ($P< 0.001$). In the new object recognition experiment, compared with the WT group, the percentage of times the AD group explored new objects was significantly reduced ($P< 0.05$). Compared with the AD group, the AS group had an increase in the percentage of time spent exploring new things and the number of times it was explored ($P< 0.05$). At the same time, the donepezil group had a significantly higher percentage of times exploring new things ($P< 0.01$). By using network pharmacology technology, 395 common targets of AS and AD were retrieved. The Cytoscape software was used to construct the protein–protein interaction (PPI) network of common targets. Using the algorithm, nine key targets were retrieved: APP, NTRK1, ESR1, CFTR, CSNK2A1, EGFR, ESR2, GSK3B, and PAK1. The results of molecular docking indicate that 11 pairs of compounds and their corresponding targets have a

significant binding ability, as the molecular binding energies were less than -7.0. In comparison to the AD group, the mRNA expression of the key target genes was significantly decreased in the AS treatment group ($P< 0.001$). The KEGG analysis showed that the MAPK signaling pathway was significantly enriched, and Western blot confirmed that the TRAF6 protein decreased significantly ($P< 0.0001$). Meanwhile, the levels of MAP3K7 and P38 phosphorylation increased, and there was also an increase in the expression of HSP27 proteins.

Conclusion: Our study indicates that the multi-component and multi-target properties of AS play an important role in the alleviation of anxiety and memory impairment caused by AD, and the mechanism is involved in the phosphorylation and activation of the MAPK signaling pathway. The results of this study could provide a novel perspective for the clinical treatment of AD.

KEYWORDS

Acanthopanax senticosus, Alzheimer's disease, network pharmacology, MAPK signaling pathway, neuroinflammation

1 Introduction

Alzheimer's disease (AD) is the most common neurodegenerative disease which is a common cause of dementia, and the incidence of AD gradually increases with age (1). The clinical manifestations include memory loss, disorientation, and language impairment. The patient's ability to handle social affairs and self-care will decline as the condition worsens (2). Current hypothesis for the pathogenesis of AD include Aβ plaque-related neurodegeneration, neurofibrillary tangles, synaptic dysfunction and neurotransmitter imbalance, and neuroinflammation (3). FDA-approved drugs including donepezil, rivastigmine, and galantamine are mainly used to treat β-amyloid deposition and tau fiber tangles, but the effect is not significant (3, 4). More and more studies showed that neuroinflammation played a key role in AD neurodegeneration, and how to control the inflammatory response caused by Aβ protein provides a new research direction for the treatment of AD (5–7).

Related research showed (8–10) that traditional Chinese medicine with multiple components, targets, and pathways can treat AD by improving neurocholine function, reducing inflammatory response, and resisting oxidative stress. *Acanthopanax senticosus* (AS) is a Wujiaceae plant that can improve sleep, enhance memory, and reduce fatigue (11). Relevant experimental studies have shown that AS extract can significantly enhance mice's object recognition memory (12); EEAK (ethanol extract of AS) can improve cognitive dysfunction caused by cholinergic blockade and improve the performance of mice in Y-maze and novel object recognition experiments (13). ML Jinc et al. found that (14) AS can induce the expression of HO-1 through the p38-CREB and Nrf2 pathways, thereby reducing the expression of pro-inflammatory mediators such as iNOS, COX-2, and NO in LPS-stimulated BV2 cells, and has a neuroprotective effect. Therefore, AS is considered to have a certain therapeutic effect on AD, but its possible mechanism is still unclear.

This study intends to verify the therapeutic effect of the traditional Chinese medicine AS on AD through system network pharmacology, molecular docking technology, and animal experiments, explore the relevant molecular mechanisms, and provide more scientific basis for the clinical treatment of AD.

2 Materials and methods

2.1 Preparation and feeding of experimental animal models

Specific-pathogen-free (SPF)-grade 5×FAD transgenic mice were obtained from the Model Animal Research Institute of Nanjing University (Animal Qualification Certificate No. 201400975) and kept under SPF conditions. The animal experiments were approved by the Animal Care and Use Committee of Shanghai University of Traditional Chinese Medicine (ethics number: PZSHUTCM210702001).

5×FAD transgenic mice were cross-bred with C57BL/6J mice. The mice were raised in separate cages according to their gender after 20 days of life. Their tails were docked at 30 days for genetic identification of mouse breeds, and 5×FAD mice were selected as the *Acanthopanax senticosus* treatment group (AS group), the donepezil hydrochloride treatment group (donepezil group), and the model group (AD group), while the C57BL/6J mice in the same litter were the blank group (WT group), with 12 mice in each group. After 2 months of regular feeding of the mice, the AS group was changed to a diet supplemented with 1.69 mg/kg of *Acanthopanax*

senticosus (Heilongjiang Ussuri River Harbin Branch, batch no. 20210501), and the donepezil group was changed to a diet containing 3.8 g/kg of the drug, donepezil hydrochloride tablets (Sibohai, Phyllanthus Bio-Technology Co. Ltd, batch no. 21030004). All the drug-containing diets were manufactured by Jiangsu Synergy Pharmaceutical and Biological Engineering Co. Ltd., and animal tissues were acquired after 3 months of continuous feeding.

2.2 Animal experiment

2.2.1 Open-field experiment

The test box for the open-field experiment consisted of four square opaque boxes with a length, width, and height dimension of 50 × 50 × 40 cm, and a square area of 20×20 cm in the center of the test box was designated as the analysis area. Each mouse was allowed to move freely in the test box for 5 min, and the total distance traveled, the average speed of movement, and the number of times the mice crossed the central area of the experimental site were recorded by using Ethovision XT 11.5 image acquisition and analysis software for the different groups. The experimental environment was kept quiet, and the test chamber was wiped with 75% alcohol after each round of experiments.

2.2.2 Novelty recognition experiment

The test chambers for the novelty recognition experiment consisted of four square opaque whiteboards measuring 50 × 50 × 40 cm in length, width, and height, with two identical X-objects and Y-objects placed in the center of each chamber and secured with a transparent tape. The detection behavior of each mouse was recorded for 5 min using Ethovision XT 11.5 image acquisition and analysis software. Approximately 1 h after the abovementioned behavioral experiments, object Y was replaced by object Z, which was different in size, shape, and color from object Y, and then the mice were placed in the experimental field in the order of the sequence and moved randomly around the experimental field for 5 min. The residence time and number of times the mice explored each object were recorded. The location preference index of the first trial was calculated as RI = Tx/(Ty + Tx) × 100%, which was used to observe whether the experimental mice had a preference for toys X and Y, and whether there was a difference in curiosity between the toys, to determine whether the curious nature of the mice's exploration was normal. The formula for the experimental position preference index for the next 1 h is RI = Tz/(Tz + Tx) × 100%, which was used to determine the curiosity index of the experimental mice toward the novel object Z.

2.3 Network pharmacology analysis

2.3.1 Component collection and target prediction

The TCMIP (http://www.tcmip.cn/TCMIP/index.php/Home/Login/login.html) and HERB (http://herb.ac.cn/) databases were searched using the keyword "ciwujia" (*Acanthopanax senticosus*, AS). The screening conditions were oral bioavailability (OB) ≥0.3, drug likeness (DL) ≥0.18, Lipinsk's five principles, and high gastrointestinal absorption, and we supplemented the literature with active ingredients that have clear utility in AS (15). The Swiss Target Prediction database (http://www.swisstargetprediction.ch/) was used to predict the targets of the relevant compounds. Using "Alzheimer's disease" as a keyword, the OMIM database (https://www.omim.org/), TTD database (http://db.idrblab.net/ttd/), and GeneCards database (https://www.genecards.org/) (score ≥5) were searched, screened, and intersected to obtain AD-related disease targets.

2.3.2 Component–target network construction of AS treatment for AD

The targets of AS and AD were imported into the Venny 2.1 online software mapping tool platform (https://bioinfogp.cnb.csic.es/tools/venny/) to draw a Venn diagram, and the common targets obtained were the potential targets of AS for AD. These potential targets and their corresponding compound data were processed with Cytoscape 3.7.2 software to construct a compound–target network (CTN) of AS for AD.

2.3.3 Construct protein–protein interaction network

Taking the target in the abovementioned CTN as the objective, IntAct, BioGrid, and STRING databases are used to construct the protein–protein (PPI) network. The MCODE algorithm was used to filter the key clusters in the PPI network, construct the PPI network, and calculate the parameters of degree, degree centrality (DC), closeness centrality (CC), and betweenness centrality (BC) of the network and then select the core clusters according to the mean value.

2.3.4 GO enrichment analysis and KEGG pathway analysis

The DAVID database (https://david.ncifcrf.gov/) was used to perform Gene Ontology (GO) functional annotation of core targets, including Biological Process (BP), Cellular Component (CC), and Molecular Function (MF), and Kyoto Encyclopedia of Genes and Genomes (KEGG) enrichment analysis was performed to predict the possible pathway mechanisms of AS for AD.

2.4 Molecular docking

The core targets obtained from the PPI network were mapped to the CTN network to find the key compounds corresponding to the core targets. The 3D protein structure of the core target was retrieved from the PDB database (https://www.rcsb.org/) as a receptor, and the receptor protein was subjected to pre-docking preparation operations such as dehydrogenation and hydrogenation by UCSF Chimera 1.16 software. Using the abovementioned key compounds as ligands, molecular docking was performed using Auto Dock Vina 1.1.2

software, and the pairs with binding energies ≤-7.5 were visualized by Pymol 2.4.0 software.

2.5 qRT-PCR detection of key protein mRNA content

mRNA was extracted from the cerebral cortex of each group of mice using the TRIzol method. cDNA reverse transcription was performed at 25°C for 5 min, 55°C for 10 min, and 85°C for 5 s. The PCR primers were purchased from Sangong Bioengineering (Shanghai) Co., Ltd., and the sequence of the primers (5′ to 3′) is shown in Table 1. The reaction program was set at 95°C for 30 s, 95°C for 15 s, and 60°C for 30 s in the quantitative PCR instrument (C1000 Touc, BIO-RAD). The results were expressed as $2^{-\Delta\Delta CT}$ values and analyzed for statistical differences.

2.6 Western blot to validate the pathway of action

An appropriate amount of mouse hippocampal tissue stored at -80°C in the refrigerator was taken out, RIPA lysis buffer was added, and the tissue was disrupted with an ultrasonic crusher and centrifuged at 12,000 rpm for 15 min. The supernatant was aspirated and 5× Protein Loading Buffer (Beyotime, P0015) was added. The protein samples were heated in a water bath at 100°C for 10 min. Electrophoresis was performed at 120 V for 80 min, and the membranes were transferred to a new membrane. After blocking with 5% BSA solution for 2 h, the primary antibody was incubated. The antibodies used for each sample were TRAF6 (#8028, CST, 1:1,000), anti-MAP3K7 (K008561P, Solarbio, 1:1,000), anti-p-MAP3K7 (K006194P, Solarbio, 1:1,000), P38 (#8690, CST, 1: 1,000), p-P38 (#4511, CST, 1:1,000), and HSP27 (#95357, CST, 1:1,000), overnight at 4°C in the refrigerator. After three washes in TBST solution, secondary antibodies were used: anti-rabbit IgG, HRP-conjugated antibody (#7074, CST, 1:2,000) was incubated for 1 h. The protein band signals were captured using the FL1000 Intelligent Imaging Scanning System (Thermo Fisher Scientific, USA). The protein band intensities were quantified using Image J (v1.45f) software.

2.7 Statistical method

The experimental data obtained from all behavioral experiments were expressed as mean ± SD ($\bar{x} \pm s$), and SPSS 26.0 software was used for statistical analysis. One-way ANOVA was used for two-way comparisons between multiple groups and when $P<0.05$ is a statistically significant difference criterion.

3 Results

3.1 Behavioral experiment results

The effects of AS on anxiety, nervousness, and other emotions of mice were analyzed by recording the distance traveled, average speed of movement, and number of times crossing the central zone of different groups of freely moving mice in the open-field experiment, and the results show that there was no significant difference between the distance traveled and the average speed of movement of mice in the WT, AD, donepezil, and AS groups in the behavioral experiments ($P< 0.05$) (Figures 1A, B). The number of times the mice in the AD group crossed the central zone was significantly lower than that of the WT group (5.38 ± 1.19 vs. 10.12 ± 3.31; $P< 0.01$), while the number of times the mice in the AS group traversed the central zone was significantly higher than that of the AD group (11.38 ± 3.11 vs. 5.38 ± 1.19; $P< 0.001$), whereas there was no significant difference in the donepezil group (6.25 ± 1.75 vs. 5.38 ± 1.19) (Figure 1C).

Mice are naturally curious and exploratory of new things, and the effect of spikenard on learning and memory impairment in

TABLE 1 qRT-PCR primer sequences.

Gene	Forward (o′– 3′)	Reverse (e′– 3′)
GAPDH	AGGTCGGTGTGAACGGATTTG	TGTAGACCATGTAGTTGAGGTCA
APP	ACCCCAGATCGCCATGTTC	CCCACTTTCCATTCTGCACATTC
NTRK1	CAGTCTGATGACTTCGTTGATGC	CTCTTCACGATGGTTAGGCTTC
ESR1	CCCGCCTTCTACAGGTCTAAT	CTTTCTCGTTACTGCTGGACAG
CFTR	CTGGACCACACCAATTTTGAGG	GCGTGGATAAGCTGGGGAT
CSNK2A1	ATGTGGTGGAATGGGGGAATC	GCAAGTGTGATGATGTTGGGC
EGFR	GCATCATGGGAGAGAACAACA	TCAGGAACCATTACTCCATAGGT
ESR2	CTGTGCCTCTTCTCACAAGGA	TGCTCCAAGGGTAGGATGGAC
GSK3B	AAGCGATTTAAGAACCGAGAGC	AGAAATACCGCAGTCGGACTAT
PAK1	GAAACACCAGCACTATGATTGGA	ATTCCCGTAAACTCCCCTGTG

GAPDH, glyceraldehyde-3-phosphate dehydrogenase; APP, amyloid precursor protein; NTRK1, neurotrophic receptor tyrosine kinase 1; ESR1, estrogen receptor 1; CFTR, CF transmembrane conductance regulator; CSNK2A1, casein kinase 2 alpha 1; EGFR, epidermal growth factor receptor; ESR2, estrogen receptor 2; GSK3B, glycogen synthase kinase 3 beta; PAK1, P21 (RAC1) activated kinase 1.

10.3389/fimmu.2024.1383464

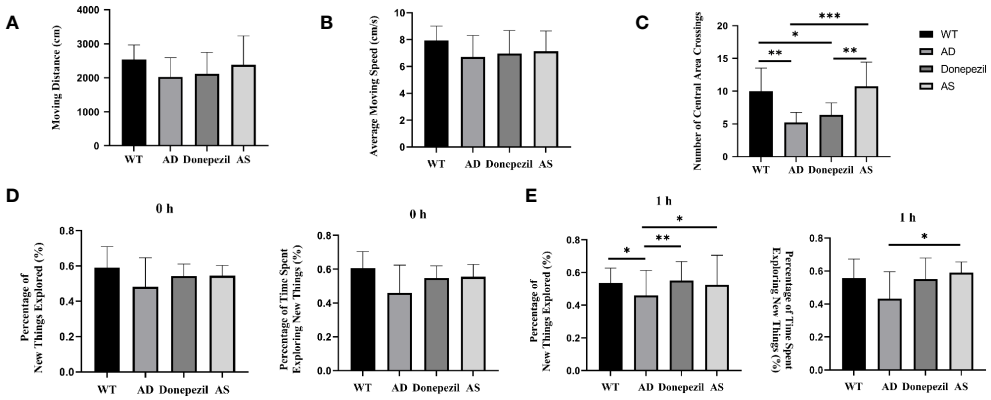

FIGURE 1
Behavioral experimental results on the open-field test and the new-object recognition experiment. **(A)** Moving distance in each group of the open-field test. **(B)** Average moving speed in each group of the open-field test. **(C)** Times of crossing the central area in each group of the open-field test. **(D)** 0 h percentage of new things explored and 0 h percentage of time exploring new things. **(E)** 1 h percentage of new things explored and 1 h percentage of time exploring new things (n = 8). *P < 0.05, **P < 0.01, ***P < 0.001.

demented mice could be determined by conducting new object recognition experiments. The experimental results showed that in the training phase (0 h) (Figure 1D), there was no significant difference in the percentage of time spent exploring unfamiliar toys (0.60 ± 0.05 vs. 0.53 ± 0.11 vs. 0.55 ± 0.06 vs. 0.57 ± 0.04; P > 0.05) and the percentage of number of explorations (0.57 ± 0.07 vs. 0.54 ± 0.11 vs. 0.56 ± 0.07 vs. 0.60 ± 0.04; P > 0.05) among the mice in the WT, AD, donepezil, and AS groups, indicating that there was no difference in the inherent curiosity for novelty among the mice in each group.

During the test phase (1 h) (Figure 1E), compared with the WT group, the AD group showed a decrease in the percentage of number of times of curious exploration of object Z (0.45 ± 0.07 vs. 0.55 ± 0.07; P< 0.05) and a decrease in the percentage of time spent exploring (0.46 ± 0.09 vs. 0.56 ± 0.05), but there was no significant difference; compared with AD group, the percentage of time spent exploring and the percentage of number of times of curious exploration of object Z are increased in the AS group (0. 56 ± 0.08 vs. 0.45 ± 0.07; 0.60 ± 0.07 vs. 0.46 ± 0.09; P< 0.05); compared with the AD group, the donepezil group had a significantly higher percentage of times exploring object Z (0.58 ± 0.05 vs. 0.45 ± 0.07; P< 0.01) and an increased percentage of time exploring object Z, but there was no statistically significant difference and it was lower than the AS group.

3.2 Active ingredients–target network of AS in treating AD

By searching the TCMIP database, the HERB database, and the Chinese Pharmacopoeia (2020 edition), 25 active ingredients (Table 2) and 395 targets for AS were obtained. GeneCards database (score ≥5), OMIM database, and TTD database were used to retrieve 3563 AD-related targets. The intersection of the two databases yielded 245 targets common to AS and AD (Figure 2A), which belonged to a total of 25 chemical components in AS, and a compound–target network (CTN) was constructed using Cytoscape-v3.7.2 software (Figure 2B).

TABLE 2 Potentially active compounds in *Acanthopanax senticosus*.

PubChem CID	Compound
72	3,4-Dihydroxybenzoic acid
338	Salicylic acid
1183	Vanillin
10742	Syringic acid
13250	Ethyl gallate
73117	(+)-Eudesmin
15699109	Coniferaldehyde glucoside
21636080	Chiisanogenin
428040	Ethyl glucoside
443023	(+)-Syringaresinol
445858	Ferulic acid
5280343	Quercetin
5280372	Coniferin
5280536	4-Hydroxy-3-methoxycinnamaldehyde
5282316	(9Z,12E)-12-Nitrooctadeca-9,12-dienoic acid
5315944	Ciwujiatone
5315945	Clausarin
5316860	Syringin
5318565	Isofraxidin
637542	4-Hydroxycinnamic acid
68289	Sesamo
689043	Caffeic acid
71312557	Eleutheroside E
72307	Sesamin
9859136	Eleutheroside C

3.3 Analysis of core targets and biological functions of AS in treating AD

Protein interaction pairs (PPI pairs) of the abovementioned 245 targets screened in IntAct (https://www.ebi.ac.uk/intact/), BioGrid (https://thebiogrid.org/), and STRING databases were transferred to Cytoscape software to construct the protein–protein interaction (PPI) network for AS of AD. The topological parameters of each node in the PPI network were calculated using the MCODE algorithm, and a total of 19 core protein interaction cluster networks were screened, of which 85 targets related to AS for AD were identified in these 19 core protein interaction clusters. The core nodes were screened by the mean values of degree, degree centrality (DC), closeness centrality (CC), betweenness centrality (BC) and other parameters, and finally nine key targets were obtained, including APP, NTRK1, ESR1, CFTR, CSNK2A1, EGFR, ESR2, GSK3B, and PAK1, which suggest that these targets play an important role in AS for AD.

The results of the GO enrichment analysis of these nine key targets showed that (Figure 2D) the biological process (BP) of AS treatment of AD was highlighted in the processes of protein phosphorylation, protein autophosphorylation, positive regulation of protein phosphorylation, cellular response to estradiol stimulation, and learning or memory; cellular composition (CC) was mainly in the processes of macromolecular complexes, axons, plasma membrane, cell surface, early endosomal membranes and receptor complexes, etc.; and molecular function (MF) focuses on the role of enzyme binding, protein serine/threonine/tyrosine kinase activity, ATP binding, binding of the same proteins, estrogen receptor activity, and nitric oxide synthase regulatory activity.

The KEGG pathway analysis identified 22 relevant biological pathways that may be significantly affected by AS in the treatment of AD (Figure 2C). AS was found to play a role in some cancer pathways, such as breast and endometrial cancer as well as in Alzheimer's disease pathways and pathways associated with neurodegenerative diseases. Others play important roles in the ErbB signaling pathway, the Ras signaling pathway, the MAPK signaling pathway, the PI3K-Akt signaling pathway, and so on.

3.4 Molecular docking

To further explore the potential mechanism of AS for the treatment of AD, these nine key targets and their corresponding 16 compounds in AS were subjected to molecular docking operations. The results (Table 3) showed that the binding free energies of each compound docked to the proteins were all less than -5.0 kJ/mol, and the lower the free binding energy, the higher the affinity between the protein receptor and the small molecule ligand, and the more likely the interaction would occur. This indicates that the compounds in AS have high affinity with all relevant proteins. Docking results below -7.5 kJ/mol were visualized using Pymol software (Figure 3).

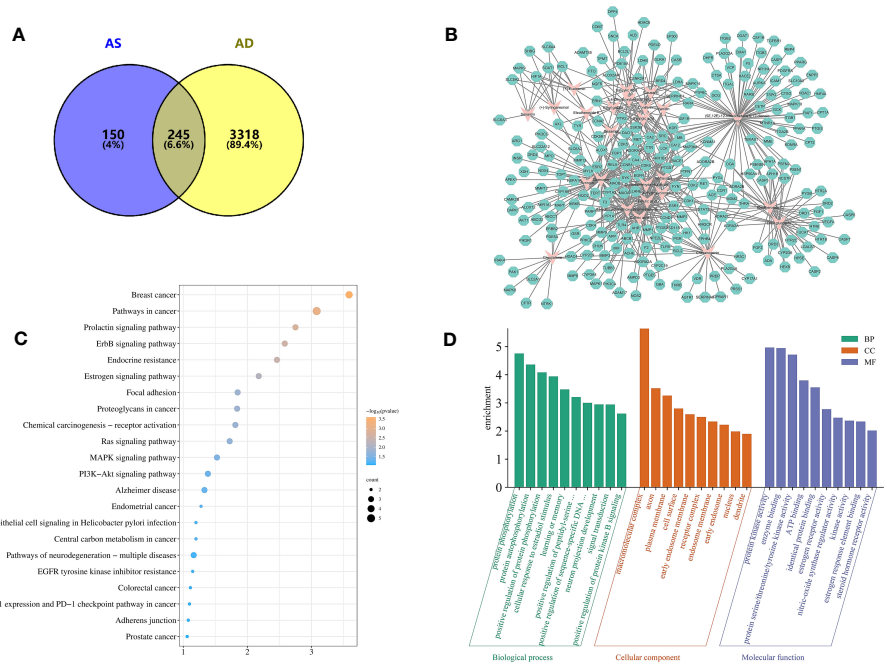

FIGURE 2
Target information and network topology analysis results of *Acanthopanax senticosus* (AS) and Alzheimer's disease. **(A)** Venn diagram. **(B)** "Compound–target" network (CTN) of common targets and compounds in AS. Pink rhombus, compounds; green polygons, targets. **(C)** Kyoto Encyclopedia of Genes and Genomes pathways enrichment analysis. The bluer the color, the larger the *P* value. The size of each bubble reflects the number of genes enriched in the terms. **(D)** Gene Ontology enrichment analysis.

10.3389/fimmu.2024.1383464

TABLE 3 Binding ability of key targets and corresponding compounds.

Target	PDB ID	Ligands	deltaG (kcal/mol)
CSNK2A1	1NA7	Quercetin	-8.7
GSK3B	1Q5K	Quercetin	-8.6
EGFR	1IVO	Quercetin	-8.2
GSK3B	1Q5K	(+)-Eudesmin	-7.7
ESR2	4J26	Quercetin	-7.7
GSK3B	1Q5K	Coniferin	-7.6
APP	1AAP	Quercetin	-7.5
GSK3B	1Q5K	Clausarin	-7.4
ESR1	1A52	(9Z,12E)-12-Nitrooctadeca-9,12-dienoic acid	-7.4
EGFR	1IVO	Coniferaldehyde glucoside	-7.4
CSNK2A1	1NA7	(9Z,12E)-12-nitrooctadeca-9,12-dienoic acid	-7.2
APP	1AAP	Caffeic acid	-6.8
ESR2	4J26	Caffeic acid	-6.4
GSK3B	1Q5K	Isofraxidin	-6.4
ESR1	1A52	Caffeic acid	-6.3
EGFR	1IVO	Isofraxidin	-6.3
ESR2	4J26	4-Hydroxycinnamic acid	-6.3
PAK1	3FXZ	Ciwujiatone	-6.2
ESR2	4J26	Ferulic acid	-6.2
ESR1	1A52	4-Hydroxy-3-methoxycinnamaldehyde	-6.1
ESR1	1A52	4-Hydroxycinnamic acid	-6.1
CFTR	1XMI	Ciwujiatone	-6.1
EGFR	1IVO	Caffeic acid	-6.1
ESR2	4J26	4-Hydroxy-3-methoxycinnamaldehyde	-6.1
ESR2	4J26	Ethyl gallate	-6.1
ESR2	4J26	Salicylic acid	-6.1
ESR2	4J26	3,4-Dihydroxybenzoic acid	-6.0
GSK3B	1Q5K	4-Hydroxy-3-methoxycinnamaldehyde	-6.0
APP	1AAP	Ferulic acid	-5.9
NTRK1	1HE7	Ciwujiatone	-5.9
EGFR	1IVO	(9Z,12E)-12-Nitrooctadeca-9,12-dienoic acid	-5.9
EGFR	1IVO	4-Hydroxy-3-methoxycinnamaldehyde	-5.8
EGFR	1IVO	Ferulic acid	-5.7
APP	1AAP	4-Hydroxy-3-methoxycinnamaldehyde	-5.4
EGFR	1IVO	Sesamol	-5.4

3.5 mRNA expression of key genes in mouse cerebral cortex

According to the statistical results of qRT-PCR (Figure 4A), the mRNA content expression of APP, NTRK1, ESR1, CFTR, CSNK2A1, EGFR, ESR2, GSK3B, and PAK1 in the hippocampus of the brains of mice in the AD group was significantly elevated compared with those of mice in the WT group ($P< 0.01$, $P< 0.001$, $P< 0.0001$). The mRNA expression of APP, NTRK1, ESR1, CFTR, CSNK2A1, EGFR, ESR2, GSK3B, and PAK1 in the AS group showed a significant decrease compared with that of the AD group ($P< 0.001$, $P< 0.0001$). It was demonstrated that the key targets of AS for the treatment of AD derived from network pharmacology were plausible and effective.

3.6 Western blot analysis of key pathways in the treatment of AD by AS

According to the results of the KEGG biological function analysis, the most relevant pathway for AS treatment of AD is involved in the MAPK pathway. The TRAF6, MAP3K7, p-MAP3K7, P38, p-P38, and HSP27 proteins in this pathway were selected for western blot analysis. The analysis showed that the expression level of TRAF6 protein in the hippocampal tissue of the AD group was significantly increased compared to that of the WT group, while the relative protein levels of p-MAP3K7/MAP3K7, the relative protein levels of p-P38/P38, and the expression of HSP27 protein were decreased. In contrast, in the hippocampus of mice after therapeutic intervention with AS, it can be found that mice in the AS group have a significant decrease in the expression level of TRAF6 protein and a notable increase in the expression level of MAPK phosphorylation and the HSP27 protein compared with the AD group; all the results were significant (Figure 4B). This suggests that AS may treat AD by regulating the phosphorylation process of the MAPK signaling pathway.

4 Discussion

It is established that the accumulation of extracellular amyloid β and neurofibrillary tangles in the brain contributes to the onset of Alzheimer's disease; however, the current study suggests that AD is significantly linked to inflammatory processes within the central nervous system (CNS) (16). Flavonoid compounds have demonstrated the ability to inhibit neuroinflammatory processes and enhance memory recognition in mice with AD (17). According to the findings of clinical trials conducted by Tohda et al., the extract of AS is safe for augmentation in cognitive function, and it effectively alleviates anxiety in healthy individuals (18). In our study, we can see that AS has some efficacy in alleviating cognitive impairment caused by AD from the results of the behavioral experiments. In the open-field experiment, although there was no statistically significant difference between the groups of mice in terms of the distance traveled and the average speed of movement, the number of times the mice in the AS group crossed the central zone was significantly

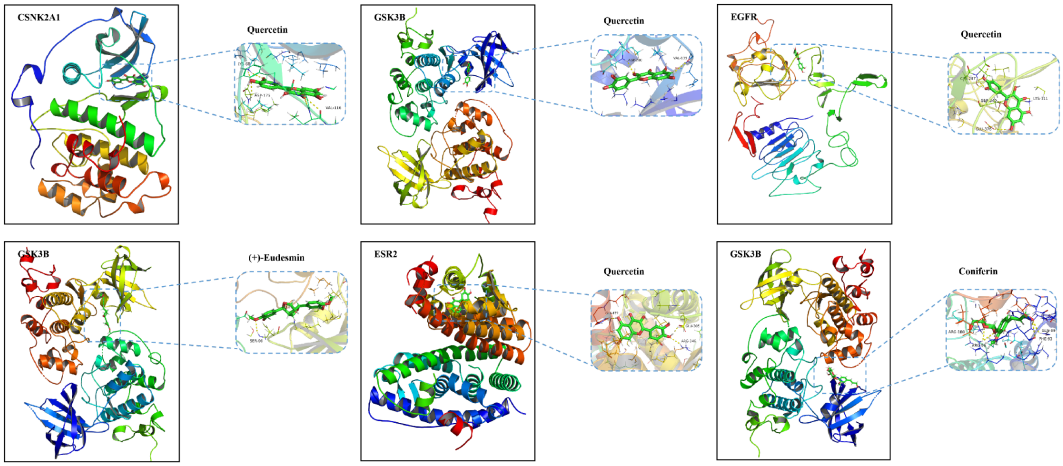

FIGURE 3
Molecular docking diagram of quercetin, (+)-eudesmin, and coniferin with related key targets.

higher, which means that the mice showed good autonomous exploratory behavior and the negative emotional responses such as anxiety and nervousness were significantly alleviated by the administration of AS. According to the novelty recognition experiment, compared with the AD group, the percentage of time spent curiously exploring Z and the percentage of frequency of curious exploration increased in the AS group, while the percentage of number of times exploring Z was significantly higher in the donepezil group. Taken in combination, this suggests that both AS and donepezil can improve transient memory impairment in AD model mice.

To elucidate the potential therapeutic targets and mechanisms of action for AS in the treatment of AD, a comprehensive analysis of 245 candidate targets was conducted using network pharmacology techniques. A topological algorithm was employed to establish a protein–interaction network (PPI), which identified nine key targets for AS in AD treatment: amyloid-beta precursor protein (APP), neurotrophic receptor tyrosine kinase 1 (NTRK1), estrogen receptor alpha (ESR1), cystic fibrosis transmembrane conductance regulator (CFTR), casein kinase 2 alpha 1 (CSNK2A1), epidermal growth factor receptor (EGFR), estrogen receptor 2 (ESR2), glycogen synthase kinase 3 beta (GSK3B), and P21 activated kinase 1 (PAK1). The quantitative real-time PCR (qRT-PCR) data revealed that the mRNA expression levels of these targets in the hippocampus of AS-treated mice significantly decreased compared to that of the AD group. Several studies have shown that in addition to amyloid deposition and tau protein hyperphosphorylation leading to AD, mice carrying mutants of the human APP gene and lacking the apoE gene also exhibit memory deficits (19). It also promotes synapse formation, dendrite sprouting, and neuronal migration (20). Chronic intracerebroventricular injection of sAPPα in mice mitigated cognitive and synaptic deficits (21). NTRK1 (TrkA), a receptor for nerve growth factor (NGF), regulates neuronal growth, differentiation, and apoptosis in the CNS (22). Inflammatory mediators, including IL-1β, TNF-α, and IL-6, stimulate the synthesis of nerve growth factor (NGF) in both neurons and glial cells, concurrently increasing the expression of the TrkA receptor. Upon Toll-like receptor (TLR)

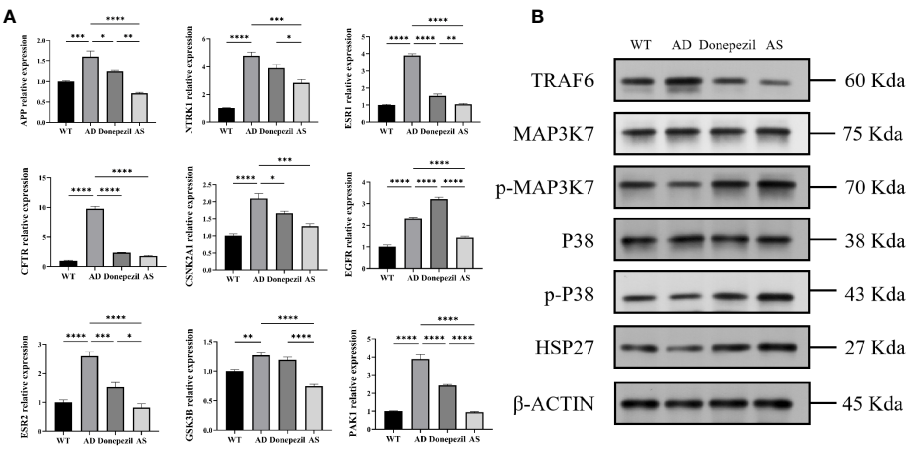

FIGURE 4
Results of qRT-PCR and Western blot (WB) about proteins related to the treatment of Alzheimer's disease by *Acanthopanax senticosus*. **(A)** mRNA level of key targets on each group. **(B)** Results of WB (n = 3). *P < 0.05, **P < 0.01, ***P< 0.001, ****P< 0.0001.

activation, NGF binds to TrkA, triggering a cascade that involves the activation of Ras, PI3K, phospholipase Cγ1, and downstream signaling pathways, such as the MAPK pathway. This cascade interferes with intracellular TLR signaling, thereby augmenting the endogenous negative feedback mechanisms that modulate excessive inflammation (23–25). R Romano et al. showed that EGFR, part of the receptor tyrosine kinase superfamily, is crucial for neural stem cell maintenance, astrocyte maturation, and neurite outgrowth in the CNS (26). Its inhibition improves astrocyte proliferation after injury, enhances autophagy, and reduces Aβ toxicity and neuroinflammation (27), correlating with a reduced risk of associated dementia (ADD) (28). ESR1 and ESR2, estrogen receptor-related genes, are implicated in neuronal degeneration due to estrogen decline, leading to cognitive difficulties (29). ERα and ERβ expression in neurons and astrocytes is associated with cognitive function maintenance in older women (30, 31). CFTR, expressed in neurons and other cell types, is linked to improved cognitive performance with physical activity in CF patients (32, 33). GSK3, a ubiquitous serine–threonine kinase with two isoforms (GSK3α and GSK3β), is widely found in the CNS (34). GSK3β overexpression promotes the BACE1 cleavage of APP, favoring Aβ plaque formation, which disrupts the Wnt pathway, leading to tau phosphorylation and accelerating AD progression (34, 35).

According to the CTN graph, it is evident that the expression of key targets is associated with several anti-inflammatory and antioxidant properties in AS, including quercetin, (+)-eudesmin, 12-nitrooctadeca-9,12-dienoic acid, coniferaldehyde glucoside, caffeic acid, and isofraxidin, which has been shown to decrease Aβ production by inhibiting BACE1 and acetylcholinesterase (AChE), regulate the NF-κB pathway to reduce COX-2 levels, and mediate the inhibition of neuroinflammatory responses *via* the Nrf2/HO1 pathway, thereby intervening in AD (36–38).

The analysis of functional enrichment can facilitate a more comprehensive understanding of the interactions among gene products. According to the results of the KEGG analysis, the MAPK signaling pathway appears to be the most promising treatment avenue for Alzheimer's disease (AD). Mitogen-activated protein kinases (MAPK) represent a group of serine–threonine kinases, comprising extracellular signal-regulated kinases (ERK), p38, and c-Jun NH2-terminal kinases (JNK) (39). Each MAPK signaling axis contains at least three components: MAPK kinase kinase kinase (MAP3K), MAPK kinase kinase (MAP2K), and MAPK kinase (40). Notably, the MAPK signaling pathway, which has been found to be significantly associated with AD development, can be triggered by inflammatory factors such as TNFα or IL-1β or in response to cellular stress (41, 42). Relevant studies have demonstrated that inhibiting the MAPK signaling pathway can effectively mitigate the inflammatory response, thereby alleviating the symptoms of AD (43, 44). The results of the Western blot analysis demonstrate that, compared with the AD group, the AS group exhibited a significant decrease in TRAF6 protein expression and an increase in p-MAP3K7/MAP3K7 relative protein content, p-P38/P38 relative protein content, and HSP27 protein expression levels. These findings suggest that AS may control the inflammatory response and improve cognitive dysfunction by inhibiting the expression of the TRAF6 protein, increasing the phosphorylation of the MAPK pathway and inhibiting the activation of pro-inflammatory factors.

In conclusion, AS can enhance short-term learning memory and effectively alleviate anxiety in 5xFAD mice. The mechanism of action is related to the activation of phosphorylation of the MAPK pathway and inhibition of the production of inflammatory factors. AS contains active compounds including quercetin, caffeic acid, and isofraxidin, with its main targets being APP, NTRK1, EGFR, GSK3B, and other genes. This study analyzes the feasibility and mechanism of action of AS in the treatment of AD, providing a novel approach to finding effective solutions for AD treatment in clinical settings.

Data availability statement

The original contributions presented in the study are included in the article/supplementary materials, further inquiries can be directed to the corresponding author/s.

Ethics statement

The animal study was approved by Animal Management and Use Committee of Shanghai University of Traditional Chinese Medicine. The study was conducted in accordance with the local legislation and institutional requirements.

Author contributions

ZZ: Data curation, Validation, Writing – original draft, Investigation, Visualization. YW: Data curation, Visualization, Writing – original draft, Writing – review & editing. DS: Conceptualization, Resources, Writing – original draft, Funding acquisition, Writing – review & editing. CJ: Validation, Writing – original draft. HC: Data curation, Writing – original draft. FJ: Software, Writing – original draft. XB: Investigation, Writing – original draft. YS: Writing – review & editing. XS: Funding acquisition, Supervision, Writing – review & editing.

Funding

The author(s) declare financial support was received for the research, authorship, and/or publication of this article. The research funds of this experiment were from the special scientific research funds of Shanghai Hospital Traditional Chinese Medicine Preparation Industry Transformation Collaborative Innovation Center and Shanghai Association for the Integration of Traditional Chinese and Western Medicine.

Conflict of interest

The authors declare that the research was conducted in the absence of any commercial or financial relationships that could be construed as a potential conflict of interest.

Publisher's note

References

1. 2023 Alzheimer's disease facts and figures. *Alzheimers Dement*. (2023) 19:1598–695. doi: 10.1002/alz.13016

2. Crump C, Sundquist J, Sieh W, Sundquist K. Risk of alzheimer's disease and related dementias in persons with glaucoma: A national cohort study. *Ophthalmology*. (2023) 17(1):19. doi: 10.1016/j.ophtha.2023.10.014

3. Khan S, Barve KH, Kumar MS. Recent advancements in pathogenesis, diagnostics and treatment of alzheimer's disease. *Curr Neuropharmacol*. (2020) 18:1106–25. doi: 10.2174/1570159X18666200528142429

4. Cummings JL, Tong G, Ballard C. Treatment combinations for alzheimer's disease: current and future pharmacotherapy options. *J Alzheimers Dis*. (2019) 67:779–94. doi: 10.3233/JAD-180766

5. Bairamian D, Sha S, Rolhion N, Sokol H, Dorothee G, Lemere CA, et al. Microbiota in neuroinflammation and synaptic dysfunction: a focus on Alzheimer's disease. *Mol Neurodegener*. (2022) 17:19. doi: 10.1186/s13024-022-00522-2

6. Parhizkar S, Holtzman DM. APOE mediated neuroinflammation and neurodegeneration in Alzheimer's disease. *Semin Immunol*. (2022) 59:101594. doi: 10.1016/j.smim.2022.101594

7. Lyketsos CG, Carrillo MC, Ryan JM, Khachaturian AS, Trzepacz P, Amatniek J, et al. Neuropsychiatric symptoms in Alzheimer's disease. *Alzheimers Dement*. (2011) 7:532–9. doi: 10.1016/j.jalz.2011.05.2410

8. Li X, Xiao KW, Chen YQ, Huang K, Xue XC, Yang CJ, et al. Visual analysis of research on traditional Chinese medicine treatment of Alzheimer's disease in recent ten years Alzheimer's disease in recent ten years. *China J Chin Materia Med*. (2023) 48:1673–81. doi: 10.19540/j.cnki.cjcmm.20221206.501

9. Ma ZY, Su XM. Thoughts and methods of traditional chineThoughts and methods of traditional chinese medicine in treating alzheimer diseaseAlzheimer disease. *Chin Med Modern Distance Educ China*. (2022) 20:201–3.

10. Lee J, Kwon S, Jin C, Cho SY, Park SU, Jung WS, et al. Traditional east asian herbal medicine treatment for alzheimer's disease: A systematic review and meta-analysis. *Pharm (Basel)*. (2022) 15:174. doi: 10.3390/ph15020174

11. Li XT, Zhou JC, Zhou Y, Ren YS, Huang YH, Wang SM, et al. Pharmacological effects of Eleutherococcus senticosus on the neurological disorders. *Phytother Res*. (2022) 36:3490–504. doi: 10.1002/ptr.7555

12. Yamauchi Y, Ge YW, Yoshimatsu K, Komastu K, Kuboyama T, Yang X, et al. Memory enhancement by oral administration of extract of eleutherococcus senticosus leaves and active compounds transferred in the brain. *Nutrients*. (2019) 11:1142. doi: 10.3390/nu11051142

13. Lee S, Park HJ, Jeon SJ, Kim E, Lee HE, Kim H, et al. Cognitive ameliorating effect of acanthopanax koreanum against scopolamine-induced memory impairment in mice. *Phytother Res*. (2017) 31:425–32. doi: 10.1002/ptr.v31.3

14. Jin ML, Park SY, Kim YH, Park G, Lee SJ. Acanthopanax senticosus exerts neuroprotective effects through HO-1 signaling in hippocampal and microglial cells. *Environ Toxicol Pharmacol*. (2013) 35:335–46. doi: 10.1016/j.etap.2013.01.004

15. Commission CP. *Pharmacopoeia of the people's republic of China. Vol. 1*. BeiJing: China Medical Science & Technology Press (2020) p. 215–6.

16. Calsolaro V, Edison P. Neuroinflammation in Alzheimer's disease: Current evidence and future directions. *Alzheimers Dement*. (2016) 12:719–32. doi: 10.1016/j.jalz.2016.02.010

17. Khan H, Ullah H, Aschner M, Cheang WS, Akkol EK. Neuroprotective effects of quercetin in alzheimer's disease. *Biomolecules*. (2019) 10:59. doi: 10.3390/biom10010059

18. Tohda C, Matsui M, Inada Y, Yang X, Kuboyama T, Kimbara Y, et al. Combined Treatment with Two Water Extracts of Eleutherococcus senticosus Leaf and Rhizome of Drynaria fortunei Enhances Cognitive Function: A Placebo-Controlled, Randomized, Double-Blind Study in Healthy Adults. *Nutrients*. (2020) 12:303. doi: 10.3390/nu12020303

19. Dodart JC, Mathis C, Bales KR, Paul SM, Ungerer A. Behavioral deficits in APP (V717F) transgenic mice deficient for the apolipoprotein E gene. *Neuroreport*. (2000) 11:603–7. doi: 10.1097/00001756-200002280-00034

20. Muller UC, Deller T, Korte M. Not just amyloid: physiological functions of the amyloid precursor protein family. *Nat Rev Neurosci*. (2017) 18:281–98. doi: 10.1038/nrn.2017.29

21. Tan VTY, Mockett BG, Ohline SM, Parfitt KD, Wicky HE, Peppercorn K, et al. Lentivirus-mediated expression of human secreted amyloid precursor protein-alpha prevents development of memory and plasticity deficits in a mouse model of Alzheimer's disease. *Mol Brain*. (2018) 11:7. doi: 10.1186/s13041-018-0348-9

22. Alberti L, Carniti C, Miranda C, Roccato E, Pierotti MA. RET and NTRK1 proto-oncogenes in human diseases. *J Cell Physiol*. (2003) 195:168–86. doi: 10.1002/jcp.10252

23. Prencipe G, Minnone G, Strippoli R, De Pasquale L, Petrini S, Caiello I, et al. Nerve growth factor downregulates inflammatory response in human monocytes through TrkA. *J Immunol*. (2014) 192:3345–54. doi: 10.4049/jimmunol.1300825

24. Minnone G, De Benedetti F, Bracci-Laudiero L. NGF and its receptors in the regulation of inflammatory response. *Int J Mol Sci*. (2017) 18:1028. doi: 10.3390/ijms18051028

25. Reichardt LF. Neurotrophin-regulated signalling pathways. *Philos Trans R Soc Lond B Biol Sci*. (2006) 361:1545–64. doi: 10.1098/rstb.2006.1894

26. Romano R, Bucci C. Role of EGFR in the nervous system. *Cells*. (2020) 9:1887. doi: 10.3390/cells9081887

27. Mansour HM, Fawzy HM, El-Khatib AS, Khattab MM. Repurposed anti-cancer epidermal growth factor receptor inhibitors: mechanisms of neuroprotective effects in Alzheimer's disease. *Neural Regener Res*. (2022) 17:1913–8. doi: 10.4103/1673-5374.332132

28. Bellenguez C, Kucukali F, Jansen IE, Kleineidam L, Moreno-Grau S, Amin N, et al. New insights into the genetic etiology of Alzheimer's disease and related dementias. *Nat Genet*. (2022) 54:412–36. doi: 10.1038/s41588-022-01024-z

29. Pinkas J, Bojar I, Gujski M, Sarecka-Hujar B, Owoc A, Raczkiewicz D. Effect of interactions between APOE and ESR1 polymorphisms on cognitive functions in postmenopausal women. *Arch Med Sci*. (2021) 17:31–9. doi: 10.5114/aoms.2018.72972

30. Liu J, Yuan S, Niu X, Kelleher R, Sheridan H. ESR1 dysfunction triggers neuroinflammation as a critical upstream causative factor of the Alzheimer's disease process. *Aging (Albany NY)*. (2022) 14:8595–614. doi: 10.18632/aging.v14i21

31. Baumgartner NE, Daniel JM. Estrogen receptor alpha: a critical role in successful female cognitive aging. *Climacteric*. (2021) 24:333–9. doi: 10.1080/13697137.2021.1875426

32. Gambazza S, Nobili RM, Biffi R, Summers PE, Colombo C, Costa A. Cystic Fibrosis, New Frontier: Exploring the Functional Connectivity of the Brain Default Mode Network. Comment on Elce et al. Impact of Physical Activity on Cognitive Functions: A New Field for Research and Management of Cystic Fibrosis. *Diagnostics*. (2020) 10:489. doi: 10.3390/diagnostics11061001

33. Elce V, Del Pizzo A, Nigro E, Frisso G, Martiniello L, Daniele A, et al. Impact of physical activity on cognitive functions: A new field for research and management of cystic fibrosis. *Diagnostics (Basel)*. (2020) 10:489. doi: 10.3390/diagnostics10070489

34. Lauretti E, Dincer O, Pratico D. Glycogen synthase kinase-3 signaling in Alzheimer's disease. *Biochim Biophys Acta Mol Cell Res*. (2020) 1867:118664. doi: 10.1016/j.bbamcr.2020.118664

35. Balaraman Y, Limaye AR, Levey AI, Srinivasan S. Glycogen synthase kinase 3beta and Alzheimer's disease: pathophysiological and therapeutic significance. *Cell Mol Life Sci*. (2006) 63:1226–35. doi: 10.1007/s00018-005-5597-y

36. Bayazid AB, Lim BO. Quercetin Is An Active Agent in Berries against Neurodegenerative Diseases Progression through Modulation of Nrf2/HO1. *Nutrients*. (2022) 14:5132. doi: 10.3390/nu14235132

37. Grewal AK, Singh TG, Sharma D, Sharma V, Singh M, Rahman MH, et al. Mechanistic insights and perspectives involved in neuroprotective action of quercetin. *BioMed Pharmacother*. (2021) 140:111729. doi: 10.1016/j.biopha.2021.111729

38. Zaplatic E, Bule M, Shah SZA, Uddin MS, Niaz K. Molecular mechanisms underlying protective role of quercetin in attenuating Alzheimer's disease. *Life Sci*. (2019) 224:109–19. doi: 10.1016/j.lfs.2019.03.055

39. Falcicchia C, Tozzi F, Arancio O, Watterson DM, Origlia N. Involvement of p38 MAPK in synaptic function and dysfunction. *Int J Mol Sci*. (2020) 21:5624. doi: 10.3390/ijms21165624

40. Kheiri G, Dolatshahi M, Rahmani F, Rezaei N. Role of p38/MAPKs in Alzheimer's disease: implications for amyloid beta toxicity targeted therapy. *Rev Neurosci*. (2018) 30:9–30. doi: 10.1515/revneuro-2018-0008

41. Thakur S, Dhapola R, Sarma P, Medhi B, Reddy DH. Neuroinflammation in alzheimer's disease: current progress in molecular signaling and therapeutics. *Inflammation*. (2023) 46:1–17. doi: 10.1007/s10753-022-01721-1

42. Liu S, Chen L, Li J, Sun Y, Xu Y, Li Z, et al. Asiaticoside mitigates alzheimer's disease pathology by attenuating inflammation and enhancing synaptic function. *Int J Mol Sci*. (2023) 24:11976. doi: 10.3390/ijms241511976

43. Lee JK, Kim NJ. Recent advances in the inhibition of p38 MAPK as a potential strategy for the treatment of alzheimer's disease. *Molecules*. (2017) 22:1287. doi: 10.3390/molecules22081287

44. Beamer E, Correa SAL. The p38(MAPK)-MK2 signaling axis as a critical link between inflammation and synaptic transmission. *Front Cell Dev Biol*. (2021) 9:635636. doi: 10.3389/fcell.2021.635636

frontiers | Frontiers in Immunology

TYPE Original Research
PUBLISHED 24 May 2024
DOI 10.3389/fimmu.2024.1402250

OPEN ACCESS

EDITED BY
Danchen Wu,
Queen's University, Canada

REVIEWED BY
Ji-Feng Li,
Capital Medical University, China
Dong Liu,
Shanghai Jiao Tong University, China

*CORRESPONDENCE
Rong Jiang
listening39@163.com
Ya-Lin Zhao
39031381@qq.com
Yu Shi
youyou_78_78@sina.com

†These authors have contributed equally to this work and share first authorship

RECEIVED 20 March 2024
ACCEPTED 26 April 2024
PUBLISHED 24 May 2024

CITATION
Xu W-J, Wang S, Zhao Q-H, Xu J-Y, Hu X-Y, Gong S-G, He J, Qiu H-L, Luo C-J, Xu J, Li H-T, Li Z-P, Wang L, Shi Y, Zhao Y-L and Jiang R (2024) Serum ASGR2 level: an efficacy biomarker for balloon pulmonary angioplasty in patients with chronic thromboembolic pulmonary hypertension.
Front. Immunol. 15:1402250.
doi: 10.3389/fimmu.2024.1402250

Serum ASGR2 level: an efficacy biomarker for balloon pulmonary angioplasty in patients with chronic thromboembolic pulmonary hypertension

Wei-Jie Xu[1†], Shang Wang[2†], Qian-Hao Zhao[2†], Jia-Yi Xu[3], Xiao-Yi Hu[2], Su-Gang Gong[2], Jing He[2], Hong-Ling Qiu[2], Ci-Jun Luo[2], Jian Xu[2], Hui-Ting Li[2], Ze-Pu Li[4], Lan Wang[2], Yu Shi[5*], Ya-Lin Zhao[6*] and Rong Jiang[2*]

[1]Department of Clinical Laboratory, Shanghai Pulmonary Hospital, Tongji University School of Medicine, Shanghai, China, [2]Department of Cardiopulmonary Circulation, Shanghai Pulmonary Hospital, School of Medicine, Tongji University, Shanghai, China, [3]School of Life Science and Technology, Tongji University, Shanghai, China, [4]Department of Cardiology, Affiliated Renhe Hospital of Shanghai University, Shanghai, China, [5]Department of Cardiology, Yantai Yu-Huangding Hospital, Medical College of Qingdao University, Yantai, China, [6]Department of Respiratory Critical Care Medicine, The First Hospital of Kunming, Kunming, China

Background: This study aimed to employ plasma proteomics to investigate the molecular changes, pathway alterations, and potential novel biochemical markers associated with balloon pulmonary angioplasty (BPA) in patients with chronic thromboembolic pulmonary hypertension (CTEPH).

Methods: Pre- and post-BPA plasma samples from five CTEPH patients in the PRACTICE study were analyzed to identify differentially expressed proteins. Proteomic and bioinformatics analyses were conducted, and the identified proteins were further validated using ELISA assays in a separate cohort of the same study. Correlation and multivariate regression analyses were performed to investigate the associations between these differentially expressed proteins and clinical parameters.

Results: Significantly higher serum levels of asialoglycoprotein receptor 2 (ASGR2) were detected in 5 CTEPH patients compared to those in healthy individuals but decreased significantly after successful BPA procedures. The decrease in serum levels of ASGR2 after the completion of BPA procedures was further validated in a separate cohort of 48 patients with CTEPH [0.70 (0.51, 1.11) ng/mL vs. 0.38 (0.27, 0.59) ng/mL, $P < 0.001$]. Significant associations were found between the pre-BPA ASGR2 level and clinical parameters, including neutrophil percentage ($R = 0.285$, $P < 0.05$), platelet (PLT) count ($R = 0.386$, $P < 0.05$), and high-density lipoprotein cholesterol (HDL-C) before BPA ($R = -0.285$, $P < 0.05$). Significant associations were detected between post-BPA serum ASGR2 levels and lymphocyte percentage (LYM%) ($R = 0.306$, $P < 0.05$), neutrophil-to-lymphocyte ratio ($R = -0.294$, $P < 0.05$), and pulmonary vascular resistance after BPA ($R = -0.35$, $P < 0.05$). Multivariate stepwise regression analysis revealed that pre-BPA ASGR2 levels were

associated with HDL-C and PLT count (both $P < 0.001$), while post-BPA ASGR2 levels were associated with LYM% ($P < 0.05$).

Conclusion: Serum levels of ASGR2 may be a biomarker for the effectiveness of BPA treatment in CTEPH patients. The pre-BPA serum level of ASGR2 in CTEPH patients was associated with HDL-C and the PLT count. The post-BPA serum level of ASGR2 was correlated with the LYM%, which may reflect aspects of immune and inflammatory status.

KEYWORDS

chronic thromboembolic pulmonary hypertension, balloon pulmonary angioplasty, proteomics, asialoglycoprotein receptor 2, immune

1 Introduction

Chronic thromboembolic pulmonary hypertension (CTEPH) is a pulmonary vascular disease characterized by pulmonary artery thrombus, pulmonary vascular remodeling leading to vascular stenosis or occlusion, and progressive elevated pulmonary artery pressure, ultimately leading to right heart failure (1). In addition to thrombotic factors, immune function and inflammatory status contribute significantly to the development of CTEPH, which is characterized by increased activation of innate and adaptive immune cells that promote inflammation and vascular disease (2).

In addition to riociguat, a targeted medicine for CTEPH, and pulmonary endarterectomy, balloon pulmonary angioplasty (BPA) is an appropriate alternative therapeutic option for patients who are not eligible for surgery or who experience persistent or recurrent pulmonary hypertension after PEA. Balloon pulmonary angioplasty effectively improves hemodynamics, right ventricular (RV) function, exercise capacity, symptoms, and prognosis (3, 4). Moreover, BPA treatment has been demonstrated to decrease interleukin (IL)-6 and C-reactive protein levels in CTEPH patients, indicating its potential to improve systemic inflammation (5). Although transcriptome sequencing and bioinformatics analysis have been used to investigate the pathogenesis of CTEPH (6), proteomic studies assessing the therapeutic efficacy of BPA are lacking.

In this study, we conducted proteomic profiling to identify changes in protein expression between pre-BPA and post-BPA samples from patients with CTEPH. Differentially expressed proteins were identified, and their correlations with clinical parameters were investigated in a cohort of patients enrolled in the PRACTICE study. We aimed to utilize plasma proteomics to uncover molecular changes, pathway alterations, and potential novel biochemical markers associated with BPA treatment in CTEPH patients.

2 Materials and methods

2.1 Study population

The CTEPH patients included in our study were selected from the PRACTICE study (ChiCTR2000032403) (7). The PRACTICE study, which was a prospective, randomized controlled study conducted at a single center, aimed to compare the effectiveness and safety of combining BPA with riociguat versus riociguat monotherapy in patients with inoperable CTEPH. All patients enrolled in the study met the diagnostic criteria for CTEPH in the ESC/ERS 2022 guidelines (8). These criteria included a mean pulmonary artery pressure (mPAP) > 20 mmHg, pulmonary artery wedge pressure (PAWP) ≤ 15 mmHg, and pulmonary vascular resistance (PVR) > 2 Wood units (WUs) via right heart catheterization (RHC). In the BPA group, patients initially underwent pre-RHC and received riociguat therapy for management of pulmonary arterial hypertension (PAH). Following a 3-month stabilization period, hospitalizations were scheduled at monthly intervals for BPA sessions until sufficient improvement in pulmonary vasculature patency was achieved. A post-RHC assessment was conducted three days after the final BPA procedure to evaluate hemodynamics. The study protocol was conducted in accordance with the revised Declaration of Helsinki, and approval was obtained from the Ethics Committee of the Shanghai Pulmonary Hospital (L20-385-1). Written informed consent was obtained from all participants.

Pre-BPA and post-BPA assessments included the World Health Organization functional class (WHC FC), 6-minute walk distance (6MWD), routine blood tests, lipid profile, N-terminal pro-B-type natriuretic peptide (NT-proBNP) levels, RHC and echocardiography parameters. Parameters that were measured and recorded during the RHC included mPAP, PAWP, cardiac output (CO), and PVR (9). Echocardiographic parameters included

right atrial area (RAA), right ventricular end-diastolic transverse diameter (RVEDTD), right ventricular end-diastolic longitudinal diameter, right atrial transverse diameter (RATD), right atrial longitudinal diameter (RALD), and tricuspid annular plane systolic excursion (TAPSE) (10).

Pre- and post-BPA serum samples from five CTEPH patients in the PRACTICE study were analyzed to identify differentially expressed proteins. Proteomic and bioinformatics analyses were conducted, and the identified proteins were further validated using enzyme-linked immunosorbent assay (ELISA) in a separate cohort of 48 CTEPH patients in the PRACTICE study.

2.2 Sample collection

Blood samples were centrifuged at 3000×g for 10 minutes at 4°C to obtain serum, which was stored at -80°C for ELISA testing.

2.3 Mass spectrometry

Plasma samples from five patients were subjected to analysis, which involved protein extraction, peptide digestion, chromatographic fractionation, and liquid chromatography-tandem mass spectrometry data acquisition.

2.4 Bioinformatics analysis

The analysis consisted of three stages: quantitative, differential expression and functional analysis (11).

2.4.1 Quantitative analysis

The detected proteins were compared with contents of the Swiss-Prot human protein database, and the number and overlap of relationships between groups were counted.

2.4.2 Differential expression analysis

The quantifiable proteins identified through mass spectrometry were carefully selected, and multiple rounds of comprehensive protein quantification experiments were conducted. The ratio of the mean values before and after treatment was calculated to assess differential expression, while the P value was used to determine the significance of protein level comparisons between the two groups.

2.4.3 Functional analysis

For subcellular localization and domain analysis, CELLO and InterProScan software, respectively, were used to investigate the functional regions and biological roles of proteins (12). Blast2GO software annotates differentially expressed protein sets with the Gene Ontology (GO) database, categorizing them into biological processes, molecular functions, and cellular components (13). KASS interprets and annotates proteins based on the KEGG pathway database (13). Fisher's exact test was performed to compare the distribution of gene ontology GO classifications and KEGG pathways in the target protein set with that in the overall protein set, enabling enrichment analysis.

2.5 Enzyme-linked immunosorbent assay

The plasma concentrations of apolipoprotein C1 (APOC1), asialoglycoprotein receptor 2 (ASGR2) and heparan sulfate proteoglycan 2 (HSPG2) were selected from 13 differentially expressed proteins and measured using a Human APOC1 ELISA Kit (catalog# EH0529, FineTest®), a Human ASGR2 ELISA Kit (catalog#EH2669, FineTest®) and a Human HSPG2 ELISA Kit (catalog#EH0955, FineTest®), respectively. The detection limits were as follows: APOC1, 9.375–600 ng/mL, ASGR2 0.156–10 ng/mL, and HSPG2 0.625–40 ng/mL. The protein concentrations were determined by measuring the absorbance at 450 nm and then using a standard curve for calculations.

2.6 Data analysis

In the proteomics analysis, logarithmic transformation with a base of 2 was applied to normalize the data. The Student's t test was then used to calculate *P* values for statistical analysis. Due to the limited number of significant differences, genes exhibiting an expression fold change ≥ 1.18 were considered significantly upregulated, while genes with an expression fold change < 0.85 were considered significantly downregulated, with a significance level of $P < 0.05$.

The serum ASGR2 levels and clinical parameters with a normal distribution are presented as the means ± standard deviations. Nonnormally distributed data are reported as medians (interquartile ranges). The Mann-Whitney U test was used to compare the serum concentrations of differentially expressed proteins (DEPs) between the CTEPH patients and individuals. The pre- and post-BPA changes in DEPs and clinical parameters were assessed using either the Wilcoxon signed-rank test or paired t test, depending on whether the data were normally distributed.

Spearman correlation analysis was performed to explore the relationships between serum ASGR2 levels and clinical parameters before and after BPA treatment.

Multiple linear stepwise regression analyses were conducted to investigate the associations between ASGR2 and clinical parameters. To address nonnormally distributed data, the natural logarithm (ln) was utilized to transform the values into normally distributed data. Covariance tests were performed on the relevant variables. GraphPad Prism 9 and IBM SPSS 23.0 software were used. A *P* value less than 0.05 was considered statistically significant.

3 Results

3.1 Characteristics of CTEPH patients undergoing proteomic analysis

The average age of the five patients was 59.2 ± 8.7 years, and three of them were female. After the completion of BPA treatment,

the mPAP significantly decreased from 40.6 ± 6.9 mmHg to 19.4 ± 4.6 mmHg ($P < 0.01$). Additionally, the PVR decreased significantly from 9.6 ± 4.2 mmHg to 3.1 ± 0.4 mmHg ($P = 0.023$) (Table 1).

3.2 Proteomic and bioinformatics analysis

A total of 625 proteins were identified in the quantitative analysis, with 559 proteins overlapping between the groups. Furthermore, 21 proteins were exclusively detected in the pre-BPA group, while 45 proteins were exclusively detected in the post-BPA group.

Volcano plots were generated based on fold change values ≥ 1.18 or ≤ 0.85 and P values < 0.1 (Figure 1A). Four downregulated differentially expressed proteins encoded by the genes IGHV3-53, CCT3, HSPG2, and ASGR2 were identified. Nine upregulated differentially expressed proteins encoded by the genes TAGLN2, PDLIM1, TPI1, APOC1, CFHR5, LTF, IGLL1, IGHV4-34, and IGKV1-12 were also identified (Figure 1B).

The GO functional annotation revealed significant enrichment of differentially expressed proteins in key biological processes (such as humoral immune response, complement activation, and cell recognition), emphasizing their relevance to immune function and cell interactions (Figures 1C, D). In terms of molecular function, these proteins were primarily involved in immunoglobulin receptor binding and antigen binding (Figure 1E) and were also significantly enriched in cellular components, such as immunoglobulin complexes and the external side of the plasma membrane (Figure 1F). Notably, APOC1, HSPG2, and ASGR2-encoded proteins were frequently found in these enriched pathways, suggesting their potential as characteristic differentially expressed proteins for further validation.

According to the KEGG pathway analysis, the top pathways were phototransduction, fructose and mannose metabolism, primary immunodeficiency, cholesterol metabolism, glycolysis/gluconeogenesis, long-term potentiation, renin secretion, amphetamine addiction, inositol phosphate metabolism and amino acid biosynthesis.

3.3 Detection of DEPs in serum samples from 5 CTEPH patients

The serum levels of APOC1 and HSPG2 in 5 CTEPH patients were significantly greater than those in healthy individuals. However, no significant differences were observed between the pre- and post-BPA treatments. Compared with those in healthy individuals, significantly greater serum levels of ASGR2 were detected in 5 CTEPH patients ($P = 0.03$) but decreased significantly after successful BPA procedures ($P = 0.028$) (Figure 2).

3.4 Validation of ASGR2 in the PRACTICE cohort

Following the completion of BPA treatment, a notable decrease in the serum ASGR2 concentration was observed in the 48 CTEPH patients in the PRACTICE study [0.70 (0.51, 1.11) ng/mL vs. 0.38 (0.27, 0.59) ng/mL, $P < 0.001$]. Of the patients, 24 were female, with a mean age of 61.8 ± 11.3 years.

Following successful BPA therapy, a significant improvement was observed in the WHO FC ($P < 0.001$). Hemodynamically, post-BPA treatment substantially reduced the mPAP and PVR (45.7 ± 11.1 mmHg vs. 25.7 ± 6.3 mmHg and 9.3 ± 6.0 mmHg vs. 3.3 ± 0.8 mmHg, respectively; both $P < 0.001$). Additionally, CO and SvO_2 significantly increased [4.8 ± 1.2 L/min vs. 5.6 ± 1.1 L/min, $P = 0.004$; 59.5 ± 8.8% vs. 68.9 ± 6.8%, $P < 0.001$, respectively]. Through

TABLE 1 Clinical information of 5 CTEPH patients undergoing proteomic analysis.

Patient	Gender	Age (years)	6MWD (m)	NT-proBNP (pg/ml)	RAP (mm Hg)	mPAP (mm Hg)	PAWP (mm Hg)	CO (L/min)	PVR (Wood U)	S_VO_2 (%)
Pre-BPA										
1	Female	65	465	151.5	1	40	6	2.41	14.10	59.8
2	Male	50	375	126.0	1.0	45	5	2.97	13.47	60.5
3	Female	57	420	235.0	3.0	31	8	6.07	3.79	70.5
4	Female	53	520	60.0	0.0	49	1	5.57	8.62	48.7
5	Male	71	195	4281.0	1	38	10	3.40	8.24	56.6
Post-BPA										
1	Female	65	450	136.5	1	14	2	3.9	3.05	69.9
2	Male	50	390	29.0	1	15	4	3.20	3.44	60.7
3	Female	57	400	125.0	1	21	6	4.23	3.55	70.3
4	Female	53	520	65.0	1	24	9	5.90	2.54	69.5
5	Male	71	455	353.7	0	23	6	5.73	2.97	58.3

6MWD, 6-minute walking distance; NT-proBNP, N-terminal pro B-type natriuretic peptide; RAP, right atrial pressure; mPAP, mean pulmonary artery pressure; PAWP, pulmonary artery wedge pressure; CO, cardiac output; PVR, pulmonary vascular resistance; S_VO_2, saturation of mixed venous blood oxygen.

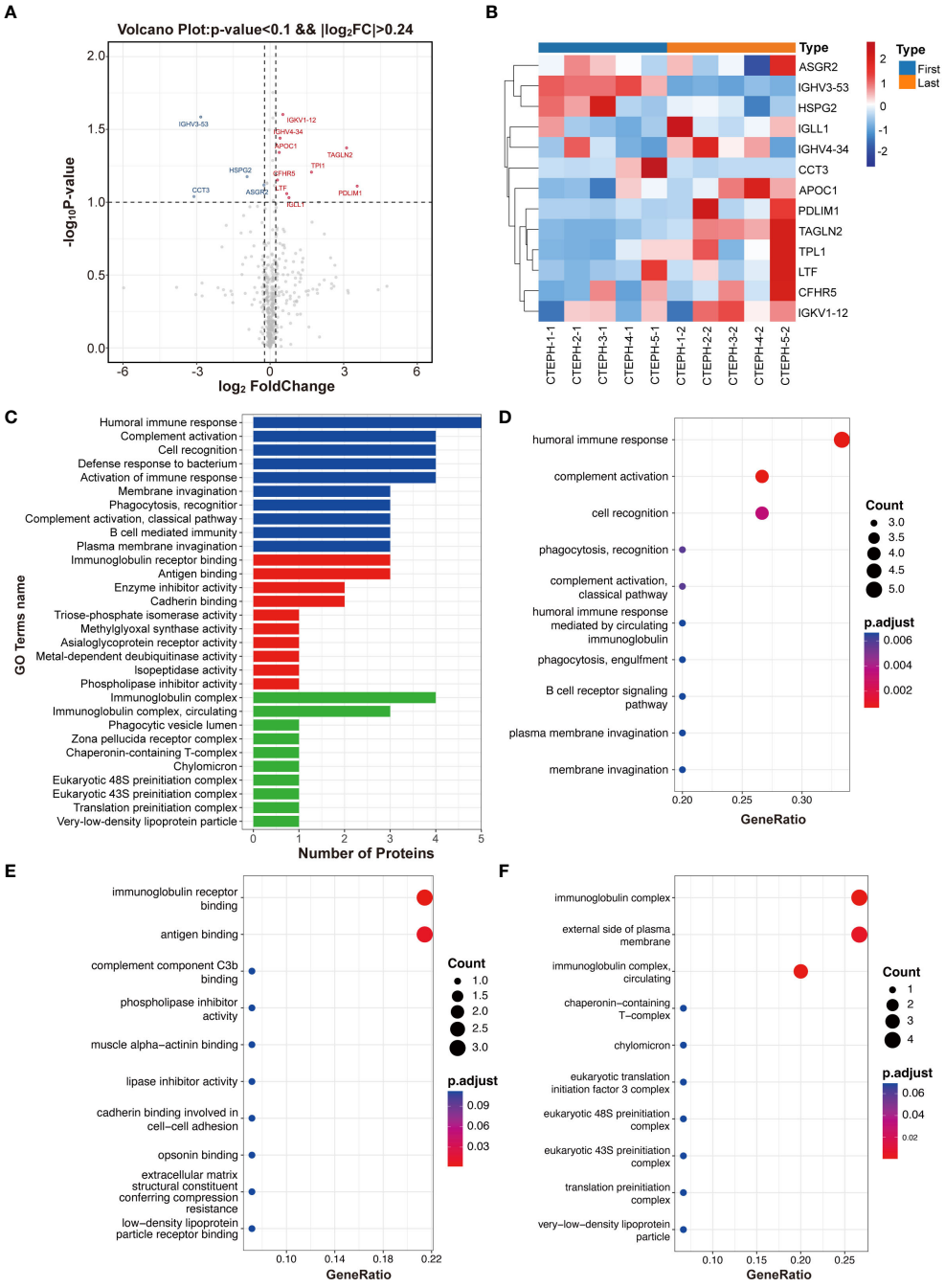

FIGURE 1
Differentially expressed protein identification and functional enrichment analysis. **(A)** Volcano plot. **(B)** Heatmap of differentially expressed proteins. **(C)** Bar plot showing the number of differentially expressed proteins at the secondary functional annotation level of GO. **(D)** The top 10 enriched terms in the biological process category. **(E)** The top 10 enriched terms in the molecular function category. **(F)** The top 10 enriched terms in the cellular component category.

echocardiography, significant reductions were observed in RV structure parameters, including RAA, RATD, RALD, and RVEDTD [18.50 (15.9, 23.2) mm^2 vs. 14.1 (11.5, 17.8) mm^2, $P < 0.01$; 18.5 (15.9, 23.2) cm vs. 14.1 (11.5, 17.8) cm, $P < 0.001$; 5.2 ± 0.8 cm vs. 4.6 ± 0.8 cm, $P < 0.001$; 4.0 ± 0.7 cm vs. 3.5 ± 0.5 cm, $P < 0.001$, respectively]. A significant increase in RV systolic function was observed for the TAPSE [11.0 (9.2, 12.0) mm vs. 13.0 (11.0, 14.0) mm, $P < 0.001$] (Table 2).

The levels of NT-proBNP decreased significantly [596.3 (110.4–1763.5) pg/ml to 125.5 (54.8–178.6) pg/ml, $P < 0.001$]. The white blood cell counts increased [5.7 (4.7–6.8) × 10^9/L vs. 6.6 (4.9–8.2) × 10^9/L) ($P = 0.011$), accompanied by an increase in the neutrophil percentage (NEU%) [56.0 ± 9.30% vs. 67.0 ± 10.9%, $P = 0.041$]. However, there was a decrease in the lymphocyte percentage (LYM%) [32.7 ± 8.1% vs. 23.5 ± 9.2%, $P = 0.005$] and eosinophil percentage [2.8 ± 2.9% vs. 1.9 ± 2.9%, $P = 0.0013$]. These changes resulted in an

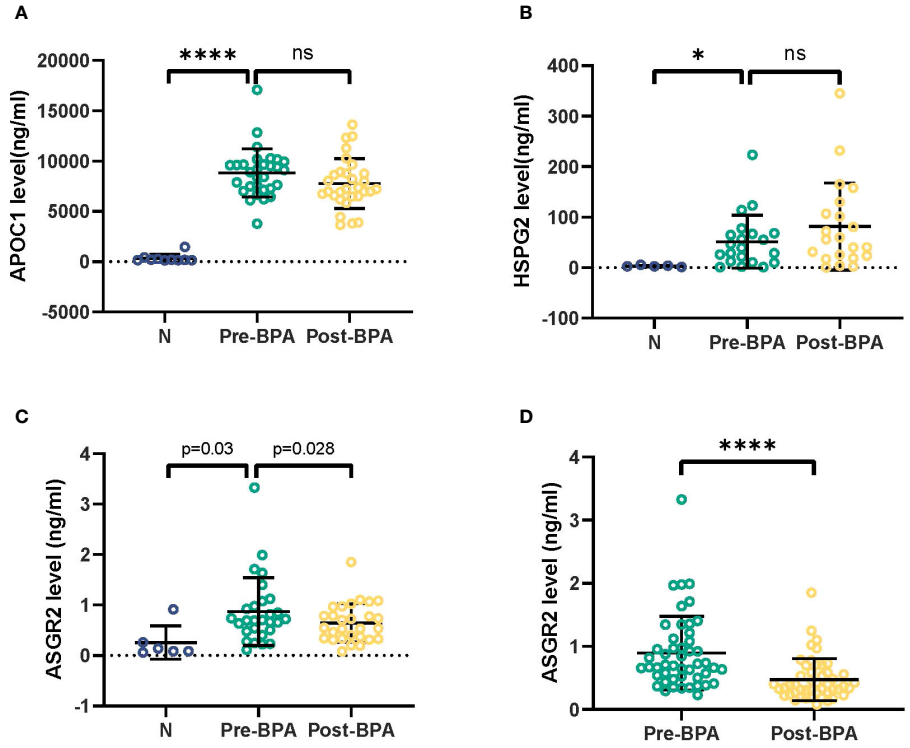

FIGURE 2
Detection of APOC1, HSPG2 and ASGR2 in serum samples from 5 CTEPH patients. CTEPH, Chronic thromboembolic pulmonary hypertension. *p< 0.05; ns, not significant; ****p<0.001.

elevated neutrophil-to-lymphocyte ratio (NLR) [1.9 ± 0.8 vs. 3.4 ± 1.6, $P = 0.021$]. Platelet counts remained unchanged.

In terms of lipid metabolism, a significant increase in apolipoprotein A-1 (ApoA-I) levels was observed [1.3 ± 0.3 g/L vs. 1.4 ± 0.2 g/L, $P = 0.003$). No significant changes were detected in total cholesterol, triglyceride, high-density lipoprotein cholesterol (HDL-C), low-density lipoprotein cholesterol (LDL-C), small dense LDL cholesterol (SDLDL-C), ApoB, ApoE, or lipoprotein (a) levels (Table 3).

3.5 Correlation analysis of serum ASGR2 levels

According to the Spearman correlation analysis, pre-BPA ASGR2 levels were positively correlated with pre-BPA NEU% and PLT count but negatively correlated with HDL-C (R = 0.285, R = 0.386, R = -0.285, all $P < 0.05$). Post-BPA ASGR2 levels were positively correlated with post-BPA LYM % and the NLR (R = 0.306; R = -0.294, both $P < 0.05$, respectively). A significant positive Spearman correlation was observed between post-BPA ASGR2 levels and post-BPA PVR (R = -0.35, $P < 0.05$) (Figure 3).

3.6 Multiple linear stepwise regression analysis of ASGR2

For the pre-BPA treatment data, the equation ln ($ASGR2_{pre\text{-}BPA}$) = -1.433 HDL-C $_{pre\text{-}BPA}$ + 1.013 PLT $_{pre\text{-}BPA}$ (R^2 = 0.407, F = 15.812, $P < 0.001$) was obtained. Notably, NEU% was excluded from the analysis due to multicollinearity. Subsequently, for the pre-BPA treatment data, ln($ASGR2_{post\text{-}BPA}$) = -2.879 + 0.388 ln(LYM% $_{post\text{-}BPA}$) (R^2 = 0.15, F = 6.016, $P < 0.05$) (Table 4).

4 Discussion

This study aimed to utilize plasma proteomics to explore the molecular changes, pathway alterations, and potential novel biochemical markers associated with BPA in CTEPH patients. The findings of the study can be summarized as follows: (I) After successful BPA procedures, the serum levels of ASGR2, which were initially greater in CTEPH patients than in healthy individuals, significantly decreased. (II) Prior to BPA treatment, a correlation was observed between serum ASGR2 levels and PLT count as well as HDL-C levels. Following BPA treatment, serum ASGR2 levels were associated with LYM%. (III) Serum ASGR2 levels may be associated with PVR.

As a subunit of the asialoglycoprotein receptor (ASGPR), ASGR2 plays a significant role in cellular processes. Known as the Ashwell–Morell receptor, ASGPR is a transmembrane protein primarily expressed in hepatocytes that specifically recognizes N-acetylgalactosamine and galactose. Its main function is to internalize and degrade glycoproteins through desialylation, contributing to the maintenance of serum glycoprotein homeostasis (14). A strong correlation of ASGR2 with gastrointestinal tumors, including hepatocellular carcinoma, gastric cancer, and colorectal cancer has been reported (14).

10.3389/fimmu.2024.1402250

TABLE 2 Hemodynamic and echocardiographic changes pre- and post-BPA.

Variable	Pre-BPA n = 48	Post-BPA n = 48	*P* value
Age (y)	61.8 ± 11.3		
Female, n (%)	24 (50)		
ASGR2, ng/mL	0.70 (0.51, 1.11)	0.38 (0.27,0.59)	< 0.001
WHO FC, n (%)			< 0.001
II	5 (10.4)	37 (77.1)	
III	42 (87.5)	11 (22.9)	
IV	1 (2.1)	0 (0)	
6MWD, m	356.5 ± 104.1	442.3 ± 67.8	< 0.001
Hemodynamics			
mPAP, mm Hg	45.7 ± 11.1	25.7 ± 6.3	< 0.001
PAWP, mm Hg	8.0 ± 3.4	7.8 ± 3.5	0.736
CO, L/min	4.8 ± 1.2	5.6 ± 1.1	0.004
PVR, Wood U	9.3 ± 6.0	3.3 ± 0.8	< 0.001
S_VO_2, %	59.5 ± 8.8	68.9 ± 6.8	< 0.001
Echocardiography			
RAA, mm^2	18.5 (15.9, 23.2)	14.1 (11.5, 17.8)	< 0.001
RATD, cm	4.4 ± 0.9	3.6 ± 0.6	< 0.001
RALD, cm	5.2 ± 0.8	4.6 ± 0.8	< 0.001
RVEDTD, cm	4.0 ± 0.7	3.5 ± 0.5	< 0.001
RVEDLD, cm	6.5 (5.8, 7.0)	6.6 (6.0, 7.0)	0.166
sPAP, mmHg	71.5 (52.3, 97.8)	42.0 (37.3, 49.0)	< 0.001
TAPSE, mm	11.0 (9.2, 12.0)	13.0 (11.0, 14.0)	< 0.001

Values are expressed as the mean ± SD or median (quartile range). BPA, balloon pulmonary angioplasty; ASGR2, asialoglycoprotein receptor 2; WHO FC, World Health Organization functional class; 6MWD, 6-minute walking distance; mPAP, mean pulmonary artery pressure; PAWP, pulmonary artery wedge pressure; CO, cardiac output; PVR, pulmonary vascular resistance; S_VO_2, saturation of mixed venous blood oxygen; RAA, right atrial area; RATD, right atrial transverse dimension; RALD, right atrial longitudinal dimension; RVEDTD, right ventricular transverse dimension; RVEDLD, right ventricular longitudinal dimension; sPAP, systolic pulmonary artery pressure; TAPSE, tricuspid annular plane systolic excursion.

TABLE 3 Blood test changes between pre- and post-BPA.

Variable	Pre-BPA n = 48	Post-BPA n = 48	*P* value
NT-proBNP, pg/ml	596.3 (110.4, 1763.5)	125.5 (54.8, 178.6)	< 0.001
ESR, mm/h	16.0 ± 12.0	14.3 ± 11.5	0.522
hs-CRP, mg/L	5.6 ± 8.9	4.1 ± 6.0	0.327
Blood routine			
WBC, $\times 10^9$/L	5.7 (4.7, 6.8)	6.6 (4.9, 8.2)	0.011
NEU%, %	56.0 ± 9.3	67.0 ± 10.9	0.041
LYM%, %	31.7 (26.2, 39.5)	20.9 (16.2, 30.4)	0.005
NLR	1.9 ± 0.8	3.4 ± 1.6	0.021
EO%, %	2.8 ± 2.9	1.9 ± 2.9	0.013
PLT, $\times 10^9$/L	225.5 ± 85.4	224.3 ± 77.6	0.839
Renal function			
UA, μmol/L	355.0 (294.5, 445.3)	339.5 (278.6, 400.3)	0.070
BUN, mmol/L	6.1 ± 1.9	6.2 ± 1.5	0.666
Crea, μmol/L	68.6 ± 16.0	66.5 ± 14.4	0.167
Lipid metabolism			
TCH, mmol/L	4.2 ± 0.8	4.5 ± 0.9	0.115
TG, mmol/L	1.4 ± 0.6	1.4 ± 0.7	0.881
HDL-C, mmol/L	1.1 ± 0.3	1.1 ± 0.3	0.213
LDL-C, mmol/L	2.7 ± 0.7	2.9 ± 0.6	0.180
SDLDL-C, mmol/L	0.8 ± 0.3	0.7 ± 0.3	0.217
ApoA-I, g/L	1.3 ± 0.3	1.4 ± 0.2	0.003
ApoB, g/L	2.0 ± 8.3	0.9 ± 0.2	0.192
ApoE, g/L	36.4 (29.4, 45.0)	36.5 (28.9, 48.0)	0.765
LP (a), mg/L	124.9 (79.4, 281.5)	143.8 (92.6, 301.1)	0.549

Values are expressed as the mean ± SD or median (quartile range). BPA, balloon pulmonary angioplasty; NTproBNP, N-terminal pro B-type natriuretic peptide; ESR, erythrocyte sedimentation rate; hs-CRP, high-sensitivity C-reactive protein; WBC, white blood cell; NEU%, neutrophil percentage; LYM%, lymphocyte percentage; NLR, neutrophil to lymphocyte ratio; EO%, eosinophil percentage; PLT, platelet; UA, uric acid; BUN, blood urea nitrogen; Crea, creatinine; TCH, total cholesterol; TG, triglyceride; HDL-C, high density lipoprotein cholesterol; LDL-C, low density lipoprotein cholesterol; SDLDL-C, small dense low density lipoprotein cholesterol; ApoA, Apolipoprotein A; ApoB, Apolipoprotein B; ApoE, Apolipoprotein E; LP (a), lipoprotein (a).

Moreover, emerging evidence suggests a potential association between ASGR2 and neuropsychiatric/neurodegenerative diseases, as well as hemophilia. Currently, there is no available research that establishes a connection between ASGR2 and PAH.

4.1 Relationship between ASGR2 and PLT count

Our study revealed a correlation between serum ASGR2 levels and PLT count in CTEPH patients before BPA intervention. Decreased PLT count and function have been recognized as factors that promote the development of CTEPH (15). In patients with CTEPH, PLTs demonstrate heightened activation, yet there is an intriguing phenomenon of reduced PLT aggregation and increased depolymerization. The activation of PLTs affects the production of proinflammatory chemokines and the aggregation of pulmonary interstitial macrophages, thereby contributing to the inflammatory state. The aggregation of PLTs and granulocytes in the peripheral blood further contributes to immune inflammation and the pathophysiology of CTEPH (16). The literature on the direct impact of ASGR2 in CTEPH patients is limited. However, studies suggest that the ASGR2 genotype may modulate von Willebrand factor, influencing the molecular link between inflammatory pathways and PLT adhesion during thrombus formation in CTEPH patients.

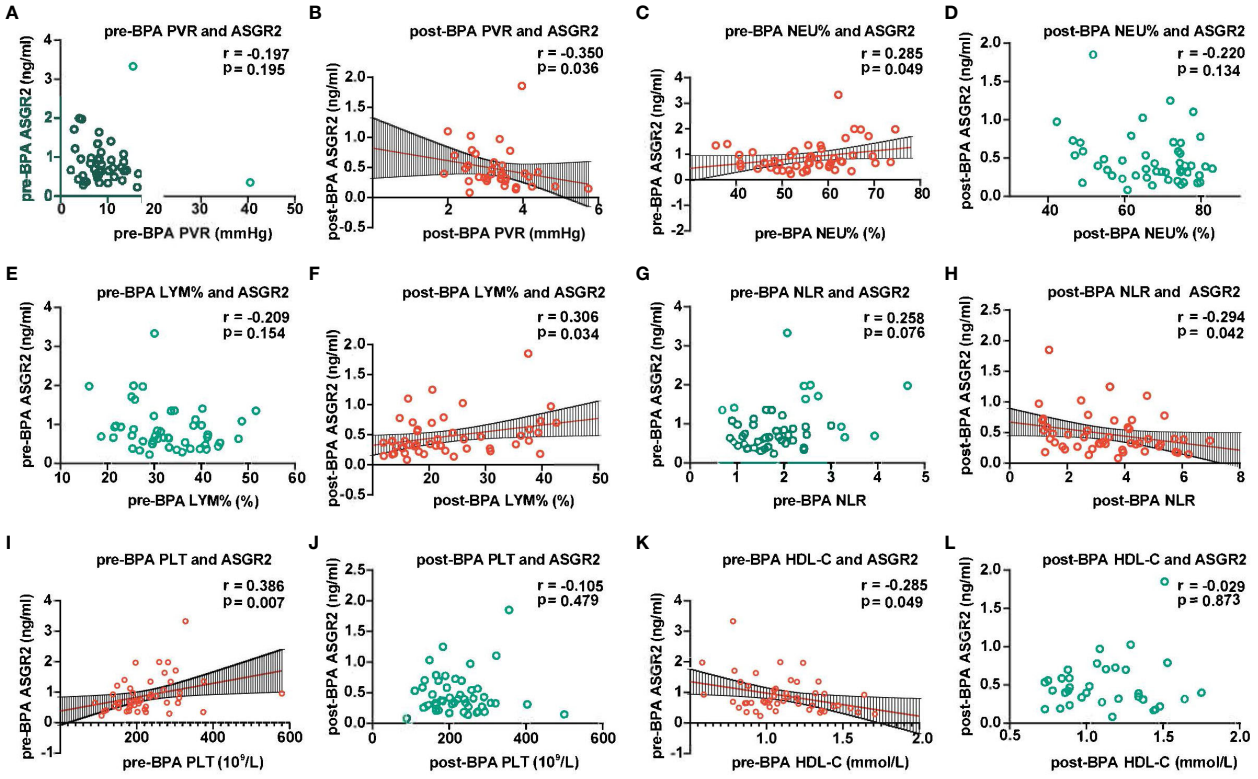

FIGURE 3
Association between ASGR2 and clinical parameters. ASGR2, asialoglycoprotein receptor 2; HDL-C, high-density lipoprotein cholesterol; PVR, pulmonary vascular resistance; LYM%, lymphocyte percentage; NLR, neutrophil-to-lymphocyte ratio; BPA, balloon pulmonary angioplasty; NEU%, neutrophil percentage. **(A)** pre-BPA PVR and ASGR2. **(B)** post-BPA PVR and ASGR2. **(C)** pre-BPA NEU% and ASGR2. **(D)** post-BPA NEU% and ASGR2. **(E)** pre-BPA LYM% and ASGR2. **(F)** post-BPA LYM% and ASGR2 **(G)** pre-BPA NLR and ASGR2. **(H)** post-BPA NLR and ASGR2. **(I)** pre-BPA PLT and ASGR2. **(J)** post-BPA PLT and ASGR2. **(K)** pre-BPA HDL-C and ASGR2. **(L)** post-BPA HDL-C and ASGR2.

However, further research is needed to fully understand the role of ASGR2 in CTEPH pathogenesis (17).

Our study revealed a correlation between the PLT count and ASGR2 level before BPA treatment. However, this correlation was no longer present after successful BPA treatment. These findings suggest that the initial abnormalities in PLT count and function observed in CTEPH patients are resolved by BPA intervention treatment, resulting in reduced inflammation and decreased PLT aggregation. The ASGR2 level may reflect the immune and inflammatory status of patients with CTEPH.

4.2 Relationship between ASGR2 and HDL-C

We observed a correlation between serum ASGR2 levels and HDL-C levels in CTEPH patients prior to BPA treatment. In CTEPH patients, dysfunctional HDL-C is associated with RV structure, PVR and proinflammatory effects (18–20). HDL-C levels are associated with peripheral blood leukocytes, including neutrophils, lymphocytes, and monocytes (21). The monocyte-to-HDL ratio is a novel marker of systemic inflammation in PH patients (21). The current understanding of the impact of ASGR2 on HDL-C formation and conversion, as well as its role in lipid metabolism and lipid levels, is still uncertain.

In our study, no significant change in HDL-C levels was observed pre- or post-BPA intervention. The correlation between ASGR2 and HDL-C, which was initially present prior to BPA

TABLE 4 Stepwise linear regression of ASGR2.

Variable	*P*	Tol	R^2	Adjusted R^2	F
Pre-BPA (n = 48)					
PLT, $\times10^9$/L	0.001		0.407	0.382	15.812
HDL-C, mmol/L	< 0.001				
NEU%, %	0.551	0.076			
Post-BPA (n = 48)					
Constant	< 0.001		0.150	0.125	6.016
LYM%, %	0.019				
NLR	0.185	0.042			
PVR, Wood U	0.063	0.969			

Tol, collinearity tolerance; ASGR2, asialoglycoprotein receptor 2; HDL-C, high density lipoprotein cholesterol; PLT, platelet; NEU%, neutrophil percentage; LYM%, lymphocyte percentage; NLR, neutrophil to lymphocyte ratio; PVR, pulmonary vascular resistance.

treatment, disappeared after BPA treatment. Inflammation has been shown to reduce the levels of ApoA-I, the protein component of HDL-C, and impair the function of HDL-C, resulting in proinflammatory effects. Notably, ApoA-I has been found to inhibit IL-6 secretion by macrophages and attenuate IL-6-induced proliferation and migration of pulmonary artery endothelial cells (22). Macrophages at inflamed sites can express ApoA-I, potentially exerting anti-inflammatory effects without affecting serum HDL-C levels (19, 23).

Our study revealed that ApoA-I levels increased after BPA treatment in CTEPH patients, indicating a potential link between inflammation and HDL-C function. Prior to BPA, inflammatory processes in CTEPH patients may lead to decreased ApoA-I levels and dysfunctional HDL-C, contributing to vascular pathologies. Following BPA intervention, the elevated ApoA-I levels, together with macrophages, suppressed inflammation and restored normal HDL function without affecting HDL-C levels. These findings support the hypothesis that ASGR2 may serve as a marker reflecting the inflammatory status and hemodynamic levels in CTEPH patients through its association with HDL-C.

4.3 Relationships between ASGR2, LYM, NEU and the NLR

In our study, a significant correlation between ASGR2 expression and the percentage of NEUs was detected before BPA treatment, but this correlation disappeared after treatment. Neutrophils and their products, including myeloperoxidase, proteases, and neutrophil extracellular traps (NETs), are key contributors to PH. They degrade vascular elastin, drive vascular remodeling, amplify the leukocyte response, and modify the local inflammatory environment (24). Additionally, neutrophils can impair the antioxidant and anti-inflammatory functions of HDL-C, potentially leading to the development of atherosclerosis (25). The interaction between NETs and platelets during programmed cell death promotes thrombosis formation in PAH patients. In addition, neutrophils can also impair the antioxidant and anti-inflammatory functions of HDL-C, leading to the development of atherosclerosis (26).

In our study, no significant correlation was found between ASGR2 expression and the LYM% or NLR before BPA treatment. However, after BPA treatment, a correlation between ASGR2 expression, LYM%, and the NLR was observed. Immune system dysfunction plays a crucial role in the pathogenesis of PH, as evidenced by alterations in circulating T-cell subsets. T lymphocytes infiltrate the pulmonary arteries of CTEPH patients and secrete cytokines, leading to damage to newly formed blood vessels and exacerbating disease progression. The upregulation of T lymphocytes and cytokines promotes the recruitment of inflammatory cells and contributes to the proliferation of smooth muscle and endothelial cells (27–29). Peripheral blood cells infiltrate affected lung tissues, leading to inflammatory cell infiltration and impacting peripheral blood cell counts and ratios (30). The decrease in the percentage of peripheral blood LYMs following BPA intervention indicated a successful improvement in immune signaling, leading to reduced lymphocyte activation and proliferation. Furthermore, importantly, the NLR is a reliable biomarker for the diagnosis of PH, risk stratification, and prognosis prediction (31). Therefore, ASGR2 may be an indicator of immune function and inflammatory status in CTEPH patients, as reflected by its association with LYM, NEU, PLT, HDL-C and the NLR.

Multiple linear stepwise regression analysis revealed no significant relationships between ASGR2 and the NEU% or NLR, likely due to multicollinearity. The LYM% explained 15% of the variation in ASGR2 after BPA treatment, while the combination of PLT and HDL-C explained 40.7% of the variation before BPA treatment. Nevertheless, there are still unidentified factors that influence ASGR2, highlighting the need for further research.

4.4 Relationship between ASGR2 and PVR

In our study, the serum levels of ASGR2 may be associated with PVR. The PVR is associated with the NLR, LYM, and pulmonary vascular remodeling (32, 33). Furthermore, PVR is negatively correlated with the levels of IL-7, a cytokine necessary for B-cell maturation and regulatory T-cell survival (34). Taken together, these findings suggest that PVR levels may be influenced by lymphocyte immune function and inflammation. We observed that the *P* value for PVR was 0.063, indicating a trend toward significance. The exclusion of PVR from the multiple regression analysis was primarily due to the limited sample size, which may have impacted the statistical power to detect a significant relationship.

4.5 Limitations

This study may be limited by its small sample size. Although our study revealed statistically significant correlations between ASGR2 and NEU, LYM%, and the NLR, the strength of these associations was modest. This may be attributed to the limited sample size employed in our study. To enhance the robustness and generalizability of our findings, future research should focus on recruiting a larger sample size for further validation and replication of our results.

5 Conclusions

The serum ASGR2 concentration may be a biomarker for BPA treatment effectiveness in CTEPH patients. The pre-BPA serum level of ASGR2 in CTEPH patients was associated with HDL-C and the PLT count. The post-BPA serum level of ASGR2 was correlated with the LYM%, which may reflect aspects of immunity and inflammatory status.

Data availability statement

The original contributions presented in the study are publicly available. This data can be found here: https://ngdc.cncb.ac.cn/omix/release/OMIX005982.

Ethics statement

The studies involving humans were approved by the ethics committee of the Shanghai Pulmonary Hospital. The studies were conducted in accordance with the local legislation and institutional requirements. The participants provided their written informed consent to participate in this study.

Author contributions

W-JX: Formal Analysis, Writing – original draft, Methodology. SW: Formal Analysis, Writing – original draft, Validation. Q-HZ: Validation, Writing – original draft, Formal Analysis. J-YX: Writing – original draft, Methodology. X-YH: Writing – original draft. S-GG: Writing – original draft, Resources. JH: Writing – original draft. H-LQ: Writing – original draft. C-JL: Writing – original draft. JX: Writing – original draft. H-TL: Writing – original draft. Z-PL: Writing – review & editing. LW: Writing – original draft, Resources. YS: Writing – review & editing. Y-LZ: Writing – review & editing, Methodology. RJ: Conceptualization, Funding acquisition, Writing – review & editing.

Funding

The author(s) declare financial support was received for the research, authorship, and/or publication of this article. This work was funded by the Clinical Research Foundation of Shanghai Pulmonary Hospital (SKPY2021004), the Shenkang-Lianying Joint Research and Development Program (SKLY2022CRT202) the Medical and Health Project of Baoshan District in 2022 (2023-E-30) and Program of National Key Research and Development Project of China (2023YFC2509500).

Conflict of interest

The authors declare that the research was conducted in the absence of any commercial or financial relationships that could be construed as a potential conflict of interest.

Publisher's note

All claims expressed in this article are solely those of the authors and do not necessarily represent those of their affiliated organizations, or those of the publisher, the editors and the reviewers. Any product that may be evaluated in this article, or claim that may be made by its manufacturer, is not guaranteed or endorsed by the publisher.

References

1. Liu J, Yang P, Tian H, Zhen K, McCabe C, Zhao L, et al. Right ventricle remodeling in chronic thromboembolic pulmonary hypertension. *J Transl Int Med.* (2022) 10:125–33. doi: 10.2478/jtim-2022-0027

2. Viswanathan G, Kirshner HF, Nazo N, Ali S, Ganapathi A, Cumming I, et al. Single-cell analysis reveals distinct immune and smooth muscle cell populations that contribute to chronic thromboembolic pulmonary hypertension. *Am J Respir Crit Care Med.* (2023) 207:1358–75. doi: 10.1164/rccm.202203-0441OC

3. Kawakami T, Matsubara H, Shinke T, Abe K, Kohsaka S, Hosokawa K, et al. Balloon pulmonary angioplasty versus riociguat in inoperable chronic thromboembolic pulmonary hypertension (MR BPA): an open-label, randomised controlled trial. *Lancet Respir Med.* (2022) 10:949–60. doi: 10.1016/S2213-2600(22)00171-0

4. Xiong C, Yang B. Revising the hemodynamic criteria for pulmonary hypertension: A perspective from China. *J Transl Int Med.* (2023) 11:1–3. doi: 10.2478/jtim-2022-0023

5. Magon W, Stepniewski J, Waligora M, Jonas K, Przybylski R, Podolec P, et al. Changes in inflammatory markers in patients with chronic thromboembolic pulmonary hypertension treated with balloon pulmonary angioplasty. *Cells.* (2022) 11(9). doi: 10.3390/cells11091491

6. Miao R, Dong X, Gong J, Li Y, Guo X, Wang J, et al. Single-cell RNA-sequencing and microarray analyses to explore the pathological mechanisms of chronic thromboembolic pulmonary hypertension. *Front Cardiovasc Med.* (2022) 9:900353. doi: 10.3389/fcvm.2022.900353

7. Zhao QH, Gong SG, He J, Yuan P, Wu WH, Luo CJ, et al. Balloon pulmonary angioplasty combined with riociguat for the treatment of inoperable chronic thromboembolic pulmonary hypertension (PRACTICE study): study protocol for a randomized controlled trial. *Trials.* (2021) 22:957. doi: 10.1186/s13063-021-05910-5

8. Humbert M, Kovacs G, Hoeper MM, Badagliacca R, Berger RMF, Brida M, et al. 2022 ESC/ERS Guidelines for the diagnosis and treatment of pulmonary hypertension. *Eur Heart J.* (2022) 43:3618–731. doi: 10.1183/13993003.00879-2022

9. Jiang R, Ai ZS, Jiang X, Yuan P, Liu D, Zhao QH, et al. Intravenous fasudil improves in-hospital mortality of patients with right heart failure in severe pulmonary hypertension. *Hypertension Res.* (2015) 38:539–44. doi: 10.1038/hr.2015.33

10. Jiang R, Wang L, Zhao QH, Wu C, Yuan P, Wang S, et al. Echocardiography nomogram for predicting survival among chronic lung disease patients with severe pulmonary hypertension. *J Clin Med.* (2022) 11(6). doi: 10.3390/jcm11061603

11. Cox J, Mann M. MaxQuant enables high peptide identification rates, individualized p.p.b.-range mass accuracies and proteome-wide protein quantification. *Nat Biotechnol.* (2008) 26:1367–72. doi: 10.1038/nbt.1511

12. Finn RD, Coggill P, Eberhardt RY, Eddy SR, Mistry J, Mitchell AL, et al. The Pfam protein families database: towards a more sustainable future. *Nucleic Acids Res.* (2016) 44:D279–85. doi: 10.1093/nar/gkv1344

13. Kanehisa M, Goto S, Sato Y, Furumichi M, Tanabe M. KEGG for integration and interpretation of large-scale molecular data sets. *Nucleic Acids Res.* (2012) 40:D109–14. doi: 10.1093/nar/gkr988

14. Grewal PK. The ashwell-morell receptor. *Methods Enzymol.* (2010) 479:223–41. doi: 10.1016/S0076-6879(10)79013-3

15. Yaoita N, Shirakawa R, Fukumoto Y, Sugimura K, Miyata S, Miura Y, et al. Platelets are highly activated in patients of chronic thromboembolic pulmonary hypertension. *Arterioscler Thromb Vasc Biol.* (2014) 34:2486–94. doi: 10.1161/ATVBAHA.114.304404

16. Delaney C, Davizon-Castillo P, Allawzi A, Posey J, Gandjeva A, Neeves K, et al. Platelet activation contributes to hypoxia-induced inflammation. *Am J Physiol Lung Cell Mol Physiol.* (2021) 320:L413–21. doi: 10.1152/ajplung.00519.2020

17. Manz XD, Szulcek R, Pan X, Symersky P, Dickhoff C, Majolee J, et al. Epigenetic modification of the von willebrand factor promoter drives platelet aggregation on the pulmonary endothelium in chronic thromboembolic pulmonary hypertension. *Am J Respir Crit Care Med.* (2022) 205:806–18. doi: 10.1164/rccm.202109-2075OC

18. Ross DJ, Hough G, Hama S, Aboulhosn J, Belperio JA, Saggar R, et al. Proinflammatory high-density lipoprotein results from oxidized lipid mediators in the pathogenesis of both idiopathic and associated types of pulmonary arterial hypertension. *Pulm Circ.* (2015) 5:640–8. doi: 10.1086/683695

19. Huang Y, Zhang J, Zhao Q, Hu X, Zhao H, Wang S, et al. Impact of reduced apolipoprotein A-I levels on pulmonary arterial hypertension. *Hellenic J Cardiol*. (2023). doi: 10.1016/j.hjc.2023.10.004

20. He M, Jiang R, Fei S, Cao JX, Wang L, Shi JY. Cardiac magnetic resonance imaging-derived septum swing index detects pulmonary hypertension: A diagnostic study. *J Transl Int Med*. (2023) 11:459–67. doi: 10.2478/jtim-2023-0114

21. Bilik MZ, Oylumlu M, Oylumlu M, Acun B, Arik B, Arslan B, et al. Novel predictor of pulmonary arterial hypertension: Monocyte to HDL cholesterol ratio. *Med (Baltimore)*. (2022) 101:e29973. doi: 10.1097/MD.0000000000029973

22. Khirfan G, Li M, Wang X, DiDonato JA, Dweik RA, Heresi GA. Abnormal levels of apolipoprotein A-I in chronic thromboembolic pulmonary hypertension. *Pulm Circ*. (2021) 11:20458940211010371. doi: 10.1177/20458940211010371

23. Tavori H, Su YR, Yancey PG, Giunzioni I, Wilhelm AJ, Blakemore JL, et al. Macrophage apoAI protects against dyslipidemia-induced dermatitis and atherosclerosis without affecting HDL. *J Lipid Res*. (2015) 56:635–43. doi: 10.1194/jlr.M056408

24. Domon H, Terao Y. The role of neutrophils and neutrophil elastase in pneumococcal pneumonia. *Front Cell Infect Microbiol*. (2021) 11:615959. doi: 10.3389/fcimb.2021.615959

25. Carlucci PM, Purmalek MM, Dey AK, Temesgen-Oyelakin Y, Sakhardande S, Joshi AA, et al. Neutrophil subsets and their gene signature associate with vascular inflammation and coronary atherosclerosis in lupus. *JCI Insight*. (2018) 3(8). doi: 10.1172/jci.insight.99276

26. Baptista de Barros Ribeiro Dourado LP, Santos M, Moreira-Goncalves D. Nets, pulmonary arterial hypertension, and thrombo-inflammation. *J Mol Med (Berl)*. (2022) 100:713–22. doi: 10.1007/s00109-022-02197-0

27. Hassoun PM, Mouthon L, Barbera JA, Eddahibi S, Flores SC, Grimminger F, et al. Inflammation, growth factors, and pulmonary vascular remodeling. *J Am Coll Cardiol*. (2009) 54:S10–9. doi: 10.1016/j.jacc.2009.04.006

28. Austin ED, Rock MT, Mosse CA, Vnencak-Jones CL, Yoder SM, Robbins IM, et al. T lymphocyte subset abnormalities in the blood and lung in pulmonary arterial hypertension. *Respir Med*. (2010) 104:454–62. doi: 10.1016/j.rmed.2009.10.004

29. Quarck R, Wynants M, Verbeken E, Meyns B, Delcroix M. Contribution of inflammation and impaired angiogenesis to the pathobiology of chronic thromboembolic pulmonary hypertension. *Eur Respir J*. (2015) 46:431–43. doi: 10.1183/09031936.00009914

30. Xu WJ, Wang S, Yuan P, Wang L, Huang JX, Jiang R. Arterial and venous thromboembolism risk associated with blood eosinophils: A systematic review and meta-analysis. *Anim Model Exp Med*. (2022) 5:470–81. doi: 10.1002/ame2.12277

31. Yogeswaran A, Tello K, Lund J, Klose H, Harbaum L, Sommer N, et al. Risk assessment in pulmonary hypertension based on routinely measured laboratory parameters. *J Heart Lung Transplant*. (2022) 41:400–10. doi: 10.1016/j.healun.2021.10.018

32. Seyfarth HJ, Hammerschmidt S, Halank M, Neuhaus P, Wirtz HR. Everolimus in patients with severe pulmonary hypertension: a safety and efficacy pilot trial. *Pulm Circ*. (2013) 3:632–8. doi: 10.1086/674311

33. Urbanowicz TK, Olasinska-Wisniewska A, Michalak M, Straburzynska-Migaj E, Jemielity M. Neutrophil to lymphocyte ratio as noninvasive predictor of pulmonary vascular resistance increase in congestive heart failure patients: Single-center preliminary report. *Adv Clin Exp Med*. (2020) 29:1313–7. doi: 10.17219/acem/126292

34. Diekmann F, Legchenko E, Chouvarine P, Lichtinghagen R, Bertram H, Happel CM, et al. Circulating interleukin-7 in human pulmonary arterial hypertension. *Front Cardiovasc Med*. (2021) 8:794549. doi: 10.3389/fcvm.2021.794549

frontiers | Frontiers in Immunology

TYPE Original Research
PUBLISHED 28 June 2024
DOI 10.3389/fimmu.2024.1420182

OPEN ACCESS

EDITED BY
Ping Yuan,
Tongji University, China

REVIEWED BY
Fan Chen,
Air Force Medical University, China
Zhen Dong,
Southwest University, China

*CORRESPONDENCE
Juxiang Chen
jxchenchhs@163.com
Hongxiang Wang
wanghongxiang27@smmu.edu.cn

†These authors have contributed equally to this work and share first authorship

RECEIVED 01 May 2024
ACCEPTED 12 June 2024
PUBLISHED 28 June 2024

CITATION
Zhang S, Cheng L, Su Y, Qian Z, Wang Z, Chen C, Li R, Zhang A, He J, Mao J, Wang H and Chen J (2024) AGBL4 promotes malignant progression of glioblastoma via modulation of MMP-1 and inflammatory pathways.
Front. Immunol. 15:1420182.
doi: 10.3389/fimmu.2024.1420182

AGBL4 promotes malignant progression of glioblastoma via modulation of MMP-1 and inflammatory pathways

Shuai Zhang[1†], Lilin Cheng[1†], Yandong Su[1†], Zhongrun Qian[2†], Zhen Wang[1], Chao Chen[1], Rong Li[1], Aikang Zhang[1], Jiawei He[1], Jiangxin Mao[1], Hongxiang Wang[1*] and Juxiang Chen[1*]

[1]Department of Neurosurgery, Changhai Hospital, Naval Medical University, Shanghai, China, [2]Department of Neurosurgery, The First Affiliated Hospital of University of Science and Technology of China, Division of Life Sciences and Medicine, Hefei, Anhui, China

Introduction: Glioblastoma multiforme (GBM), the most common primary malignant brain tumor, is notorious for its aggressive growth and dismal prognosis. This study aimed to elucidate the molecular underpinnings of GBM, particularly focusing on the role of AGBL4 and its connection to inflammatory pathways, to discover viable therapeutic targets.

Methods: Single-cell sequencing was utilized to examine the expression levels of AGBL4 and functional assays were performed to assess the effects of AGBL4 modulation.

Results: Our findings identified the significant upregulation of AGBL4 in GBM, which correlated with adverse clinical outcomes. Functional assays demonstrated that AGBL4 knockdown inhibited GBM cell proliferation, migration, and invasion and influenced inflammatory response pathways, while AGBL4 overexpression promoted these activities. Further investigation revealed that AGBL4 exerted its oncogenic effects through modulation of MMP-1, establishing a novel regulatory axis critical for GBM progression and inflammation.

Discussion: Both AGBL4 and MMP-1 may be pivotal molecular targets, offering new avenues for targeted therapy in GBM management.

KEYWORDS

glioblastoma, prognosis, AGBL4, MMP-1, single-cell sequencing

1 Introduction

Gliomas are the most common malignant primary tumors in the central nervous system, derived from glial or precursor cells and encompass diverse histopathological subtypes, including GBM, astrocytoma, oligodendroglioma, ependymoma, and oligoastrocytoma. GBM is the most common and aggressive form, making up the majority of cases (1). Despite standard treatment involving maximal safe resection, chemotherapy, radiotherapy, and tumor treating fields, GBM remains therapeutically challenging due to its aggressive nature, tendency to infiltrate the surrounding brain, and develop resistance to therapies (2). This results in a dismal 5-year survival rate of merely 4.7% (3). Consequently, there is an urgent need to elucidate the molecular underpinnings of GBM to improve diagnostic efficacy and develop novel targeted therapies (4).

The advent of single-cell sequencing technology has revolutionized our understanding of cellular processes in biology (5). By enabling the measurement of individual cell genomes, single-cell sequencing facilitates the analysis of differentially expressed genes (DEGs), the identification of key factors dysregulated during tumorigenesis, and the construction of regulatory network and clonality trees within tumor lesions. It also enables the study of tumor heterogeneity across multiple levels, which is crucial for understanding resistance to therapy and for creating new treatment approaches (6). Therefore, single-cell sequencing has been widely employed for detecting mutations and studying the epigenomic changes during tumor progression.

Emerging evidence implicates the ATP/GTP-binding protein-like 4 gene (AGBL4) in various pathological processes, including antituberculosis drug-induced hepatotoxicity (7), cardiometabolic risk (8), and colorectal cancer, where it is anticipated to serve as a novel biomarker (9). However, its role in gliomas, particularly GBM, remains largely unexplored. In this study, we employed single-cell sequencing to confirm high expression levels of AGBL4 in GBM tissues linked to poor outcomes, supported by data from The Cancer Genome Atlas (TCGA) and Changhai Hospital. Functional assays demonstrated its capacity to promote GBM cell proliferation, migration, and invasion. Subsequent investigations identified matrix metalloproteinase-1 (MMP-1) as a key gene increased in GBM tissues and a likely target of AGBL4. Reducing AGBL4 levels significantly hindered GBM growth in xenograft models, a process that MMP-1 could reverse.

Further analysis indicated that AGBL4-related DEGs like MMP-1, Fos proto-oncogene (FOS), and FosB proto-oncogene (FOSB) are involved in the interleukin (IL)-17 signaling pathway, suggesting that AGBL4 and MMP-1 could influence GBM progression via inflammatory pathways. Subsequent analyses showed a complex relationship among AGBL4, MMP-1, and other inflammatory genes in regulating the GBM tumor microenvironment, affecting tumor behavior and patient survival. These findings highlight the potential of inflammation-related factors as focal points for future research and the development of novel therapeutic strategies for GBM.

2 Materials and methods

2.1 Patients and tissue samples

Specimen collection and clinical data were approved by the Research Ethics Committee of Changhai Hospital, Naval Medical University. Written informed consent was secured from each participant. The study included three primary and three recurrent GBM samples from six Chinese patients for single-cell sequencing. Additionally, eight fresh GBM samples and four normal brain tissues from traumatic injury patients were obtained. Sixty-five paraffin-embedded primary GBM specimens from January 2005 to December 2019, with clinical data and follow-up, were analyzed. GBM patient datasets from TCGA database provided external validation.

2.2 Single-cell sequencing

GBM sample single-cell sequencing libraries were constructed following the Chromium Next GEM Single Cell 3' Reagent Kits v3.1. Gene expression matrices were generated and processed using Cell Ranger software on the 10×Genomics platform. Genomic and transcriptomic mapping was done using Spliced Trans Alignment to a Reference software, producing gene counts matrices per cell. Cell filtration, standardization, classification, differential gene expression analysis, and marker gene screening were conducted using the Seurat package in R studio. Sequencing was outsourced to Oebiotech Co., Ltd., Shanghai, China.

2.3 Western blot analysis

Samples were lysed using RIPA buffer (cat R0010, Solarbio, Beijing, China) with protease inhibitors (SKU 11836153001, Roche, Basel, Switzerland). Proteins were separated on 10% SDS-PAGE gels (cat 20325ES62, Yeason, Shanghai, China) and transferred onto PVDF membranes (cat GVWP02500, Millipore, MA, USA). Membranes were incubated with anti-human AGBL4 antibody (1:1000) and anti-actin antibody (1:10,000) overnight at 4°C, then with secondary antibodies for 1 hour at room temperature. Protein bands were visualized using an ECL kit (cat PI32209, Thermo Scientific Pierce, Waltham, MA, USA).

2.4 Quantitative real-time PCR

Total RNA was extracted with TRIzol ® reagent (cat 15596026CN, Thermo Fisher Scientific, Waltham, MA, USA). Complementary DNA was synthesized using HiScript II RT SuperMix (cat R223–01, Vazyme, Nanjing, China). RT-PCR quantified AGBL4 mRNA levels using GAPDH as an endogenous control with primers Human-AGBL4-F (AATCTACCAGCAGACCAAAATG) and Human-AGBL4-R (TCAAAACAAAAGGCAAAGGAC).

2.5 Cell culture and transfection

GBM cell lines T98G, U251-MG, U87-MG, and A172, sourced from the Cell Bank of Chinese Academy of Science, were maintained in Dulbecco's Modified Eagle's Medium supplemented with 10% fetal bovine serum at 37°C in a 5% CO_2 atmosphere. Lentiviral vectors for AGBL4 knockdown (KD) and overexpression (OE) were produced by Hanyin Biotech, Shanghai, China. Specific AGBL4-KD and AGBL4-OE lentiviruses were used to transduce U87-MG and A172, and T98G and U251-MG cell lines, respectively. The sequences for AGBL4-shRNAs were: shRNA1: GAGGGAA TGTGAGCAAATA, shRNA2: CCGGACCATAGGAAGAACT, shRNA3: GCTTACTGCTACCCATATA.

2.6 Cell viability, colony formation, scratch assay, and Matrigel-transwell assay

Cell viability was assessed using the Cell Counting Kit-8 (CCK-8, cat CK04–01, Dojindo, Japan) by measuring the optical density at 450 nm at 24, 48, 72, 96, and 120 hours post-treatment. Colony formation efficiency was evaluated by seeding cells in 6-well plates and staining emerging colonies with 0.1% crystal violet. To assess cell migration, a scratch assay was performed. Cells were grown in 6-well plates and a scratch was made in the center of the wells using a 200 µL pipette tip. After washing away the cellular debris and further incubating, images of the scratch were captured to evaluate the migration rate by measuring the gap closure. For invasion assays, the upper chamber of a transwell apparatus was coated with Matrigel (cat CLS3422, 8-µm pores, Millipore, MA, US) and seeded with 5×10^4 cells in 100 µL of serum-free medium. The lower chamber was filled with 600 µL of complete culture medium. After overnight incubation, cells that migrated to the underside of the membrane were stained with 0.1% crystal violet, and five random fields were counted under a light microscope.

2.7 Immunohistochemical analysis

Immunohistochemistry was performed to detect AGBL4 expression in a GBM tissue microarray with 65 samples from the Department of Neurosurgery, Changhai hospital, Naval Medical University. The procedure included fixing, dehydrating, embedding, and sectioning tissues, which were then deparaffinized and rehydrated. Heat-mediated antigen retrieval was performed, followed by blocking of endogenous peroxidase and nonspecific binding. Sections were incubated with primary and secondary antibodies, developed with chromogen, counterstained with hematoxylin, and finally, dehydrated, cleared, and mounted for microscopic examination. The percentage of positive cells was divided into 0 (0–5%), 1 (6–25%), 2 (26–50%), 3 (51–75%) and 4 (76–100%). The intensity of protein expression was determined as 0 (no staining), 1 (weakly staining), 2 (moderately staining) and 3 (strongly staining). The scores was calculated by multiplying the percentage of positive cells and the intensity of protein expression as follows: 0 (-), 2–3 (+), 4–6 (++), and >6 (+++). A total score of ≥4 points categorizes the specimens into the high AGBL4 group, while scores <4 points indicate low AGBL4 group.

2.8 Xenograft animal model

Male athymic nu/nu mice aged 6 weeks, obtained from Shanghai Jiao Tong University, were used in compliance with guidelines set by the Institutional Animal Care and Use Committee of Changhai Hospital, Naval Medical University. For tumor induction, we used three groups of mice (6 mice per group) injected with different cell lines: U87-MG control cells (U87MG-NC), AGBL4-knockdown U87-MG cells (U87MG-AGBL4-KD), and U87-MG cells with both AGBL4 knockdown and MMP-1 overexpression (U87MG-AGBL4-KD+MMP1-OE). Each mouse was anesthetized and their heads were secured in a stereotaxic instrument for precise intracranial injection of 5×10^5 cells into the corpus striatum. Post-injection, the mice were monitored every three days for changes in behavior and body weight. Magnetic resonance imaging (MRI) was utilized to assess tumor development when clinical signs such as reduced eating, decreased movement, circling behavior, or weight loss were observed. Tumor volumes were calculated based on the MRI data, and body weight differences among the three groups were compared on the day of MRI scanning. Mice were euthanized at humane endpoints, which were clearly defined by severe neurological dysfunction, inability to access food or water, unrelieved pain, or other signs indicating a severe decline in quality of life. The overall survival periods were recorded and the brains were harvested for further histopathological examination.

2.9 Statistics

Statistical analyses were performed using SPSS software (version 19.0). Student's t-test was used to compare the mean differences between two groups. Kaplan-Meier survival analysis and log-rank test were employed to evaluate the survival outcomes among different groups. All statistical analyses were two-sided, and $P < 0.05$ was considered statistically significant. Statistical graphs were drawn using GraphPad Prism 7 software (GraphPad Software Inc., San Diego, CA, USA).

Methods for Hematoxylin-Eosin (H&E) staining and bioinformatics analysis are detailed in the Supplementary Materials.

3 Results

3.1 AGBL4 is highly expressed in GBM and predicts poor prognosis

Single-cell sequencing was performed on both primary and recurrent GBM specimens. Dimensionality reduction via the t-distributed stochastic neighbor embedding (t-SNE) algorithm revealed nineteen distinct clusters (Figure 1A). AGBL4 expression was observed across a majority of these tumor clusters (Figure 1B), with a significant upregulation in recurrent GBM compared to

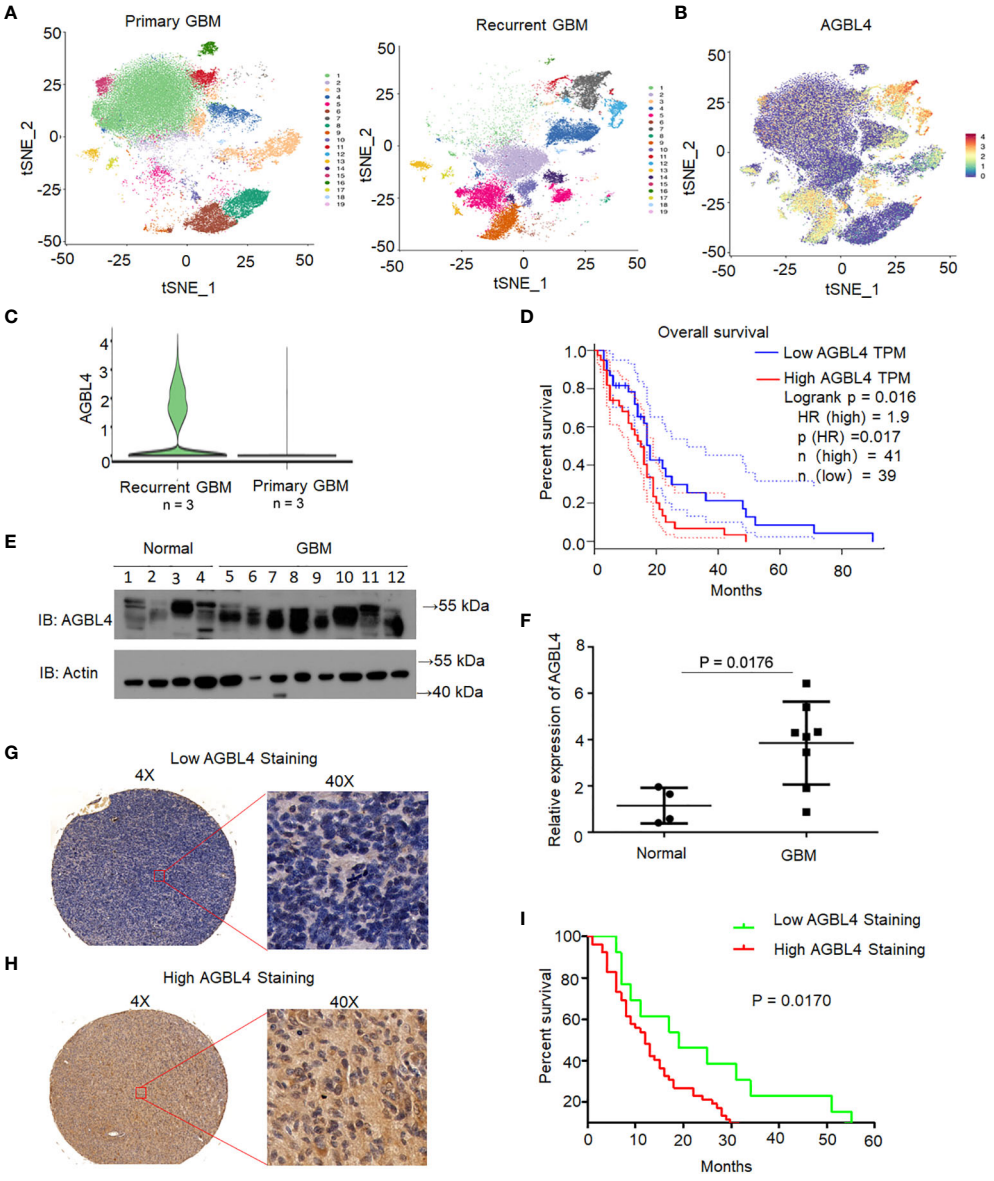

FIGURE 1
AGBL4 was highly expressed in GBM and predicted poor prognosis. **(A)** t-SNE visualization of 19 distinct clusters identified from single-cell RNA sequencing of primary and recurrent GBM samples. **(B)** Expression of AGBL4 across the clusters revealed by t-SNE plot. **(C)** AGBL4 expression is significantly higher in recurrent GBM compared to primary GBM samples. **(D)** Survival curves of GBM patients with low AGBL4 or high AGBL4 expression, obtained from TCGA database, P=0.017. **(E)** WB analysis confirms elevated AGBL4 protein levels in GBM tissues compared to normal brain samples. **(F)** Quantification of qRT-PCR verifies the upregulation of AGBL4 in GBM relative to normal brain tissues, P=0.0176. **(G, H)** Representative images of immunohistochemical staining show **(G)** low and **(H)** high AGBL4 expression in GBM tissues. Scale bars: 100 µm (4X), 25 µm (40X). **(I)** Kaplan-Meier analysis demonstrates that GBM patients with high AGBL4 staining have significantly shorter survival times compared to those with low AGBL4 expression, P = 0.0170.

primary GBM (Figure 1C). Survival analysis using TCGA database indicated that elevated AGBL4 levels were associated with a worse prognosis in GBM patients (Figure 1D).

To validate the role of AGBL4 in GBM prognosis, we analyzed AGBL4 expression in normal brain tissues (n=4) and GBM tissues (n=8) through RT-PCR and WB. The WB results confirmed a marked increase in AGBL4 levels in GBM tissues relative to normal brain samples (Figures 1E, F). Immunohistochemical analysis was conducted on primary GBM tissue microarray. Based on the scoring criteria outlined before, samples were classified into low and high AGBL4 expression groups. Representative images of low (Figure 1G) and high (Figure 1H) AGBL4 groups illustrate the distinctions in staining intensity and cellular distribution. Survival analysis demonstrated a significant association between AGBL4 expression levels and patient outcomes. Specifically, patients categorized into the high AGBL4 group (scores ≥4) exhibited notably shorter survival times compared to those in the low AGBL4 group (scores <4) (P=0.017) (Figure 1I).

Altogether, these results demonstrate that AGBL4 expression is significantly elevated in GBM and its overexpression is predictive of poor prognosis in both our cohort and TCGA dataset.

3.2 Knockdown of AGBL4 inhibits GBM cell proliferation, migration, and invasion

To determine the roles of AGBL4 in GBM cell functions, we first analyzed AGBL4 expression in various GBM cell lines. Using the $2^{-\Delta\Delta Ct}$ method, RT-PCR results showed differential expression levels of AGBL4, with U87-MG and A172 cells exhibiting higher expression compared to T98G and U251-MG cells (Figure 2A). Additionally, WB analysis confirmed these findings, showing protein expression levels consistent with the RT-PCR results (Figure 2B). Following the knockdown of AGBL4 using the most effective shRNA sequence (shRNA2: CCGGACCATAGGAAGAACT) in U87-MG and A172 cell lines, WB analysis confirmed the efficient reduction of AGBL4 expression The knockdown efficiency was quantified at approximately 70% in the U87-MG cell line and around 65% in the A172 cell line (Figures 2C–E).

Functional assays were then performed to investigate the effect of AGBL4 on GBM cell pathology. The CCK-8 assay and colony formation assay, both indicative of cell proliferative capacity, showed that AGBL4 knockdown significantly decreased proliferation in U87-MG and A172 cells (Figures 3A–F). Scratch assays demonstrated that AGBL4 knockdown also decreased the migratory capabilities of these cells (Figures 3G–J). Finally, Matrigel-transwell assays provided quantitative and visual evidence of the diminished invasion capacity following AGBL4 knockdown (Figures 3K–N).

These findings collectively suggest that AGBL4 is integral to the proliferative, migratory, and invasive characteristics of GBM cells, confirming its potential as a target for GBM therapy.

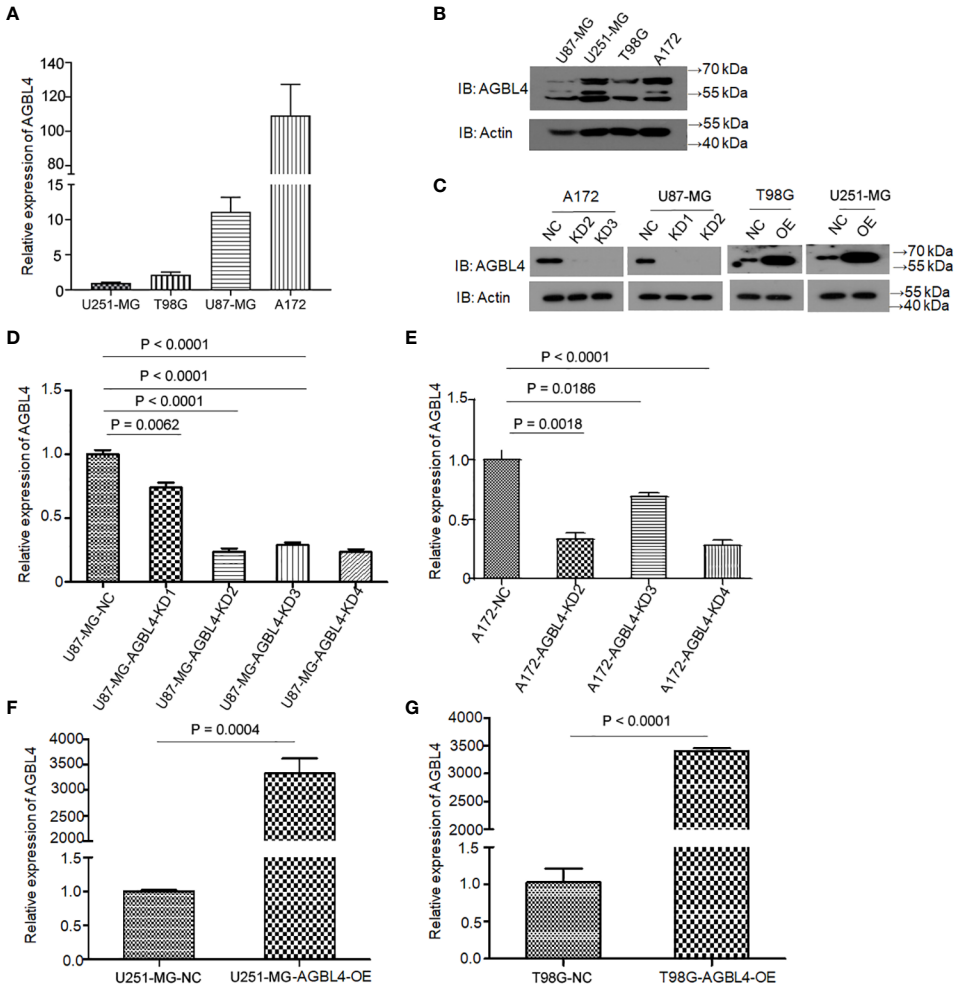

FIGURE 2
Relative expression levels of AGBL4 in GBM cells. **(A)** QRT-PCR analysis shows varying expression levels of AGBL4 across different GBM cell lines, with U87-MG and A172 exhibiting higher expression compared to T98G and U251-MG. **(B, C)** WB analysis confirms the protein expression patterns of AGBL4 in **(B)** U87-MG, U251-MG, T98G, and A172 cell lines and **(C)** after AGBL4 knockdown in A172 and U87-MG cells, and overexpression in T98G and U251-MG cells. **(D–G)** Quantification of qRT-PCR demonstrates successful AGBL4-KD in **(D)** U87-MG and **(E)** A172 cells, and successful AGBL4-OE in **(F)** U251-MG and **(G)** T98G cells.

10.3389/fimmu.2024.1420182

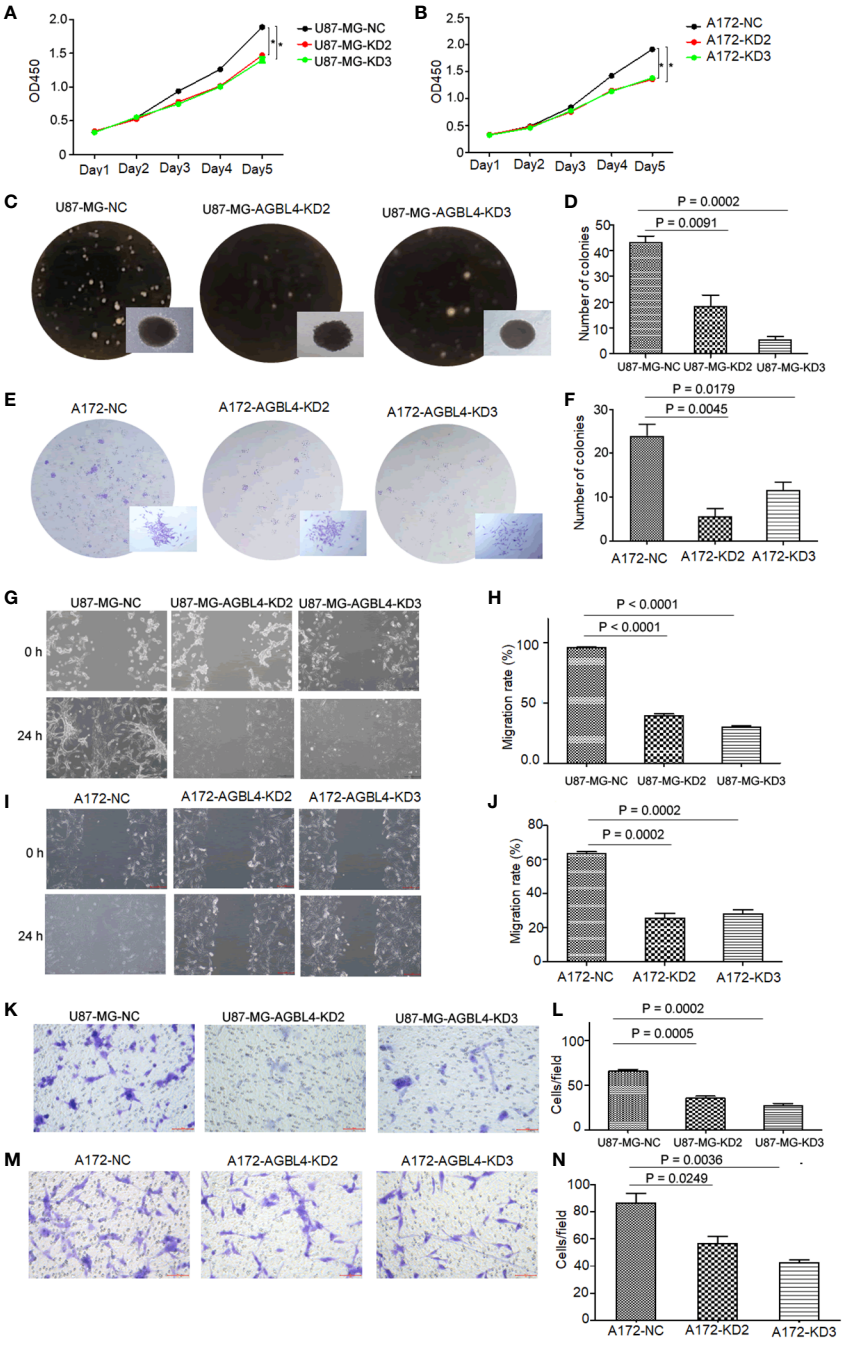

FIGURE 3
Knockdown of AGBL4 inhibits GBM cell proliferation, migration and invasion abilities. **(A, B)** CCK-8 assays show reduced proliferation in **(A)** U87-MG and **(B)** A172 cells after AGBL4 knockdown. **(C–F)** Colony formation assays demonstrate decreased colony numbers and sizes in **(C, D)** U87-MG and **(E, F)** A172 cells after AGBL4 knockdown. **(G–J)** Scratch migration assays reveal impaired migratory ability of **(G, H)** U87-MG and **(I, J)** A172 cells following AGBL4 knockdown. **(K–N)** Matrigel transwell invasion assays illustrate diminished invasive potential in **(K, L)** U87-MG and **(M, N)** A172 cells upon AGBL4 knockdown.

3.3 Overexpression of AGBL4 improves GBM cell proliferation, migration and invasion

To investigate the roles of AGBL4 in GBM growth, we overexpressed AGBL4 in T98G and U251-MG cells. WB results verified the overexpression of AGBL4 in these cells (Figure 2C). RT-PCR also confirmed that the relative expression levels of AGBL4 were significantly increased in both U251-MG and T98G overexpression groups (Figures 2F, G). The CCK-8 assay demonstrated that AGBL4 overexpression enhanced the proliferation ability of GBM cells (Figures 4A, B). Additionally,

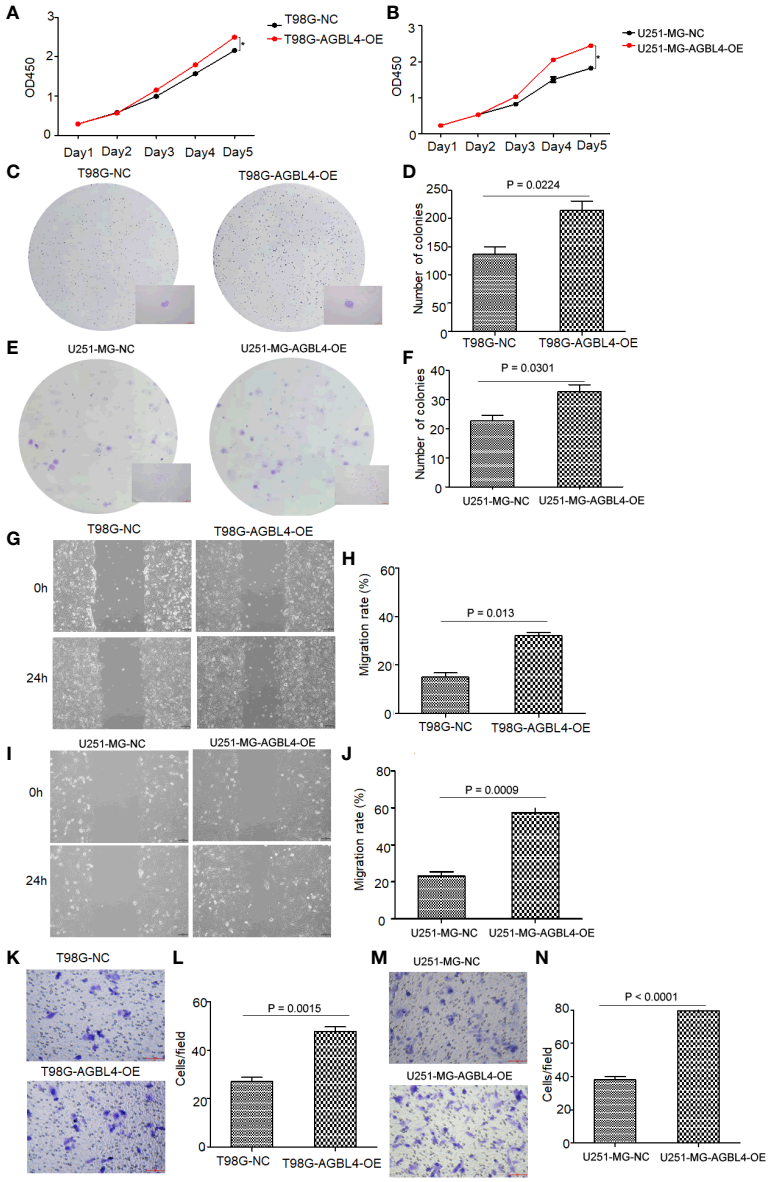

FIGURE 4
High expression of AGBL4 improves GBM cell proliferation, migration and invasion abilities. **(A, B)** CCK-8 assays demonstrate enhanced proliferation in **(A)** T98G and **(B)** U251-MG cells after AGBL4 overexpression. **(C–F)** Colony formation assays show increased colony numbers and sizes in **(C, D)** T98G and **(E, F)** U251-MG cells after AGBL4 overexpression. **(G–J)** Scratch migration assays indicate improved migratory ability of **(G, H)** T98G and **(I, J)** U251-MG cells following AGBL4 overexpression. **(K–N)** Matrigel transwell invasion assays reveal elevated invasive potential in **(K, L)** T98G and **(M, N)** U251-MG cells upon AGBL4 overexpression.

the colony formation assay revealed that AGBL4 overexpression led to an increased number of colonies (Figures 4C–F). Scratch assays indicated that the high expression of AGBL4 promoted the migration of GBM cells (Figures 4G–J). Furthermore, the Matrigel-transwell assays demonstrated a significant increase in invasion, with more cell visible in the fields of view compared to the controls (Figures 4K–N).

These findings highlight a critical role for AGBL4 in promoting the proliferation, migration, and invasion of GBM cells.

3.4 AGBL4 knockdown significantly reduces a range of classic factors associated with cancer-related pathways

To elucidate the molecular mechanism of AGBL4 in GBM, we conducted transcriptome sequencing on A172 cells with or without AGBL4 knockdown. The heatmap revealed distinct differences and pairwise correlations in gene expression between the various GBM cell samples (Figure 5A). Analysis identified

10.3389/fimmu.2024.1420182

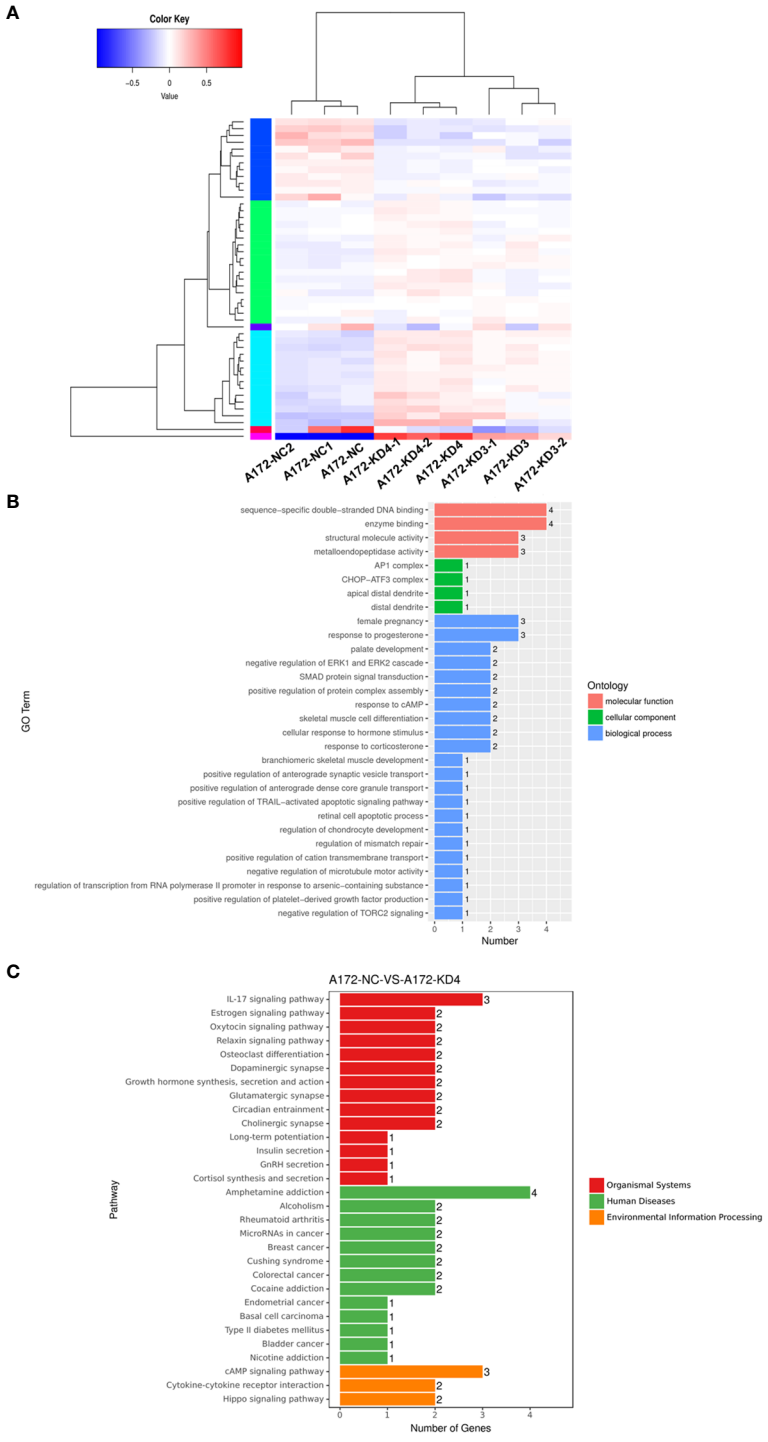

FIGURE 5
AGBL4 knockdown significantly reduces a range of classic factors associated with cancer-related pathways. **(A)** Heatmap showing differential gene expression between NC and AGBL4-KD in A172 cells. Each column represents a different sample, and each row represents a gene. Red indicates upregulated genes, blue indicates downregulated genes, and color intensity correlates with expression level. **(B)** GO annotations analysis of DEGs in A172 cells comparing NC and KD. The bar chart categorizes GO terms by biological processes, cellular components, and molecular functions, with the number of associated genes indicated. **(C)** KEGG analysis of DEGs in A172 cells after AGBL4-KD. The bar chart categorizes pathway terms by organismal systems, human diseases, and environmental information processing, with the number of genes involved in each pathway.

nearly 42 DEGs, with 30 up-regulated and 12 down-regulated (Supplementary Figure 1).

Bioinformatics analysis indicated that these DEGs were primarily involved in processes such as enzyme binding, positive regulation of protein complex assembly, positive regulation of TRAIL-activated apoptotic signaling pathway, and negative regulation of microtubule motor activity, according to GO annotations (Figure 5B). Furthermore, KEGG enrichment analysis

suggested that AGBL4-associated DEGs might participate in pathways related to microRNAs in human cancer and contribute to the IL-17 signaling pathway, which is frequently recognized as a reference index to judge the malignancy of gliomas (Figure 5C). Based on these findings, we speculated that AGBL4-related DEGs might play significant roles in tumor progression within the central nervous system.

3.5 AGBL4 promotes GBM cell proliferation, migration, and invasion abilities via MMP-1

From the DEGs identified in our transcriptome analysis (Supplementary Table 1), eight candidate genes were selected based on fold change and prognostic correlation in TCGA database (Table 1). RT-PCR analysis revealed that among these candidates, MMP-1 exhibited the most significant differential expression (Supplementary Figure 2), identifying it as a target for further investigation to clarify the specific signaling pathway through which AGBL4 may promote GBM tumor progression.

Microarray data revealed elevated MMP-1 expression in GBM tissues, categorized samples into high and low MMP-1 groups. Histologically, cells in the low MMP-1 group displayed uniform morphology, with regular arrangement and clear tissue structures, as confirmed by H&E staining. In contrast, the high MMP-1 group exhibited cells of varying sizes, irregular shapes, disorganized arrangement, significant nuclear atypia, and frequent mitosis, indicating a more aggressive cellular phenotype (Supplementary Figure 3A). Survival analysis displayed that patients with high MMP-1 expression had significantly shorter survival times than those with low expression (P=0.0149), indicating that MMP-1 levels are inversely correlated with GBM patient survival (Supplementary Figure 3B).

RT-PCR confirmed that compared to the U87-MG negative control (U87MG-NC group), knocking down AGBL4 (U87MG-AGBL4-KD2 group) significantly reduced the expression of MMP-1. Overexpressing MMP-1 in the AGBL4 knockdown cells (U87MG-AGBL4-KD2+MMP1-OE group) restored MMP-1 expression levels to those comparable with the control group (Figures 6A, B). Overexpression of MMP-1 on the basis of AGBL4 knockdown could counteract the inhibitory effect of AGBL4-decrease on GBM cells, which was manifested as the improvement of the proliferation capacity of AGBL4-knockdown U87-MG and A172 cells after complementing MMP-1 in CCK-8 assay (Figures 6C, D). Colony formation assays further supported this trend. Colony formation assays further supported this trend, with the MMP1-OE group demonstrating the strongest ability to form colonies. The AGBL4-KD2+MMP1-OE group's colony-forming capacity was comparable to the NC. The AGBL4-KD2 group had the least robust colony-forming ability, reinforcing the significant role of MMP-1 in GBM cell proliferation (Figures 6E–G). The Matrigel-transwell and scratch assays indicated that, the MMP1-OE group exhibited the highest levels of invation and migration, followed by the AGBL4-KD2 +MMP1-OE group, which displayed similar levels to the NC gtoup. Both of these groups exhibited enhanced capabilities compared to the AGBL4-KD2 group, which showed the lowest levels of invasion and migration (Figure 7).

TABLE 1 Candidate genes for downstream targets of AGBL4.

Candidate genes			
CDCP1	PRUNE2	AXIN2	FRAS1
MMP-1	MIAT	HSD17B6	SLITRK3

3.6 Inhibition of AGBL4 suppresses GBM progression and prolongs survival via MMP-1 in animal models

To determine the effect of AGBL4 and MMP-1 in GBM *in vivo*, we injected U87MG-NC, U87MG-AGBL4-KD2 and U87MG-AGBL4-KD2+MMP1-OE cells into nude mice (n=6). After intracranial tumor implantation, the mice were monitored every 3 days for behavioral changes and weight loss. On approximately day 15, MRI was performed to assess tumor growth when clinical symptoms were noted. The MRI data revealed that the U87MG-AGBL4-KD2 group exhibited significantly slower tumor growth compared to the U87MG-NC group. Conversely, the U87MG-AGBL4-KD2+MMP1-OE group showed accelerated tumor progression relative to the U87MG-AGBL4-KD group (Figures 8A, C). Survival analysis indicated that the U87MG-AGBL4-KD2 mice had the longest survival time, followed by the U87MG-AGBL4-KD2+MMP1-OE and U87MG-NC groups (Figure 8B). H&E staining of nude mice's brain tissues displayed that there were more mitotic figures in U87MG-NC mice, followed by U87MG-AGBL4-KD2+MMP1-OE mice, while the morphology of cells from AGBL4-KD2 mice was relatively less irregular as well as fewer mitotic figures (Figure 8D). The protein content of tumor cells in the three group of nude mice differed from one another, that is, the degree of tumor progression was quite different. The proliferation level and the malignancy degree of U87MG-NC mice and U87MG-AGBL4-KD2+MMP1-OE mice were both higher than AGBL4-KD2 mice (Figure 8E).

3.7 AGBL4-MMP-1 axis is associated with inflammatory response pathways in GBM

Enrichment analysis of AGBL4-related DEGs suggests that 3 genes, including MMP-1, FOS, and FOSB, are significantly concentrated in IL-17 signaling pathway. This may indicate that upregulated AGBL4, along with downstream MMP-1, could intervene in the progression of GBM by influencing key components within inflammation-related pathways. In the TIMER database, an immune cell correlation analysis of MMP-1, FOS, and FOSB revealed a negative correlation between MMP-1 gene expression and the infiltration levels of B cells, CD8+ T cells, CD4+ T cells, and macrophages, after purity adjustment. Conversely, a positive correlation with dendritic cell infiltration was observed. Meanwhile, FOS gene expression showed a positive

10.3389/fimmu.2024.1420182

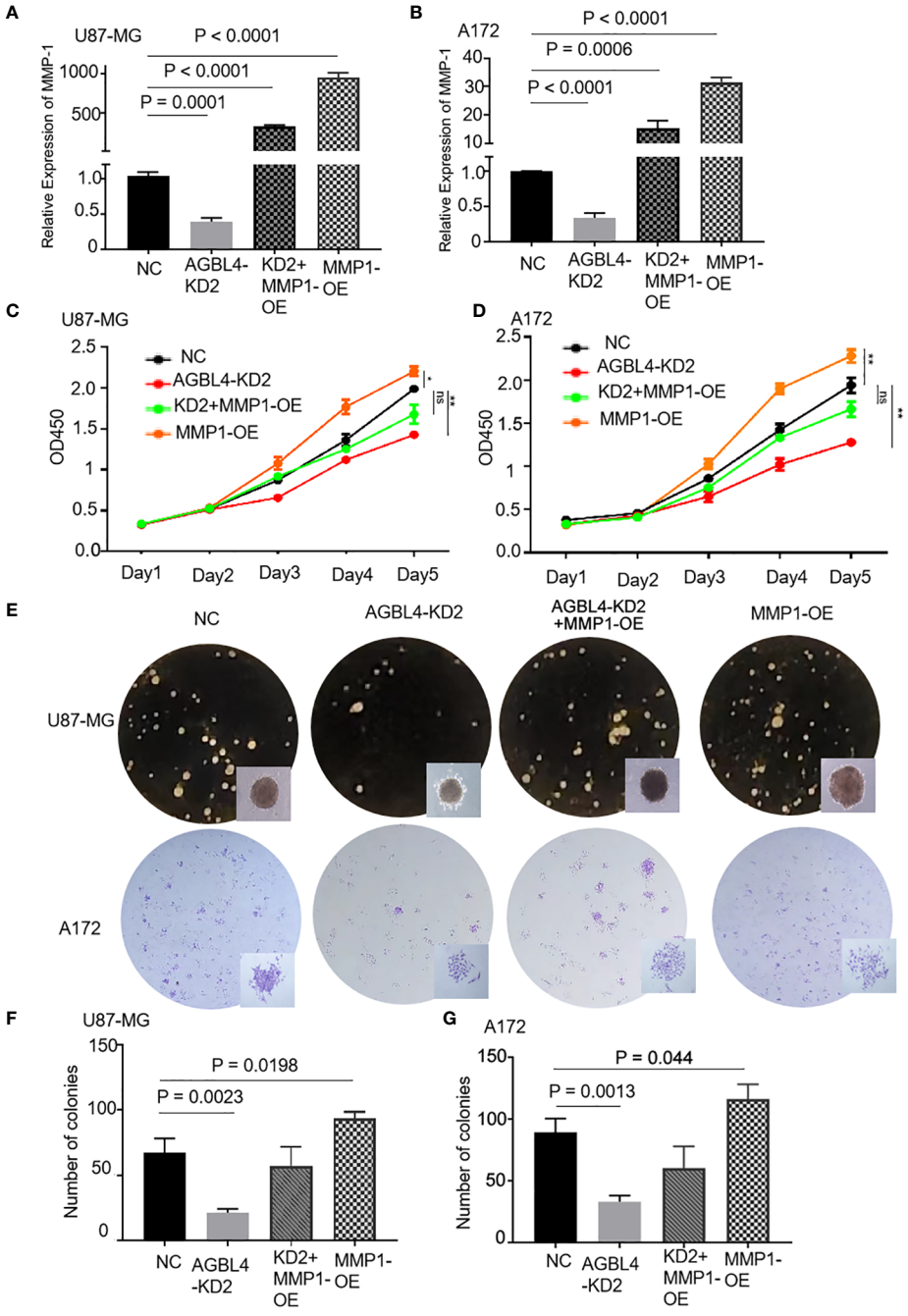

FIGURE 6
AGBL4 promotes GBM via MMP-1 and high expression of MMP-1 improves GBM cell proliferation abilities. **(A, B)** Relative expression levels of MMP-1 in NC, AGBL4-KD2, AGBL4-KD2+MMP1-OE, and MMP1-OE A172 and U87-MG cells. **(C, D)** Proliferation abilities of NC, AGBL4-KD2, AGBL4-KD2 +MMP1-OE, and MMP1-OE A172 and U87-MG cells. **(E–G)** Number of formed colonies of NC, AGBL4-KD2, AGBL4-KD2+MMP1-OE, and MMP1-OE A172 and U87-MG cells.

correlation with the infiltration levels of CD4+ T cells, neutrophils, and dendritic cell infiltration. Besides, FOSB gene expression demonstrated a negative correlation with CD4+ T cell infiltration and macrophage infiltration levels (Figure 9A). These findings suggest that the expression levels of MMP-1, FOS, and FOSB are closely related to immune cell activity in GBM, hinting at the role of these genes, particularly MMP-1, in modulating the GBM immune microenvironment.

3.8 PPI network and correlation analysis of MMP-1 and inflammatory response genes

We then constructed an interaction network integrating MMP-1 with 737 genes from the Inflammatory Response annotation cluster (GO:0006954) of GO database to identify key molecules interacting with MMP-1, which resulted in a PPI network comprising 15 nodes and 87 edges (Figure 9B). Excavation of this network yielded the top

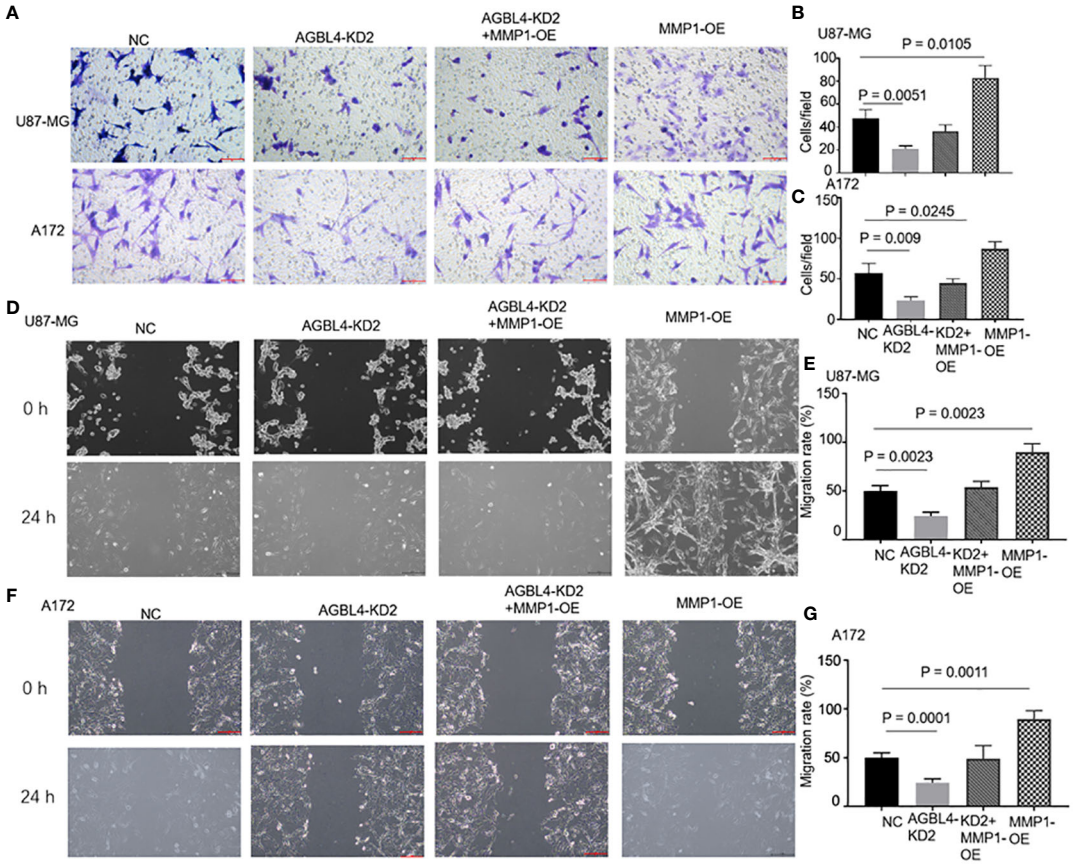

FIGURE 7
AGBL4 promotes GBM via MMP-1 and high expression of MMP-1 improves GBM cells migration and invasion abilities. **(A–C)** The numbers of invading cells in random fields of NC, AGBL4-KD2, AGBL4-KD2+MMP1-OE, and MMP1-OE A172 and U87-MG cells. **(D–G)** Migration levels of NC, AGBL4-KD2, AGBL4-KD2+MMP1-OE, and MMP1-OE A172 and U87-MG cells.

10 hub genes, which were then subjected to GO and KEGG enrichment analyses. The results, as shown in Figures 9C, D, revealed that these hub genes are predominantly localized to the cell surface, extracellular space, and extracellular region, and are involved in various inflammatory and immune regulatory processes such as the inflammatory response, positive regulation of transcription from RNA polymerase II promoter, and positive regulation of interleukin-6 production. KEGG pathway analysis also indicated significant enrichment in several pathways related to inflammation and immune responses. Collectively, these findings underscore the role of genes interacting with MMP-1 in regulating inflammatory responses, immune signal transduction, and cell proliferation, invasion, and migration, indirectly reflecting the importance of MMP-1 in maintaining tissue structure and signal transduction within the inflammatory and tumor microenvironment.

To further examine the correlation between MMP-1 expression levels and the expression of inflammatory response genes in GBM samples, we utilized data from TCGA database. The results indicated a moderate positive correlation between MMP-1 and several genes, including NFKB1, SELE, TGFB1, THBS1, TIMP1, and TNFAIP6. A weaker positive correlation was observed between MMP-1 and PTX3, STAT3, TLR2 (Supplementary Figure 4). These findings corroborate, at the expression level, the involvement of MMP-1 with these genes in certain biological processes or pathological mechanisms within GBM, particularly in pathways related to the inflammatory response.

3.9 Mutation profile and prognostic value of inflammatory response genes interacting with MMP-1

Figure 10A presents the mutation profile of the 14 inflammatory response genes that interact with MMP-1 in GBM from TCGA database. It is observed that over 10% of the samples harbor mutations in at least one of the aforementioned genes, with THBS1 exhibiting the highest mutation frequency, nearing 4%. The predominant type of mutation found in most inflammation-related genes is missense mutation. VCAM1 harbors frame shift deletions, while THBS1, VCAM1, and TGFB1 contain nonsense mutations, and NOX4 shows splice site mutations. These mutation data provide insight into the functional roles of MMP-1 and associated inflammatory response genes in GBM, suggesting they may influence protein function through alterations in amino acid sequences, premature protein translation termination, protein inactivation, or changes in protein structure, thereby affecting inflammatory and immune responses and ultimately contributing

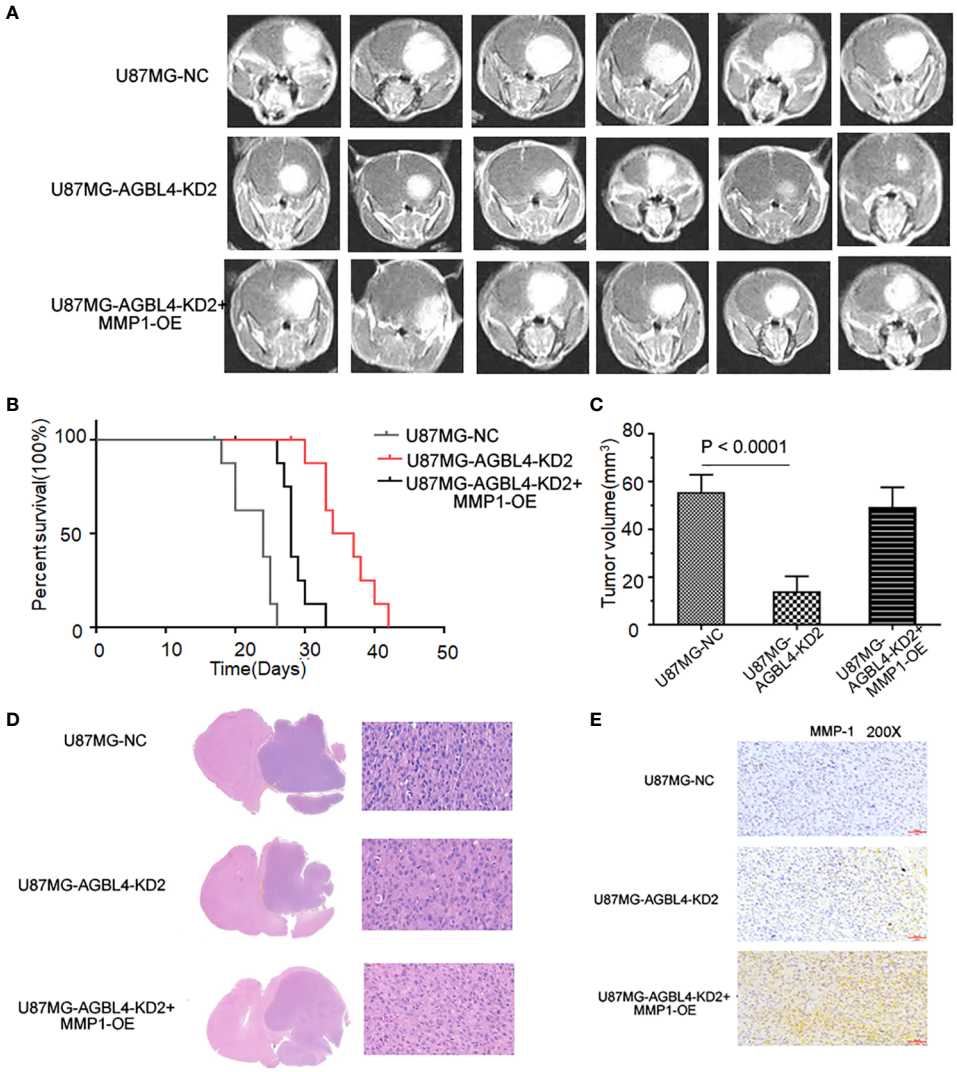

FIGURE 8
Inhibition of AGBL4 suppresses GBM progression and prolongs survival time in animal models. **(A)** MRI images showing the growth of intracranial tumors in mice implanted with U87-MG cells that are either NC, AGBL4-KD2, or AGBL4-KD2+MMP1-OE. **(B)** Kaplan-Meier survival curves of mice implanted with U87 cells that are either NC, AGBL4-KD2, or AGBL4-KD2+MMP1-OE, indicating the survival rate over time. **(C)** The quantification of tumor volumes of mice implanted with U87-MG cells that are either NC, AGBL4-KD2, or AGBL4-KD2+MMP1-OE, measured from the MRI images, with statistical significance indicated by P<0.0001. **(D)** H&E staining of intracranial tissues of the nude mice with U87MG-NC, U87MG-AGBL4-KD2, and U87MG-AGBL4-KD2+MMP1-OE. **(E)** Immunohistochemistry of intracranial tissues of the nude mice with U87MG-NC, U87MG-AGBL4-KD2, and U87MG-AGBL4-KD2+MMP1-OE (Magnification: 200×).

to tumor progression. Bioinformatic analyses of these inflammatory response genes revealed that high expression levels of THBS1 correlate with a lower overall survival rate in GBM patients (Figure 10B), implying that THBS1 may be an adverse prognostic factor. Figure 10C reconfirms the expression levels of THBS1 in GBM from TCGA database compared to normal brain tissue in GTEx database, where THBS1 is significantly overexpressed in tumor tissues. These findings may signify a detrimental role of THBS1 in the pathological process of GBM, where its elevated expression reflects more aggressive biological characteristics of the tumor and provides direction for the development of future biomarkers.

Combining immune cell correlation analysis, PPI network construction, gene mutation profiling, and correlative studies, we can tentatively conclude that the interactions among AGBL4, MMP-1, and other inflammatory response genes, especially THBS1, may constitute a complex network in the pathological process of GBM. This network potentially regulates the tumor microenvironment, influencing tumor proliferation, invasion, migration, and patient survival. These findings highlight the potential of inflammation-related factors as focal points for future research, offering the possibility to further explore the precise mechanisms of these molecules and provide critical information for the development of novel therapeutic strategies.

4 Discussion

AGBL4, also named as cytosolic carboxypeptidase 6, is part of the family of enzymes that catalyze the deglutamylation of

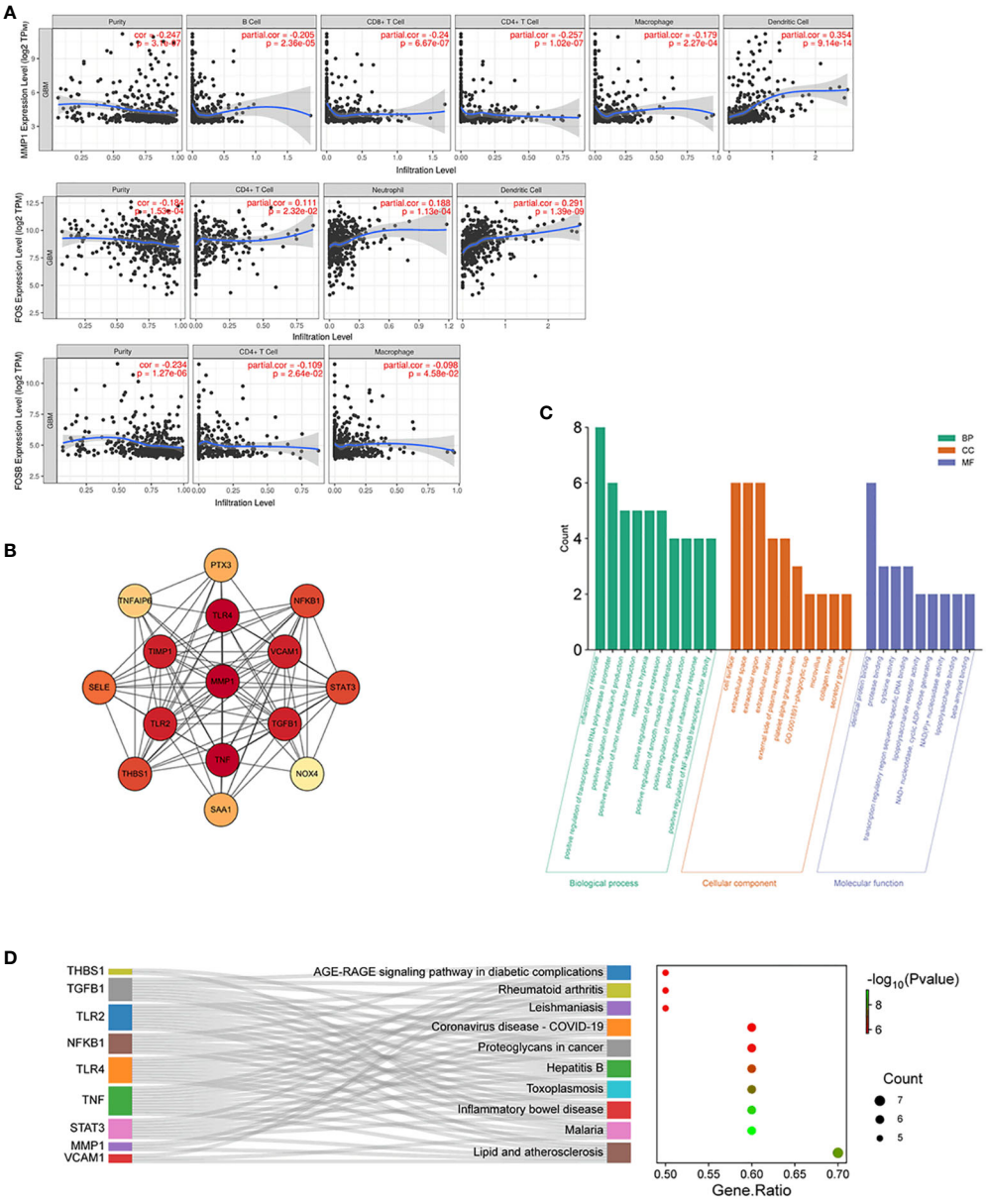

FIGURE 9
Immune cell correlation and molecular interaction analysis in GBM. **(A)** Scatter plots illustrating correlation between MMP-1, FOS, and FOSB gene expression and the infiltration levels of immune cells in GBM, adjusted for tumor purity, $P < 0.05$. **(B)** PPI network of MMP-1 with associated genes from the Inflammatory Response annotation cluster (GO:0006954), consisting of 15 nodes and 87 edges with MMP-1 centrally positioned. **(C)** GO annotations analysis for the top 10 hub genes from the PPI network. **(D)** KEGG pathway enrichment analysis for the top 10 hub genes from the PPI network, and the relationship between genes and pathways.

polyglutamate side chains on proteins such as tubulins and nucleosome assembly proteins (10). Polyglutamylation is a reversible post-translational protein modification and has been found playing a critical role in tubulin regulation as well as in cellular processes such as chromatin remodeling or hematopoiesis (10, 11). Besides, alterations in polyglutamylation levels have been associated with several pathologies, including neurodegenerative processes or cancer progression (12, 13). As a member of cytosolic carboxypeptidase family, although the role of AGBL4 in various cellular and pathological processes such as antiviral activity, immunomodulatory activity, and renal adenocarcinamo is documented (14–16), its function in central nervous system tumors, particularly GBM, has been less explored. Our study made an approach to the involvement of AGBL4 in GBM pathogenesis and its potential mechanism of action through the modulation of MMP-1.

Our finding indicate that elevated AGBL4 expression correlates with poor prognosis in GBM patients, which aligns with data from both TCGA and our tissue microarray experiments. The promotion of GBM cell proliferation, invasion, and migration by AGBL4 was substantiated through phenotypic experiments. Transcriptomic and bioinformatic analyses further revealed that AGBL4-realted DEGs

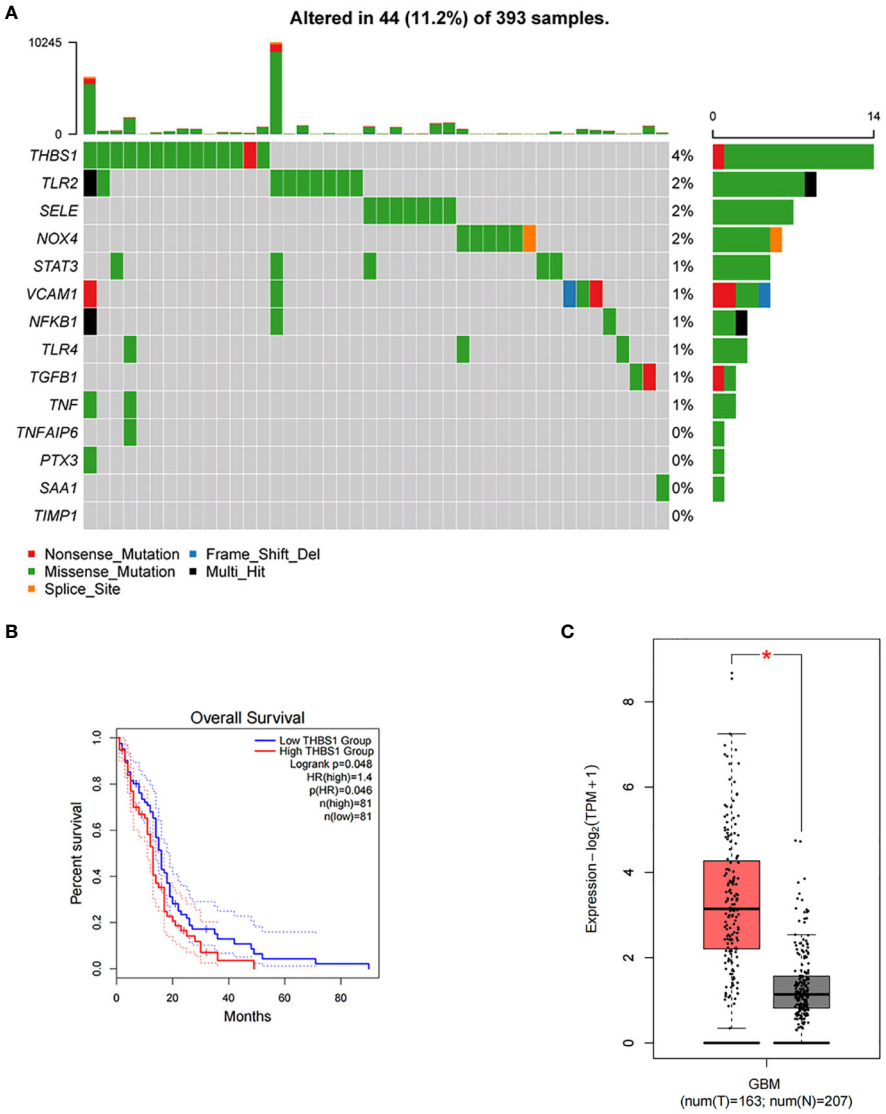

FIGURE 10
Mutational landscape of inflammatory response genes and their impact on survival in GBM. **(A)** A mutational landscape displaying the frequency and types of genetic alterations in inflammatory response genes across 393 GBM samples from TCGA with each row representing a gene, and each column a sample. Alterations, including nonsense mutations, frame shift deletions, missense mutations, multi-hit events, and splice site alterations, are color-coded. The graph on the right side indicates the percentage of samples with mutations in each gene, with the graph on the top showing the total number of mutations per sample. **(B)** Kaplan-Meier survival curves comparing overall survival between GBM patients with high and low expression of THBS1, P=0.046. **(C)** A box plot illustrating the differential expression of THBS1 between tumor (T) tissue samples in GBM patients from TCGA and normal (N) brain tissue samples from GTEx database, with the red asterisk denoting a statistically significant higher expression in the tumor samples.

were enriched in cancer-associated microRNA-related pathways and IL-17 signaling pathway, the latter being notably related to malignancy in central nervous system tumors. This suggests a possible link between AGBL4's oncogenic effects and inflammatory pathways, highlighting its role in the tumor microenvironment's immune responses.

The matrix metalloproteinase family, particularly MMP-1, known for its role in cleaving collagenous extracellular matrix (17), appears to be a critical downstream effector of AGBL4. Elevated MMP-1 expression is a hallmark of highly malignant gliomas and is implicated in enhancing tumor invasiveness and malignancy (18, 19). Pullen et al. demonstrated a regulatory pathway linking nitric oxide to high-grade glioma cell motility via MMP-1 (20). Anand et al. identified that EGFR regulates MMP-1 predominantly through the MAPK signaling pathway in GBM cells (21). Malik et al. found an association between the 2G/2G genotype and 2G allele of -1607 MMP-1 polymorphism and GBM occurrence (22). Additionally, increased MMP-1 and PAR1 expression correlates with higher histological malignancy and poorer clinical outcomes in gliomas (23). While much research has focused on MMP-1's downstream mechanisms in gliomas, its upstream regulators remain underexplored, which is crucial for understanding glioma invasiveness.

Our study not only confirms the upregulation of MMP-1 in high-grade gliomas but also identifies AGBL4 as a novel upstream

regulator of MMP-1. Existing studies on AGBL4 are relatively few and mainly focus on its role in cellular component (24), neurodegeneration (25), and immunomodulatory activities (16, 26). However, its implications in oncology, particularly in GBM, have been less explored. Our study marks a significant advancement by first identifying the differential expression of AGBL4 in GBM and verifying its negative correlation with patient survival through analysis of public databases and gene chips. This groundbreaking research links AGBL4 to the aggressive nature of central nervous system tumors at the molecular level for the first time. Further, our experimental findings underscore the critical role of AGBL4 in tumor biology, revealing that knocking down AGBL4 inhibits the proliferation, migration, and invasion of GBM cells, thertby highlighting its importance in tumor viability and progression. Importantly, this research not only pioneers the investigation of the interaction of AGBL4 with GBM, but also introduces the novel concept that AGBL4 may contribute to GBM in an MMP-1-dependent manner.

In addition, the interaction between AGBL4 and MMP-1 highlights a potential connection to the inflammatory processes within the tumor microenvironment of GBM. The upregulation of MMP-1, mediated by AGBL4, may not only promote tumor invasiveness through structural modifications but could also exacerbate inflammation, thereby creating a more conducive environment for tumor growth and spread. Our data indicates that the expression levels of MMP-1, FOS, and FOSB are closely related to immune cell activity in GBM, suggesting their pivotal roles in modulating the GBM immune microenvironment.

Our constructed PPI network, integrating MMP-1 with genes from the Inflammatory Response cluster of the GO database, identified key molecules that interact with MMP-1. These interacting genes are primarily involved in inflammatory response, positive regulation of transcription from RNA polymerase II promoter, and positive regulation of interleukin-6 production, indirectly reflecting the importance of MMP-1 in maintaining tissue structure and signal transduction within the inflammatory and tumor microenvironment.

Further analysis from TCGA database on the correlation between MMP-1 expression levels and the expression of inflammatory response genes in GBM samples showed a moderate positive correlation between MMP-1 and several genes, exemplified by THBS1, confirming the involvement of AGBL4-MMP-1 axis in GBM-related inflammatory pathways.

However, understanding the molecular pathogenesis of GBM remains a challenge. It is speculated that AGBL4 and MMP-1 may contribute to the occurrence, development, and spread of GBM, but the specific mechanism and interactions between AGBL4 and MMP-1 still require further investigation.

5 Conclusion

In summary, this study demonstrates that AGBL4 expression in GBM is upregulated and links with poor prognosis of GBM patients by enhancing tumor cell proliferation, migration, and invasion. Our findings reveal a novel mechanistic pathway where AGBL4 enhances GBM malignancy primarily through modulation of MMP-1 expression, which in turn influences the inflammatory response pathways within the tumor microenvironment (Figure 11). The identification of AGBL4 and MMP-1 not only deepens our understanding of the molecular dynamics of GBM but also highlights their involvement in inflammatory processes that

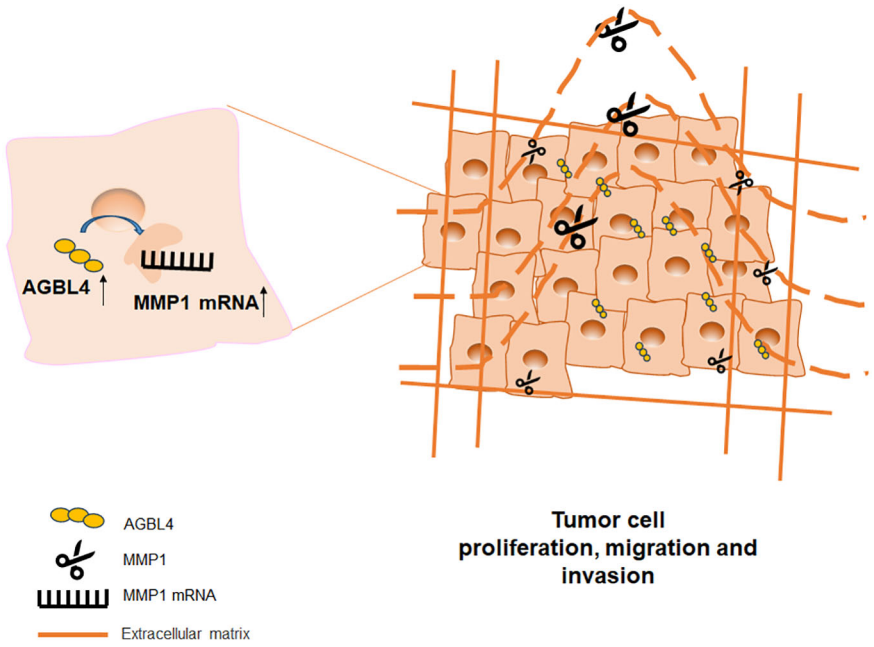

FIGURE 11
Model for the mechanism of AGBL4 in GBM tumorigenesis.

may contribute to tumor aggressiveness, suggesting the potential of AGBL4 and MMP-1 as strategic targets for gene-directed therapy, as well as advocating for the development of targeted inhibitors against these proteins as a promising new direction for therapeutic intervention in glioma treatment.

Data availability statement

The datasets presented in this study can be found in online repositories. The names of the repository/repositories and accession number(s) can be found below: GSA-Human: HRA003631 (Genome Sequence Archive in the National Genomics Data Center, China National Center for Bioinformation / Beijing Institute of Genomics, Chinese Academy of Sciences, https://ngdc.cncb.ac.cn/gsa-human).

Ethics statement

The studies involving humans were approved by the Ethical Committee of Changhai Hospital, Naval Medical University. The studies were conducted in accordance with the local legislation and institutional requirements. The participants provided their written informed consent to participate in this study. The animal study was approved by the Institutional Animal Care and Use Committee of Changhai Hospital, Naval Medical University. The study was conducted in accordance with the local legislation and institutional requirements.

Author contributions

SZ: Writing – review & editing, Conceptualization, Data curation, Formal analysis, Investigation, Methodology, Writing – original draft, Visualization. LC: Visualization, Writing – review & editing, Data curation, Formal analysis, Investigation, Methodology, Software, Writing – original draft. YS: Writing – review & editing, Data curation, Formal analysis, Software, Supervision, Visualization, Writing – original draft. ZQ: Writing – review & editing, Data curation, Formal analysis, Investigation, Software, Writing – original draft, Resources. ZW: Software, Supervision, Visualization, Writing – review & editing, Validation. CC: Software, Supervision, Writing – review & editing, Validation. RL: Writing – review & editing, Formal analysis, Investigation. AZ: Software, Writing – review & editing, Formal analysis. JH: Validation, Writing – review & editing, Visualization. JM: Supervision, Writing – review & editing, Software. HW: Writing – review & editing, Conceptualization, Data curation, Project administration, Supervision, Validation, Visualization. JC: Conceptualization, Funding acquisition, Methodology, Project administration, Resources, Supervision, Validation, Writing – review & editing.

Funding

The author(s) declare financial support was received for the research, authorship, and/or publication of this article. This study was supported by National Natural Science Foundation of China (Nos. 82003222).

Acknowledgments

The authors wish to express sincere gratitude to the technical staff of Naval Medical University for providing the necessary facilities and resources for conducting our experiments.

Conflict of interest

The authors declare that the research was conducted in the absence of any commercial or financial relationships that could be construed as a potential conflict of interest.

Publisher's note

Supplementary material

The Supplementary Material for this article can be found online at: https://www.frontiersin.org/articles/10.3389/fimmu.2024.1420182/full#supplementary-material

References

1. Ostrom QT, Price M, Neff C, Cioffi G, Waite KA, Kruchko C, et al. CBTRUS statistical report: primary brain and other central nervous system tumors diagnosed in the United States in 2015–2019. *Neuro-oncology*. (2022) 24:v1–v95. doi: 10.1093/neuonc/noac202

2. Barnholtz-Sloan JS, Ostrom QT, Cote D. Epidemiology of brain tumors. *Neurologic Clinics*. (2018) 36:395–419. doi: 10.1016/j.ncl.2018.04.001

3. Ostrom QT, Bauchet L, Davis FG, Deltour I, Fisher JL, Langer CE, et al. The epidemiology of glioma in adults: a "state of the science" review. *Neuro-oncology*. (2014) 16:896–913. doi: 10.1093/neuonc/nou087

4. Louis DN, Perry A, Wesseling P, Brat DJ, Cree IA, Figarella-Branger D, et al. The 2021 WHO classification of tumors of the central nervous system: a summary. *Neuro-oncology*. (2021) 23:1231–51. doi: 10.1093/neuonc/noab106

5. Hwang B, Lee JH, Bang D. Single-cell RNA sequencing technologies and bioinformatics pipelines. *Exp Mol Med*. (2018) 50:1–14. doi: 10.1038/s12276-018-0071-8

6. Lei Y, Tang R, Xu J, Wang W, Zhang B, Liu J, et al. Applications of single-cell sequencing in cancer research: progress and perspectives. *J Hematol Oncol*. (2021) 14:91. doi: 10.1186/s13045-021-01105-2

7. Pan H, Yang M, Lu L, Tao B, He X, Chen H, et al. Association of FAM65B, AGBL4, and CUX2 genetic polymorphisms with susceptibility to antituberculosis drug-induced hepatotoxicity: validation study in a Chinese Han population. *Pharmacogenetics Genomics*. (2019) 29:84–90. doi: 10.1097/FPC.0000000000000370

8. Guo T, Yin R-X, Yao L-M, Huang F, Pan L, Lin W-X, et al. Integrative mutation, haplotype and G× G interaction evidence connects ABGL4, LRP8 and PCSK9 genes to cardiometabolic risk. *Sci Rep*. (2016) 6:37375. doi: 10.1038/srep37375

9. Lin P-C, Lin J-K, Lin C-H, Lin H-H, Yang S-H, Jiang J-K, et al. Clinical relevance of plasma DNA methylation in colorectal cancer patients identified by using a genome-wide high-resolution array. *Ann Surg Oncol*. (2015) 22:1419–27. doi: 10.1245/s10434-014-4277-2

10. Rodriguez-Calado S, Van Damme P, Avilés FX, Candiota AP, Tanco S, Lorenzo J. Proximity mapping of CCP6 reveals its association with centrosome organization and cilium assembly. *Int J Mol Sci*. (2023) 24:1273. doi: 10.3390/ijms24021273

11. Ruse CI, Chin HG, Pradhan S. Polyglutamylation: biology and analysis. *Amino Acids*. (2022) 54:529–42. doi: 10.1007/s00726-022-03146-4

12. Shashi V, Magiera MM, Klein D, Zaki M, Schoch K, Rudnik-Schöneborn S, et al. Loss of tubulin deglutamylase CCP 1 causes infantile-onset neurodegeneration. *EMBO J*. (2018) 37:e100540. doi: 10.15252/embj.2018100540

13. Wang L-L, Jin X-H, Cai M-Y, Li H-G, Chen J-W, Wang F-W, et al. AGBL2 promotes cancer cell growth through IRGM-regulated autophagy and enhanced Aurora A activity in hepatocellular carcinoma. *Cancer Lett*. (2018) 414:71–80. doi: 10.1016/j.canlet.2017.11.003

14. Li C, Wang J, Hao J, Dong B, Li Y, Zhu X, et al. Reduced cytosolic carboxypeptidase 6 (CCP6) level leads to accumulation of serum polyglutamylated DNAJC7 protein: A potential biomarker for renal cell carcinoma early detection. *Oncotarget*. (2016) 7:22385. doi: 10.18632/oncotarget.v7i16

15. Xia P, Ye B, Wang S, Zhu X, Du Y, Xiong Z, et al. Glutamylation of the DNA sensor cGAS regulates its binding and synthase activity in antiviral immunity. *Nat Immunol*. (2016) 17:369–78. doi: 10.1038/ni.3356

16. Serrano I, Luque A, Mitjavila F, Blom AM, Rodríguez de Córdoba S, Vega MC, et al. The hidden side of complement regulator C4BP: dissection and evaluation of its immunomodulatory activity. *Front Immunol*. (2022) 13:883743. doi: 10.3389/fimmu.2022.883743

17. Jabłońska-Trypuć A, Matejczyk M, Rosochacki S. Matrix metalloproteinases (MMPs), the main extracellular matrix (ECM) enzymes in collagen degradation, as a target for anticancer drugs. *J Enzyme inhibition medicinal Chem*. (2016) 31:177–83. doi: 10.3109/14756366.2016.1161620

18. Oldak L, Chludzinska-Kasperuk S, Milewska P, Grubczak K, Reszec J, Gorodkiewicz E. MMP-1, UCH-L1, and 20S proteasome as potential biomarkers supporting the diagnosis of brain glioma. *Biomolecules*. (2022) 12:1477. doi: 10.3390/biom12101477

19. Tomko N, Kluever M, Wu C, Zhu J, Wang Y, Salomon RG. 4-Hydroxy-7-oxo-5-heptenoic acid lactone is a potent inducer of brain cancer cell invasiveness that may contribute to the failure of anti-angiogenic therapies. *Free Radical Biol Med*. (2020) 146:234–56. doi: 10.1016/j.freeradbiomed.2019.11.009

20. Pullen NA, Fillmore HL. Induction of matrix metalloproteinase-1 and glioma cell motility by nitric oxide. *J Neuro-oncology*. (2010) 96:201–9. doi: 10.1007/s11060-009-9965-6

21. Anand M, Van Meter T, Fillmore H. Epidermal growth factor induces matrix metalloproteinase-1 (MMP-1) expression and invasion in glioma cell lines *via* the MAPK pathway. *J neuro-oncology*. (2011) 104:679–87. doi: 10.1007/s11060-011-0549-x

22. Malik N, Kumar R, Prasad KN, Kawal P, Srivastava A, Mahapatra AK. Association of matrix metalloproteinase-1 gene polymorphism with glioblastoma multiforme in a northern Indian population. *J neuro-oncology*. (2011) 102:347–52. doi: 10.1007/s11060-010-0337-z

23. Zhang Y, Zhan H, Xu W, Yuan Z, Lu P, Zhan L, et al. Upregulation of matrix metalloproteinase-1 and proteinase-activated receptor-1 promotes the progression of human gliomas. *Pathology-Research Pract*. (2011) 207:24–9. doi: 10.1016/j.prp.2010.10.003

24. Wang Y, Zhang Y, Guo X, Zheng Y, Zhang X, Feng S, et al. CCP5 and CCP6 retain CP110 and negatively regulate ciliogenesis. *BMC Biol*. (2023) 21:124. doi: 10.1186/s12915-023-01622-1

25. Rogowski K, Van Dijk J, Magiera MM, Bosc C, Deloulme J-C, Bosson A, et al. A family of protein-deglutamylating enzymes associated with neurodegeneration. *Cell*. (2010) 143:564–78. doi: 10.1016/j.cell.2010.10.014

26. Ye B, Li C, Yang Z, Wang Y, Hao J, Wang L, et al. Cytosolic carboxypeptidase CCP6 is required for megakaryopoiesis by modulating Mad2 polyglutamylation. *J Exp Med*. (2014) 211:2439–54. doi: 10.1084/jem.20141123

frontiers | Frontiers in Immunology

TYPE Original Research
PUBLISHED 16 July 2024
DOI 10.3389/fimmu.2024.1440262

OPEN ACCESS

EDITED BY
Wen-Hui Wu,
Tongji University, China

REVIEWED BY
Xiaoli Zhao,
Nanjing Medical University, China
Shuyuan Xue,
Northwest University, China
Qinghua Yang,
Zhengzhou University, China

*CORRESPONDENCE
Hu Zhao
zxj1204@163.com
Chaoyan Yue
20111250007@fudan.edu.cn

†These authors have contributed equally to this work

RECEIVED 29 May 2024
ACCEPTED 04 July 2024
PUBLISHED 16 July 2024

CITATION
Cao C, Li Q, Cai D, Yue C and Zhao H (2024) Causal effect of COVID-19 on optic nerve and visual pathway disorders: genetic evidence of lung-brain axis.
Front. Immunol. 15:1440262.
doi: 10.3389/fimmu.2024.1440262

Causal effect of COVID-19 on optic nerve and visual pathway disorders: genetic evidence of lung-brain axis

Chunge Cao [1†], Qiong Li [2†], Dajun Cai [1], Chaoyan Yue [3*] and Hu Zhao [1*]

[1]Department of Obstetrics and Gynecology, Second Affiliated Hospital of Zhengzhou University, Zhengzhou, China, [2]Department of Obstetrics and Gynecology, First People's Hospital of Chenzhou, Chenzhou, China, [3]Department of Laboratory Medicine, Obstetrics and Gynecology Hospital of Fudan University, Shanghai, China

Purpose: To investigate the potential causal association between COVID-19 exposure and optic nerve and visual pathway disorders through a two-sample bidirectional Mendelian randomization (MR) analysis, and to provide empirical support for the lung-brain axis.

Methods: This MR analysis utilized publicly accessible summary-level data from genome-wide association studies on COVID-19 (n=158,783) and optic nerve and visual pathway diseases (n=412,181), primarily involving individuals of European descent. The random-effect inverse-variance weighted estimation was applied as the main analytical approach, complemented by MR-Egger, weighted median, and weighted mode methods. The heterogeneity and pleiotropy of the instrumental variables were assessed using Cochran's Q test, leave-one-out sensitivity analysis, MR-Egger intercept test, MR-PRESSO, and funnel plot evaluations.

Results: In the forward analysis, the inverse-variance weighted method identified a significant causal effect of COVID-19 on optic nerve and visual pathway disorders (odds ratio = 1.697, 95% confidence interval: 1.086–2.652, p = 0.020). Directionally consistent results were also observed with MR-Egger regression, weighted median, and weighted mode approaches. Conversely, the reverse analysis revealed no causal effects of optic nerve and visual pathway disorders on COVID-19 susceptibility.

Conclusion: Our findings suggest that COVID-19 exposure may increase the risk of developing optic nerve and visual pathway disorders, supporting the lung-brain axis hypothesis. These results underscore the importance of vigilant monitoring of the visual system in patients recovering from COVID-19 and suggest potential avenues for future therapeutic strategies.

KEYWORDS

COVID-19, optic nerve, visual pathways, Mendelian randomization, lung-brain axis

Introduction

The COVID-19 pandemic has triggered a worldwide health emergency with far-reaching repercussions, surpassing the initial respiratory symptoms to include prolonged neurological complications, often termed 'long COVID' (1). Observational studies have potentially shown that COVID-19 can lead to disorders of optic nerve and visual pathways, including uveitis, optic neuritis, macular degeneration, and retinal vascular diseases (2, 3). These conditions may manifest as a variety of symptoms, such as vision loss, visual field defects, reduced sensitivity to light and contrast, as well as alterations in color perception (4).

The burgeoning concept of the lung-brain axis delineates a sophisticated biological network facilitating communication between the lungs and brain via neural, inflammatory, immune, and neuroendocrine signaling pathways (5). The central nervous system (CNS) plays a critical role in modulating the pulmonary response to stress and inflammation through neuroendocrine mechanisms (6). Brain injuries may provoke pulmonary complications by eliciting the release of necrotic substances (7), while pulmonary conditions have the potential to instigate cerebrovascular diseases through the induction of white matter lesions (8). Additionally, the significant influence of the lung microbiome on brain autoimmunity has been increasingly acknowledged (9). This reciprocal communication highlights the symbiotic interplay between respiratory and neurological health. Early hypotheses suggested that the SARS-CoV-2 might penetrate the CNS via the nasal cavity and olfactory pathway or the blood-brain barrier (BBB) (10, 11). However, cerebrospinal fluid analyses in patients presenting neuropsychiatric symptoms have revealed minimal detection of viral RNA, with only 8.6% (3 out of 35) identified through reverse transcription polymerase chain reaction (12). This suggests that neurological symptoms do not typically result from direct SARS-CoV-2 infection of the brain tissue.

Although there has been considerable research, the connection between COVID-19 and optic nerve or visual pathway disorders is yet to be conclusively proven, hindered by insufficient large-scale cohort studies and conclusive evidence. Concurrently, the varied symptoms experienced by individuals with Long COVID, coupled with the challenge of distinguishing symptoms caused by COVID-19 from those that are aggravations of existing or sporadic illnesses, significantly complicate the understanding of underlying mechanisms and the development of therapeutic strategies.

Mendelian randomization (MR) is an innovative approach in epidemiology, utilizing genetic variants as proxies for deducing the causal impact of various exposures on outcomes (13). These genetic markers are randomly segregated and allocated during the formation of gametes and at conception, remaining uninfluenced by the development or progression of the outcome (14). As a result, MR typically protects against biases and unmeasured confounding factors, providing a more robust basis for causal deduction than is possible with traditional observational studies (15). In this study, we aim to investigate the causal link between COVID-19 and disorders of optic nerve and visual pathways through the MR method, to assess its impact size, and to furnish evidence supporting the lung-brain axis hypothesis.

Materials and methods

Study design

Figure 1 depicts a graphical abstract illustrating the bidirectional MR study. The forward MR assessed the causal effect of COVID-19 on disorders of optic nerve and visual pathways. The reverse MR assessed the causal effect of optic nerve and visual pathway disorders on COVID-19 susceptibility. This study used datasets from extensive genome-wide association studies (GWAS). Single-nucleotide polymorphisms (SNPs) from these GWAS datasets served as instrumental variables (IVs) for the exposure. The MR analysis is based on three critical assumptions: firstly, the IVs are strongly associated with the exposure; secondly, the IVs are related to the outcome solely through the exposure under investigation; and thirdly, the IVs are independent of any confounding factors (16). This research employed publicly accessible, summary-level GWAS data from studies that had previously received institutional review board approval. Additional ethical approval or informed consent was not requisite for this study's data usage, given its public, anonymized, and de-identified nature.

Data sources

The GWAS datasets for COVID-19 (GWAS ID: ebi-a-GCST011071) and optic nerve and visual pathway disorders (GWAS ID: finn-b-H7_OPTNERVE) came from the IEU Open GWAS Project. The COVID-19 dataset included 29,071 cases and 1,559,712 controls, with a total of 8,103,014 SNPs. The dataset for optic nerve and visual pathway disorders comprised 1,301 cases and 217,491 controls, encompassing 16,380,466 SNPs. The majority of participants in both GWAS datasets were of European descent.

Selection of IVs

We first selected SNPs that were strongly associated with the exposure, using a genome-wide significance threshold of $p < 5e\text{-}08$. To ensure a sufficient number of SNPs for the exposure, we allowed for a relaxed threshold of $p < 5e\text{-}07$ or $p < 5e\text{-}06$. We used the European ancestry data from the 1000 Genomes Project (RRID: SCR_008801) and employed stringent clumping parameters with a distance greater than 10,000 kb and an ($r^2 < 0.001$) to minimize linkage disequilibrium among the variables. To enhance the accuracy of our results, we excluded palindromic SNPs with intermediate allele frequencies. Potential confounders were identified and removed by querying the PhenoScanner V2 database for SNPs associated with possible confounding factors. Weak IVs were discarded using the F statistic to ensure a robust association between the exposure factors and the IVs. The F statistic was determined by the squared beta coefficient divided by its variance for the SNP-exposure association, with an F statistic greater than 10 indicating a strong association (17).

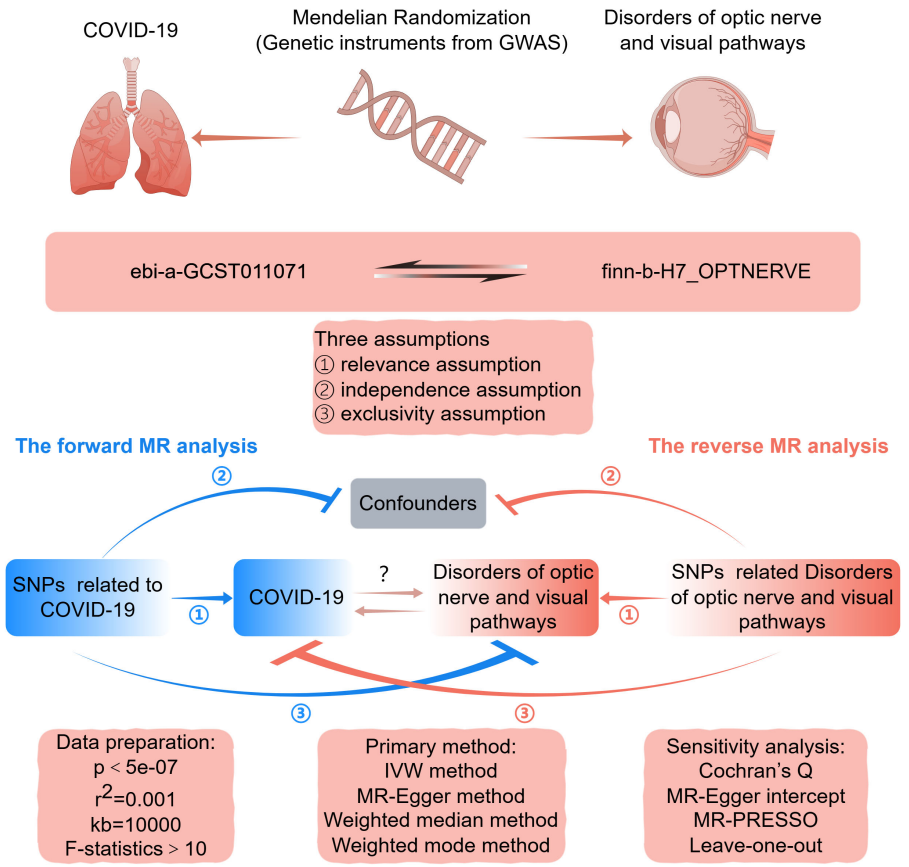

FIGURE 1
Graphical abstract for this MR study between COVID-19 and disorders of optic nerve and visual pathways. GWAS, genome-wide association study; MR, Mendelian randomization; SNP, single nucleotide polymorphism; IVW, inverse-variance weighted. By FigDraw.

MR analysis

Assessing the causal link between COVID-19 and disorders of optic nerve and visual pathways, we employed four MR methods: the random-effect inverse-variance weighted (IVW) estimation method, MR-Egger regression method, weighted-median estimator method, and weighted mode-based method. The IVW method, when directional pleiotropy is absent, offers a more stable and precise estimation of causal effects by integrating the Wald ratio estimates from each instrumental variant (18, 19). Consequently, IVW served as the primary method for this study, while the other three methods served as supplementary analyses. Consistent results across all four methods bolster the credibility of the causality estimates. In cases of discrepancy, the IVW outcome is given precedence as the principal finding. However, we consider the IVW results reliable only if they are directionally concordant with the findings of the supplementary methods.

Sensitivity analysis

The Cochran's Q test was applied to assess the heterogeneity among IVs, with a *p*-value below 0.05 indicating significant heterogeneity. A leave-one-out sensitivity analysis was performed to ensure no single SNP disproportionately influenced the causal estimate. This involved sequentially discarding each SNP associated with the exposure and repeating the IVW analysis to verify the stability of the causal effects of each SNP. The MR-Egger intercept test was employed to detect and adjust for bias from directional pleiotropy; a non-zero intercept suggests the presence of such bias (20). Additionally, the MR-PRESSO method was employed to identify and correct for horizontal pleiotropy; a global test resulting in a *p*-value under 0.05 signifies horizontal pleiotropy between IVs and outcomes; the outlier test pinpoints SNPs that may be outliers, potentially violating MR assumptions, necessitating their exclusion from the analysis (21).

Statistical analysis

The MR analysis used TwoSampleMR (version 4.3.1), an R statistical software package that facilitates the two-sample MR approach. Causal estimates were presented as odds ratios (ORs) with 95% confidence intervals (CIs). Statistical significance was determined by a two-tailed p-value of less than 0.05.

Results

Genetic instruments and strength

In our bidirectional analysis, we identified nine SNPs significantly associated with COVID-19, showing a genome-wide significance threshold of p<5e-07, and fourteen SNPs linked to disorders of optic nerve and visual pathways, with a threshold of p<5e-06. These associations were established after linkage disequilibrium clumping, data harmonization, and mining of the Phenoscanner V2 database, as detailed in Supplementary Tables 1, 2. The F-statistics for each SNP were above 10, indicating a negligible risk of weak instrument bias.

The causal effect of COVID-19 on optic nerve and visual pathway disorders

Figure 2 illustrates the causal relationship between COVID-19 and the incidence of optic nerve and visual pathway disorders. The IVW method indicates a notable causal influence of COVID-19 on optic nerve and visual pathway disorders, with an OR of 1.697 and a 95% CI ranging 1.086 to 2.652 (p = 0.020). Complementary methods, including MR-Egger, Weighted Median, and Weighted Mode, yielded directionally consistent but not statistically significant results compared to IVW. The robustness of these findings is supported by sensitivity analyses presented in Table 1 and Figure 3. Cochran's Q test indicates uniformity across SNP effect estimates (p = 0.841), and the MR-Egger intercept negates the presence of directional pleiotropy (intercept = -0.039, p = 0.495). The MR-PRESSO test also finds no evidence of horizontal pleiotropy or outliers (p = 0.866), and the leave-one-out analysis substantiates the consistency of our results.

The causal effect of optic nerve and visual pathway disorders on COVID-19

As shown in Figure 2, the IVW analysis suggests that optic nerve and visual pathway disorders do not causally affect COVID-19 susceptibility (OR = 0.991, 95% CI: 0.969-1.012; p = 0.429). This finding is supported by MR-Egger, Weighted Median, and Weighted Mode methods. Detailed in Table 1 and Figure 4, the sensitivity analyses affirm the reliability of our conclusions. Cochran's Q test confirms no variability among the SNP effect estimates (p = 0.967), and the MR-Egger intercept indicates an absence of directional pleiotropy (Intercept = -0.001, p = 0.835). Additionally, the MR-PRESSO test reveals no horizontal pleiotropy or outliers (p = 0.967), and the leave-one-out test reinforces the dependability of our findings.

Discussion

In this study, we employed a two-sample bidirectional MR approach to explore the relationship between COVID-19 and disorders of optic nerve and visual pathways. The forward results provide compelling genetic evidence that COVID-19 may increase the risk of disorders of optic nerve and visual pathways. The reverse results show that disorders of optic nerve and visual pathways have no causal effect on COVID-19 susceptibility. Sensitivity analyses have reinforced the robustness of our results.

Our research has unearthed critical insights that could be transformative for clinical practice and public health policy. These findings highlight a significant correlation between viral infections and an increased risk of optic nerve and visual pathway disorders. Such knowledge is vital for physicians, enabling them to diagnose and treat these conditions more proactively, which may lead to better patient outcomes. Moreover, our study supports the need for public health authorities to intensify visual health monitoring and preventive actions during the pandemic, with a particular focus on vulnerable groups. Educating the public and patients about the ocular risks linked to COVID-19 is essential, as it encourages early medical intervention when symptoms are detected. This research also marks a pivotal step in understanding the lung-brain axis, potentially reshaping our comprehension of how respiratory infections influence neurological health. It paves the way for further investigations into the specific mechanisms by which COVID-19 impacts the optic nerve and visual pathways, spurring the creation of novel prophylactic and therapeutic approaches. In addition, these discoveries could be instrumental in guiding the development of vaccines and shaping public health strategies aimed at mitigating the long-term sequelae of COVID-19.

A comprehensive retrospective case-control study involving 2,351 patients revealed a notable increase in immune-mediated ocular conditions like uveitis and optic neuritis, potentially linked to

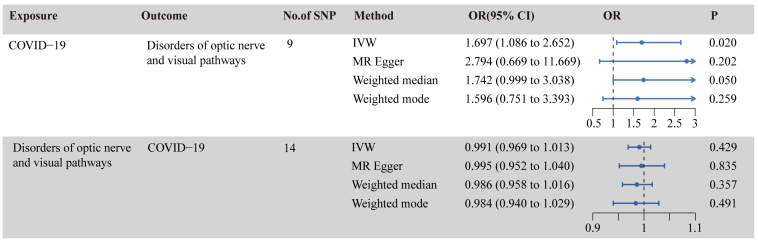

FIGURE 2
Causal relationship between COVID-19 and disorders of optic nerve and visual pathways in the MR analyses. SNPs, single-nucleotide polymorphisms; OR, odds ratio; CI, confidence interval; IVW, inverse-variance weighted; MR, Mendelian randomization.

TABLE 1 Results of pleiotropy and heterogeneity analyses.

Exposure	Outcome	Cochran's Q test		MR-Egger test		MR-PRESSO test	
		IVW Q	*p*-value	Intercept	*p*-value	Global test *p*	Outliers
COVID-19	Disorders of optic nerve and visual pathways	4.177	0.841	-0.039	0.495	0.866	None
Disorders of optic nerve and visual pathways	COVID-19	5.336	0.967	-0.001	0.835	0.967	None

IVW, inverse-variance weighted; SNPs, single-nucleotide polymorphisms.

COVID-19 (2). Concurrently, an observational cross-sectional study indicated that patients with neurological symptoms of COVID-19 exhibited a decrease in the thickness of the retinal nerve fiber layer and ganglion cell complex, as well as a reduced vessel density (22). In contrast, other research indicated an elevation in the thickness of the retinal nerve fiber layer, implying potential inflammation of the optic nerve or temporary alterations during acute COVID-19 infection (23). Additionally, a separate study observed increased intraocular pressure and specific changes in the outer retina in severe cases 80 days post-COVID-19 infection, although no evidence of uveitis was detected (24). The discrepancies observed across these studies could be attributed to a variety of

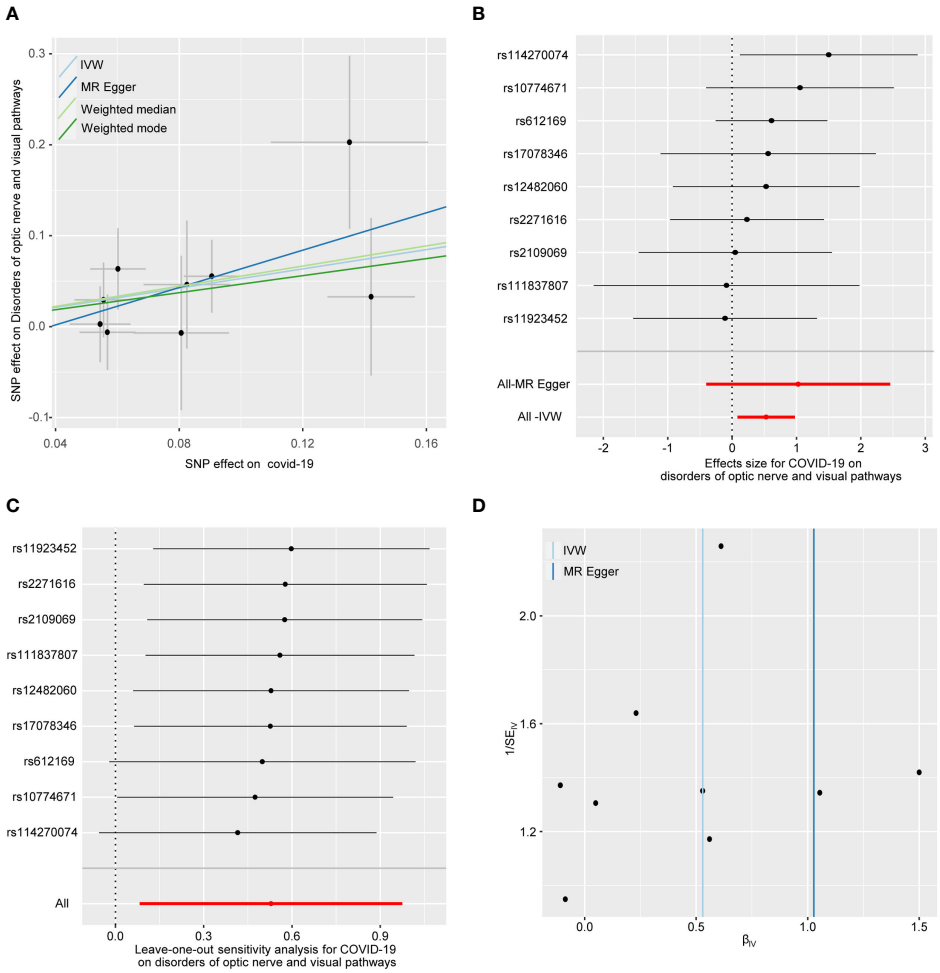

FIGURE 3
The forward MR analyses: Casual effect of COVID-19 on disorders of optic nerve and visual pathways. **(A)** Scatter plot of the association between COVID-19 and disorders of optic nerve and visual pathways. **(B)** Forest plot to show the causal effect size estimate of COVID-19 on disorders of optic nerve and visual pathways (red line segment) and 95% CI values (gray line segment) for each SNP. **(C)** Leave-one-out analyses to evaluate the impact of each SNP on the overall result. **(D)** Funnel plot to detect obvious heterogeneity and system bias. IVW, inverse variance weighted; SNPs, single-nucleotide polymorphisms.

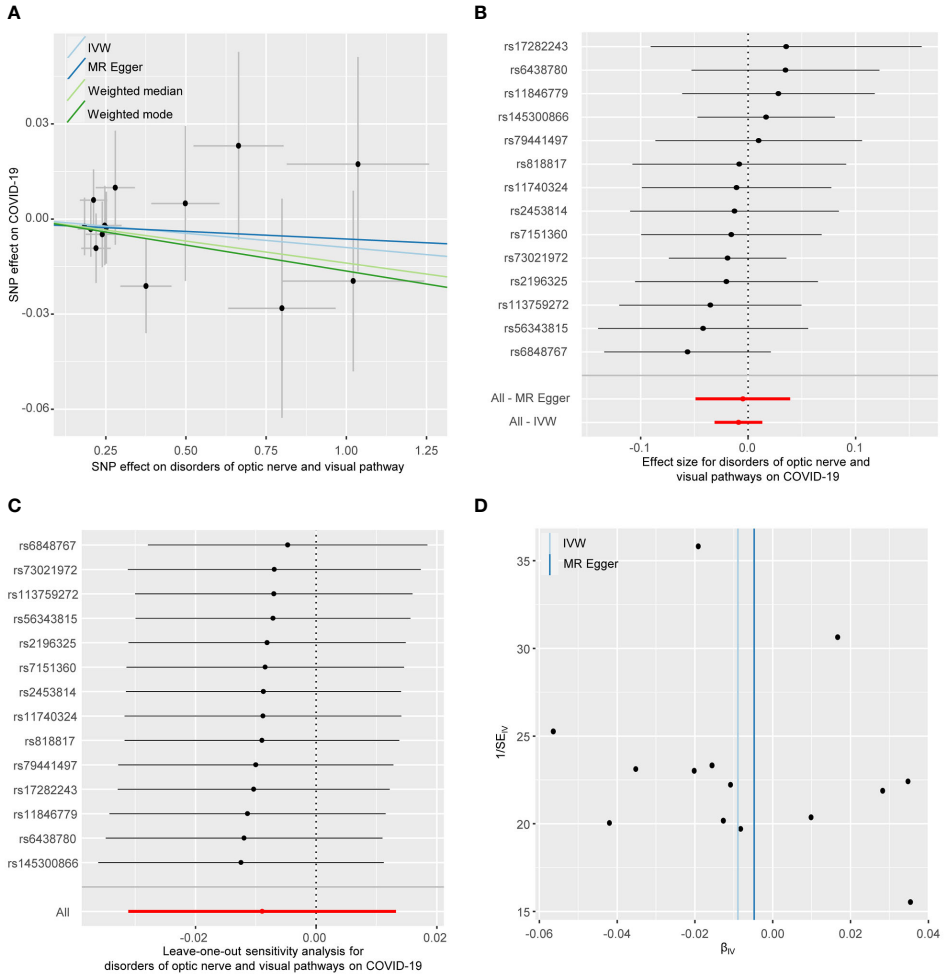

FIGURE 4
The reverse MR analyses: Casual effect of disorders of optic nerve and visual pathways on COVID-19. **(A)** Scatter plot of the association between disorders of optic nerve and visual pathways and COVID-19. **(B)** Forest plot to show the causal effect size estimate of disorders of optic nerve and visual pathways on COVID-19 (red line segment) and 95% CI values (gray line segment) for each SNP. **(C)** Leave-one-out analyses to evaluate the impact of each SNP on the overall result. **(D)** Funnel plot to detect obvious heterogeneity and system bias. IVW, inverse variance weighted; SNPs, single-nucleotide polymorphisms.

factors, including study design, methodological variances, sample size differences, reporting biases, the timing of assessments, the expertise of the investigators, the specific definitions of disorders, and the level of control over confounding variables.

Several host receptors facilitate the entry of SARS-CoV-2 into human cells, with the angiotensin-converting enzyme 2 (ACE2) receptor being paramount. The viral spike protein (S protein) binds to ACE2, triggering the cleavage of the S protein into S1 and S2 subunits. The S1 subunit, containing the receptor binding domain, attaches to ACE2, and subsequent cleavage of the S2 subunit by host proteases facilitates membrane fusion and viral entry (25). Multiple tissues including mucosa of the nose, mouth, and eyes, respiratory tract, lungs, heart, liver, kidney, brain, gastrointestinal tract, placenta, and other organs express ACE2 with a high level (10). Current researches indicate that SARS-CoV-2 could invade the human brain through multiple pathways (26). Initially, the virus may progress from the nasal cavity to the olfactory bulb via olfactory nerves. Secondly, the virus might access the bloodstream via damaged respiratory epithelium and proceed to penetrate the BBB, utilizing ACE2-mediated transcellular pathways or disrupting the barrier's tight-junctions. Lastly, the virus has the potential to invade ocular tissues and navigate along the optic nerve to the occipital cortex. However, CSF testing in patients with COVID-19 to find evidence of viral neuroinvasion by SARS-CoV-2 showed that of 304 patients whose CSF was tested for SARS-CoV-2 viral RNA, there were 17 (6%) whose test was positive, all of whom had symptoms that localized to the CNS, of 58 patients whose CSF was tested for SARS-CoV-2 antibody, 7 (12%) had positive antibodies with evidence of intrathecal synthesis, all of whom had symptoms that localized to the CNS, of 132 patients who had oligoclonal bands evaluated, 3 (2%) had evidence of intrathecal antibody synthesis (27). The above results indicate that most neurological complications associated with SARS- CoV-2 are unlikely to be related to direct viral neuroinvasion.

Recent studies have illuminated the lung-brain axis, which allows two-way communication between the lungs and CNS. This axis consists of the following multiple interrelated pathways. As part of the autonomic nervous system, neuroanatomical pathway involves neurons and cells for respiratory communication, involving the phrenic nerve for breathing and the vagus nerve for involuntary functions. Pulmonary receptors coordinate with the brain to regulate breathing, with increased sensitivity in diseases like asthma and COPD causing dyspnea. Quick signaling of this pathway is essential for cough reflexes and adjusting respiration to maintain homeostasis and adapt to health changes. In the endocrine pathway, the hypothalamus-pituitary-adrenal axis releases glucocorticoids during lung stress or inflammation, while the sympathetic system secretes adrenaline and noradrenaline for 'fight or flight' responses. They work together to maintain balance and respond to diseases. In immune pathway, CNS conditions can cause lung damage via cytokines, and lung infections can negatively affect the CNS. Systemic inflammation is linked to CNS issues like paraneoplastic syndromes and autoimmune diseases. The lung serves as a critical site for the reactivation of autoreactive T cells, which can then migrate to the CNS and trigger autoimmune disorders. The lung's microbial balance affects CNS susceptibility to autoimmune conditions. Metabolites and microorganisms pathway involves the transfer of biological substances like exosomes and outer-membrane vesicles, ferrying proteins, lipids, nucleic acids, and other bioactive molecules between the CNS and lungs, crossing the BBB. Exosomes can carry cytokines that intensify lung injury and affect microglial activity in the brain, impacting conditions like Alzheimer's disease. Similarly, outer-membrane vesicles from bacteria can provoke central neuropathy and neuroinflammatory diseases. The gas pathway is crucial for how respiratory gases impact the CNS. Air pollutants, like ozone, can indirectly influence CNS functions by altering neuronal activity and activating stress response pathways, which may result in cognitive and behavioral changes. Diseases of the lungs that lead to hypoxemia and hypercapnia are associated with CNS disorders. Chronic hypoxemia is known to cause white matter changes that are associated with Alzheimer's disease. On the other hand, mild hypercapnia might offer neuroprotection, while severe hypercapnia can aggravate brain injury (28).

In a prospective study assessing the prevalence of serum myelin oligodendrocyte glycoprotein antibody (MOG-Ab) and aquaporin-4 antibody (AQP4-Ab) among 35 patients with clinical optic neuritis and confirmed COVID-19, it was found that serum MOG-Ab and AQP4-Ab were detected in 28.6% (10/35) and 5.7% (2/35) optic neuritis cases after COVID-19 (29). Positivity for MOG-Ab is generally indicative of MOG antibody-associated disease, an immune-mediated condition that demyelinates the optic nerves, brain, and spinal cord (30). AQP4-Ab positivity is a strong marker for neuromyelitis optica spectrum disorder, a severe autoimmune inflammatory disorder of the CNS, marked by intense optic neuritis and myelitis (31). The identification of these antibodies, coupled with a favorable response to pulse steroid therapy, suggests that optic neuritis related to COVID-19 represents a post-infectious, immune-mediated inflammatory response (29). Furthermore, a comprehensive multicenter study has shown that recipients of the mRNA vaccines BNT162b2 and mRNA-1273 have a notably higher risk of retinal vascular occlusion within two years post-vaccination, suggesting that SARS-CoV-2 may cause neuro-ophthalmic damage via mechanisms beyond direct viral invasion (32).

Integrating the available evidence, we propose that SARS-CoV-2 may precipitate conditions affecting the optic nerve and visual pathways via the lung-brain axis routes. Initially, SARS-CoV-2 might penetrate the CNS through BBB, directly targeting neurons within the optic nerve and visual pathways. Furthermore, lung inflammation from SARS-CoV-2 could amplify the release of inflammatory mediators like cytokines, enhancing BBB permeability and leading to optic neuritis and retinal vascular occlusion. Additionally, lung impairment due to SARS-CoV-2 might disrupt oxygen and carbon dioxide exchange, compromising the oxygenation of the brain and optic nerve, with sustained hypoxemia and hypercapnia potentially causing damage to these structures. Moreover, the infection could disrupt lung microbial homeostasis and metabolic outputs, which might, via the bloodstream, impact the optic nerve and visual pathways' functionality. SARS-CoV-2 could also present antigens mimicking MOG or AQP4 proteins on astrocytes, eliciting a pathogenic T cell response and antigen-antibody reaction, leading to inflammation and demyelination, thereby impairing vision. A less likely but possible pathway for the generation of MOG-Ab may involve the incidental unveiling of MOG protein to the immune system's antigen-presenting cells during inflammation in the CNS's white matter or optic nerve, instigated by COVID-19. The specific mechanisms by which COVID-19 causes disorders of optic nerve and visual pathways require further and more in-depth research.

Our study presents several notable strengths. Primarily, the MR approach we employed was less prone to confounding factors, such as inflammation, vascular disease, and tumor compression, which could also lead to optic nerve and visual pathway disorders. This robustness stems from our utilization of multiple COVID-19-associated SNPs, derived from extensive GWAS, as IVs. We further refine our analysis by excluding SNPS associated with potential confounders, identified through the PhenoScanner V2 database, to negate the impact of these confounders on our results. These measures provided substantial statistical power to establish causal relationships. Moreover, we implemented stringent criteria for the selection of IVs to uphold the foundational assumptions of MR, thereby mitigating the risk of weak instrument bias. To account for any anomalies induced by horizontal or directional pleiotropy, we utilized advanced methods such as MR-Egger and MR-PRESSO for detection and correction. Additionally, we confined the genetic background of our participants predominantly to European ancestry, which curtailed potential confounding effects arising from a more diverse population mix.

Our study has several limitations that warrant consideration. The datasets analyzed were primarily composed of individuals of

European descent, potentially limiting the generalizability of our findings across different ethnic groups. Furthermore, the ongoing mutation of SARS-CoV-2 could influence factors such as viral transmissibility, viral load, disease severity, and the virus's ability to evade immune responses. These mutations may complicate the causal inference regarding disorders of optic nerve and visual pathways. Currently, there is a lack of GWAS data on post-mutation SARS-CoV-2. Should such data become available for various SARS-CoV-2 strains in the future, we aim to conduct further investigations. Additionally, our MR analysis is based on publicly accessible summary-level data rather than individual-level data, precluding us from performing subgroup analyses based on COVID-19 severity. This limitation may result in less precise causal estimates and could impact the interpretation and generalization of our results.

Conclusions

In summary, this MR study provides evidence suggesting that COVID-19 may elevate the risk of developing optic nerve and visual pathway disorders. Beyond deepening our comprehension of the interplay between COVID-19 and diseases of optic nerve and visual pathways, this research also introduces fresh perspectives and robust data to bolster lung-brain axis studies. These insights are pivotal for devising preventive measures and therapeutic interventions for nervous system diseases associated with infections. Moreover, they are instrumental in enhancing the quality of clinical care delivered to patients. Additionally, these discoveries lay the groundwork for the development of innovative therapeutic approaches for patients with infections.

Data availability statement

The original contributions presented in the study are included in the article/Supplementary Material. Further inquiries can be directed to the corresponding authors.

Ethics statement

Ethics approval and consent to participate were waived for this study because this study used publicly available summary-level GWAS data from published studies that had obtained institutional review board approval for their respective studies, and the data was public, anonymized, and de-identified.

Author contributions

CC: Conceptualization, Funding acquisition, Investigation, Methodology, Project administration, Writing – original draft. QL: Data curation, Formal analysis, Writing – review & editing. DC: Conceptualization, Methodology, Writing – review & editing. CY: Data curation, Formal analysis, Methodology, Software, Supervision, Visualization, Writing – review & editing. HZ: Funding acquisition, Resources, Validation, Writing – review & editing.

Funding

The author(s) declare financial support was received for the research, authorship, and/or publication of this article. Henan Province Medical Science and Technology Research Plan Joint Construction Project (LHGJ20230321) and Henan Provincial Department of Education Key Research Project for Institutions of Higher Learning (24B320029) financially supported this study.

Acknowledgments

We acknowledge the availability of their data through the IEU open GWAS project.

Conflict of interest

The authors declare that the research was conducted in the absence of any commercial or financial relationships that could be construed as a potential conflict of interest.

Publisher's note

Supplementary material

The Supplementary Material for this article can be found online at: https://www.frontiersin.org/articles/10.3389/fimmu.2024.1440262/full#supplementary-material

References

1. Spudich S, Nath A. Nervous system consequences of COVID-19. *Science*. (2022) 375:267–9. doi: 10.1126/science.abm2052

2. Przybek-Skrzypecka J, Szewczuk A, Kamińska A, Skrzypecki J, Pyziak-Skupień A, Szaflik JP. Effect of COVID-19 lockdowns on eye emergency department, increasing prevalence of uveitis and optic neuritis in the COVID-19 era. *Healthcare(Basel)*. (2022) 10:1422. doi: 10.3390/healthcare10081422

3. Shi J, Danesh-Meyer HV. A review of neuro-ophthalmic sequelae following COVID-19 infection and vaccination. *Front Cell Infect Microbiol*. (2024) 14:1345683. doi: 10.3389/fcimb.2024.1345683

4. Midi I. *Disorders of optic nerve and visual pathways*. London, UK: IntechOpen (2014) p. 1–22. doi: 10.5772/58312

5. Bajinka O, Simbilyabo L, Tan Y, Jabang J, Saleem SA. Lung-brain axis. *Crit Rev Microbiol*. (2022) 48:257–69. doi: 10.1080/1040841X.2021.1960483

6. Trueba AF, Ritz T. Stress, asthma, and respiratory infections: pathways involving airway immunology and microbial endocrinology. *Brain Behav Immun*. (2013) 29:11–27. doi: 10.1016/j.bbi.2012.09.012

7. Bai W, Li W, Ning YL, Li P, Zhao Y, Yang N, et al. Blood glutamate levels are closely related to acute lung injury and prognosis after stroke. *Front Neurol*. (2018) 8:755. doi: 10.3389/fneur.2017.00755

8. Lahousse L, Tiemeier H, Ikram MA, Brusselle GG. Chronic obstructive pulmonary disease and cerebrovascular disease: A comprehensive review. *Respir Med*. (2015) 109:1371–80. doi: 10.1016/j.rmed.2015.07.014

9. Hosang L, Canals RC, van der Flier FJ, Hollensteiner J, Daniel R, Flügel A, et al. The lung microbiome regulates brain autoimmunity. *Nature*. (2022) 603:138–44. doi: 10.1038/s41586-022-04427-4

10. Baig AM, Sanders EC. Potential neuroinvasive pathways of SARS-CoV-2: deciphering the spectrum of neurological deficit seen in coronavirus disease-2019 (COVID-19). *J Med Virol*. (2020) 92:1845–57. doi: 10.1002/jmv.26105

11. Nuzzo D, Picone P. Potential neurological effects of severe COVID-19 infection. *Neurosci Res*. (2020) 158:1–5. doi: 10.1016/j.neures.2020.06.009

12. Dimitriadis K, Meis J, Neugebauer H, Barlinn K, Neumann B, Gahn G, et al. Neurologic manifestations of COVID-19 in critically ill patients: results of the prospective multicenter registry PANDEMIC. *Crit Care*. (2022) 26:217. doi: 10.1186/s13054-022-04080-3

13. Bowden J, Holmes MV. Meta-analysis and Mendelian randomization: A review. *Res Sythesis Methods*. (2019) 10:486–96. doi: 10.1002/jrsm.1346

14. Smith GD, Hemani G. Mendelian randomization: Genetic anchors for causal inference in epidemiological studies. *Hum Mol Genet*. (2014) 23:R89–98. doi: 10.1093/hmg/ddu328

15. Smith GD, Ebrahim S. 'Mendelian randomization': Can genetic epidemiology contribute to understanding environmental determinants of disease? *Int J Epidemiol*. (2003) 32:1–22. doi: 10.1093/ije/dyg070

16. Lawlor DA, Harbord RM, Sterne JAC, Timpson N, Smith GD. Mendelian randomization: Using genes as instruments for making causal inferences in epidemiology. *Stat Med*. (2008) 27:1133–63. doi: 10.1002/sim.3034

17. Bowden J, Fabiola Del Greco M, Minelli C, Smith GD, Sheehan NA, Thompson JR. Assessing the suitability of summary data for two-sample mendelian randomization analyses using MR-Egger regression: The role of the I2 statistic. *Int J Epidemiol*. (2016) 45:1961–74. doi: 10.1093/ije/dyw220

18. Burgess S, Scott RA, Timpson NJ, Smith GD, Thompson SG. Using published data in Mendelian randomization: A blueprint for efficient identification of causal risk factors. *Eur J Epidemiol*. (2015) 30:543–52. doi: 10.1007/s10654-015-0011-z

19. Burgess S, Dudbridge F, Thompson SG. Combining information on multiple instrumental variables in Mendelian randomization: Comparison of allele score and summarized data methods. *Stat Med*. (2016) 35:1880–906. doi: 10.1002/sim.6835

20. Bowden J, Smith GD, Burgess S. Mendelian randomization with invalid instruments: effect estimation and bias detection through Egger regression. *Int J Epidemiol*. (2015) 44:512–25. doi: 10.1093/ije/dyv080

21. Verbanck M, Chen CY, Neale B, Do R. Detection of widespread horizontal pleiotropy in causal relationships inferred from Mendelian randomization between complex traits and diseases. *Nat Genet*. (2018) 50:693–8. doi: 10.1038/s41588-018-0099-7

22. Ugurlu A, Agcayazi SB, Icel E, Budakoglu O, Unver E, Barkay O, et al. Assessment of the optic nerve, macular, and retinal vascular effects of COVID-19. *Can J Ophthalmol*. (2023) 58:570–6. doi: 10.1016/j.jcjo.2022.06.016

23. Burgos-Blasco B, Güemes-Villahoz N, Donate-Lopez J, Vidal-Villegas B, García-Feijóo J. Optic nerve analysis in COVID-19 patients. *J Med Virol*. (2021) 93:190–1. doi: 10.1002/jmv.26290

24. Costa ÍF, Bonifácio LP, Bellissimo-Rodrigues F, Rocha EM, Jorge R, Bollela VR, et al. Ocular findings among patients surviving COVID-19. *Sci Rep*. (2021) 11:11085. doi: 10.1038/s41598-021-90482-2

25. Yan R, Zhang Y, Li Y, Xia L, Guo Y, Zhou Q. Structural basis for the recognition of SARS-CoV-2 by full-length human ACE2. *Science*. (2020) 367:1444–8. doi: 10.1126/science.abb2762

26. Ding Q, Zhao HJ. Long-term effects of SARS-CoV-2 infection on human brain and memory. *Cell Death Discov*. (2023) 9:196. doi: 10.1038/s41420-023-01512-z

27. Lewis A, Frontera J, Placantonakis DG, Lighter J. Cerebrospinal fluid in COVID-19: A systematic review of the literature. *J Neurol Sci*. (2021) 421:117316. doi: 10.1016/j.jns.2021.117316

28. Li CY, Chen WL, Lin F, Bin L, Wang P, Liao GL, et al. Functional two-way crosstalk between brain and lung: the brain-lung axis. *Cell Mol Neurobiol*. (2023) 43:991–1003. doi: 10.1007/s10571-022-01238-z

29. Sun CB. Prevalence of serum MOG antibody and AQP4 antibody in optic neuritis after SARS-CoV-2 infection. *Front Immunol*. (2023) 14:1296518. doi: 10.3389/fimmu.2023.1296518

30. Sechi E, Cacciaguerra L, Chen JJ, Mariotto S, Fadda G, Dinoto A, et al. Myelin oligodendrocyte glycoprotein antibody-associated disease (MOGAD): a review of clinical and MRI features, diagnosis, and management. *Front Neurol*. (2022) 13:885218. doi: 10.3389/fneur.2022.885218

31. Wang L, Du L, Li QY, Li F, Wang B, Zhao YQ, et al. Neuromyelitis optica spectrum disorder with anti-Aquaporin-4 antibody: outcome prediction models. *Front Immunol*. (2022) 13:873576. doi: 10.3389/fimmu.2022.873576

32. Li JX, Wang YH, Bair H, Hsu SB, Chen C, Wei JCC, et al. Risk assessment of retinal vascular occlusion after COVID-19 vaccination. *NPJ Vaccines*. (2023) 8:64. doi: 10.1038/s41541-023-00661-7

frontiers | Frontiers in Immunology

TYPE Original Research
PUBLISHED 24 July 2024
DOI 10.3389/fimmu.2024.1441838

OPEN ACCESS

EDITED BY
Ping Yuan,
Tongji University, China

REVIEWED BY
Lan Jiang,
First Affiliated Hospital of Wannan Medical College, China
Wei Tan,
Shandong Second Medical University, China
Qun Zhao,
Fourth Hospital of Hebei Medical University, China

*CORRESPONDENCE
Wen Gu
guwen@xinhuamed.com.cn
Xuejun Guo
guoxuejun@xinhuamed.com.cn

†These authors have contributed equally to this work

RECEIVED 31 May 2024
ACCEPTED 05 July 2024
PUBLISHED 24 July 2024

CITATION
Qin Q, Yu H, Zhao J, Xu X, Li Q, Gu W and Guo X (2024) Machine learning-based derivation and validation of three immune phenotypes for risk stratification and prognosis in community-acquired pneumonia: a retrospective cohort study. *Front. Immunol.* 15:1441838. doi: 10.3389/fimmu.2024.1441838

Machine learning-based derivation and validation of three immune phenotypes for risk stratification and prognosis in community-acquired pneumonia: a retrospective cohort study

Qiangqiang Qin[1†], Haiyang Yu[1†], Jie Zhao[2†], Xue Xu[1], Qingxuan Li[3], Wen Gu[1*] and Xuejun Guo[1*]

[1]Department of Respiratory Medicine, Xinhua Hospital, Shanghai Jiaotong University School of Medicine, Shanghai, China, [2]Department of Hematology, Xinhua Hospital, Shanghai Jiaotong University School of Medicine, Shanghai, China, [3]Department of Respiratory and Critical Care Medicine, The Second Hospital of Jilin University, Changchun, Jilin, China

Background: The clinical presentation of Community-acquired pneumonia (CAP) in hospitalized patients exhibits heterogeneity. Inflammation and immune responses play significant roles in CAP development. However, research on immunophenotypes in CAP patients is limited, with few machine learning (ML) models analyzing immune indicators.

Methods: A retrospective cohort study was conducted at Xinhua Hospital, affiliated with Shanghai Jiaotong University. Patients meeting predefined criteria were included and unsupervised clustering was used to identify phenotypes. Patients with distinct phenotypes were also compared in different outcomes. By machine learning methods, we comprehensively assess the disease severity of CAP patients.

Results: A total of 1156 CAP patients were included in this research. In the training cohort (n=809), we identified three immune phenotypes among patients: Phenotype A (42.0%), Phenotype B (40.2%), and Phenotype C (17.8%), with Phenotype C corresponding to more severe disease. Similar results can be observed in the validation cohort. The optimal prognostic model, SuperPC, achieved the highest average C-index of 0.859. For predicting CAP severity, the random forest model was highly accurate, with C-index of 0.998 and 0.794 in training and validation cohorts, respectively.

Abbreviations: CAP, Community-acquired pneumonia; ML, Machine learning; SCAP: Severe community-acquired pneumonia; MV, mechanical ventilation; IRVS, intensive respiratory or vasopressor support; IDSA, Infectious Diseases Society of America; ATS, American Thoracic Society; ARDS, Acute respiratory distress syndrome; t-SNE, t-distributed Stochastic Neighbor Embedding; PCA, Principal Component Analysis; UMAP, Uniform Manifold Approximation and Projection; CDF, Cumulative distribution function; ROC, Receiver Operating Characteristic; IRB, Institutional Review Board; ARDS, Acute Respiratory Distress Syndrome; RCT, Randomized Controlled Trial.

Conclusion: CAP patients can be categorized into three distinct immune phenotypes, each with prognostic relevance. Machine learning exhibits potential in predicting mortality and disease severity in CAP patients by leveraging clinical immunological data. Further external validation studies are crucial to confirm applicability.

KEYWORDS

community-acquired pneumonia, immune phenotype, machine learning, unsupervised clustering, risk stratification

Introduction

Community-acquired pneumonia (CAP) is an acute parenchymal lung infection caused by a variety of microorganisms outside the hospital. Despite advancements in rapid diagnostic testing, novel treatment options, and vaccine development, CAP continues to be one of the predominant causes of hospitalization, morbidity, and mortality globally (1). Severe community-acquired pneumonia (SCAP) is presently defined as the condition of patients requiring admission to the Intensive Care Unit (ICU) for mechanical ventilation (MV) or intensive respiratory or vasopressor support (IRVS) (2). Among 7,449 patients enrolled in the United States between 2014 and 2016, the 30-day mortality rate for SCAP was 6% (3). Consequently, the prompt identification and immediate management of SCAP are crucial for reducing its mortality rate. Presently, numerous methods are employed to evaluate the severity of CAP, primarily relying on established scores and guidelines. Nonetheless, these methods exhibit multiple limitations that impede their utility as clinical decision support tools (4–6).

In recent decades, machine learning (ML) algorithms have shown better performance in predicting various diseases or clinical conditions. Research has consistently illustrated the efficacy of ML in managing critically ill patients by predicting length of stay, risk of ICU readmission, and mortality rates. Recently, Jeon Et al. established that ML models significantly outperform traditional severity-of-illness scoring systems in predicting ICU mortality among patients with severe pneumonia (7). Xu et al. found that the ML model based on available clinical features is feasible and effective in predicting adverse outcomes such as mortality inCAP patients and ICU admission (8).

The clinical manifestations of CAP are highly variable. As a result, patients with CAP who are hospitalized present with a wide range of clinical symptoms, vital signs, and laboratory findings. Previously, Stefano Aliberti et al. divided patients into three different clinical phenotypes based on the presence or absence of acute respiratory failure and severe sepsis at admission, which showed significant differences in mortality (9). As infections advance, a range of resident and mobilized immune cells are activated to combat the invading pathogens. Research indicates that both the inflammatory response and immune regulation are pivotal in the pathogenesis of SCAP and acute respiratory distress syndrome (ARDS) (10). However, to date, limited studies have explored the immune phenotypes associated with CAP and their correlation with patient clinical outcomes. Therefore, we hypothesize that distinct clusters of characteristics present in CAP patients at admission may form identifiable subgroups or phenotypes, potentially signaling disparate prognoses for the illness and serving a vital function in the early detection of SCAP. This study sought to ascertain if immune phenotypes in patients with CAP can be identified using immunological data, to evaluate their correlation with prognosis, and to predict the likelihood of SCAP.

Methods

Study design

In this research, electronic health records of patients diagnosed with CAP admitted to the Respiratory and Critical Care department of Xin Hua Hospital Affiliated to Shanghai Jiao Tong University School of Medicine between January 1, 2020 and October 31, 2023 were retrospectively collected. All patients incorporated in this research were required to meet the diagnostic criteria of CAP and to have blood samples collected within the first 24 hours of admission. However, the study excluded patients who met any of the following exclusion criteria: (1) age under 18 years; (2) diagnosis of an autoimmune or hematologic malignancy; (3) a subsequent diagnosis of conditions such as pulmonary tuberculosis or idiopathic pulmonary fibrosis; and (4) those who declined further treatment or were transferred to another hospital. (see Figure 1, Supplementary Figure S1 for details). Additionally, in this study, we exclusively consider data from the initial hospital admission for individuals who experienced multiple admissions (11). Vital signs (heart rate, systolic blood pressure and diastolic blood pressure, temperature, respiratory rate and mentation), demographic information(age, sex, height, weight), laboratory indicators(WBC, Neutrophil cell count, IgA, IgE, IgM, IL-6, IL-8, CD3, CD4, CD8, etc.) were collected within 24h after admission, and other variables

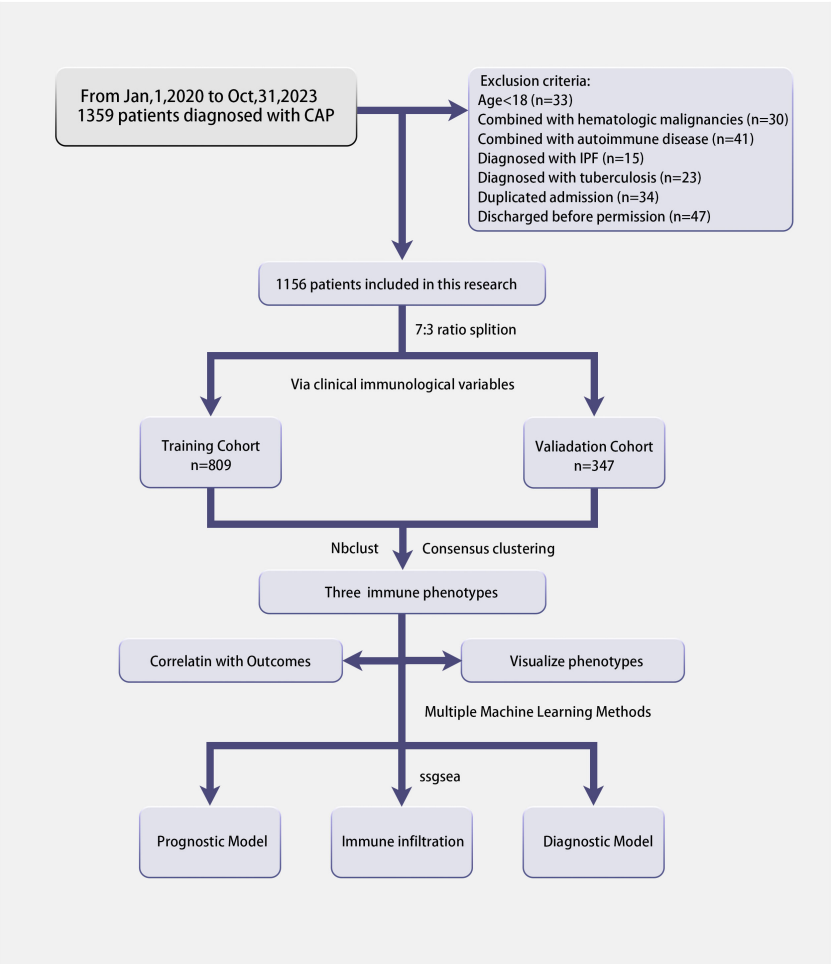

FIGURE 1
The flowchart of this research.

(days from symptom onset, chief complaint, length of stay, application of assisted ventilation, and clinical outcome) were also extracted after patients discharged. Upon applying our predefined inclusion and exclusion criteria, we successfully enrolled a cohort of 1,165 eligible patients for this study.

Candidate variables for clustering and phenotyping

Patients were randomly allocated to the training and validation cohorts in a ratio of 7:3 to ensure reproducibility and consistency in the modeling outcomes (12). And a meticulously curated dataset comprising various laboratory indicators has been compiled for this analysis. When addressing missing values, we employed two distinct strategies. For variables with less than 20% missing data, imputation was performed using the Multivariate Imputation by Chained Equations (MICE) package (13). Conversely, variables with 20% or more missing data were excluded entirely to preserve the integrity and robustness of the study (14). This methodological approach refined our dataset to encompass 79 laboratory indicators.

Moreover, given the study's emphasis on exploring the immune phenotype of community-acquired pneumonia, we cumulatively identified 31 immunological laboratory variables as the focal point for clustering analysis. To identify commonalities among different patients based on laboratory examinations, we applied the unsupervised 'consensus clustering' algorithm within the training cohort to ascertain the optimal number of clusters. Subsequently, we corroborated the findings in both the validation cohort and the meta-cohort. Additionally, to verify the integrity of the clustering process, our dataset underwent analysis using the NBclust (15) clustering algorithm. Additionally, we employed an alluvial plot to visualize the discrepancies between conventional grading systems and our machine learning approach. Lastly, we presented chord diagrams to illustrate the associations between laboratory indicators and clinical immune phenotypes.

Definitions and clinical outcomes

CAP patients were classified into three distinct immune phenotypes (Phenotype A, Phenotype B, and Phenotype C).

Utilizing prior knowledge and clinical expertise, indicators such as the necessity for mechanical ventilation, admission to the intensive care unit, or mortality due to the disease were employed as surrogate markers of SCAP in this investigation. The primary outcome was the in-hospital mortality rate. Secondary outcomes included the 28-day mortality rate, the likelihood of progressing to severe pneumonia, length of stay, days of ventilation, days in the ICU, ICU-free days, and the probability of respiratory support. Upon stratification of pneumonia patients into three immune phenotypes, we assessed differences in all-cause in-hospital mortality rates across the meta, training, and validation cohorts. Simultaneously, we examined the 28-day mortality rate and the risk of severe disease progression within these cohorts. This approach facilitated a detailed evaluation of mortality outcomes associated with different immune phenotypes in community-acquired pneumonia.

Integrated machine learning based model construction and evaluation

To assess the predictive performance of machine learning (ML) methods based on Zaoqu liu's framework (16), nine algorithms were employed for patient prognosis prediction in both the training and validation cohorts. The model with the highest average concordance index (C-index) across these cohorts will be considered the most effective. Additionally, this study expanded its methodology to include thirteen ML algorithms for forecasting the risk of severity in CAP patients, specifically: Lasso, Ridge, Elastic Net (Enet), Stepwise GLM (Stepglm), Support Vector Machine (SVM), Gradient Boosting Machine (GBM), Linear Discriminant Analysis (LDA), Partial Least Squares and Logistic Regression Model (plsRglm), Random Forest, and Naive Bayes (17–19). Consistently, the model that exhibits superior performance across both cohorts will be identified as the optimal model. To guarantee the robustness and reliability of our models, we meticulously selected only those comprising more than five variables. This strategy enabled clinicians to concentrate on the most informative and stable combinations of predictors. Moreover, we incorporated the publicly accessible dataset GSE188309 (20), which concentrates on community-acquired pneumonia, into our analysis to ascertain potential immune infiltration from a transcriptomic perspective.

Association between clinical immune phenotype and traditional scoring system

Generally, CURB-65 and PSI scoring systems were frequently utilized in clinical settings to evaluate the severity of pneumonia patients with CAP. However, recent studies have highlighted significant limitations within these systems (21, 22). In response, we developed a model utilizing machine learning techniques and evaluated its predictive accuracy using the Receiver Operating Characteristic (ROC) curve, in comparison to traditional scoring systems.

Statistical analysis

In this study, the Shapiro-Wilk test was utilized to assess the normality of continuous variables prior to the formal analysis. For comparisons, the Mann–Whitney U-test was applied to non-normally distributed continuous variables, while the Student's t-test was used for those with a normal distribution, as appropriate. For categorical variables, the Kruskal-Wallis test or the Chi-square test was employed where relevant. Continuous variables were presented as mean ± SD for normally distributed data and as median (interquartile range, IQR) for non-normally distributed data. Categorical variables were reported as frequencies and percentages. All data generation, processing, statistical analyses, and plotting were performed using R software version 4.2.0. A p-value of less than 0.05 was considered statistically significant, although this was not explicitly mentioned in the report.

IRB statement

Approval was obtained from the Institutional Review Board (IRB) of Xinhua Hospital, Shanghai Jiao Tong University School of Medicine, Shanghai, China, and a waiver of consent was granted because the study used electronic medical record data and blood test results from normal clinical visits (Approval Number: XHEC-C-2024-026-1; Approval Date: 2024-03-19; Study Title: Clinical Study Based on Comprehensive Multi-omics Analysis of Peripheral Blood for Community Acquired Pneumonia). All procedures were followed in accordance with the IRBs standards on human experimentation and the Helsinki Declaration of 1975.

Results

Baseline characteristics of CAP patients

This study reviewed the records of 12,000 individuals discharged from the Respiratory Department of Xinhua Hospital between January 1, 2020, and October 31, 2023. Of these, 1,379 were diagnosed with CAP. Following the application of exclusion criteria, 223 patients were omitted from the study. Consequently, a cohort of 1,156 CAP patients was established for inclusion in the research. Patients were allocated into two groups: a training cohort consisting of 809 patients and a validation cohort of 347 patients, using a randomization ratio of 7:3. Table 1 presents the baseline characteristics of the combined meta-cohort, along with those of the training and validation cohorts separately. Among the participants, 8 required treatment with an invasive ventilator, 96 received non-invasive ventilation, and 46 underwent therapy with high-flow nasal cannula. In this study, 53 patients succumbed to their conditions, while 239 required admission to the intensive care unit. The median hospital stay for the meta cohort was 9 days, with an interquartile range (IQR) of 7–14 days. The three most frequent symptoms among the patients were cough (76%, n=880), fever (54%, n=626), and sputum production (52%, n=600). Consistent

10.3389/fimmu.2024.1441838

TABLE 1 Characteristics of the study population and outcomes of community acquired pneumonia patients.

Variables	Total (n = 1156)	test (n = 347)	train (n = 809)	P Value
Demographics				
Sex, n (%)				0.715
Female	492 (43)	151 (44)	341 (42)	
Male	664 (57)	196 (56)	468 (58)	
Age (years), median (IQR)	65 (54, 73)	66 (58, 73)	65 (53, 73)	0.534
Height (cm), median (IQR)	166 (160, 172)	167 (160, 173)	166 (160, 172)	0.783
Weight (kg), median (IQR)	64 (56, 73)	64.75 (57, 73.08)	64 (55, 73)	0.356
Mentation, n (%)				0.721
1	1141 (99)	343 (99)	798 (99)	
2	4 (0)	1 (0)	3 (0)	
3	5 (0)	2 (1)	3 (0)	
4	2 (0)	0 (0)	2 (0)	
5	1 (0)	0 (0)	1 (0)	
6	0 (0)	0 (0)	0 (0)	
7	2 (0)	0 (0)	2 (0)	
8	1 (0)	1 (0)	0 (0)	
Vital signs				
Fever peak, median (IQR)	38.1 (37.3, 39)	38 (37.3, 39)	38.1 (37.3, 39)	0.661
Temperature admission, median (IQR)	37 (36.6, 37.7)	37 (36.7, 37.7)	37 (36.6, 37.7)	0.568
Tmax during the course, median (IQR)	37.4 (37.1, 38)	37.3 (37.05, 38)	37.4 (37.1, 38)	0.405
Heart rate, median (IQR)	92 (83, 101)	90 (82, 101)	92 (83, 101)	0.202
Respiration Rate, median (IQR)	20 (18, 20)	20 (19, 20)	20 (18, 20)	0.204
Systolic blood pressure, median (IQR)	132 (120, 149)	131 (120, 148.75)	133 (120, 149)	0.684
Diastolic blood pressure, median (IQR)	79 (71, 87)	79 (72, 86)	78 (70, 88)	0.762
CURB-65 score, n (%)				0.883
0	452 (39)	130 (37)	322 (40)	
1	444 (38)	137 (39)	307 (38)	
2	222 (19)	70 (20)	152 (19)	
3	37 (3)	10 (3)	27 (3)	
4	1 (0)	0 (0)	1 (0)	
PSI score, median (IQR)	70 (53, 89)	71 (54, 88)	69 (52, 90)	0.274
Chief Complaint				
Cough, n (%)				0.339
No	276 (24)	76 (22)	200 (25)	
Yes	880 (76)	271 (78)	609 (75)	
Sputum, n (%)				0.281
No	556 (48)	158 (46)	398 (49)	
Yes	600 (52)	189 (54)	411 (51)	

(Continued)

10.3389/fimmu.2024.1441838

TABLE 1 Continued

Variables	Total (n = 1156)	test (n = 347)	train (n = 809)	P Value
Chief Complaint				
Chest Pain, n (%)				0.792
No	1081 (94)	326 (94)	755 (93)	
Yes	75 (6)	21 (6)	54 (7)	
Dyspnea, n (%)				0.469
No	874 (76)	257 (74)	617 (76)	
Yes	282 (24)	90 (26)	192 (24)	
Chest Tightness, n (%)				0.329
No	1025 (89)	313 (90)	712 (88)	
Yes	131 (11)	34 (10)	97 (12)	
Fever, n (%)				0.661
No	530 (46)	163 (47)	367 (45)	
Yes	626 (54)	184 (53)	442 (55)	
Fatigue, n (%)				0.364
No	1112 (96)	337 (97)	775 (96)	
Yes	44 (4)	10 (3)	34 (4)	
Consciousness Disorder, n (%)				0.207
No	1149 (99)	343 (99)	806 (100)	
Yes	7 (1)	4 (1)	3 (0)	
Difficulty Breathing, n (%)				0.706
No	1128 (98)	340 (98)	788 (97)	
Yes	28 (2)	7 (2)	21 (3)	
Hemoptysis, n (%)				0.364
No	1112 (96)	337 (97)	775 (96)	
Yes	44 (4)	10 (3)	34 (4)	
Comorbidity				
Respiratory system				
COPD, n (%)				0.537
No	1007 (87)	306 (88)	701 (87)	
Yes	149 (13)	41 (12)	108 (13)	
Bronchiectasis, n (%)				0.602
No	1088 (94)	329 (95)	759 (94)	
Yes	68 (6)	18 (5)	50 (6)	
Emphysema bullae, n (%)				1
No	1105 (96)	332 (96)	773 (96)	
Yes	51 (4)	15 (4)	36 (4)	
Pulmonary hypertension, n (%)				0.842
No	1126 (97)	337 (97)	789 (98)	
Yes	30 (3)	10 (3)	20 (2)	

(Continued)

10.3389/fimmu.2024.1441838

TABLE 1 Continued

Variables	Total (n = 1156)	test (n = 347)	train (n = 809)	P Value
Respiratory system				
Lung cancer, n (%)				0.602
No	1097 (95)	327 (94)	770 (95)	
Yes	59 (5)	20 (6)	39 (5)	
PE, n (%)				0.379
No	1116 (97)	338 (97)	778 (96)	
Yes	40 (3)	9 (3)	31 (4)	
Asthma, n (%)				0.188
No	1108 (96)	328 (95)	780 (96)	
Yes	48 (4)	19 (5)	29 (4)	
OSAHS, n (%)				0.225
No	1110 (96)	329 (95)	781 (97)	
Yes	46 (4)	18 (5)	28 (3)	
Bronchitis, n (%)				1
No	1136 (98)	341 (98)	795 (98)	
Yes	20 (2)	6 (2)	14 (2)	
Cardiovascular system				
Hypertension, n (%)				0.107
No	689 (60)	194 (56)	495 (61)	
Yes	467 (40)	153 (44)	314 (39)	
Atrial fibrillation, n (%)				0.08
No	1086 (94)	333 (96)	753 (93)	
Yes	70 (6)	14 (4)	56 (7)	
Coronary heart disease, n (%)				1
No	1026 (89)	308 (89)	718 (89)	
Yes	130 (11)	39 (11)	91 (11)	
Arrhythmia, n (%)				0.015
No	1005 (87)	315 (91)	690 (85)	
Yes	151 (13)	32 (9)	119 (15)	
Heart failure, n (%)				0.694
No	994 (86)	301 (87)	693 (86)	
Yes	162 (14)	46 (13)	116 (14)	
Digestive system				
Liver dysfunction, n (%)				1
No	992 (86)	298 (86)	694 (86)	
Yes	164 (14)	49 (14)	115 (14)	
Gastric cancer, n (%)				1
No	1146 (99)	344 (99)	802 (99)	
Yes	10 (1)	3 (1)	7 (1)	

(Continued)

10.3389/fimmu.2024.1441838

TABLE 1 Continued

Variables	Total (n = 1156)	test (n = 347)	train (n = 809)	P Value
Digestive system				
Colorectal cancer, n (%)				0.132
No	1138 (98)	345 (99)	793 (98)	
Yes	18 (2)	2 (1)	16 (2)	
Esophageal cancer, n (%)				0.33
No	1151 (100)	347 (100)	804 (99)	
Yes	5 (0)	0 (0)	5 (1)	
Hepatitis, n (%)				0.163
No	1151 (100)	344 (99)	807 (100)	
Yes	5 (0)	3 (1)	2 (0)	
Urinary system				
Renal Insufficiency, n (%)				0.163
No	1076 (93)	329 (95)	747 (92)	
Yes	80 (7)	18 (5)	62 (8)	
Urological tumors, n (%)				0.573
No	1141 (99)	344 (99)	797 (99)	
Yes	15 (1)	3 (1)	12 (1)	
Kidney Stones, n (%)				0.473
No	1125 (97)	340 (98)	785 (97)	
Yes	31 (3)	7 (2)	24 (3)	
Endocrine system				
Diabetes, n (%)				0.065
No	904 (78)	259 (75)	645 (80)	
Yes	252 (22)	88 (25)	164 (20)	
Nervous system				
Senile dementia, n (%)				0.465
No	1147 (99)	343 (99)	804 (99)	
Yes	9 (1)	4 (1)	5 (1)	
Cerebral infarction, n (%)				1
No	1056 (91)	317 (91)	739 (91)	
Yes	100 (9)	30 (9)	70 (9)	
PD, n (%)				1
No	1144 (99)	344 (99)	800 (99)	
Yes	12 (1)	3 (1)	9 (1)	
History of mlignancy, n (%)				0.572
No	1042 (90)	309 (89)	733 (91)	
Yes	114 (10)	38 (11)	76 (9)	

(Continued)

10.3389/fimmu.2024.1441838

TABLE 1 Continued

Variables	Total (n = 1156)	test (n = 347)	train (n = 809)	P Value
Full Blood Count				
Hemoglobin (g/L), median (IQR)	125 (113, 135)	125 (116, 135.5)	125 (112, 135)	0.284
Neutrophil percent (%), median (IQR)	69 (58.9, 80.6)	69.8 (58.4, 80.3)	68.6 (59.3, 80.8)	0.789
Neutrophil count (*10^9/L), median (IQR)	4.43 (3.18, 6.75)	4.32 (3.1, 6.78)	4.46 (3.23, 6.72)	0.683
MCV (fl), median (IQR)	90.7 (88.3, 94)	90.8 (88.5, 93.95)	90.7 (88.1, 94)	0.435
MCH (pg), median (IQR)	30.3 (29.1, 31.4)	30.4 (29.3, 31.45)	30.2 (29.1, 31.4)	0.225
MCHC (g/L), median (IQR)	333 (325, 340)	334 (325, 341)	332 (325, 340)	0.295
MPV (fl), median (IQR)	9.4 (8.6, 10.2)	9.5 (8.7, 10.4)	9.3 (8.6, 10.2)	0.278
WBC Count (*10^9/L), median (IQR)	6.66 (5.18, 8.77)	6.61 (5.18, 8.62)	6.7 (5.18, 8.81)	0.925
Lymphocyte percent (%), median (IQR)	20.4 (11.6, 30)	20.1 (11.9, 29.65)	20.5 (11.2, 30)	0.86
Lymphocyte count (*10^9/L), median (IQR)	1.3 (0.86, 1.78)	1.34 (0.86, 1.78)	1.29 (0.87, 1.78)	0.481
Eosinophil percent (%), median (IQR)	1.5 (0.5, 2.9)	1.5 (0.5, 2.9)	1.5 (0.5, 2.8)	0.75
Monocyte percent (%), median (IQR)	6.7 (5.2, 8.53)	6.7 (5.2, 8.55)	6.8 (5.2, 8.5)	0.942
Monocyte count (*10^9/L), median (IQR)	0.44 (0.33, 0.61)	0.44 (0.32, 0.62)	0.44 (0.33, 0.61)	0.885
RDW (%), median (IQR)	13 (12.5, 13.6)	12.9 (12.4, 13.5)	13 (12.5, 13.6)	0.148
Arterial Blood Gas				
HCO3 (mmol/L), median (IQR)	25.4 (23.3, 27.4)	25.5 (23.35, 27.4)	25.3 (23.3, 27.3)	0.513
HCO3std (mmol/L), median (IQR)	25.3 (23.7, 26.9)	25.4 (23.7, 26.85)	25.2 (23.7, 26.9)	0.72
pCO2 (kPa), median (IQR)	5.21 (4.72, 5.66)	5.23 (4.75, 5.66)	5.21 (4.7, 5.65)	0.352
pH, median (IQR)	7.42 (7.4, 7.45)	7.42 (7.4, 7.45)	7.42 (7.4, 7.45)	0.996
pO2 (kPa), median (IQR)	11.95 (10.3, 14.6)	11.7 (10.1, 14.15)	12.1 (10.5, 14.7)	0.061
TCO2 (mmol/L), median (IQR)	49.9 (44.98, 54.4)	50.1 (45.5, 54.45)	49.8 (44.7, 54.4)	0.556
Glu (mmol/L), median (IQR)	5.28 (4.66, 6.66)	5.3 (4.69, 6.76)	5.26 (4.64, 6.64)	0.264
Renal Function				
Cr (umol/L), median (IQR)	60 (51, 73)	58.8 (50, 72)	60 (51, 74)	0.141
BUN (mmol/L), median (IQR)	5.2 (4.02, 7)	5.2 (4.02, 7)	5.2 (4.02, 6.99)	0.963
GFR (mL/min per1.75m^2), median (IQR)	104.72 (84.94, 125.35)	106.05 (87.31, 125.96)	104.37 (84.2, 124.44)	0.522
UA (umol/L), median (IQR)	269 (213, 338)	264 (217, 313.5)	269 (210, 345)	0.354
ACE (U/L), median (IQR)	23.5 (17.28, 30.2)	23.4 (17, 29.9)	23.6 (17.5, 30.5)	0.97
Blood lipids				
LDL-C (mmol/L), median (IQR)	2.41 (1.89, 2.97)	2.53 (1.94, 3.08)	2.38 (1.87, 2.95)	0.05
TG (mmol/L), median (IQR)	1.04 (0.77, 1.41)	1.08 (0.79, 1.43)	1.02 (0.76, 1.4)	0.303
ApoE (mg/dL), median (IQR)	3.6 (2.9, 4.6)	3.7 (2.9, 4.5)	3.6 (2.9, 4.7)	0.846
Coagulation				
D-Dimer (mg/L), median (IQR)	0.61 (0.34, 1.16)	0.61 (0.32, 1.14)	0.61 (0.34, 1.17)	0.513
TT (s), median (IQR)	13.7 (12.8, 14.7)	13.8 (12.8, 14.65)	13.7 (12.8, 14.8)	0.773
APTT (s), median (IQR)	11.9 (11, 12.9)	11.8 (11, 12.9)	11.9 (11.1, 13)	0.31
INR, median (IQR)	1.05 (0.97, 1.14)	1.04 (0.97, 1.14)	1.05 (0.97, 1.15)	0.346
PTT (s), median (IQR)	30.9 (28.5, 33.4)	30.5 (28.05, 32.95)	31.1 (28.7, 33.6)	0.024

(Continued)

10.3389/fimmu.2024.1441838

TABLE 1 Continued

Variables	Total (n = 1156)	test (n = 347)	train (n = 809)	P Value
Coagulation				
ATA (%), median (IQR)	83 (72, 93)	84 (71.5, 95)	83 (72, 93)	0.258
Inflammatory Cytokine				
IL-10 (pg/mL), median (IQR)	5 (5, 5)	5 (5, 5)	5 (5, 5)	0.085
IL-1B (pg/mL), median (IQR)	5 (5, 9.76)	5 (5, 9.93)	5 (5, 9.72)	0.874
IL-2R (U/mL), median (IQR)	573.5 (409, 880.5)	569 (397, 851)	582 (412, 899)	0.218
IL-6 (pg/mL), median (IQR)	6.97 (3.09, 19.2)	6.83 (2.91, 18.4)	7.18 (3.18, 19.4)	0.553
IL-8 (pg/mL), median (IQR)	26.3 (14.67, 62.12)	28.2 (14.8, 66.35)	25.6 (14.4, 61)	0.628
TNF-α (pg/mL), median (IQR)	14.65 (8.97, 28.52)	14.9 (9.14, 29.6)	14.6 (8.91, 28.4)	0.441
IgG4 (g/L), median (IQR)	0.5 (0.26, 0.9)	0.48 (0.25, 0.86)	0.5 (0.27, 0.93)	0.541
Electrolytes				
P (mmol/L), median (IQR)	1.08 (0.93, 1.22)	1.08 (0.95, 1.21)	1.07 (0.92, 1.22)	0.394
Cl (mmol/L), median (IQR)	105 (102, 107)	105 (102, 107)	105 (102, 107)	0.554
Mg (mmol/L), median (IQR)	0.92 (0.85, 0.97)	0.92 (0.85, 0.97)	0.92 (0.85, 0.98)	0.356
Potassium (mmol/L), median (IQR)	3.96 (3.69, 4.21)	3.95 (3.69, 4.19)	3.96 (3.68, 4.22)	0.748
Ca (mmol/L), median (IQR)	2.08 (1.99, 2.16)	2.09 (1.99, 2.15)	2.08 (1.99, 2.16)	0.969
Sodium (mmol/L), median (IQR)	139 (136, 141)	139 (136, 141)	139 (136, 141)	0.277
Inflammation Measurements				
CRP (mg/L), median (IQR)	24 (4, 76)	21 (3, 68.5)	25 (4, 78)	0.261
PCT(ng/mL), median (IQR)	0.05 (0.04, 0.15)	0.05 (0.04, 0.14)	0.05 (0.04, 0.15)	0.149
ESR (mm/h), median (IQR)	41.5 (21, 70)	42 (21, 70)	41 (21, 69)	0.875
Myocardial Enzyme				
CK-MB (U/L), median (IQR)	5 (3, 7)	5 (3.1, 8)	5 (3, 7)	0.983
cTnI (ng/ml), median (IQR)	0.01 (0, 0.01)	0.01 (0, 0.01)	0.01 (0, 0.01)	0.291
CK (U/L), median (IQR)	63 (41, 99.25)	58 (41, 88)	65 (41, 103)	0.123
α-HBDH (U/L), median (IQR)	142 (113.75, 173)	141 (114.5, 173)	142 (113, 173)	0.711
LDH (U/L), median (IQR)	212 (176, 264)	214 (176, 262)	211 (176, 264)	0.702
Cell immunity				
CD3T (%), median (IQR)	70.5 (62.97, 77.29)	69.95 (61.91, 77.15)	70.67 (63.58, 77.37)	0.282
CD4T (%), median (IQR)	41.8 (34.47, 48.45)	41.01 (33.45, 48.59)	41.99 (35.02, 48.31)	0.431
CD8T (%), median (IQR)	24.13 (18.48, 30.66)	24.07 (18.59, 30.9)	24.22 (18.43, 30.56)	0.915
CD3T (Cells/uL), median (IQR)	932.35 (567.65, 1285.11)	932.52 (557.31, 1291.49)	932.18 (578.03, 1284.19)	0.827
CD4T (Cells/uL), median (IQR)	532.42 (320.8, 785.7)	515.96 (305.94, 800.39)	537.39 (332.43, 776.03)	0.742
CD64 infection index	0.84 (0.43, 2.06)	0.89 (0.43, 2.06)	0.84 (0.42, 2.06)	0.892
CD8T (Cells/uL), median (IQR)	314.12 (185.76, 461.07)	316.69 (185.76, 461.9)	313.71 (185.79, 459.57)	0.805
Humoral Immunity				
Ig A (g/L), median (IQR)	2.5 (1.86, 3.31)	2.49 (1.85, 3.29)	2.5 (1.86, 3.33)	0.792
Ig E (IU/mL), median (IQR)	59.45 (21.7, 197.25)	62.3 (22.15, 184.5)	57.9 (21.2, 211)	0.921
Ig G (g/L), median (IQR)	12.3 (10.5, 14.5)	12 (10.4, 14.2)	12.4 (10.6, 14.6)	0.122

(Continued)

TABLE 1 Continued

Variables	Total (n = 1156)	test (n = 347)	train (n = 809)	P Value
Humoral Immunity				
Ig M (g/L), median (IQR)	0.86 (0.62, 1.21)	0.89 (0.58, 1.22)	0.86 (0.62, 1.2)	0.949
Liver Function				
GGT (U/L), median (IQR)	29 (18, 53)	28 (19, 49)	29 (18, 55)	0.583
Alb (g/L), median (IQR)	35.8 (32.1, 39)	35.9 (32.3, 38.8)	35.8 (32, 39.1)	0.977
AST (U/L), median (IQR)	20 (13, 34)	22 (13, 34)	20 (12, 34)	0.356
ALT (U/L), median (IQR)	21 (16, 31)	20 (16, 29.5)	21 (16, 31)	0.147
ALP (U/L), median (IQR)	75 (61, 95)	76 (60.5, 95)	75 (61, 94)	0.79
PA (mg/L), median (IQR)	158 (111, 206)	156 (116, 206)	159 (109, 207)	0.597
TB (umol/L), median (IQR)	8.7 (6.4, 11.4)	8.6 (6.2, 10.9)	8.7 (6.5, 11.5)	0.311
TP (g/L), median (IQR)	63.9 (59.5, 67.8)	63.5 (59.2, 67.8)	64 (59.8, 67.8)	0.471
FIB (g/L), median (IQR)	4.05 (3.24, 4.94)	3.9 (3.24, 4.95)	4.06 (3.24, 4.92)	0.903
Complement system				
C3 (g/L), median (IQR)	1.17 (1, 1.35)	1.17 (1.01, 1.34)	1.17 (1, 1.36)	0.976
C4 (g/L), median (IQR)	0.29 (0.23, 0.37)	0.29 (0.23, 0.37)	0.29 (0.23, 0.37)	0.898
CH50 (U/mL), Mean ± SD	49.59 _ 15.19	49.31 _ 15.27	49.71 _ 15.16	0.685
Respiratory support				
HFNC, n (%)				0.668
No	1110 (96)	335 (97)	775 (96)	
Yes	46 (4)	12 (3)	34 (4)	
NIMV, n (%)				0.941
No	1060 (92)	319 (92)	741 (92)	
Yes	96 (8)	28 (8)	68 (8)	
IMV, n (%)				1
No	1148 (99)	345 (99)	803 (99)	
Yes	8 (1)	2 (1)	6 (1)	
Clinical Outcomes				
ICU duration (days), median (IQR)	0 (0, 0)	0 (0, 0)	0 (0, 0)	0.444
Ventilation duration (days), median (IQR)	0 (0, 0)	0 (0, 0)	0 (0, 0)	0.44
Length of stay, median (IQR)	9 (7, 14)	10 (7, 14)	9 (7, 14)	0.372
Inpatient Outcome, n (%)				0.46
Alive	1103 (95)	334 (96)	769 (95)	
Dead	53 (5)	13 (4)	40 (5)	
ICU free days (days), median (IQR)	8 (4, 11)	8 (5, 12)	7 (4, 10)	0.12
Outcome at 28 days, n (%)				0.433
Alive	1117 (97)	338 (97)	779 (96)	
Dead	39 (3)	9 (3)	30 (4)	
Days from symptom onset (days), median (IQR)	10 (6, 14)	10 (5, 14)	10 (6, 14)	0.811

(Continued)

TABLE 1 Continued

Variables	Total (n = 1156)	test (n = 347)	train (n = 809)	P Value
Clinical Outcomes				
ICU admission, n (%)				0.502
No	917 (79)	280 (81)	637 (79)	
Yes	239 (21)	67 (19)	172 (21)	

COPD, Chronic obstructive pulmonary disease; OSAHS, Obstructive sleep apnea hypopnea syndrome; MCV, Mean corpuscular volume; MCH, Mean corpuscular hemoglobin; MCHC, Mean corpuscular hemoglobin concentration; WBC, White bold cell; MPV, Mean platelet volume; RDW, Red blood cell distribution width; HCO3, Carbonic acid hydrogen radical; HCO3std, Standard bicarbonate; pCO2, Partial pressure of carbon dioxide; Ph, Potential of hydrogen; pO2, Partial pressure of oxygen; TCO2, Total carbon dioxide; Glu, Glucose; Cr,Creatinine; BUN, Blood urea nitrogen; GFR, Glomerular Filtration Rate; UA, Urine Acid; ACE, Angiotensin-Converting Enzyme; LDL-C, Low-Density Lipoprotein Cholesterol; TG, Triglyceride; ApoE, Apolipoprotein E; TT, Thrombin time; APTT, Activated partial thromboplastin time; INR, International normalized ratio; PTT, Partial thromboplastin time; ATA, Antithrombin Activity; IL-10, Lnterleukin-10; IL-1B, Lnterleukin-1B; IL-2R, Lnterleukin-2 Receptor; IL-6, Lnterleukin-6; IL-8, Lnterleukin-8; TNF-α, Tumor necrosis factor-alpha; IgG4, Immunoglobulin G4; CK-MB, Creatine kinase MB; cTnI, Cardiac troponin I; CK, Creatine kinase; α-HBDH, Alpha-hydroxybutyric dehydroge; LDH, Lactate dehydrogenase; Ig A, Immunoglobulin A; Ig E, Immunoglobulin E; Ig G, Immunoglobulin G; Ig M, Immunoglobulin M; GGT, γ-Glutamyl transferase GGT; Alb, Albumin; AST, Aspartate aminotransferase; ALT, Alanine aminotransferase; ALP, Alkaline phosphatase; PA, Prealbumin; TB, Total bilirubin; TP, Total Protein; FIB, Fibrinogen; C3, Complement C3; C4, Complement C4; CH50, 50% Hemolytic unit of Complement; HFNC, High Flow Nasal Cannula; NIMV, Noninvasive Mechanical Ventilation; IMV, Invasive Mechanical Ventilation.

TABLE 2 Characteristics and outcomes of community acquired pneumonia patients divided by immune phe Notypes in training cohort.

Phenotype	Phenotype A(n=322)	Phenotype B(n=351)	Phenotype C(n=136)	Total (n=809)	P value
Demographics					
Sex, n (%)					0
Female	173 (54%)	134 (38%)	34 (25%)	341 (42%)	
Male	149 (46%)	217 (62%)	102 (75%)	468 (58%)	
Age (years), median (IQR)	60 [39; 67]	68 [60; 76]	72 [64; 79]	65 [53; 73]	0
Height (cm), median (IQR)	165 [160; 171]	166 [160; 172]	170 [163; 175]	166 [160; 172]	0.008
Weight (kg), median (IQR)	64 [56; 73]	65 [55; 73]	63 [55; 74]	64 [55; 73]	0.977
Mentation, n (%)					0.46
1	322(39.80%)	344(42.52%)	132(16.32%)	798(98.64%)	
2	0(0%)	2(0.25%)	1(0.12%)	3(0.37%)	
3	0(0%)	2(0.25%)	1(0.12%)	3(0.37%)	
4	0(0%)	1(0.12%)	1(0.12%)	2(0.25%)	
5	0(0%)	1(0.12%)	0(0%)	1(0.12%)	
6	0(0%)	0(0%)	0(0%)	0(0%)	
7	0(0%)	1(0.12%)	1(0.12%)	2(0.25%)	
8	0(0%)	0(0%)	0(0%)	0(0%)	
Vital signs					
Fever peak, median (IQR)	38 [37; 39]	38 [37; 39]	38 [38; 39]	38 [37; 39]	0.002
Temperature admission, median (IQR)	37 [36; 37]	37 [37; 38]	37 [37; 38]	37 [37; 38]	0.001
Tmax during the course, median (IQR)	37 [37; 38]	37 [37; 38]	38 [37; 39]	37 [37; 38]	0
Heart rate, median (IQR)	92 [83; 100]	92 [83; 101]	91 [84; 103]	92 [83; 101]	0.824
Respiration Rate, median (IQR)	20 [18; 20]	20 [19; 20]	20 [18; 21]	20 [18; 20]	0.043
Systolic blood pressure, median (IQR)	132 [120; 145]	134 [122; 150]	133 [118; 151]	133 [120; 149]	0.228
Diastolic blood pressure, median (IQR)	80 [71; 89]	78 [70; 87]	77 [70; 85]	78 [70; 88]	0.062

(Continued)

10.3389/fimmu.2024.1441838

TABLE 2 Continued

Phenotype	Phenotype A(n=322)	Phenotype B(n=351)	Phenotype C(n=136)	Total (n=809)	P value
CURB-65 score, n (%)					
0	183 (57%)	113 (32%)	26 (19%)	322 (40%)	
1	116 (36%)	136 (39%)	55 (40%)	307 (38%)	
2	20 (6%)	88 (25%)	44 (32%)	152 (19%)	
3	3 (1%)	14 (4%)	10 (7%)	27 (3%)	
4	0 (0.0%)	0 (0.0%)	1 (1%)	1 (0%)	
5	0 (0.0%)	0 (0.0%)	0 (0.0%)	0 (0.0%)	
PSI score, median (IQR)	55 [38; 69]	74 [60; 94]	93 [75; 112]	69 [52; 90]	0
Chief Complaint					
Cough, n (%)					0.009
No	63 (20%)	93 (26%)	44 (32%)	200 (25%)	
Yes	259 (80%)	258 (74%)	92 (68%)	609 (75%)	
Sputum, n (%)					0.117
No	144 (45%)	183 (52%)	71 (52%)	398 (49%)	
Yes	178 (55%)	168 (48%)	65 (48%)	411 (51%)	
Chest Pain, n (%)					0.225
No	296 (92%)	328 (93%)	131 (96%)	755 (93%)	
Yes	26 (8%)	23 (7%)	5 (4%)	54 (7%)	
Dyspnea, n (%)					0
No	271 (84%)	259 (74%)	87 (64%)	617 (76%)	
Yes	51 (16%)	92 (26%)	49 (36%)	192 (24%)	
Chest Tightness, n (%)					0.233
No	288 (89%)	310 (88%)	114 (84%)	712 (88%)	
Yes	34 (11%)	41 (12%)	22 (16%)	97 (12%)	
Fever, n (%)					0.215
No	158 (49%)	149 (42%)	60 (44%)	367 (45%)	
Yes	164 (51%)	202 (58%)	76 (56%)	442 (55%)	
Fatigue, n (%)					0.024
No	314 (98%)	336 (96%)	125 (92%)	775 (96%)	
Yes	8 (2%)	15 (4%)	11 (8%)	34 (4%)	
Consciousness Disorder, n (%)					0.299
No	322 (100%)	348 (99%)	136 (100%)	806 (100%)	
Yes	0 (0.0%)	3 (1%)	0 (0.0%)	3 (0%)	
Difficulty Breathing, n (%)					0.001
No	319 (99%)	343 (98%)	126 (93%)	788 (97%)	
Yes	3 (1%)	8 (2%)	10 (7%)	21 (3%)	
Hemoptysis, n (%)					0.6
No	306 (95%)	339 (97%)	130 (96%)	775 (96%)	

(Continued)

10.3389/fimmu.2024.1441838

TABLE 2 Continued

Phenotype	Phenotype A(n=322)	Phenotype B(n=351)	Phenotype C(n=136)	Total (n=809)	P value
Chief Complaint					
Yes	16 (5%)	12 (3%)	6 (4%)	34 (4%)	
Comorbidity					
Respiratory system					
COPD, n (%)					0.04
No	291 (90%)	296 (84%)	114 (84%)	701 (87%)	
Yes	31 (10%)	55 (16%)	22 (16%)	108 (13%)	
Bronchiectasis, n (%)					0.546
No	302 (94%)	332 (95%)	125 (92%)	759 (94%)	
Yes	20 (6%)	19 (5%)	11 (8%)	50 (6%)	
Emphysema bullae, n (%)					0.223
No	312 (97%)	334 (95%)	127 (93%)	773 (96%)	
Yes	10 (3%)	17 (5%)	9 (7%)	36 (4%)	
Pulmonary hypertension, n (%)					0.122
No	318 (99%)	338 (96%)	133 (98%)	789 (98%)	
Yes	4 (1%)	13 (4%)	3 (2%)	20 (2%)	
Lung cancer, n (%)					0.003
No	315 (98%)	332 (95%)	123 (90%)	770 (95%)	
Yes	7 (2%)	19 (5%)	13 (10%)	39 (5%)	
PE, n (%)					0.261
No	314 (98%)	334 (95%)	130 (96%)	778 (96%)	
Yes	8 (2%)	17 (5%)	6 (4%)	31 (4%)	
Asthma, n (%)					1
No	311 (97%)	338 (96%)	131 (96%)	780 (96%)	
Yes	11 (3%)	13 (4%)	5 (4%)	29 (4%)	
OSAHS, n (%)					0.203
No	311 (97%)	342 (97%)	128 (94%)	781 (97%)	
Yes	11 (3%)	9 (3%)	8 (6%)	28 (3%)	
Bronchitis, n (%)					0.316
No	319 (99%)	343 (98%)	133 (98%)	795 (98%)	
Yes	3 (1%)	8 (2%)	3 (2%)	14 (2%)	
Cardiovascular system					
Hypertension, n (%)					0
No	223 (69%)	204 (58%)	68 (50%)	495 (61%)	
Yes	99 (31%)	147 (42%)	68 (50%)	314 (39%)	
Atrial fibrillation, n (%)					0.001
No	312 (97%)	322 (92%)	119 (88%)	753 (93%)	
Yes	10 (3%)	29 (8%)	17 (12%)	56 (7%)	

(Continued)

10.3389/fimmu.2024.1441838

TABLE 2 Continued

Phenotype	Phenotype A(n=322)	Phenotype B(n=351)	Phenotype C(n=136)	Total (n=809)	P value
Cardiovascular system					
Coronary heart disease, n (%)					0.01
No	299 (93%)	303 (86%)	116 (85%)	718 (89%)	
Yes	23 (7%)	48 (14%)	20 (15%)	91 (11%)	
Arrhythmia, n (%)					0.003
No	290 (90%)	293 (83%)	107 (79%)	690 (85%)	
Yes	32 (10%)	58 (17%)	29 (21%)	119 (15%)	
Heart failure, n (%)					0
No	305 (95%)	296 (84%)	92 (68%)	693 (86%)	
Yes	17 (5%)	55 (16%)	44 (32%)	116 (14%)	
Digestive system					
Liver dysfunction, n (%)					0.013
No	290 (90%)	294 (84%)	110 (81%)	694 (86%)	
Yes	32 (10%)	57 (16%)	26 (19%)	115 (14%)	
Gastric cancer, n (%)					0.129
No	321 (100%)	348 (99%)	133 (98%)	802 (99%)	
Yes	1 (0%)	3 (1%)	3 (2%)	7 (1%)	
Colorectal cancer, n (%)					0.093
No	318 (99%)	345 (98%)	130 (96%)	793 (98%)	
Yes	4 (1%)	6 (2%)	6 (4%)	16 (2%)	
Esophageal cancer, n (%)					0.152
No	322 (100%)	347 (99%)	135 (99%)	804 (99%)	
Yes	0 (0.0%)	4 (1%)	1 (1%)	5 (1%)	
Hepatitis, n (%)					0.654
No	322 (100%)	349 (99%)	136 (100%)	807 (100%)	
Yes	0 (0.0%)	2 (1%)	0 (0.0%)	2 (0%)	
Urinary system					
Renal Insufficiency, n (%)					0
No	315 (98%)	315 (90%)	117 (86%)	747 (92%)	
Yes	7 (2%)	36 (10%)	19 (14%)	62 (8%)	
Urological tumors, n (%)					0.006
No	321 (100%)	346 (99%)	130 (96%)	797 (99%)	
Yes	1 (0%)	5 (1%)	6 (4%)	12 (1%)	
Kidney Stones, n (%)					0.578
No	311 (97%)	343 (98%)	131 (96%)	785 (97%)	
Yes	11 (3%)	8 (2%)	5 (4%)	24 (3%)	
Endocrine system					
Diabetes, n (%)					0

(Continued)

10.3389/fimmu.2024.1441838

TABLE 2 Continued

Phenotype	Phenotype A(n=322)	Phenotype B(n=351)	Phenotype C(n=136)	Total (n=809)	P value
Endocrine system					
No	277 (86%)	271 (77%)	97 (71%)	645 (80%)	
Yes	45 (14%)	80 (23%)	39 (29%)	164 (20%)	
Nervous system					
Senile dementia, n (%)					0.122
No	322 (100%)	348 (99%)	134 (99%)	804 (99%)	
Yes	0 (0.0%)	3 (1%)	2 (1%)	5 (1%)	
Cerebral infarction, n (%)					0
No	306 (95%)	319 (91%)	114 (84%)	739 (91%)	
Yes	16 (5%)	32 (9%)	22 (16%)	70 (9%)	
PD, n (%)					0.023
No	322 (100%)	344 (98%)	134 (99%)	800 (99%)	
Yes	0 (0.0%)	7 (2%)	2 (1%)	9 (1%)	
History of mlignancy, n (%)					0
No	307 (95%)	312 (89%)	114 (84%)	733 (91%)	
Yes	15 (4%)	39 (11%)	22 (16%)	76 (9%)	
Full Blood Count					
Hemoglobin (g/L), Mean ± SD	128 ± 15	123 ± 18	115 ± 21	124 ± 18	0
Neutrophil percent (%), median (IQR)	60 [52; 67]	75 [65; 83]	81 [70; 88]	69 [59; 81]	0
Neutrophil count (*10^9/L), median (IQR)	4 [3; 5]	5 [3; 7]	7 [4; 10]	4 [3; 7]	0
MCV (fl), median (IQR)	90 [87; 94]	91 [89; 94]	91 [89; 95]	91 [88; 94]	0.002
MCH (pg), median (IQR)	30 [29; 31]	30 [29; 32]	31 [29; 32]	30 [29; 31]	0.022
MCHC (g/L), median (IQR)	332 [326; 339]	331 [325; 341]	333 [325; 341]	332 [325; 340]	0.786
MPV (fl), median (IQR)	9 [9; 10]	9 [9; 10]	9 [8; 10]	9 [9; 10]	0.189
WBC Count (*10^9/L), median (IQR)	6 [5; 8]	6 [5; 9]	8 [6; 12]	7 [5; 9]	0
Lymphocyte percent (%), median (IQR)	30 [22; 37]	16 [10; 23]	10 [6; 17]	20 [11; 30]	0
Lymphocyte count (*10^9/L), median (IQR)	2 [2; 2]	1 [1; 1]	1 [1; 1]	1 [1; 2]	0
Eosinophil percent (%), median (IQR)	2 [1; 4]	1 [0; 2]	1 [0; 2]	2 [0; 3]	0
Monocyte percent (%), median (IQR)	7 [6; 8]	7 [5; 9]	6 [4; 9]	7 [5; 8]	0.141
Monocyte count (*10^9/L), median (IQR)	0 [0; 1]	0 [0; 1]	0 [0; 1]	0 [0; 1]	0.194
RDW (%), median (IQR)	13 [12; 13]	13 [12; 14]	14 [13; 14]	13 [12; 14]	0
Arterial Blood Gas					
HCO3 (mmol/L), median (IQR)	25 [24; 27]	25 [23; 28]	25 [21; 27]	25 [23; 27]	0.03
HCO3std (mmol/L), median (IQR)	25 [24; 26]	26 [24; 27]	25 [22; 27]	25 [24; 27]	0.223
pCO2 (kPa), median (IQR)	5 [5; 6]	5 [5; 6]	5 [4; 5]	5 [5; 6]	0
pH, median (IQR)	7 [7; 7]	7 [7; 7]	7 [7; 7]	7 [7; 7]	0
pO2 (kPa), median (IQR)	12 [11; 14]	12 [11; 15]	12 [9; 15]	12 [10; 15]	0.234
TCO2 (mmol/L), median (IQR)	50 [46; 54]	50 [45; 55]	48 [41; 55]	50 [45; 54]	0.134

(Continued)

10.3389/fimmu.2024.1441838

TABLE 2 Continued

Phenotype	Phenotype A(n=322)	Phenotype B(n=351)	Phenotype C(n=136)	Total (n=809)	P value
Arterial Blood Gas					
Glu	5 [4; 6]	6 [5; 7]	6 [5; 8]	5 [5; 7]	0
Renal Function					
Cr (umol/L), median (IQR)	57 [49; 69]	61 [52; 74]	65 [56; 88]	60 [51; 74]	0
BUN (mmol/L), median (IQR)	5 [4; 6]	5 [4; 7]	7 [5; 10]	5 [4; 7]	0
GFR (mL/min per1.75m^2), median (IQR)	108 [93; 127]	103 [81; 122]	96 [74; 121]	104 [84; 124]	0
UA (umol/L), median (IQR)	280 [226; 354]	262 [200; 329]	270 [184; 350]	269 [210; 345]	0.007
ACE (U/L), median (IQR)	24 [18; 31]	22 [17; 30]	24 [17; 30]	24 [18; 30]	0.237
Blood lipids					
LDL-C (mmol/L), median (IQR)	3 [2; 3]	2 [2; 3]	2 [1; 2]	2 [2; 3]	0
TG (mmol/L), median (IQR)	1 [1; 2]	1 [1; 1]	1 [1; 1]	1 [1; 1]	0.018
ApoE (mg/dL), median (IQR)	4 [3; 5]	3 [3; 5]	4 [3; 5]	4 [3; 5]	0.436
Coagulation					
D-Dimer (mg/L), median (IQR)	0 [0; 1]	1 [0; 1]	1 [1; 2]	1 [0; 1]	0
TT (s), median (IQR)	14 [13; 15]	14 [13; 15]	14 [13; 15]	14 [13; 15]	0.014
APTT (s), median (IQR)	12 [11; 12]	12 [11; 13]	13 [12; 14]	12 [11; 13]	0
INR, median (IQR)	1 [1; 1]	1 [1; 1]	1 [1; 1]	1 [1; 1]	0
PTT (s), median (IQR)	31 [29; 34]	31 [28; 33]	31 [28; 34]	31 [29; 34]	0.102
ATA (%), median (IQR)	89 [79; 97]	81 [71; 90]	73 [62; 85]	83 [72; 93]	0
Inflammatory Cytokine					
IL-10 (pg/mL), median (IQR)	5 [5; 5]	5 [5; 5]	5 [5; 7]	5 [5; 5]	0
IL-1B (pg/mL), median (IQR)	5 [5; 7]	5 [5; 10]	7 [5; 14]	5 [5; 10]	0
IL-2R (U/mL), median (IQR)	440 [327; 583]	606 [465; 808]	1468 [1290;1964]	582 [412; 899]	0
IL-6 (pg/mL), median (IQR)	5 [3; 10]	9 [4; 22]	20 [8; 51]	7 [3; 19]	0
IL-8 (pg/mL), median (IQR)	23 [12; 67]	25 [15; 53]	39 [21; 77]	26 [14; 61]	0
TNF-α (pg/mL), median (IQR)	12 [8; 28]	14 [9; 28]	19 [12; 30]	15 [9; 28]	0.001
IgG4 (g/L), median (IQR)	1 [0; 1]	0 [0; 1]	1 [0; 1]	0 [0; 1]	0.188
Electrolytes					
P (mmol/L), median (IQR)	1 [1; 1]	1 [1; 1]	1 [1; 1]	1 [1; 1]	0
Cl (mmol/L), median (IQR)	105 [104; 107]	104 [102; 107]	103 [100; 106]	105 [102; 107]	0
Mg (mmol/L), median (IQR)	1 [1; 1]	1 [1; 1]	1 [1; 1]	1 [1; 1]	0.014
Potassium (mmol/L), median (IQR)	4 [4; 4]	4 [4; 4]	4 [4; 4]	4 [4; 4]	0.184
Ca (mmol/L), median (IQR)	2 [2; 2]	2 [2; 2]	2 [2; 2]	2 [2; 2]	0
Sodium (mmol/L), median (IQR)	140 [138; 142]	139 [136; 141]	136 [131; 140]	139 [136; 141]	0
Inflammation Measurements					
CRP (mg/L), median (IQR)	8 [2; 30]	34 [7; 80]	107 [37; 160]	25 [4; 78]	0
PCT(ng/mL), median (IQR)	0 [0; 0]	0 [0; 0]	0 [0; 1]	0 [0; 0]	0
ESR (mm/h), median (IQR)	32 [16; 53]	45 [24; 71]	64 [35; 90]	41 [21; 69]	0

(Continued)

10.3389/fimmu.2024.1441838

TABLE 2 Continued

Phenotype	Phenotype A(n=322)	Phenotype B(n=351)	Phenotype C(n=136)	Total (n=809)	P value
Myocardial Enzyme					
CK-MB (U/L), median (IQR)	4 [3; 6]	5 [4; 8]	6 [4; 9]	5 [3; 7]	0
cTnI (ng/ml), median (IQR)	0 [0; 0]	0 [0; 0]	0 [0; 0]	0 [0; 0]	0
CK (U/L), median (IQR)	63 [42; 94]	67 [41; 114]	60 [34; 122]	65 [41; 103]	0.329
α-HBDH (U/L), median (IQR)	124 [104; 153]	150 [120; 182]	166 [128; 233]	142 [113; 173]	0
LDH (U/L), median (IQR)	190 [160; 220]	220 [188; 266]	268 [203; 336]	211 [176; 264]	0
Cell immunity					
CD3T (%), median (IQR)	75 [69; 80]	67 [59; 74]	69 [59; 76]	71 [64; 77]	0
CD4T (%), median (IQR)	45 [40; 50]	40 [33; 46]	40 [31; 47]	42 [35; 48]	0
CD8T (%), median (IQR)	25 [20; 31]	23 [17; 30]	24 [17; 32]	24 [18; 31]	0.023
CD3T (Cells/uL), median (IQR)	1360 [1157;1630]	687 [482; 902]	494 [343; 826]	932 [578;1284]	0
CD4T (Cells/uL), median (IQR)	827 [687;1013]	414 [267; 519]	293 [205; 480]	537 [332; 776]	0
CD64 infection index	1 [0; 1]	1 [0; 2]	2 [1; 5]	1 [0; 2]	0
CD8T (Cells/uL), median (IQR)	462 [369; 604]	226 [152; 324]	183 [100; 301]	314 [186; 460]	0
Humoral Immunity					
Ig A (g/L), median (IQR)	2 [2; 3]	3 [2; 3]	2 [2; 4]	2 [2; 3]	0.869
Ig E (IU/mL), median (IQR)	49 [18; 186]	57 [21; 162]	137 [29; 791]	58 [21; 211]	0
Ig G (g/L), median (IQR)	12 [11; 14]	12 [10; 15]	12 [10; 15]	12 [11; 15]	0.275
Ig M (g/L), median (IQR)	1 [1; 1]	1 [1; 1]	1 [0; 1]	1 [1; 1]	0
Liver Function					
GGT (U/L), median (IQR)	26 [16; 46]	30 [18; 58]	37 [24; 68]	29 [18; 55]	0
Alb (g/L), Mean ± SD	38 ± 4	35 ± 5	30 ± 5	35 ± 5	0
AST (U/L), median (IQR)	18 [12; 31]	21 [13; 34]	24 [15; 40]	20 [12; 34]	0.003
ALT (U/L), median (IQR)	18 [15; 26]	22 [17; 32]	27 [20; 46]	21 [16; 31]	0
ALP (U/L), median (IQR)	73 [59; 90]	74 [62; 92]	88 [68; 124]	75 [61; 94]	0
PA (mg/L), median (IQR)	192 [148; 230]	142 [103; 193]	98 [70; 142]	159 [109; 207]	0
TB (umol/L), median (IQR)	8 [6; 11]	9 [7; 11]	9 [7; 14]	9 [6; 12]	0.047
TP (g/L), median (IQR)	66 [63; 70]	62 [58; 67]	61 [55; 65]	64 [60; 68]	0
FIB (g/L), median (IQR)	4 [3; 5]	4 [3; 5]	5 [4; 5]	4 [3; 5]	0
Complement system					
C3 (g/L), median (IQR)	1 [1; 1]	1 [1; 1]	1 [1; 1]	1 [1; 1]	0.032
C4 (g/L), median (IQR)	0 [0; 0]	0 [0; 0]	0 [0; 0]	0 [0; 0]	0.622
CH50 (U/mL), Mean ± SD	51 ± 14	49 ± 15	48 ± 17	50 ± 15	0.11
Respiratory support					
HFNC, n (%)					0
No	319 (99%)	338 (96%)	118 (87%)	775 (96%)	
Yes	3 (1%)	13 (4%)	18 (13%)	34 (4%)	
NIMV, n (%)					0

(Continued)

10.3389/fimmu.2024.1441838

TABLE 2 Continued

Phenotype	Phenotype A(n=322)	Phenotype B(n=351)	Phenotype C(n=136)	Total (n=809)	P value
Respiratory support					
No	317 (98%)	311 (89%)	113 (83%)	741 (92%)	
Yes	5 (2%)	40 (11%)	23 (17%)	68 (8%)	
IMV, n (%)					0.485
No	321 (100%)	347 (99%)	135 (99%)	803 (99%)	
Yes	1 (0%)	4 (1%)	1 (1%)	6 (1%)	
Clinical Outcomes					
ICU duration (days), median (IQR)	0 [0; 0]	0 [0; 6]	0 [0; 17]	0 [0; 0]	0
Ventilation duration (days), median (IQR)	0 [0; 0]	0 [0; 0]	0 [0; 4]	0 [0; 0]	0
Length of stay, median (IQR)	8 [7; 10]	10 [8; 15]	14 [9; 20]	9 [7; 14]	0
Inpatient Outcome, n (%)					0
Alive	322 (100%)	332 (95%)	115 (85%)	769 (95%)	
Dead	0 (0.0%)	19 (5%)	21 (15%)	40 (5%)	
ICU free days (days), median (IQR)	7 [6; 9]	8 [1; 11]	5 [0; 11]	7 [4; 10]	0.005
Outcome at 28 days, n (%)					0
Alive	322 (100%)	338 (96%)	119 (88%)	779 (96%)	
Dead	0 (0.0%)	13 (4%)	17 (12%)	30 (4%)	
Days from symptom onset (days), median (IQR)	10 [7; 14]	9 [5; 14]	10 [6; 14]	10 [6; 14]	0.199
ICU admission, n (%)					0
No	300 (93%)	261 (74%)	76 (56%)	637 (79%)	
Yes	22 (7%)	90 (26%)	60 (44%)	172 (21%)	

COPD, Chronic obstructive pulmonary disease; OSAHS, Obstructive sleep apnea hypopnea syndrome; MCV, Mean corpuscular volume; MCH, Mean corpuscular hemoglobin; MCHC, Mean corpuscular hemoglobin concentration; WBC, White bold cell; MPV, Mean platelet volume; RDW, Red blood cell distribution width; HCO3, Carbonic acid hydrogen radical; HCO3std, Standard bicarbonate; pCO2, Partial pressure of carbon dioxide; Ph, Potential of hydrogen; pO2, Partial pressure of oxygen; TCO2, Total carbon dioxide; Glu, Glucose; Cr, Creatinine; BUN, Blood urea nitrogen; GFR, Glomerular Filtration Rate; UA, Urine Acid; ACE, Angiotensin-Converting Enzyme; LDL-C, Low-Density Lipoprotein Cholesterol; TG, Triglyceride; ApoE, Apolipoprotein E, TT, Thrombin time; APTT, Activated partial thromboplastin time; INR, International normalized ratio; PTT, Partial thromboplastin time; ATA, Antithrombin Activity; IL-10, Lnterleukin-10; IL-1B, Lnterleukin-1B; IL-2R, Lnterleukin-2 Receptor; IL-6, Lnterleukin-6; IL-8, Lnterleukin-8; TNF-α, Tumor necrosis factor-alpha; IgG4, Immunoglobulin G4; CK-MB, Creatine kinase MB; cTnI, Cardiac troponin I; CK, Creatine kinase; α-HBDH, Alpha-hydroxybutyric dehydroge; LDH, Lactate dehydrogenase; Ig A, Immunoglobulin A; Ig E, Immunoglobulin E; Ig G, Immunoglobulin G; Ig M, Immunoglobulin M; GGT, γ-Glutamyl transferase GGT; Alb, Albumin; AST, Aspartate aminotransferase; ALT, Alanine aminotransferase; ALP, Alkaline phosphatase; PA, Prealbumin; TB, Total bilirubin; TP, Total Protein; FIB, Fibrinogen; C3, Complement C3; C4, Complement C4; CH50, 50% Hemolytic unit of Complement; HFNC, High Flow Nasal Cannula; NIMV, Noninvasive Mechanical Ventilation; IMV, Invasive Mechanical Ventilation.

with prior research (23, 24), the most prevalent comorbidities included hypertension (40%, n=467) and type 2 diabetes mellitus (22%, n=252). To determine the latent immune phenotypes of CAP, the "Consensus Cluster Plus" package was utilized for consensus clustering across the training, validation, and meta cohorts. This analysis identified three distinct immune phenotypes within each cohort, as demonstrated in Figures 2A, B, Supplementary Figures S3A, B, and S4A, B, indicating that a tripartite classification was most suitable for the data. The "nbclust" package (15, 25) was routinely utilized for unsupervised clustering to ascertain the optimal number of clusters. In agreement with the majority rule, three distinct clusters were deemed to be ideal for all cohorts, as depicted in the Supplementary Materials (Supplementary Figures S2A, S3C, and S4C). Grounded on these findings and informed by prior knowledge, a tripartite classification of phenotypes was determined to be most appropriate. The results of clustering were visualized by t-distributed stochastic neighbor embedding (t-SNE), Principal Component Analysis (PCA) and Uniform Manifold Approximation and Projection (UMAP) plot, as shown in Figure 2C, Supplementary Figures S2B, C, S3D–F, and S4D–F. The baseline characteristics of each cohort are presented in Table 2 and Supplementary Tables S1, S2. The three distinct immune phenotypes varied in size, ranging from 16.8% to 43.4% of the cohorts, and demonstrated differences in clinical presentations and patterns of organ dysfunction. These variances are detailed in Supplementary Tables S1, S2, and Figures 3A–D, Supplementary Figures S7A–D, and S8A–D. Within the training cohort, patients with CAP were grouped into three phenotypes based on distinct laboratory features. Phenotype A patients exhibited elevated levels of prealbumin. In contrast, phenotype B was characterized by

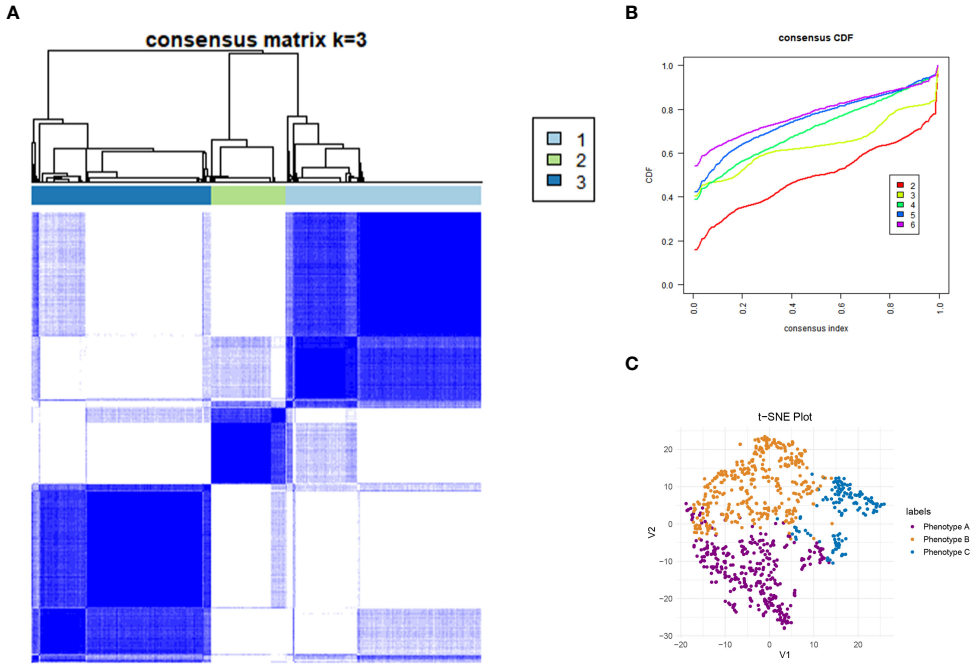

FIGURE 2
Consensus Clustering and visualization. **(A)** Identification of three immune phenotypes of community acquired pneumonia (CAP) patients by consensus clustering. **(B)** Cumulative distribution function (CDF) curve illustrated consensus distribution for each phenotype. **(C)** T-distributed stochastic neighbor embedding (t-SNE) method successfully divided CAP patients into three distinct immune phenotypes. The purple dot represent patients belong to phenotype A. Patients with phenotype B are represented by a yellow dot, and those with phenotype C by a blue dot. CAP, community acquired pneumonia; t-SNE, T-distributed stochastic neighbor embedding; CDF, Cumulative distribution function.

reduced IgG4, triglycerides, and uric acid levels. Patients classified as phenotype C tended to be older males with a higher likelihood of being admitted to the ICU. Variations in laboratory indicators were apparent among the three immune phenotypes. According to the standardized mean difference between phenotypes (Figures 3E–G), phenotype A patients showed fewer laboratory abnormalities and less evidence of organ dysfunction. Conversely, phenotype B patients had indicators suggestive of renal dysfunction, while

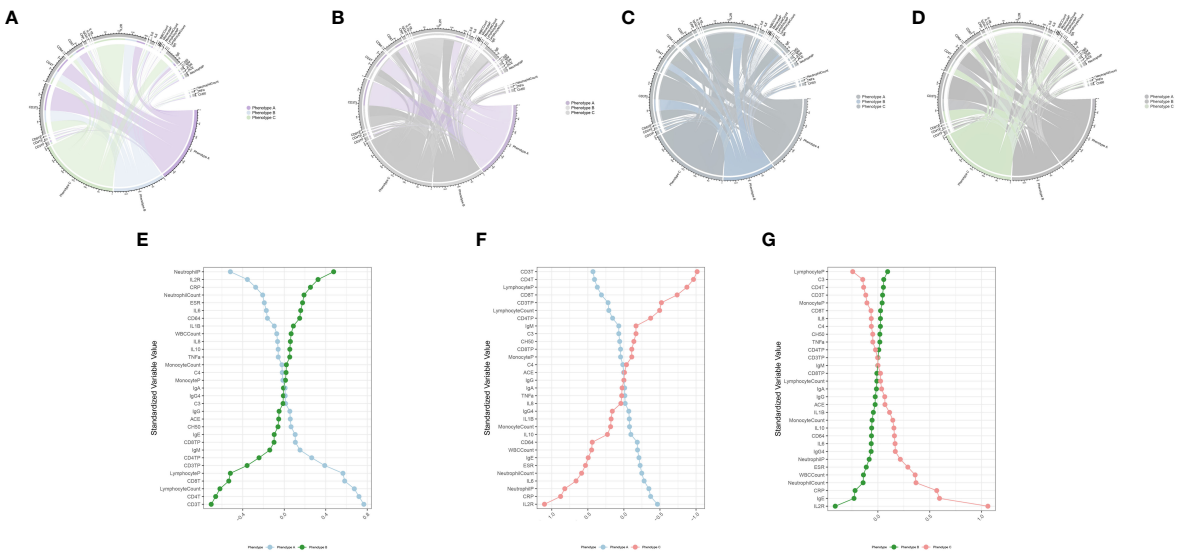

FIGURE 3
Association and variation between clinical immunological indicators and three phenotypes. Chord diagram **(A–D)** of the association between clinical immunological variables and each phenotype in training cohort. Different phenotypes were shown in different colors: phenotype A is purple, phenotype B is blue, and phenotype C is green. Rank plot **(E–G)** of variable mean among various phenotypes in training cohort. Variables were normalized by mean and standard error.

those in phenotype C were more likely to display increased inflammatory markers (such as IL-2R, IL-8, IL-6), alongside reduced immunologic parameters of inflammation (e.g., CD3, CD4, CD8), lower albumin levels, and elevated body temperatures. Patients classified as Phenotype B tend to demonstrate moderate abnormalities in their laboratory tests. Relative to Phenotype A, those with Phenotype B show elevated levels of neutrophils, C-reactive protein (CRP), and erythrocyte sedimentation rate (ESR). In addition, there is a concurrent suppression of lymphocytes and their subsets. The levels of IgG4 do not vary significantly between these phenotypes. Patients identified as Phenotype C also manifest a similar pattern, with increased inflammatory markers (IL-2R, neutrophil count, and ESR) and decreased immunological indicators (CD3+CD4+CD8+ lymphocytes); however, IgG, IgA, and TNF-α levels remain statistically unchanged. When drawing comparisons between Phenotypes B and C, a rise in IL-2R, CRP, ESR, and IgE is noted, along with a reduction in lymphocyte-related indicators. These differential markers underscore their importance in phenotype classification and, indirectly, the robustness of this classification scheme. Further corroboration of these findings is evident in the validation and meta cohorts, as depicted in Supplementary Figures S7E–G and S8E–G.

Relationship between distinct clinical immune phenotypes and clinical outcomes

In current research, distinct immune phenotypes were correlated with primary and secondary outcomes. Within the training cohort, Phenotype C had the highest inpatient mortality rate, with 21 deaths (15.4%, n=136), markedly higher than that observed in Phenotype A (0 deaths, 0%, n=322) and Phenotype B (19 deaths, 5.4%, n=351) (P<0.001). Furthermore, Phenotype C experienced the highest 28-day mortality rate with 17 deaths (12.5%, n=136) compared to Phenotypes A (0 deaths, 0%, n=322) and B (13 deaths, 3.7%, n=351). Similar trends in survival outcomes were observed in the meta and validation cohorts, as detailed in Supplementary Tables S1 and S2. Across all three cohorts, patients characterized as Phenotype C consistently exhibited a poorer prognosis compared to those classified as Phenotypes A and B (P<0.001; Figures 4A, B, Supplementary Figures S5A, B, and S6A, B). Furthermore, the three clinically derived immune phenotypes showed notable differences across all primary and secondary outcomes (Figures 4C–H, Supplementary Figures S5C–H, and S6C–H). Our investigation also explored the correspondence between the immune phenotypes identified in this study and traditional clinical categorizations such as CURB-65 and PSI. The results indicate that our immune phenotyping operates independently of these conventional classifications (Figure 6I, Supplementary Figures S9A, B), firmly establishing the utility and precision of our clustering approach. The presented evidence highlights distinct clinical outcomes among the phenotypes and underscores the significance of adopting this new classification in clinical practice, thereby demonstrating its practical relevance.

Construction and evaluation of integrated machine learning signatures

Based on the immunological laboratory indicators available at Xinhua Hospital, variables exhibiting a missing rate exceeding 20% were excluded. Consequently, 31 clinical immunological laboratory indicators were selected for model development. Contrary to previous research (7, 26), our investigation not only concentrates on the prognosis of patients with CAP but also considers the likelihood of disease severity. In recent years, machine learning has gained widespread application in medical research, demonstrating robust predictive performance (27–29). Several studies have also examined the application of machine learning in forecasting CAP outcomes (7, 30, 31). However, these investigations have predominantly utilized a narrow range of machine learning algorithms and have focused primarily on predicting mortality. Physicians should, however, consider strategies for the early identification of potentially severe pneumonia patients. To address the limitations of previous research, this study has developed survival models for patients and predictive models for assessing the severity of the risk. Nine machine learning algorithms —namely, SuperPC, PlsRocx, Elastic Net, Ridge, Lasso, stepwise Cox, Random Survival Forests (RSF), and Gradient Boosting Machine (GBM)—were applied to both training and validation cohorts to facilitate optimal model selection. The results indicated that SuperPC exhibited strong predictive performance with a training cohort C-index of 0.784 and a validation cohort C-index of 0.935, averaging at 0.86 (Figure 5A). Consequently, it was chosen as the superior prognostic model. The variables included in the prognostic model were presented in Supplementary Table S3. Additionally, in order to identify severe patients earlier, we utilized 12 common machine learning algorithms (RF, GBM, Stepglm, Lasso, Enet, Glmboost, LDA, Ridge, plsRglm, xgboost, naivebayes, and SVM) to construct a predictive model for severe pneumonia. The results indicate that the random forest algorithm demonstrated the highest predictive performance in both the training cohort and the validation cohort (training cohort C-index: 0.998, validation cohort C-index: 0.794, average C-index: 0.896, Figure 5B). The variables encompassed in this model are also detailed in Supplementary Table S3. In this study, we conducted a rigorous evaluation of ourmodels' performance through a comparative analysis with conventional evaluationmetrics by examining their Receiver Operating Characteristic (ROC) curves (see Figures 6C–H). Remarkably, the machine learning approaches we employed demonstrated superior performance to traditional evaluation criteria, not only within the training cohort but also in the validation cohort and meta cohort (see Supplementary Figure S10). This finding underscores the potential of machine learning methodologies in enhancing predictive accuracy in this context.

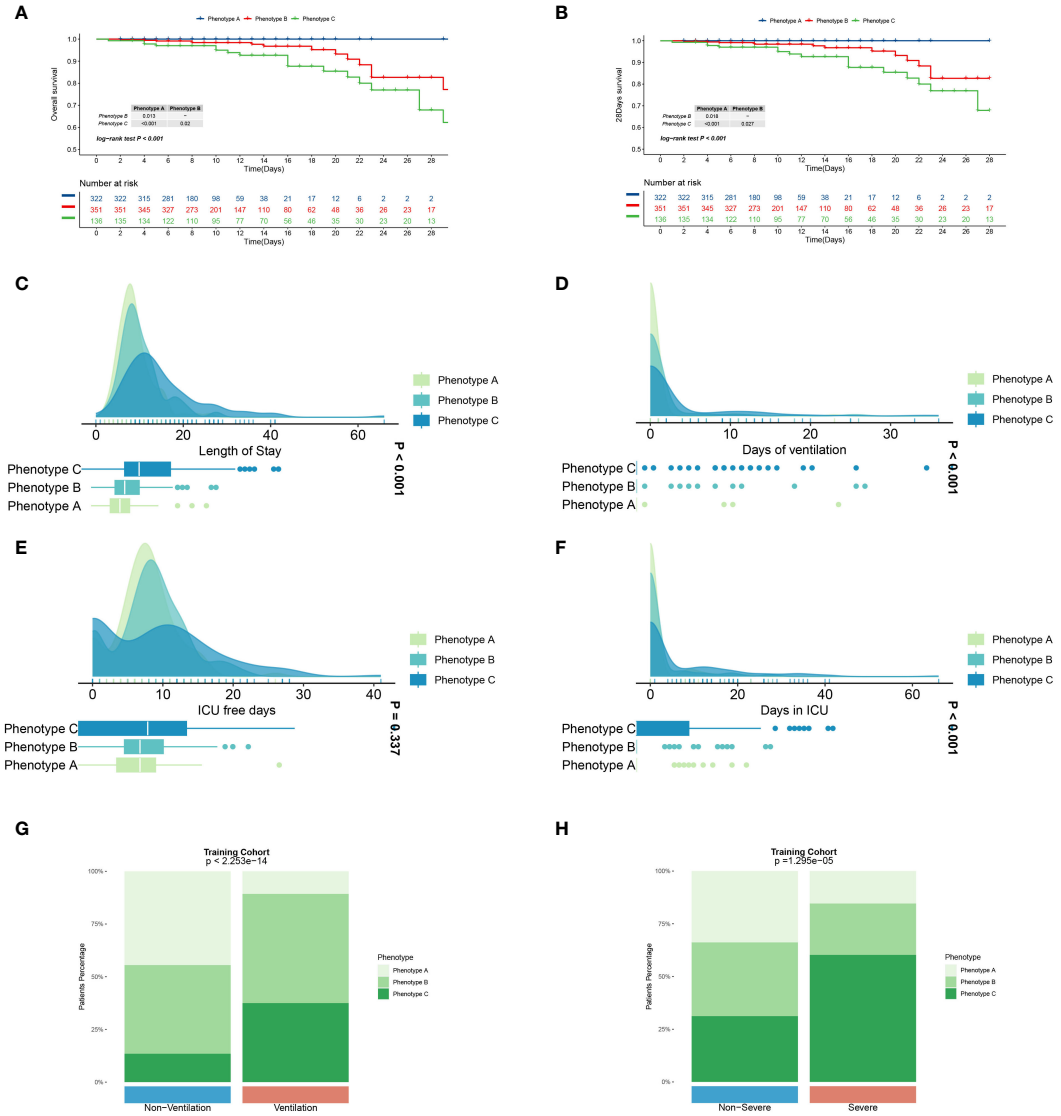

FIGURE 4
Primary and secondary outcomes among three distinct immune phenotypes in training cohort. **(A)** Survival curves for various phenotype patients during their hospitalization. **(B)** Survival curves for various phenotype patients over 28 days. Blue line represents Phenotype A patients, red for Phenotype B patients, and green for Phenotype C patients. CAP patients in Phenotype A had a better prognosis than those in Phenotype A and C (P<0.05).Phenotype C CAP patients experience extended hospital stays **(C)** and ICU stays **(F)**, prolonged ventilation days **(D)**, and fewer ICU-free days **(E)** in comparison to patients with the other two phenotypes. Green represents Phenotype A patients, light blue for Phenotype B patients, and dark blue for Phenotype C patients. Patients with phenotype C comprise a greater proportion of patients requiring assisted ventilation **(G)** and those with severe pneumonia **(H)**. Differences are observed in patient composition with respect to ventilation and the presence of severe pneumonia. P<0.001.

Furthermore, we leveraged a transcriptome database related to CAP, GSE188309, which includes data from 198 patients (refer to Supplementary Tables S4 and S5 for details) (20, 32). Using Single Sample Gene Set Enrichment Analysis (ssGSEA), an algorithm frequently utilized for assessing immune infiltration (33), we analyzed the GSE188309 dataset and identified differences in activated CD4+ T cell levels between survivors and nonsurvivors (see Supplementary Figure S11). This underscores the significance of CD4+ T cells as a crucial variable in our models. Surprisingly, CD4+ T cells were incorporated into both the prognostic and predictive models, highlighting their critical role in forecasting the severity and clinical outcomes for patients with CAP. Additionally, to validate the performance of our models, we compared their Receiver Operating Characteristic (ROC) curves with those derived from conventional evaluation criteria. Collectively, our results bolster the credibility of using machine learning to predict patient prognosis.

Discussion

In this investigation, we identified and substantiated three distinct immune phenotypes through dual clustering techniques, analyzing data from 1,165 hospitalized patients with CAP. Phenotype C emerged as indicative of a poorer prognosis, lengthier hospitalization, and an increased need for assisted

10.3389/fimmu.2024.1441838

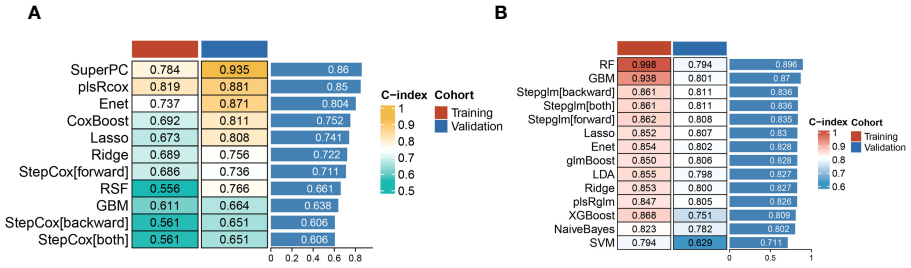

FIGURE 5
Heatmap dipicted C-index of various machine learning method in training and validation cohort for patients' outcome **(A)** and pneumonia severity **(B)**.

ventilation. Moreover, the study employed over 20 machine-learning algorithms to forecast both the prognosis and severity of CAP.

Current literature includes descriptions of phenotypes in patients with ARDS and sepsis. In their work, Calfee et al. identified two distinct ARDS phenotypes through latent class analysis (LCA), employing biomarkers and clinical data in a retrospective examination of two randomized controlled trials (RCTs) (34). Similarly, Christopher W. Seymour and colleagues (11) delineated four sepsis phenotypes, establishing correlations between host-response patterns and clinical outcomes via retrospective analysis. The secretion of inflammatory cytokines and the modulation of immune cell activity are critical in the pathogenesis of SCAP. Consequently, assessment of the immune phenotype in individuals with CAP can enable clinicians to more accurately distinguish patients at risk of progressing to SCAP. In a study conducted by Raul M. Mackenzie (35), a cohort of 217 hospitalized CAP patients underwent evaluation of lymphocyte subsets, inflammatory mediators, and immunoglobulin subclasses, revealing a distinctive lymphopenicCAP profile. This profile, characterized by diminished CD4+ lymphocytes, elevated inflammatory responses, and reduced IgG2 concentrations, was associated with increased disease severity upon admission and a poorer overall prognosis. Notwithstanding these findings, the study was limited by a relatively small sample size and predominantly included immunocompetent patients. By contrast, our research encompasses a broader demographic and a significantly larger sample size, thus providing a more comprehensive understanding of the immunological landscape in CAP. This study aimed to delineate immune phenotypes that correlate with the prognosis of patients with CAP. Analysis of 31 immunological and inflammatory parameters was conducted through unsupervised clustering, employing the "Consensus clustering" algorithm. We identified three distinct CAP immune phenotypes: Phenotype A emerged as the least severe, characterized by the lowest deviations in laboratory markers and organ function. In stark contrast, Phenotype C represented the most critical illness phenotype, marked by an increased frequency of ICU admissions and prevalence among elderly patients. Phenotype B represented an intermediate level of severity. The early detection of Phenotype C is thus crucial for improving outcomes in SCAP patients. Intriguingly, these immunophenotypes could not be completely accounted for by traditional severity scores such as the PSI and CURB-65. Most patients with low PSI and CURB-65 scores were classified under Phenotypes A and B; however, a minority presented with the high-risk Phenotype C. Therefore, incorporating immunophenotyping into the assessment offers a valuable tool for the early recognition of high-risk patients, who score low on CURB-65 and PSI indices, significantly contributing to the enhancement of their clinical prognosis.

Although immune phenotypes offer valuable insights, they do not achieve the prognostic precision of predictive models. To assess the reliability of immune phenotypes in real-world clinical contexts, we examined the association between immune phenotype classification and clinical outcomes. Our findings indicated that the three deduced immune phenotypes exhibited significant disparities across all primary and secondary outcomes measured. Notably, patients categorized within Phenotype C experienced poorer prognostic outcomes compared to those with Phenotypes A and B. These observations underscore the utility of immune phenotype classification for prognostic evaluation in patients with CAP.

Multiple studies have demonstrated the efficacy of ML in enhancing mortality predictions for patients with CAP. Cilloniz et al. reported that an adapted SeF model employing ML exhibited promise in augmenting the accuracy of mortality predictions for CAP patients within the context of a derivation-validation retrospective study (6). Despite such advancements, research on prognostic models for CAP that incorporate immunological markers remains scarce. In our investigation, we performed an analysis of data derived from the immunological laboratory indicators of CAP patients. Our findings indicate that the prognostic model established via the SuperPC algorithm demonstrates a robust predictive capability. When juxtaposed with existing models, such as CURB-65 and PSI, our model achieves a comparable mean C-index, suggesting its utility as an adjunctive tool for the clinical assessment of CAP patients. Our research not only corroborates the existing literature regarding CAP patient prognosis but also extends the analysis to encompass the likelihood of the severity of the disease. In evaluating 12 different ML algorithms, we ascertained that the Random Forest algorithm delivers a superior mean C-index, which signifies a more potent predictive performance specifically for patients with SCAP.

Lymphocytopenia has been acknowledged as an independent risk factor for adverse outcomes in patients with CAP (36). The cause of lymphocytopenia is unknown, although several causes have been

10.3389/fimmu.2024.1441838

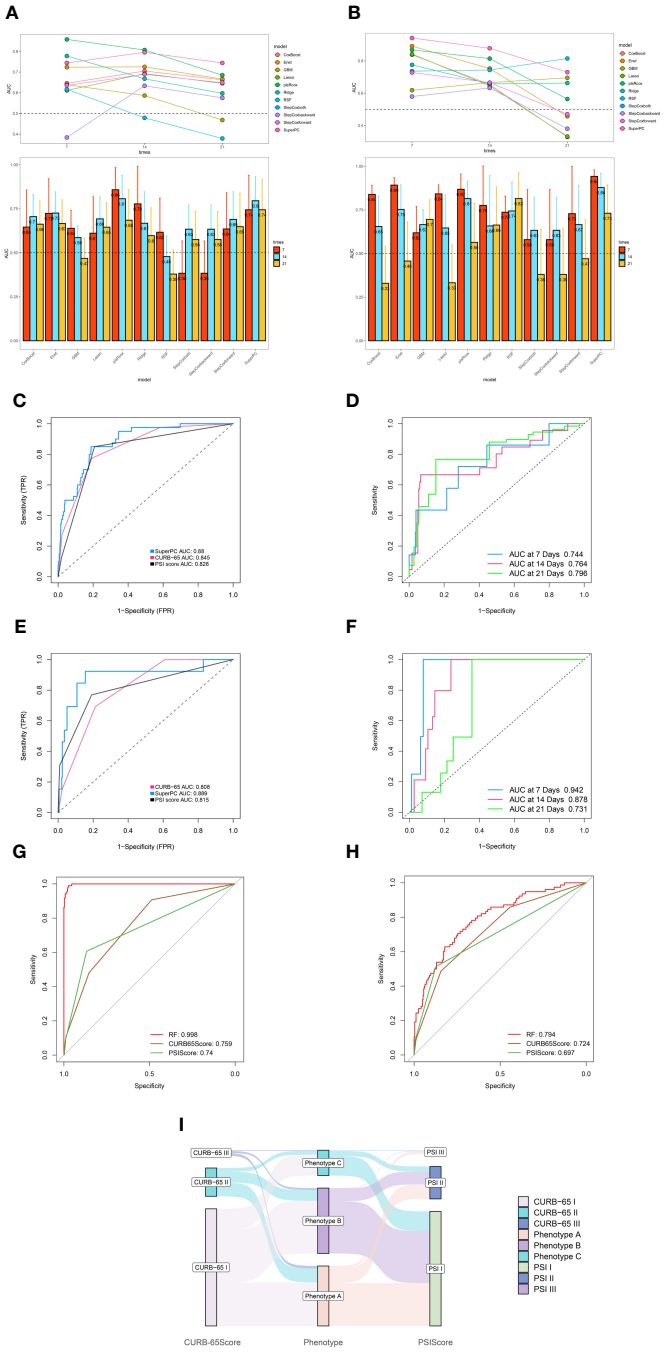

FIGURE 6
Robust performance of machine learning algorithm. **(A)** Time dependent bar and line graph of 9 machine learning methods at 7 days, 14days, and 21 days in training cohort. **(B)** Time dependent bar and line graph of 9 machine learning methods at 7 days, 14days, and 21 days in validation cohort. **(C)** The performance of SuperPC method and conventional PSI and CURB-65 evaluation criteria in training cohort. **(D)** Time dependent ROC curve of SuperPC method at 7 days, 14 days, 21 days in training cohort. **(E)** The performance of SuperPC method and conventional PSI and CURB-65 evaluation criteria in validation cohort. **(F)** Time dependent ROC curve of SuperPC method at 7 days, 14 days, 21 days in validation cohort. The performance of Random forest method and conventional PSI and CURB-65 evaluation criteria in training **(G)** and validation **(H)** cohort for predicting severe pneumonia. **(I)** Sankey plot illustrated the relationship between immune phenotypes and conventional pneumonia severity index (PSI) and CURB-65 evaluation criteria in Training cohort.

proposed, such as increased apoptosis, limitations in the host immune system's mobilization of these cells, or compartmentation at the site of infection ADDIN EN.CITE (35). Variations in lymphocyte subsets, particularly in CD4 T cells, have been implicated in the immunopathogenesis of CAP. Indeed, alterations in CD4 T cells have been associated with increased disease severity, particularly in the elderly and frail patient populations (37, 38). Our study corroborates these findings by demonstrating the prognostic and predictive significance of CD4 T cell changes. Furthermore, an analysis of the GSE188309 dataset reinforced the observation of a

discernible difference in the activation levels of CD4 T cells between survivors and non-survivors of CAP. These results underscore the pivotal role of CD4 T cells in forecasting clinical outcomes and determining disease severity in CAP patients. At present, the mechanism of CD4 T cells participating in CAP is complex and not completely clear. More studies are focused on the mechanism of CD4+T cells in pneumonia caused by viral infection, especially pneumonia caused by SARS-CoV-2. CD4+T cells can differentiate into a range of helper and effector cell types, thereby exerting antiviral capabilities. Virus-specific CD4+ T cells differentiate into Th1 cells and T follicular help-er cells (Tfh). Th1 cells have antiviral activity by producing IFNγ and related cytokines. Specific circulating Tfh cells (cTfh) are produced during acute SARS-CoV-2 infection (39). A study by Liu et al. analyzed the lymphocyte subsets of COVID-19-associated pneumonia and CAP and showed that CD16+CD56+%, CD4+/CD8+ ratio, CD19+, and CD3+CD4+ independently predicted differentiation of COVID-19 and CAP. CD3+CD4+ and CD3+CD8+ counts were independent predictors of disease severity (40).

For pneumonia caused by other pathogens, regulatory CD4 +CD25+ T cells were found to suppress respiratory inflammation by promoting IL-17 and IFN-γ responses in a mouse model of mycoplasma pneumonia (41). However, the exact mechanisms underlying these observations in our study warrant comprehensive investigation through basic experimental research.

Conclusion

Our study's principal finding demonstrates that evaluating immunological parameters upon hospital admission assists in stratifying CAP patients into three distinct immune phenotypes. Moreover, these immune phenotypes show a strong correlation with patient prognoses. We also discerned significant predictive capabilities within the SuperPC algorithm, suggesting its utility as an ancillary tool for assessing CAP. Notably, our investigation constitutes the most extensive analysis of CAP clinical phenotypes to date. An additional strength of this study is its breadth; rather than focusing on CAP related to specific pathogens, it encompasses a comprehensive evaluation of the immunophenotypes across the spectrum of CAP. This approach allows for patient classification and tailored intervention prior to the confirmation of precise etiologic agents, offering crucial guidance, especially for cases where pathogen identification proves challenging. Moreover, the rigorous application of inclusion and exclusion criteria enhances the applicability of our findings, rendering the results of significant relevance to the broader patient population.

Limitation

Our study possesses several limitations. Firstly, its scope is confined to a single center, which may not be representative of broader populations, in contrast to multi-center studies. Secondly, the retrospective nature of our research necessitates the implementation of a prospective study to corroborate our findings and inform future clinical practice. Looking ahead, the inclusion of a wider range of variables beyond immunological indicators will enable a more comprehensive assessment of multi-organ involvement in patients with CAP. And finally, other experiment methods for example flow mass spectrometry can be applied in figuring out the potential mechanism of CD4 T cells in CAP.

Data availability statement

The data analyzed in this study is subject to the following licenses/restrictions: Contact corresponding author for the dataset. Requests to access these datasets should be directed guoxuejun@xinhuamed.com.cn.

Ethics statement

The studies involving humans were approved by Institutional Review Board (IRB) of Xinhua Hospital, Shanghai Jiao Tong University School of Medicine, Shanghai, China. The studies were conducted in accordance with the local legislation and institutional requirements. Written informed consent for participation was not required from the participants or the participants' legal guardians/ next of kin in accordance with the national legislation and institutional requirements.

Author contributions

QQ: Writing – review & editing, Writing – original draft, Visualization, Validation, Software, Resources, Project administration, Methodology, Investigation, Formal Analysis, Data curation, Conceptualization. HY: Writing – original draft, Investigation, Conceptualization. JZ: Writing – original draft, Investigation, Conceptualization. XX: Writing – review & editing, Data curation. QL: Writing – review & editing, Visualization, Conceptualization. WG: Writing – review & editing, Writing – original draft, Supervision, Software, Funding acquisition, Conceptualization. XG: Writing – review & editing, Supervision, Conceptualization.

Funding

The author(s) declare financial support was received for the research, authorship, and/or publication of this article. This work received funding from the Shanghai Science and Technology Commission (Grant No. 22Y11901700).

Conflict of interest

The authors declare that the research was conducted in the absence of any commercial or financial relationships that could be construed as a potential conflict of interest.

Publisher's note

Supplementary material

The Supplementary Material for this article can be found online at: https://www.frontiersin.org/articles/10.3389/fimmu.2024.1441838/full#supplementary-material

SUPPLEMENTARY TABLE 1
Characteristics and outcomes of patients divided by immune phenotypes in validation cohort.

SUPPLEMENTARY TABLE 2
Characteristics and outcomes of patients divided by immune phenotypes in meta cohort.

SUPPLEMENTARY TABLE 3
Features incorporated in prognostic and diagnostic model.

SUPPLEMENTARY TABLE 4
Expression matrix of GSE188309.

SUPPLEMENTARY TABLE 5
Clinical information of GSE188309.

SUPPLEMENTARY FIGURE 1
Graphic flowchart of this research.

SUPPLEMENTARY FIGURE 2
Visualization of clustering and dimensionality reduction results of training cohort. **(A)** Nbclust method illustrated the optimal groups of training cohort was three. **(B)** Principal Component Analysis (PCA) method successfully divided CAP patients into three distinct immune phenotypes. **(C)** Uniform Manifold Approximation and Projection (UMAP) method successfully divided CAP patients into three distinct immune phenotypes. Patients with phenotype B are represented by a yellow dot, the blue dots represent patients belong to phenotype and those with phenotype C by a purple dot.

SUPPLEMENTARY FIGURE 3
Consensus Clustering and dimensionality reduction visualization in validation cohort. **(A)** Identification of three immune phenotypes of community acquired pneumonia (CAP) patients by consensus clustering. **(B)** Cumulative distribution function (CDF) curve illustrated consensus distribution for each phenotype. **(C)** Visualization of Nbclust method in determining optimal clusters of CAP patients. **(D)** T-distributed stochastic neighbor embedding (t-SNE) method successfully divided CAP patients into three distinct immune phenotypes. **(E)** Uniform Manifold Approximation and Projection (UMAP) method successfully divided CAP patients into three distinct immune phenotypes. **(F)** Principal Component Analysis (PCA) method successfully divided CAP patients into three distinct immune phenotypes.

SUPPLEMENTARY FIGURE 4
Consensus Clustering and dimensionality reduction visualization in meta cohort. **(A)** Identification of three immune phenotypes of community acquired pneumonia(CAP) patients by consensus clustering. **(B)** Cumulative distribution function(CDF) curve illustrated consensus distribution for each phenotype. **(C)** Visualization of Nbclust method in determining optimal clusters of CAP patients. **(D)** T-distributed stochastic neighbor embedding (t-SNE) method successfully divided CAP patients into three distinct immune phenotypes. **(E)** Uniform Manifold Approximation and Projection(UMAP) method successfully divided CAP patients into three distinct immune phenotypes. **(F)** Principal Component Analysis (PCA) method successfully divided CAP patients into three distinct immune phenotypes.

SUPPLEMENTARY FIGURE 5
Primary and secondary outcomes among three distinct immune phenotypes in validation cohort. **(A)** Survival curves for various phenotype patients during their hospitalization. **(B)** Survival curves for various phenotype patients over 28 days. Blue line represents Phenotype A patients, red for Phenotype B patients, and green for Phenotype C patients. Phenotype A had a better prognosis than those in Phenotype A and C ($P<0.05$).Phenotype C CAP patients experience extended hospital stays **(C)**, prolonged ventilation days **(D)**, ICU stays **(F)** and fewer ICU-free days **(E)** in comparison to patients with the other two phenotypes. Green represents Phenotype A patients, light blue for Phenotype B patients, and dark blue for Phenotype C patients. CAP patients in Patients with phenotype C comprise a greater proportion of patients requiring assisted ventilation **(G)** and those with severe pneumonia **(H)**. Differences are observed in patient composition with respect to ventilation and the presence of severe pneumonia. $P<0.001$.

SUPPLEMENTARY FIGURE 6
Primary and secondary outcomes among three distinct immune phenotypes in meta cohort. **(A)** Survival curves for various phenotype patients during their hospitalization. **(B)** Survival curves for various phenotype patients over 28 days. Blue line represents Phenotype A patients, red for Phenotype B patients, and green for Phenotype C patients. Phenotype A had a better prognosis than those in Phenotype A and C ($P<0.05$).Phenotype C CAP patients experience extended hospital stays **(C)**, prolonged ventilation days **(D)**, ICU stays **(F)** and fewer ICU-free days **(E)** in comparison to patients with the other two phenotypes. Green represents Phenotype A patients, light blue for Phenotype B patients, and dark blue for Phenotype C patients. CAP patients in Patients with phenotype C comprise a greater proportion of patients requiring assisted ventilation **(G)** and those with severe pneumonia **(H)**. Differences are observed in patient composition with respect to ventilation and the presence of severe pneumonia. $P<0.001$.

SUPPLEMENTARY FIGURE 7
Association and variation between clinical immunological indicators and three phenotypes. Chord diagram **(A-D)** of the association between clinical immunological variables and each phenotype in validation cohort. Different phenotypes were shown in different colors: phenotype A is purple, phenotype B is blue, and phenotype C is green. Rank plot **(E-G)** of variable mean among various phenotypes in training cohort. Variables were normalized by mean and standard error.

SUPPLEMENTARY FIGURE 8
Association and variation between clinical immunological indicators and three phenotypes. Chord diagram **(A-D)** of the association between clinical immunological variables and each phenotype in meta cohort. Different phenotypes were shown in different colors: phenotype A is purple, phenotype B is blue, and phenotype C is green. Rank plot **(E-G)** of variable mean among various phenotypes in training cohort. Variables were normalized by mean and standard error.

SUPPLEMENTARY FIGURE 9
Sankey plot illustrated the relationship between immune phenotypes and conventional pneumonia severity index (PSI) and CURB-65 evaluation criteria in validation **(A)** cohort and meta cohort **(B)**.

SUPPLEMENTARY FIGURE 10
Robust performance of machine learning algorithm. **(A)** The performance of riskscore and conventional PSI and CURB-65 evaluation criteria in meta cohort. **(B)** Time dependent ROC curve of riskscore method at 7 days, 14 days, 21 days in meta cohort. **(C)** The performance of Random forest method and conventional PSI and CURB-65 evaluation criteria in meta cohort.

SUPPLEMENTARY FIGURE 11
The immune infiltration landscape of patients with community acquired pneumonia. **(A)** Box plot illustrated different types of immune cell between alive and deceased CAP patients. **(B)** Cellular interaction of immune cell types. Positive correlation is indicated in red and negative correlation in blue.

References

1. Phua J, Dean NC, Guo Q, Kuan WS, Lim HF, Lim TK. Severe community-acquired pneumonia: timely management measures in the first 24 hours. *Crit Care (London England)*. (2016) 20:237. doi: 10.1186/s13054-016-1414-2

2. Torres A, Chalmers J, Dela Cruz C, Dominedò C, Kollef M, Martin-Loeches I, et al. Challenges in severe community-acquired pneumonia: a point-of-view review. *Intensive Care Med*. (2019) 45:159–71. doi: 10.1007/s00134-019-05519-y

3. Peyrani P, Arnold FW, Bordon J, Furmanek S, Luna CM, Cavallazzi R, et al. Incidence and mortality of adults hospitalized with community-acquired pneumonia according to clinical course. *Chest*. (2020) 157:34–41. doi: 10.1016/j.chest.2019.09.022

4. Zhang ZX, Yong Y, Tan WC, Shen L, Ng HS, Fong KY. Prognostic factors for mortality due to pneumonia among adults from different age groups in Singapore and mortality predictions based on PSI and CURB-65. *Singapore Med J*. (2018) 59:190–8. doi: 10.11622/smedj.2017079

5. Parsonage M, Nathwani D, Davey P, Barlow G. Evaluation of the performance of CURB-65 with increasing age. *Clin Microbiol infection*. (2009) 15:858–64. doi: 10.1111/j.1469-0691.2009.02908.x

6. Cilloniz C, Ward L, Mogensen M, Pericàs J, Méndez R, Gabarrús A, et al. Machine-learning model for mortality prediction in patients with community-acquired pneumonia: development and validation study. *Chest*. (2023) 163:77–88. doi: 10.1016/j.chest.2022.07.005

7. Jeon E, Lee H, Park T, Jin K, Ryu B, Lee H, et al. Machine learning-based prediction of in-ICU mortality in pneumonia patients. *Sci Rep*. (2023) 13:11527. doi: 10.1038/s41598-023-38765-8

8. Zhixiao X, Kun G, Weiwei C, Jingwen L, Chengshui C. Performance of machine learning algorithms for predicting adverse outcomes in community-acquired pneumonia. *Front Bioeng Biotechnol*. (2022) 10:903426. doi: 10.3389/fbioe.2022.903426

9. Aliberti S, Brambilla AM, Chalmers JD, Cilloniz C, Ramirez J, Bignamini A, et al. Phenotyping community-acquired pneumonia according to the presence of acute respiratory failure and severe sepsis. *Respir Res*. (2014) 15(1):27. doi: 10.1186/1465-9921-15-27

10. Ning L, Shishi Z, Bo W, Huiqing L. Targeting immunometabolism against acute lung injury. *Clin Immunol*. (2023) 249:109289. doi: 10.1016/j.clim.2023.109289

11. Seymour C, Kennedy J, Wang S, Chang C, Elliott C, Xu Z, et al. Derivation, validation, and potential treatment implications of novel clinical phenotypes for sepsis. *JAMA*. (2019) 321:2003–17. doi: 10.1001/jama.2019.5791

12. Chen Q, Pan T, Wang Y, Schoepf U, Bidwell S, Qiao H, et al. A coronary CT angiography radiomics model to identify vulnerable plaque and predict cardiovascular events. *Radiology*. (2023) 307:e221693. doi: 10.1148/radiol.221693

13. Zhang Z. Multiple imputation with multivariate imputation by chained equation (MICE) package. *Ann Trans Med*. (2016) 4:30. doi: 10.3978/j.issn.2305-5839.2015.12.63

14. Liang W, Liang H, Ou L, Chen B, Chen A, Li C, et al. Development and validation of a clinical risk score to predict the occurrence of critical illness in hospitalized patients with COVID-19. *JAMA Internal Med*. (2020) 180:1081–9. doi: 10.1001/jamainternmed.2020.2033

15. Mueller Y, Schrama T, Ruijten R, Schreurs M, Grashof D, van de Werken H, et al. Stratification of hospitalized COVID-19 patients into clinical severity progression groups by immuno-phenotyping and machine learning. *Nat Commun*. (2022) 13:915. doi: 10.1038/s41467-022-28621-0

16. Liu Z, Liu L, Weng S, Guo C, Dang Q, Xu H, et al. Machine learning-based integration develops an immune-derived lncRNA signature for improving outcomes in colorectal cancer. *Nat Commun*. (2022) 13:816. doi: 10.1038/s41467-022-28421-6

17. Dam T, Roggeveen L, van Diggelen F, Fleuren L, Jagesar A, Otten M, et al. Predicting responders to prone positioning in mechanically ventilated patients with COVID-19 using machine learning. *Ann Intensive Care*. (2022) 12:99. doi: 10.1186/s13613-022-01070-0

18. Wei Q, Chen Z, Tang Y, Chen W, Zhong L, Mao L, et al. External validation and comparison of MR-based radiomics models for predicting pathological complete response in locally advanced rectal cancer: a two-centre, multi-vendor study. *Eur radiology*. (2023) 33:1906–17. doi: 10.1007/s00330-022-09204-5

19. Li X, Zhang H, Zhao S, Tang K. Predicting risky sexual behavior among college students through machine learning approaches: cross-sectional analysis of individual data from 1264 universities in 31 provinces in China. *JMIR Public Health surveillance*. (2023) 9:e41162. doi: 10.2196/41162

20. Viasus D, Simonetti AF, Nonell L, Vidal O, Meije Y, Ortega L, et al. Whole-blood gene expression profiles associated with mortality in community-acquired pneumonia. *Biomedicines*. (2023) 11(2):429. doi: 10.3390/biomedicines11020429

21. Viasus D, Del Rio-Pertuz G, Simonetti A, Garcia-Vidal C, Acosta-Reyes J, Garavito A, et al. Biomarkers for predicting short-term mortality in community-acquired pneumonia: A systematic review and meta-analysis. *J infection*. (2016) 72:273–82. doi: 10.1016/j.jinf.2016.01.002

22. Cerda-Mancillas M, Santiago-Germán D, Andrade-Bravo B, Pedraza-Olivares F, Valenzo-Hernández F, Leaños-Miranda A, et al. D-dimer as A biomarker of severity and adverse outcomes in patients with community acquired pneumonia. *Arch Med Res*. (2020) 51:429–35. doi: 10.1016/j.arcmed.2020.04.014

23. Artero A, Madrazo M, Fernández-Garcés M, Muiño Miguez A, González García A, Crestelo Vieitez A, et al. Severity scores in COVID-19 pneumonia: a multicenter, retrospective, cohort study. *J Gen Internal Med*. (2021) 36:1338–45. doi: 10.1007/s11606-021-06626-7

24. Peña J, Rascón-Pacheco R, Ascencio-Montiel I, González-Figueroa E, Fernández-Gárate J, Medina-Gómez O, et al. Hypertension, diabetes and obesity, major risk factors for death in patients with COVID-19 in Mexico. *Arch Med Res*. (2021) 52:443–9. doi: 10.1016/j.arcmed.2020.12.002

25. Zhang H, Zang C, Xu Z, Zhang Y, Xu J, Bian J, et al. Data-driven identification of post-acute SARS-CoV-2 infection subphenotypes. *Nat Med*. (2023) 29:226–35. doi: 10.1038/s41591-022-02116-3

26. Wang B, Li Y, Tian Y, Ju C, Xu X, Pei S. Novel pneumonia score based on a machine learning model for predicting mortality in pneumonia patients on admission to the intensive care unit. *Respir Med*. (2023) 217:107363. doi: 10.1016/j.rmed.2023.107363

27. Balch J, Chen U, Liesenfeld O, Starostik P, Loftus T, Efron P, et al. Defining critical illness using immunological endotypes in patients with and without sepsis: a cohort study. *Crit Care*. (2023) 27:292. doi: 10.1186/s13054-023-04571-x

28. Guan C, Ma F, Chang S, Zhang J. Interpretable machine learning models for predicting venous thromboembolism in the intensive care unit: an analysis based on data from 207 centers. *Crit Care*. (2023) 27:406. doi: 10.1186/s13054-023-04683-4

29. Evrard B, Woillard J, Legras A, Bouaoud M, Gourraud M, Humeau A, et al. Diagnostic, prognostic and clinical value of left ventricular radial strain to identify paradoxical septal motion in ventilated patients with the acute respiratory distress syndrome: an observational prospective multicenter study. *Crit Care*. (2023) 27:424. doi: 10.1186/s13054-023-04716-y

30. Zhao Y, Zhang R, Zhong Y, Wang J, Weng Z, Luo H, et al. Statistical analysis and machine learning prediction of disease outcomes for COVID-19 and pneumonia patients. *Front Cell infection Microbiol*. (2022) 12:838749. doi: 10.3389/fcimb.2022.838749

31. Chen S, Zhou Z, Wang Y, Chen S, Jiang J. Machine learning-based identification of cuproptosis-related markers and immune infiltration in severe community-acquired pneumonia. *Clin Respir J*. (2023) 17:618–28. doi: 10.1111/crj.13633

32. Li W, Liu P, Liu H, Zhang F, Fu Y. Integrative analysis of genes reveals endoplasmic reticulum stress-related immune responses involved in dilated cardiomyopathy with fibrosis. *Apoptosis*. (2023) 28:1406–21. doi: 10.1007/s10495-023-01871-z

33. Mo S, Jin B, Tseng Y, Lin L, Lin L, Shen X, et al. A precise molecular subtyping of ulcerative colitis reveals the immune heterogeneity and predicts clinical drug responses. *J Trans Med*. (2023) 21:466. doi: 10.1186/s12967-023-04326-w

34. Calfee C, Delucchi K, Parsons P, Thompson B, Ware L, Matthay M. Subphenotypes in acute respiratory distress syndrome: latent class analysis of data from two randomised controlled trials. *Lancet Respir Med*. (2014) 2:611–20. doi: 10.1016/S2213-2600(14)70097-9

35. Méndez R, Menéndez R, Amara-Elori I, Feced L, Piró A, Ramírez P, et al. Lymphopenic community-acquired pneumonia is associated with a dysregulated immune response and increased severity and mortality. *J infection*. (2019) 78:423–31. doi: 10.1016/j.jinf.2019.04.006

36. Bermejo-Martin J, Cilloniz C, Mendez R, Almansa R, Gabarrus A, Ceccato A, et al. Lymphopenic community acquired pneumonia (L-CAP), an immunological phenotype associated with higher risk of mortality. *EBioMedicine*. (2017) 24:231–6. doi: 10.1016/j.ebiom.2017.09.023

37. Wang J, Pei L, Zhao T, Liu X, Wang Q, Zhang S, et al. CD4 T cells related to disease severity in elderly and frailty community-acquired pneumonia patients: A retrospective cohort study. *Immunity Inflammation disease*. (2023) 11:e1009. doi: 10.1002/iid3.1009

38. Bian L, Bi Y, Zhou S, Chen Z, Wen J, Shi J, et al. T cell responses in senior patients with community-acquired pneumonia related to disease severity. *Exp Cell Res*. (2017) 361:56–62. doi: 10.1016/j.yexcr.2017.09.041

39. Alessandro S, Shane C. Adaptive immunity to SARS-CoV-2 and COVID-19. *Cell*. (2021) 184(4):861–80. doi: 10.1016/j.cell.2021.01.007

40. Guohong L, Xianghu J, Xiaojiao Z, Yunbao P, Haibo X. Analysis of lymphocyte subpopulations and cytokines in COVID-19-associated pneumonia and community-acquired pneumonia. *J Immunol Res*. (2021) 2021:6657894. doi: 10.1155/2021/6657894

41. Odeh A, Simecka J. Regulatory CD4+CD25+ T cells dampen inflammatory disease in murine mycoplasma pneumonia and promote IL-17 and IFN-γ Responses. *PLoS One*. (2016) 11:e0155648. doi: 10.1371/journal.pone.0155648

frontiers | Frontiers in Immunology

TYPE Review
PUBLISHED 17 September 2024
DOI 10.3389/fimmu.2024.1464762

OPEN ACCESS

EDITED BY
Ping Yuan,
Tongji University, China

REVIEWED BY
Xiao Song,
Tongji University, China
Rong Jiang,
Tongji University, China
Jin-Ming Liu,
Tongji University, China

*CORRESPONDENCE
Baoquan Dai
wffydai@163.com

†These authors have contributed equally to this work and share first authorship

RECEIVED 15 July 2024
ACCEPTED 02 September 2024
PUBLISHED 17 September 2024

CITATION
Li Z, Ma J, Wang X, Zhu L, Gan Y and Dai B (2024) The role of immune cells in the pathogenesis of connective tissue diseases-associated pulmonary arterial hypertension. *Front. Immunol.* 15:1464762. doi: 10.3389/fimmu.2024.1464762

The role of immune cells in the pathogenesis of connective tissue diseases-associated pulmonary arterial hypertension

Zhe Li[1†], Juan Ma[1†], Xuejing Wang[2†], Liquan Zhu[1], Yu Gan[1] and Baoquan Dai[1*]

[1]Department 5 of Pediatric, Weifang Maternal and Child Health Hospital, Weifang, China, [2]School of Rehabilitation Medicine, Shandong Second Medical University, Weifang, China

Connective tissue diseases-related pulmonary arterial hypertension (CTD-PAH) is a disease characterized by an elevated pulmonary artery pressure that arises as a complication of connective tissue diseases. The number of patients with CTD-PAH accounts for 25.3% of all PAH patients. The main pathological features of CTD-PAH are thickening of intima, media and adventitia of pulmonary arterioles, increased pulmonary vascular resistance, autoimmune activation and inflammatory reaction. It is worth noting that abnormal immune activation will produce autoantibodies and release cytokines, and abnormal immune cell recruitment will promote inflammatory environment and vascular remodeling. Therefore, almost all forms of connective tissue diseases are related to PAH. In addition to general therapy and targeted drug therapy for PAH, high-dose glucocorticoid combined with immunosuppressant can quickly alleviate and stabilize the basic CTD-PAH disease. Given this, the development of therapeutic approaches targeting immune dysregulation and heightened inflammation is recognized as a promising strategy to prevent or reverse the progression of CTD-PAH. This review explores the potential mechanisms by which immune cells contribute to the development of CTD-PAH and examines the clinical application of immunosuppressive therapies in managing CTD-PAH.

KEYWORDS

inflammation, immunity, cytokines, chemokines, pulmonary hypertension, immunosuppressive therapy

1 Introduction

Connective tissue disease-associated pulmonary arterial hypertension (CTD-PAH) refers to the progressive elevation of pulmonary artery caused by connective tissue disease, which is a common complication of CTD (1, 2). CTD-PAH belongs to the category of PAH. CTD-PAH patients account for 25.3% of all PAH patients, and it is the

second most common cause of PAH, second only to the idiopathic form. The pathological features of CTD-PAH are mainly pulmonary vascular remodeling, including pulmonary arteriole middle-layer hypertrophy, intimal fibrosis, plexiform lesions and tiny pulmonary artery occlusion, etc (3, 4). These changes are closely related to vascular endothelial injury, proliferation and migration of smooth muscle cells (SMCs), extracellular matrix deposition and chronic inflammatory reaction mediated by immune abnormalities, which together lead to increased pulmonary artery pressure and increased pulmonary circulation resistance (5, 6). Among them, immune imbalance is an important feature of CTD-PAH, which is very important for the initiation and maintenance of vascular remodeling (7). For example, the change of vascular cell phenotype leads to the change of sensitivity to inflammatory trigger, the enhancement of self-staged inflammatory response and the active secretion of cytokines and chemokines (8). At present, in clinical treatment, in addition to general treatment and targeted drug therapy for PAH, high-dose glucocorticoid combined with immunosuppressant can quickly alleviate and stabilize the basic CTD condition, and can effectively improve CTD-PAH (9).

CTD encompass a broad range of systemic autoimmune rheumatic conditions that affect multiple organ systems, such as systemic lupus erythematosus related PAH (SLE-PAH), systemic sclerosis related PAH (SSc-PAH), connective tissue disease related PAH (MCTD-PAH), and rheumatoid arthritis related PAH, etc (10, 11). CTD-PAH is different in different regions. For example, in Europe and the United States, systemic sclerosis is the main cause, while in Asia, systemic lupus erythematosus is more common (11). Notably, patients with SLE-PAH tend to respond more favorably to treatm (12–14). These conditions are characterized by immune dysregulation and the production of disease-specific autoantibodies (15, 16). In addition, the pathogenesis of these diseases involves immunity and vascular remodeling. In patients with CTD-PAH, antibodies and immune complexes are often deposited on the pulmonary artery wall, especially anti-U1RNP antibodies (17). These antibodies can significantly up-regulate the expression of adhesion factors (such as ICAM21 and ELAM21) and MHC class II molecules in pulmonary artery endothelial cells (ECs), leading to inflammatory cells infiltrating the vascular wall. The deposition of immune complex will attract inflammatory cells (such as neutrophils, macrophages, etc.) to infiltrate into the blood vessel wall, causing vasculitis and cellulose necrosis, further aggravating blood vessel injury (6). The autoimmune reaction of CTD-PAH patients is extremely active, which leads to inflammatory reaction and fibrosis changes in pulmonary vascular wall, which is an important basis for the formation of pulmonary hypertension (6). Due to the infiltration of inflammatory cells and the deposition of immune complexes, the inner ECs are damaged, resulting in intima thickening. Stimulated by inflammatory factors, vascular SMCs will proliferate abnormally, aggravating lumen stenosis (18). So, this paper reviews the potential pathogenesis of CTD-PAH in autoimmune and immune dysregulation in recent years. And further put forward the feasibility of immunosuppressive treatment strategy in CTD-PAH.

2 Immune activation in CTD-PAH

The pathogenesis of CTD-PAH is intricate and not fully elucidated. Currently, the predominant theory associates PAH with extensive vascular remodeling (19). Its main characteristics are proliferation of ECs and SMCs, fibrinoid necrosis caused by vasculitis, and deposition of immunoglobulin and complement components in intima and medial layers of pulmonary blood vessels (20). Under normal conditions, blood vessels maintain a balanced state between constriction and dilation (8, 21). However, in the context of an immune-inflammatory response, a cascade of inflammatory mediators and reactive oxygen species is unleashed, leading to endothelial dysfunction (22, 23). This dysfunction manifests as reduced production of pulmonary vasodilators, increased production of pulmonary vasoconstrictors, and enhanced expression of proliferation-inducing factors, thereby elevating vascular tension and ultimately driving vascular remodeling (24). Chronic inflammatory aggregates and the formation of tertiary lymphoid organs (TLOs) (25, 26). TLOs, which structurally resemble lymph nodes, include specialized zones for T-cells with dendritic cells (DCs), organized B-cell clusters containing germinal centers, high endothelial venules, and lymphatic vessels (27). TLOs are thought to develop in response to sustained local immune activation and are considered a hallmark of chronic diseases (28). Within TLOs, tissue-migrated DCs present antigens to naïve T-cells, inducing their activation and differentiation (27). Immune cells such as T cells, B cells, and macrophages are activated, releasing inflammatory mediators that contribute to vascular remodeling and endothelial dysfunction.

In CTD-PAH, various pro-inflammatory molecules, such as interleukin (IL)-1, IL-6, tumor necrosis factor (TNF)-α and chemokines (such as chemokine ligand 2(CCL2)/monocyte chemoattractant protein-1 (MCP-1), RANTES chemokines or fracta) are synthesized by fibroblasts, ECs and vascular SMCs (9, 29, 30). In SSc-PAH, this pro-inflammatory signal involves oxidative stress and the production of a large number of pro-inflammatory molecules (31). For example, in SSc-PAH, autoreactive T cells infiltrate the pulmonary vasculature and secrete cytokines like interferon (IFN)-γ and IL-17, which promote smooth muscle cell proliferation and fibrosis (32). Furthermore, SLE patients with severe PAH exhibit enhanced expression of various growth factors and chemokines such as RANTES/CCL5 and fractalkine/fractalkine (CX3CL1) within the pulmonary artery, emphasizing the complex interplay of factors involved in this condition.

Notably, immunoglobulins and complement have been found to accumulate on arterial walls, triggering pulmonary vasculitis (33). The presence of these immune complexes within pulmonary vascular walls may contribute to the development of SLE-PAH (34). In SLE-PAH, immune complexes preferentially adhere to larger blood vessels, whereas in SLE-induced pneumonia, smaller vessels may be the primary sites of immune complex deposition (34). However, some researchers argue that inflammation appears to be less significant in the pathogenesis of SSc-PAH and MCTD-PAH, in contrast to SLE-PAH, where the features closely resemble the

plexogenic lesions observed in IPAH (35). These variations in the inflammatory profile of SSc-PAH may account for the limited efficacy of immunosuppressive therapies in this condition. Additionally, genetic abnormalities are less common in CTD-PAH compared to IPAH, although they may still contribute in specific cases. An analysis of 79 CTD-PAH patients screened for a panel of 35 PAH-specific genes identified abnormalities in 9 individuals (11.4%) (36). Left ventricular dysfunction, prevalent in CTD, can result in pulmonary venous hypertension, particularly evident in SSc-PAH, where pulmonary veno-occlusive lesions are more pronounced (37).

3 DCs in CTD-PAH

DCs are effective and multifunctional antigen presenting cells, and their migration ability is the key to start protective pro-inflammatory and tolerant immune response (38). At the crossroads of innate immunity and adaptive immunity, dendritic cells do play a prominent role in the immune monitoring of self and non-self antigens and the initiation and coordination of specific adaptive immune responses of different types of antigens (39). Therefore, the first line of defense is very important at the barrier, especially in the lungs. However, they are also involved in the pathogenesis and progress of highly prevalent respiratory diseases (40).

Recent studies have demonstrated that DCs become activated and accumulate in the lungs of patients with CTD-PAH (27). These activated DCs enhance the production of inflammatory cytokines and chemokines, which in turn lead to pulmonary vascular remodeling and increased pulmonary vascular resistance. Additionally, the levels of inflammatory cytokines and chemokines produced by these DCs are elevated. In patients with SSc, circulating type 2 conventional DCs (cDCs) exhibit increased production of IL-6, IL-10, and tumor necrosis factor-α (TNF-α) following stimulation with TLR2 and TLR4 (41, 42). These cytokines are believed to play a crucial role in the immunopathology of PAH. Notably, IL-6 stands out as a critical cytokine in the pathogenesis of PAH, as evidenced by the development of pulmonary hypertension symptoms in mice overexpressing IL-6, whereas IL-6-deficient mice do not develop pulmonary hypertension under hypoxic conditions (43, 44). These findings indicate that DCs contribute to the development and progression of CTD-related PAH through their pro-inflammatory effects.

Plasmacytoid DCs (pDCs) are primarily found in lymphoid tissues and blood under normal conditions. The severity of lung diseases in SSc patients is related to the incidence of pDCs found in the lungs (45). Importantly, pDC plays a direct role in causing and maintaining fibrosis, because their consumption has been proved to improve pulmonary fibrosis. During inflammation, pDCs migrate to peripheral tissues, where they produce IFNs and facilitate the activation of immune cells. Several autoimmune diseases are associated with the interferon gene signature, to which different cells contribute. In patients with SLE and SSc, the number of circulating pDCs is reduced compared to healthy controls, likely due to their migration to affected tissues (46, 47). In SSc patients, elevated serum levels of C-X-C motif chemokine 10 (CXCL10) are linked with PAH, suggesting that pDCs may have a significant role in the immunopathology of the disease (48). Besides IFN, pDCs are also the primary producers of CXCL4 in SSc (49). The pDC of SSc patients abnormally expressed Toll-like receptor (TLR) 8, while TLR8 was not expressed in healthy conditions (47). This abnormal expression contributes to the disease progression, because the signal transduction through TLR8 will induce the production of CXCL4 (47). CXCL4 can attract CD45-positive cells into target tissues, potentially contributing to tissue remodeling and disease progression. In addition, the expression of TLR8 leads to the infiltration of pDCs into tissues, which aggravates the disease and leads to fibrosis (47). Activation of TLR9 under anoxic conditions has also been proved to induce the production of CXCL4 (50).

Additionally, monocytes serve as precursors for mo-DCs, which are produced under inflammatory conditions (51), and there is an observed increase in the number of non-classical monocytes in SSc-PAH (52). Non-classical monocytes, which express CD16, are known to monitor the endothelium for danger signals. They can differentiate into tissue-resident macrophages under steady-state conditions or into anti-inflammatory macrophages during inflammation to assist in tissue repair. At the same time, non-classical monocytes expressing CXCL10, CXCL8, and CCL4 are involved in SSc pathology, with higher numbers observed in SSc patients compared to controls (41). In summary, the increased pulmonary expression of chemokines may draw monocytes to the lungs of CTD-PAH patients, where they become activated and undergo gene expression changes due to the pro-inflammatory environment. These modified monocytes may then give rise to mo-DCs at the site of inflammation, capable of inducing T cell activation. The roles of cDCs, pDCs, mo-DCs and their inflammatory mediators in CTD-PAH are shown in Figure 1.

4 Lymphocytes in CTD-PAH

Lymphocytes are the main immune cells in the body, which are responsible for removing pathogens such as bacteria, viruses and parasites, thus protecting the human body from infection. They play a central role in the immune system by secreting cytokines, participating in cellular immunity and humoral immunity (53). The immune cells that mainly play a role include B cells and T cells, which participate in the immune activation in the process of vascular remodeling. The roles of c B cells, T cells and their inflammatory mediators in CTD-PAH are shown in Figure 2.

B cells have the ability to differentiate into plasma cells, which are responsible for producing autoantibodies. B cells achieve this goal by presenting antigen, producing various cytokines and promoting the differentiation of T effector cells (22, 54). B cells play a significant role in the formation of autoantibodies in SSc. In recent years, there has been growing recognition that B cells are a major source of pro-inflammatory cytokines, particularly IL-6 and

10.3389/fimmu.2024.1464762

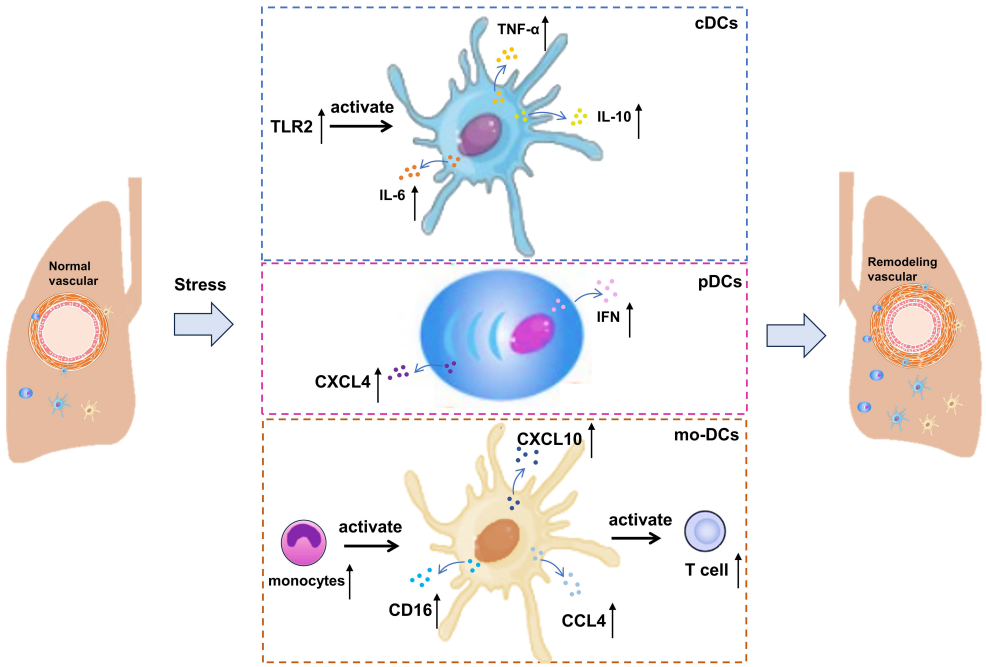

FIGURE 1
Involvement of cDCs, pDCs and mo-DCs in CTD-PAH. cDCs, circulating type 2 conventional; pDCs, plasmacytoid DCs; IL, interleukin; CCL, C-C motif chemokine ligand; TNF, tumor necrosis factor-alpha; CXCL, C-X-C motif chemokine ligand.

IFN-γ, in autoimmune diseases (55). IL-6, a potent pro-inflammatory cytokine, also has strong fibrotic effects (56). For example, circulating B cells in SSc patients produce more IL-6 compared to healthy controls (57, 58). However, there is limited data on these pro-inflammatory characteristics in PAH. In a novel approach to studying SSc-PAH using female mice deficient in P-selectin glycoprotein ligand-1, IFN-γ-producing B cells showed greater lung infiltration compared to the control group (59). Additionally, in a rat model of PAH induced by the combination of anti-vascular endothelial growth factor (VEGF) Sugen-5416

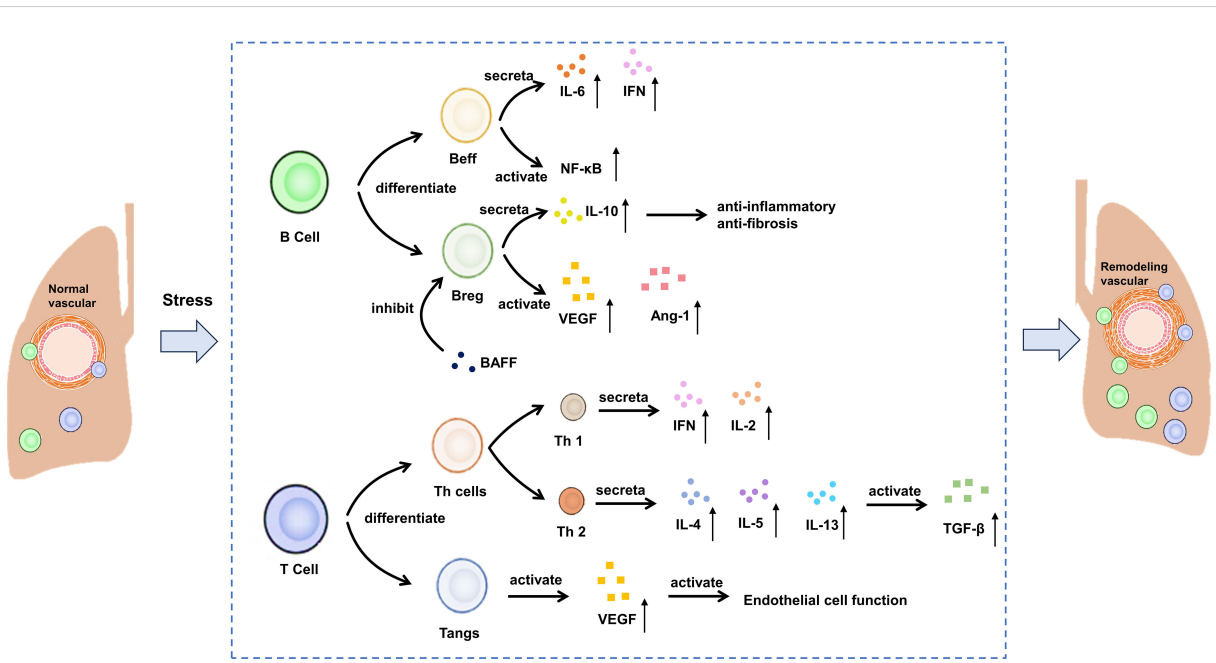

FIGURE 2
Potential mechanism of B cells and T cells on CTD-PAH. Beff: effector B cells, Breg, regulatory B cells; BAFF, B cell activating factor; VEGF, vascular endothelial growth factor; TGF-β, transforming growth factor-beta; IL, interleukin; IFN, interferon.

injection and ovalbumin immunization, the depletion of B cells correlated with reduced IL-6 expression in the lung (60). Besides, for the peripheral blood mononuclear cells of SSc-PAH patients, the genes involved in B-cell receptor signaling and NF-κB pathway in the disease group were significantly up-regulated (61, 62). Unlike effector B cells (Beffs), regulatory B cell (Bregs) produce IL-10, an anti-inflammatory and anti-fibrotic cytokine (63). Furthermore, the role of serum B cell-activating factor (BAFF) has been well established in a murine model of SSc induced by bleomycin (64). BAFF inhibits Bregs and their ability to produce IL-10. In individuals with SSc-PAH, the levels of circulating $CD24^{hi}$ CD27 Bregs are lower compared to SSc patients without PAH (65). While the existence and role of this subset in pulmonary arterial hypertension are yet to be thoroughly investigated, indirect evidence suggests a direct involvement of B cells in the vascular system of these patients (66). In SSc, B cells exhibit a higher tendency to produce vasculogenic mediators such as vascular endothelial growth factor and angiopoietin-1 compared to healthy controls, with no difference observed between patients with and without PAH (67).

T cells are an important part of adaptive immune response, including helper T cells (Th cells), regulatory T cells (Tregs) and angiogenic T cells (Tang), etc (68). Different types of T cells have specific functions and reactions in the inflammatory cascade reaction. Th cells produce a pro-inflammatory response, while Tregs exert a balanced response to achieve self-tolerance and prevent autoimmune (53). Similar to B cells, T cells can be categorized into two main opposing subpopulations: type 1 T cells, which primarily produce IFN-γ and IL-2, and type 2 T cells, which release IL-4, IL-5, and IL-13, thereby activating fibroblasts via the transforming growth factor (TGF)-β pathway (63, 69). An examination of T cell subpopulations in SSc has revealed a complex phenotype (70). Alongside Th2 cells, Th22, Th17, and CD4+ T cells reactive to topo-I play an active role in initiating pulmonary involvement in SSc (70, 71). Specifically, the topo-I-reactive CD4+ T cells demonstrate a Th17 phenotype and, along with Th22 cells, are elevated in patients, showing a negative correlation with pulmonary function parameters. Th17 cells produce IL-17, known for its fibrotic properties (72). At the same time, it was found that the expressions of IL-7R, LCK and HDAC1 were positively correlated with the number of T cell CD4 initiation and T cell CD4 memory. They reduce T cells in SSc-PAH PBMCs by regulating T cell activation (32). Although an increase in regulatory Tregs has been linked to decreased functional capacities in SSc, the precise role of these cells remains poorly understood (73). Studies have also delved into the involvement of T cells in angiogenesis. Hur et al. explored T cell subsets expressing CD31 and CXCR4, categorizing them as angiogenic T cells (Tang) due to their significant impact on vascular formation (74, 75). A recent study revealed their role in SSc pathogenesis. The presence of Tang cells is higher in SSc-PAH patients compared to those without PAH and healthy individuals (76). Moreover, there is a positive correlation between Tang cell numbers and VEGF levels in SSc-PAH, suggesting a connection between Tang cell activity and endothelial function.

5 Macrophages in CTD-PAH

Macrophages can remove pathogens and foreign bodies through their powerful phagocytosis, and serve as antigen presenting cells, presenting the treated antigens to T cells and B cells, thus initiating specific immune response (77). At the same time, macrophages can secrete a variety of inflammatory mediators, regulate immune response and promote inflammation regression (77). Macrophages play a crucial role in local innate immunity and provide comprehensive protection of the lungs against external substances (78). M1 macrophages are activated during the early inflammatory phase and induce tissue damage, with this differentiation pathway being regulated by damaged epithelial cells and IFN-γ (79). On the other hand, M2 macrophages, which exhibit fibrotic characteristics, are predominant during the proliferative phase (80–82). These activated macrophages can mitigate the differentiation of fibroblasts into myofibroblasts, a process particularly notable in SSc (82, 83). M2 macrophages, identifiable by their CD163+ and CD204+ markers, accumulate in the skin and serum of SSc patients (79). Additionally, M2 macrophages produce the chemokine CCL18, which can induce T cell migration and stimulate fibroblasts to produce collagen (84). Consequently, elevated levels of CCL18 in SSc patients are regarded as markers of lung fibrotic remodeling (85). While M2 cells are known for their fibrotic attributes, other cell populations also contribute to this complementary remodeling process. In fact, a mixed M1/M2 macrophage population is associated with SSc-PAH in both human and murine models (86, 87). Furthermore, alterations in macrophage-endothelial interactions can precipitate vascular pathologies and subsequent fibrosis. In models of bleomycin-induced injury, endothelial-derived cells exacerbate fibrosis and exhibit markers indicative of endothelial-mesenchymal transition (88). Notably, by knocking out RGC32, macrophage activation shifts from M2 to M1, which consequently reduces the skin and lung manifestations of bleomycin-induced pulmonary fibrosis (89). In addition, recent studies have shown that Regnase-1 is a multifunctional protein with RNAse activity, which can bind and degrade the mRNA of various inflammatory cytokines, thus inhibiting the inflammatory reaction. In patients with CTD-PAH, the expression level of Regnase-1 is decreased, which may lead to the over-expression of inflammatory cytokines, and then promote the development of pulmonary hypertension (90). The lack of Regnase-1 in macrophages will lead to the spontaneous development of severe CTD-PAH-like lesions in mice. This indicates that Regnase-1 in macrophages plays a key role in maintaining immune homeostasis and preventing the occurrence of CTD-PAH (90).

Macrophage migration inhibitory factor (MIF) is a substance that can limit the activity of macrophages *in vivo*. Its main function is to limit the excessive movement of macrophages, promote the infiltration of macrophages in inflammatory sites, and participate in immune regulation (91). A study investigated the role of MIF in SLE-PAH (92). Circulating MIF levels were measured in SLE

patients, SLE-PAH patients, and healthy donors. The results showed that circulating MIF was elevated in SLE-PAH patients compared to both SLE patients and healthy donors. In SLE mice, those with higher right ventricular systolic pressure (RVSP) produced more MIF protein in the pulmonary arteries than those with lower RVSP. Treatment with MIF098 reduced RVSP and inhibited excessive proliferation, muscularization, and collagen deposition in the distal pulmonary arteries of hypoxia-challenged mice. Additionally, MIF098 suppressed pulmonary arterial smooth muscle cell proliferation and migration by modulating the Mitogen-Activated Protein Kinase/Extracellular Signal-Regulated Kinase 1/2 signaling pathway and cell cycle-related proteins. In cell experiments, MIF098 also decreased collagen synthesis by inhibiting the TGF-β1/Smad2/Smad3 pathway. These findings suggest that MIF could serve as a biomarker and therapeutic target for SLE-PAH. MIF antagonists may be an effective means to improve SLE-PAH. The pathological mechanism involved above is shown in Figure 3.

6 Vascular cells in CTD-PAH

Immune cells can regulate angiogenesis by secreting cytokines such as VEGF and TNF-α. Immune cells can promote angiogenesis (such as tumor-associated macrophages) and inhibit angiogenesis (such as CD8+T cells) (93). Angiogenesis can affect the recruitment and infiltration of immune cells, and then affect the effect of immune response. Although vascular ECs are not professional antigen presenting cells, they can present antigens to T cells and express adhesion factors and cytokines to participate in immune response. ECs play a key role in maintaining vascular homeostasis under various stimuli, and regulate inflammation through mediators such as NO, ET, cell adhesion molecules, cytokines and chemokines (22). It is found that leptin derived from s plays a role in the immune pathogenesis of SSc-PAH by controlling regulatory T cells (94). At the same time, endothelial activation occurs in SSc, and Bosentan can block T cell/endothelial interaction in SSc-PAH and regulate the expression of vascular factors in serum (95). In addition, the researchers detected the response of human pulmonary artery ECs to BMPR2 signal and pyrophosphate factor stimulated by lipopolysaccharide. In PAECs interfered by autologous BMPR2 +/R899X ECs and SIMPR 2, the expressions of IL-8 and E- selectin were up-regulated. The defect of BMPR2 signal transduction and proinflammatory factors promote vascular remodeling in SLE-PAH (96).

As an important vascular cell, fibroblasts also play an important role in CTD-PAH. Pulmonary fibrosis is a sign of patients with SSc-PAH, and fibroblasts are the main target cells in this process. Fibroblasts express TGF-β and platelet-derived growth factor receptor (97). Overregulation of Wnt/β-catenin signaling pathway (98) and increased expression of insulin-like growth factor binding protein regulate the induction of TGF-β in fibroblasts. All these overexpressed protein induce fibrosis by transforming fibroblasts into myofibroblasts (99). At the same time, the study showed that in TGF-β-dependent SSc-PAH mouse model, bone morphogenetic protein receptor (BMPR)2 decreased, signal transduction was damaged and receptor turnover activity changed. Similarly, the expression of BMPR2 was significantly decreased in SSc lung tissue and fibroblasts. The increase of proteasome degradation of BMPR2 seems to be the basis, which may be caused by the increase of TGF-β activity. This suggests that the damage of BMP signal transduction caused by the increase of TGF-β dependent receptor degradation may promote the susceptibility of PAH in SSc (100).

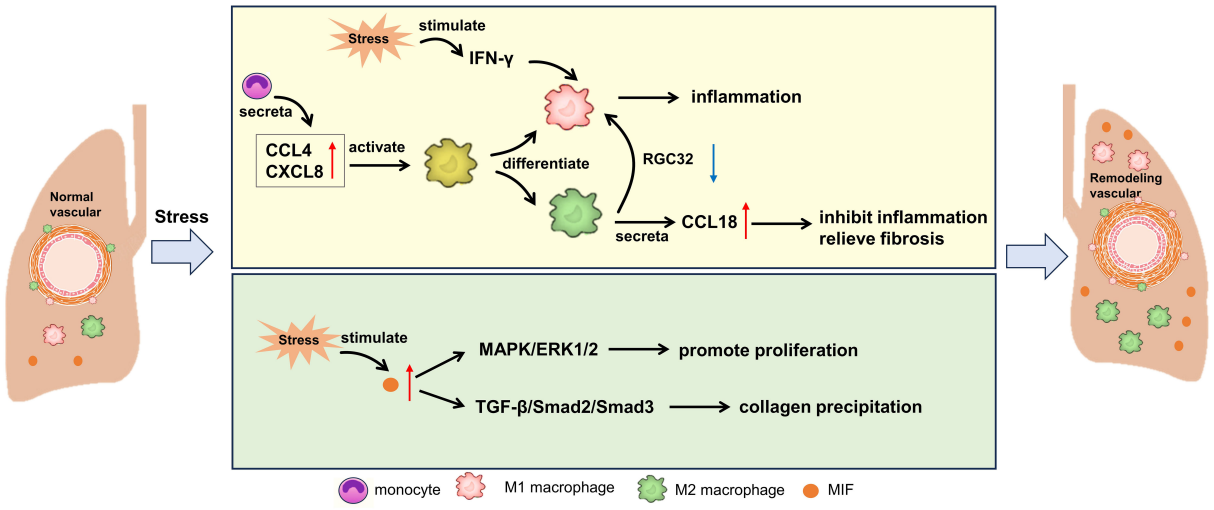

FIGURE 3
Potential mechanism of macrophages on CTD-PAH. MIF, macrophage migration inhibitory factor; CCL, C-C motif chemokine ligand; CXCL, C-X-C motif chemokine ligand; IFN, interferon; RGC32, response gene to complement 32; MAPK, mitogen-activated protein kinases; ERK, extracellular signal-regulated kinase; TGF, transforming growth factor.

7 Immunosuppression therapy in CTD-PAH

At present, the clinical treatment of CTD-PAH includes specific treatment for PAH and treatment for primary CTD. The specific treatment for PAH is to use targeted drugs. For example, Bosentan can improve exercise tolerance, cardiac function classification, hemodynamic parameters and clinical deterioration time of patients with CTD-PAH (101). At the same time, the study confirmed that Bosentan can prevent endothelial activation in SSc by restoring T cell function (95). For the treatment of primary CTD, high-dose glucocorticoids (cyclophosphamide, mycophenolate mofetil, azathioprine, methotrexate or hydroxychloroquine, etc.) combined with immunosuppressants are usually used to alleviate the condition of CTD and effectively improve CTD-PAH (9). Different from all previous therapeutic drugs for PAH, Sotatercept is an activin signal inhibitor and a First-in-class activin receptor IIA-Fc (ActRIIA Fc) fusion protein, which can selectively bind TGF-β family ligands, restore the balance between pro-proliferation and anti-proliferation signal pathways related to pulmonary artery wall and right ventricular remodeling, and play the role of inhibiting cell proliferation, reversing vascular remodeling and smoothing blood vessels (102). It was found that the treatment with ActRIIA-Fc significantly reversed the expression of pro-inflammatory and proliferative genes and normalized macrophage infiltration in the lungs of diseased rodents (7). This shows that sotatercept may have anti-inflammatory activity besides its anti-proliferation effect on vascular cells.

Growing evidence confirms the significant involvement of the immune system in the occurrence and development of CTD-PAH. Some studies have explored the potential of immunosuppressive therapy as a treatment target for CTD-PH. Among these, rituximab (an anti-CD20 monoclonal antibody)-induced B cell depletion has been the most researched intervention. Patients treated with rituximab exhibited reductions in rheumatoid factor, IL-12, and IL-17 (103). Several reports indicated that CTD-PAH patients experienced improvements in conditions other than pulmonary vascular diseases following rituximab treatment (104–106). However, the role of immunosuppression in SSc-PAH remains unclear, as there has been no observed response to corticosteroid or cytotoxic therapies. The pathophysiological differences between SSc-PAH and other types of CTD-PAH may explain the varying responses to immunosuppressive treatments. A recent study by Zamanian et al. revealed that after 24 weeks of rituximab treatment, there was no significant change in the six-minute walk distance (6MWD) for SSc-PAH patients, although an improving trend was noted (103). The authors suggest that low levels of rheumatoid factor, IL-2, and IL-17 might predict a favorable response to rituximab. For non-SSc CTD-PAH patients, immunosuppressive therapy, such as glucocorticoids or macitentan, could be considered, especially if they present with non-cardiopulmonary manifestations, potentially benefiting from the treatment. Further research is essential to better understand the role of rituximab in specific SSc-PAH patients (11). Variability in study outcomes may be attributed to differences in sample sizes, leading to experimental errors. Moreover, during the research, the primary outcome measure was changed from hemodynamic improvement to 6MWD variability due to the unexpectedly low baseline pulmonary vascular resistance in SSc-PAH patients, which significantly reduced the utility of the original primary outcome measure (66). Interestingly, an independent reanalysis of trial data focused on identifying biomarker characteristics that could indicate rituximab efficacy within subgroups, uncovering noteworthy findings. It is also noteworthy that in studies using a pulmonary arterial hypertension animal model, anti-CD20 therapy began during disease induction, making it more of a preventive rather than a curative treatment (107, 108). Therefore, further research is required to determine the relevance and positioning of B-cell depletion in the PAH treatment arsenal.

The Bruton tyrosine kinase (BTK) inhibitor has shown promising results in improving hemodynamics, reducing right ventricular hypertrophy, and mitigating pulmonary arterial remodeling and fibrosis, as well as reversing endothelial-to-mesenchymal transition in PAH rats (109). BTK expression primarily co-localizes with macrophages, suggesting that the inhibitor's effects are largely mediated through its action on macrophage BTK (109). Moreover, an increase in intracellular BTK in the B cells of CTD-PAH patients was associated with elevated serum autoantibodies (6). This indicates that BTK inhibition might alleviate PAH, at least in part, through its impact on B cells. In SSc patients, ibrutinib, a BTK inhibitor, has been found to reduce the production of pro-inflammatory cytokines and autoantibodies by peripheral B cells, while not affecting their IL-10 secretion (110). These findings suggest that BTK inhibitors could potentially serve as a therapeutic strategy for PAH by targeting both macrophages and B cells, thereby addressing multiple facets of the disease.

8 Conclusion and prospect

It is generally believed that autoimmune activation plays a key role in the pathophysiology of various subtypes of CTD-PAH. Their abnormal activation promotes the inflammatory environment and vascular remodeling characteristics of this devastating disease through various mechanisms, including autoantibody production, cytokine release and direct cell interaction. In the pathophysiology of CTD-PAH, the meaning of immune imbalance and immune cell activation is "enemy", which leads to vascular cell damage and enlarges vascular inflammation. However, many molecular and cellular mechanisms behind this process remain unsolved. A better understanding of how immunity promotes the development of CTD-PAH is very important to promote the immunosuppressive treatment of this disease.

Author contributions

ZL: Conceptualization, Writing – original draft, Validation. JM: Conceptualization, Writing – original draft, Investigation. XW: Writing – original draft, Writing – review & editing. LZ: Writing – original draft, Validation. YG: Validation, Writing – original draft. BD: Conceptualization, Software, Writing – original draft, Writing – review & editing.

Funding

The author(s) declare that no financial support was received for the research, authorship, and/or publication of this article.

Conflict of interest

The authors declare that the research was conducted in the absence of any commercial or financial relationships that could be construed as a potential conflict of interest.

Publisher's note

References

1. Humbert M, Kovacs G, Hoeper MM, Badagliacca R, Berger RMF, Brida M, et al. 2022 ESC/ERS Guidelines for the diagnosis and treatment of pulmonary hypertension. *Eur Respir J.* (2023) 61:2200879. doi: 10.1183/13993003.00879-2022

2. Humbert M, Guignabert C, Bonnet S, Dorfmüller P, Klinger JR, Nicolls MR, et al. Pathology and pathobiology of pulmonary hypertension: state of the art and research perspectives. *Eur Respir J.* (2019) 53:1801887. doi: 10.1183/13993003.01887-2018

3. Southgate L, MaChado RD, Gräf S, Morrell NW. Molecular genetic framework underlying pulmonary arterial hypertension. *Nat Rev Cardiol.* (2020) 17:85–95. doi: 10.1038/s41569-019-0242-x

4. Yuan K, Shamskhou EA, Orcholski ME, Nathan A, Reddy S, Honda H, et al. Loss of endothelium-derived wnt5a is associated with reduced pericyte recruitment and small vessel loss in pulmonary arterial hypertension. *Circulation.* (2019) 139:1710–24. doi: 10.1161/CIRCULATIONAHA.118.037642

5. Zeng H, Liu X, Zhang Y. Identification of potential biomarkers and immune infiltration characteristics in idiopathic pulmonary arterial hypertension using bioinformatics analysis. *Front Cardiovasc Med.* (2021) 8:624714. doi: 10.3389/fcvm.2021.624714

6. Heukels P, Corneth OBJ, van Uden D, van Hulst JAC, van den Toorn LM, van den Bosch AE, et al. Loss of immune homeostasis in patients with idiopathic pulmonary arterial hypertension. *Thorax.* (2021) 76:1209–18. doi: 10.1136/thoraxjnl-2020-215460

7. Joshi SR, Liu J, Bloom T, Karaca Atabay E, Kuo TH, Lee M, et al. Sotatercept analog suppresses inflammation to reverse experimental pulmonary arterial hypertension. *Sci Rep.* (2022) 12:7803. doi: 10.1038/s41598-022-11435-x

8. Hu Y, Chi L, Kuebler WM, Goldenberg NM. Perivascular inflammation in pulmonary arterial hypertension. *Cells.* (2020) 9:2338. doi: 10.3390/cells9112338

9. Thoreau B, Mouthon L. Pulmonary arterial hypertension associated with connective tissue diseases (CTD-PAH): Recent and advanced data. *Autoimmun Rev.* (2024) 23:103506. doi: 10.1016/j.autrev.2023.103506

10. Mulhearn B, Tansley SL, McHugh NJ. Autoantibodies in connective tissue disease. *Best Pract Res Clin Rheumatol.* (2020) 34:101462. doi: 10.1016/j.berh.2019.101462

11. Khangoora V, Bernstein EJ, King CS, Shlobin OA. Connective tissue disease-associated pulmonary hypertension: A comprehensive review. *Pulm Circ.* (2023) 13: e12276. doi: 10.1002/pul2.12276

12. Condliffe R, Kiely DG, Peacock AJ, Corris PA, Gibbs JS, Vrapi F, et al. Connective tissue disease-associated pulmonary arterial hypertension in the modern treatment era. *Am J Respir Crit Care Med.* (2009) 179:151–7. doi: 10.1164/rccm.200806-953OC

13. Chung L, Liu J, Parsons L, Hassoun PM, McGoon M, Badesch DB, et al. Characterization of connective tissue disease-associated pulmonary arterial hypertension from REVEAL: identifying systemic sclerosis as a unique phenotype. *Chest.* (2010) 138:1383–94. doi: 10.1378/chest.10-0260

14. Rhee RL, Gabler NB, Sangani S, Praestgaard A, Merkel PA, Kawut SM. Comparison of treatment response in idiopathic and connective tissue disease-associated pulmonary arterial hypertension. *Am J Respir Crit Care Med.* (2015) 192:1111–7. doi: 10.1164/rccm.201507-1456OC

15. Joy GM, Arbiv OA, Wong CK, Lok SD, Adderley NA, Dobosz KM, et al. Prevalence, imaging patterns and risk factors of interstitial lung disease in connective tissue disease: a systematic review and meta-analysis. *Eur Respir Rev.* (2023) 32:220210. doi: 10.1183/16000617.0210-2022

16. Hirsch K, Nolley S, Ralph DD, Zheng Y, Altemeier WA, Rhodes CJ, et al. Circulating markers of inflammation and angiogenesis and clinical outcomes across subtypes of pulmonary arterial hypertension. *J Heart Lung Transplant.* (2023) 42:173–82. doi: 10.1016/j.healun.2022.10.026

17. Zhao J, Wang Q, Liu Y, Tian Z, Guo X, Wang H, et al. Clinical characteristics and survival of pulmonary arterial hypertension associated with three major connective tissue diseases: A cohort study in China. *Int J Cardiol.* (2017) 236:432–7. doi: 10.1016/j.ijcard.2017.01.097

18. Moccaldi B, De Michieli L, Binda M, Famoso G, Depascale R, Perazzolo Marra M, et al. Serum biomarkers in connective tissue disease-associated pulmonary arterial hypertension. *Int J Mol Sci.* (2023) 24:4178. doi: 10.3390/ijms24044178

19. Dai Z, Zhu MM, Peng Y, Machireddy N, Evans CE, MaChado R, et al. Therapeutic targeting of vascular remodeling and right heart failure in pulmonary arterial hypertension with a HIF-2α Inhibitor. *Am J Respir Crit Care Med.* (2018) 198:1423–34. doi: 10.1164/rccm.201710-2079OC

20. Parperis K, Velidakis N, Khattab E, Gkougkoudi E, Kadoglou NPE. Systemic lupus erythematosus and pulmonary hypertension. *Int J Mol Sci.* (2023) 24:5085. doi: 10.3390/ijms24065085

21. Thenappan T, Ormiston ML, Ryan JJ, Archer SL. Pulmonary arterial hypertension: pathogenesis and clinical management. *Bmj.* (2018) 360:j5492. doi: 10.1136/bmj.j5492

22. Zhao H, Song J, Li X, Xia Z, Wang Q, Fu J, et al. The role of immune cells and inflammation in pulmonary hypertension: mechanisms and implications. *Front Immunol.* (2024) 15:1374506. doi: 10.3389/fimmu.2024.1374506

23. Zheng D, Liu J, Piao H, Zhu Z, Wei R, Liu K. ROS-triggered endothelial cell death mechanisms: Focus on pyroptosis, parthanatos, and ferroptosis. *Front Immunol.* (2022) 13:1039241. doi: 10.3389/fimmu.2022.1039241

24. Zanatta E, Polito P, Famoso G, Larosa M, De Zorzi E, Scarpieri E, et al. Pulmonary arterial hypertension in connective tissue disorders: Pathophysiology and treatment. *Exp Biol Med (Maywood).* (2019) 244:120–31. doi: 10.1177/1535370218824101

25. Perros F, Dorfmüller P, Montani D, Hammad H, Waelput W, Girerd B, et al. Pulmonary lymphoid neogenesis in idiopathic pulmonary arterial hypertension. *Am J Respir Crit Care Med.* (2012) 185:311–21. doi: 10.1164/rccm.201105-0927OC

26. Cool CD, Kennedy D, Voelkel NF, Tuder RM. Pathogenesis and evolution of plexiform lesions in pulmonary hypertension associated with scleroderma and human immunodeficiency virus infection. *Hum Pathol.* (1997) 28:434–42. doi: 10.1016/S0046-8177(97)90032-0

27. van Uden D, Boomars K, Kool M. Dendritic cell subsets and effector function in idiopathic and connective tissue disease-associated pulmonary arterial hypertension. *Front Immunol.* (2019) 10:11. doi: 10.3389/fimmu.2019.00011

28. Neyt K, Perros F, GeurtsvanKessel CH, Hammad H, Lambrecht BN. Tertiary lymphoid organs in infection and autoimmunity. *Trends Immunol.* (2012) 33:297–305. doi: 10.1016/j.it.2012.04.006

29. Sanchez O, Marcos E, Perros F, Fadel E, Tu L, Humbert M, et al. Role of endothelium-derived CC chemokine ligand 2 in idiopathic pulmonary arterial hypertension. *Am J Respir Crit Care Med.* (2007) 176:1041–7. doi: 10.1164/rccm.200610-1559OC

30. Cracowski JL, Chabot F, Labarère J, Faure P, Degano B, Schwebel C, et al. Proinflammatory cytokine levels are linked to death in pulmonary arterial hypertension. *Eur Respir J.* (2014) 43:915–7. doi: 10.1183/09031936.00151313

31. Thoreau B, Chaigne B, Renaud A, Mouthon L. Pathophysiology of systemic sclerosis. *Presse Med*. (2021) 50:104087. doi: 10.1016/j.lpm.2021.104087

32. Tu J, Jin J, Chen X, Sun L, Cai Z. Altered cellular immunity and differentially expressed immune-related genes in patients with systemic sclerosis-associated pulmonary arterial hypertension. *Front Immunol*. (2022) 13:868983. doi: 10.3389/fimmu.2022.868983

33. Tselios K, Gladman DD, Urowitz MB. Systemic lupus erythematosus and pulmonary arterial hypertension: links, risks, and management strategies. *Open Access Rheumatol*. (2017) 9:1–9. doi: 10.2147/OARRR.S123549

34. Quismorio FP Jr., Sharma O, Koss M, Boylen T, Edmiston AW, Thornton PJ, et al. Immunopathologic and clinical studies in pulmonary hypertension associated with systemic lupus erythematosus. *Semin Arthritis Rheum*. (1984) 13:349–59. doi: 10.1016/0049-0172(84)90015-5

35. Sasaki N, Kamataki A, Sawai T. A histopathological study of pulmonary hypertension in connective tissue disease. *Allergol Int*. (2011) 60:411–7. doi: 10.2332/allergolint.11-RAI-0337

36. Hernandez-Gonzalez I, Tenorio-Castano J, Ochoa-Parra N, Gallego N, Pérez-Olivares C, Lago-Docampo M, et al. Novel genetic and molecular pathways in pulmonary arterial hypertension associated with connective tissue disease. *Cells*. (2021) 10:1488. doi: 10.3390/cells10061488

37. Mathai SC, Bueso M, Hummers LK, Boyce D, Lechtzin N, Le Pavec J, et al. Disproportionate elevation of N-terminal pro-brain natriuretic peptide in scleroderma-related pulmonary hypertension. *Eur Respir J*. (2010) 35:95–104. doi: 10.1183/09031936.00074309

38. Worbs T, Hammerschmidt SI, Förster R. Dendritic cell migration in health and disease. *Nat Rev Immunol*. (2017) 17:30–48. doi: 10.1038/nri.2016.116

39. Guignabert C. Dendritic cells in pulmonary hypertension: foot soldiers or hidden enemies? *Am J Respir Cell Mol Biol*. (2020) 63:551–2. doi: 10.1165/rcmb.2020-0330ED

40. Lambrecht BN, Hammad H. The role of dendritic and epithelial cells as master regulators of allergic airway inflammation. *Lancet*. (2010) 376:835–43. doi: 10.1016/S0140-6736(10)61226-3

41. Carvalheiro T, Horta S, van Roon JAG, Santiago M, Salvador MJ, Trindade H, et al. Increased frequencies of circulating CXCL10-, CXCL8- and CCL4-producing monocytes and Siglec-3-expressing myeloid dendritic cells in systemic sclerosis patients. *Inflammation Res*. (2018) 67:169–77. doi: 10.1007/s00011-017-1106-7

42. van Bon L, Popa C, Huijbens R, Vonk M, York M, Simms R, et al. Distinct evolution of TLR-mediated dendritic cell cytokine secretion in patients with limited and diffuse cutaneous systemic sclerosis. *Ann Rheum Dis*. (2010) 69:1539–47. doi: 10.1136/ard.2009.128207

43. Steiner MK, Syrkina OL, Kolliputi N, Mark EJ, Hales CA, Waxman AB. Interleukin-6 overexpression induces pulmonary hypertension. *Circ Res*. (2009) 104:236–44. doi: 10.1161/CIRCRESAHA.108.182014

44. Savale L, Tu L, Rideau D, Izziki M, Maitre B, Adnot S, et al. Impact of interleukin-6 on hypoxia-induced pulmonary hypertension and lung inflammation in mice. *Respir Res*. (2009) 10:6. doi: 10.1186/1465-9921-10-6

45. Kafaja S, Valera I, Divekar AA, Saggar R, Abtin F, Furst DE, et al. pDCs in lung and skin fibrosis in a bleomycin-induced model and patients with systemic sclerosis. *JCI Insight*. (2018) 3:e98380. doi: 10.1172/jci.insight.98380

46. Migita K, Miyashita T, Maeda Y, Kimura H, Nakamura M, Yatsuhashi H, et al. Reduced blood BDCA-2+ (lymphoid) and CD11c+ (myeloid) dendritic cells in systemic lupus erythematosus. *Clin Exp Immunol*. (2005) 142:84–91. doi: 10.1111/j.1365-2249.2005.02897.x

47. Ah Kioon MD, Tripodo C, Fernandez D, Kirou KA, Spiera RF, Crow MK, et al. Plasmacytoid dendritic cells promote systemic sclerosis with a key role for TLR8. *Sci Transl Med*. (2018) 10:eaam8458. doi: 10.1126/scitranslmed.aam8458

48. Eloranta ML, Franck-Larsson K, Lövgren T, Kalamajski S, Rönnblom A, Rubin K, et al. Type I interferon system activation and association with disease manifestations in systemic sclerosis. *Ann Rheum Dis*. (2010) 69:1396–402. doi: 10.1136/ard.2009.121400

49. van Bon L, Affandi AJ, Broen J, Christmann RB, Marijnissen RJ, Stawski L, et al. Proteome-wide analysis and CXCL4 as a biomarker in systemic sclerosis. *N Engl J Med*. (2014) 370:433–43. doi: 10.1056/NEJMoa1114576

50. Ottria A, Zimmermann M, Paardekooper LM, Carvalheiro T, Vazirpanah N, Silva-Cardoso S, et al. Hypoxia and TLR9 activation drive CXCL4 production in systemic sclerosis plasmacytoid dendritic cells via mtROS and HIF-2α. *Rheumatol (Oxford)*. (2022) 61:2682–93. doi: 10.1093/rheumatology/keab532

51. Guilliams M, Ginhoux F, Jakubzick C, Naik SH, Onai N, Schraml BU, et al. Dendritic cells, monocytes and macrophages: a unified nomenclature based on ontogeny. *Nat Rev Immunol*. (2014) 14:571–8. doi: 10.1038/nri3712

52. Lescoat A, Lecureur V, Roussel M, Sunnaram BL, Ballerie A, Coiffier G, et al. CD16-positive circulating monocytes and fibrotic manifestations of systemic sclerosis. *Clin Rheumatol*. (2017) 36:1649–54. doi: 10.1007/s10067-017-3597-6

53. Rabinovitch M, Guignabert C, Humbert M, Nicolls MR. Inflammation and immunity in the pathogenesis of pulmonary arterial hypertension. *Circ Res*. (2014) 115:165–75. doi: 10.1161/CIRCRESAHA.113.301141

54. Kherbeck N, Tamby MC, Bussone G, Dib H, Perros F, Humbert M, et al. The role of inflammation and autoimmunity in the pathophysiology of pulmonary arterial hypertension. *Clin Rev Allergy Immunol*. (2013) 44:31–8. doi: 10.1007/s12016-011-8265-z

55. Matsushita T. Regulatory and effector B cells: Friends or foes? *J Dermatol Sci*. (2019) 93:2–7. doi: 10.1016/j.jdermsci.2018.11.008

56. Khanna D, Denton CP, Jahreis A, van Laar JM, Frech TM, Anderson ME, et al. Safety and efficacy of subcutaneous tocilizumab in adults with systemic sclerosis (faSScinate): a phase 2, randomised, controlled trial. *Lancet*. (2016) 387:2630–40. doi: 10.1016/S0140-6736(16)00232-4

57. Dumoitier N, Chaigne B, Régent A, Lofek S, Mhibik M, Dorfmüller P, et al. Scleroderma peripheral B lymphocytes secrete interleukin-6 and transforming growth factor β and activate fibroblasts. *Arthritis Rheumatol*. (2017) 69:1078–89. doi: 10.1002/art.40016

58. Matsushita T, Hasegawa M, Yanaba K, Kodera M, Takehara K, Sato S. Elevated serum BAFF levels in patients with systemic sclerosis: enhanced BAFF signaling in systemic sclerosis B lymphocytes. *Arthritis Rheum*. (2006) 54:192–201. doi: 10.1002/art.21526

59. González-Tajuelo R, de la Fuente-Fernández M, Morales-Cano D, Muñoz-Callejas A, González-Sánchez E, Silván J, et al. Spontaneous pulmonary hypertension associated with systemic sclerosis in P-selectin glycoprotein ligand 1-deficient mice. *Arthritis Rheumatol*. (2020) 72:477–87. doi: 10.1002/art.41100

60. Mizuno S, Farkas L, Al Husseini A, Farkas D, Gomez-Arroyo J, Kraskauskas D, et al. Severe pulmonary arterial hypertension induced by SU5416 and ovalbumin immunization. *Am J Respir Cell Mol Biol*. (2012) 47:679–87. doi: 10.1165/rcmb.2012-0077OC

61. Zhang T, Huang C, Luo H, Li J, Huang H, Liu X, et al. Identification of key genes and immune profile in limited cutaneous systemic sclerosis-associated pulmonary arterial hypertension by bioinformatics analysis. *Life Sci*. (2021) 271:119151. doi: 10.1016/j.lfs.2021.119151

62. Duo M, Liu Z, Zhang Y, Li P, Weng S, Xu H, et al. Construction of a diagnostic signature and immune landscape of pulmonary arterial hypertension. *Front Cardiovasc Med*. (2022) 9:940894. doi: 10.3389/fcvm.2022.940894

63. Doskaliuk B, Zaiats L, Yatsyshyn R, Gerych P, Cherniuk N, Zimba O. Pulmonary involvement in systemic sclerosis: exploring cellular, genetic and epigenetic mechanisms. *Rheumatol Int*. (2020) 40:1555–69. doi: 10.1007/s00296-020-04658-6

64. Matsushita T, Kobayashi T, Mizumaki K, Kano M, Sawada T, Tennichi M, et al. BAFF inhibition attenuates fibrosis in scleroderma by modulating the regulatory and effector B cell balance. *Sci Adv*. (2018) 4:eaas9944. doi: 10.1126/sciadv.aas9944

65. Ricard L, Malard F, Riviere S, Laurent C, Fain O, Mohty M, et al. Regulatory B cell imbalance correlates with Tfh expansion in systemic sclerosis. *Clin Exp Rheumatol*. (2021) 39 Suppl 131:20–4. doi: 10.55563/clinexprheumatol/fq8tm9

66. Sanges S, Tian W, Dubucquoi S, Chang JL, Collet A, Launay D, et al. B-cells in pulmonary arterial hypertension: friend, foe or bystander? *Eur Respir J*. (2024) 63:2301949. doi: 10.1183/13993003.01949-2023

67. Sanges S, Guerrier T, Duhamel A, Guilbert L, Hauspie C, Largy A, et al. Soluble markers of B cell activation suggest a role of B cells in the pathogenesis of systemic sclerosis-associated pulmonary arterial hypertension. *Front Immunol*. (2022) 13:954007. doi: 10.3389/fimmu.2022.954007

68. Wang RR, Yuan TY, Wang JM, Chen YC, Zhao JL, Li MT, et al. Immunity and inflammation in pulmonary arterial hypertension: From pathophysiology mechanisms to treatment perspective. *Pharmacol Res*. (2022) 180:106238. doi: 10.1016/j.phrs.2022.106238

69. Wynn TA. Fibrotic disease and the T(H)1/T(H)2 paradigm. *Nat Rev Immunol*. (2004) 4:583–94. doi: 10.1038/nri1412

70. Fava A, Cimbro R, Wigley FM, Liu QR, Rosen A, Boin F. Frequency of circulating topoisomerase-I-specific CD4 T cells predicts presence and progression of interstitial lung disease in scleroderma. *Arthritis Res Ther*. (2016) 18:99. doi: 10.1186/s13075-016-0993-2

71. Ugor E, Simon D, Almanzar G, Pap R, Najbauer J, Németh P, et al. Increased proportions of functionally impaired regulatory T cell subsets in systemic sclerosis. *Clin Immunol*. (2017) 184:54–62. doi: 10.1016/j.clim.2017.05.013

72. Ahmed S, Misra DP, Agarwal V. Interleukin-17 pathways in systemic sclerosis-associated fibrosis. *Rheumatol Int*. (2019) 39:1135–43. doi: 10.1007/s00296-019-04317-5

73. Truchetet ME, Brembilla NC, Montanari E, Allanore Y, Chizzolini C. Increased frequency of circulating Th22 in addition to Th17 and Th2 lymphocytes in systemic sclerosis: association with interstitial lung disease. *Arthritis Res Ther*. (2011) 13:R166. doi: 10.1186/ar3486

74. Hur J, Yang HM, Yoon CH, Lee CS, Park KW, Kim JH, et al. Identification of a novel role of T cells in postnatal vasculogenesis: characterization of endothelial progenitor cell colonies. *Circulation*. (2007) 116:1671–82. doi: 10.1161/CIRCULATIONAHA.107.694778

75. Kushner EJ, MacEneaney OJ, Morgan RG, Van Engelenburg AM, Van Guilder GP, DeSouza CA. CD31+ T cells represent a functionally distinct vascular T cell phenotype. *Blood Cells Mol Dis*. (2010) 44:74–8. doi: 10.1016/j.bcmd.2009.10.009

76. Lv T, Yang F, Zhang K, Lv M, Zhang Y, Zhu P. The risk of circulating angiogenic T cells and subsets in patients with systemic sclerosis. *Int Immunopharmacol*. (2020) 81:106282. doi: 10.1016/j.intimp.2020.106282

77. Varol C, Mildner A, Jung S. Macrophages: development and tissue specialization. *Annu Rev Immunol*. (2015) 33:643–75. doi: 10.1146/annurev-immunol-032414-112220

78. Tan SY, Krasnow MA. Developmental origin of lung macrophage diversity. *Development*. (2016) 143:1318–27. doi: 10.1242/dev.129122

79. Higashi-Kuwata N, Jinnin M, Makino T, Fukushima S, Inoue Y, Muchemwa FC, et al. Characterization of monocyte/macrophage subsets in the skin and peripheral blood derived from patients with systemic sclerosis. *Arthritis Res Ther*. (2010) 12:R128. doi: 10.1186/ar3066

80. He J, Mu M, Wang H, Ma H, Tang X, Fang Q, et al. Upregulated IGF−1 in the lungs of asthmatic mice originates from alveolar macrophages. *Mol Med Rep*. (2019) 19:1266–71. doi: 10.3892/mmr.2018.9726

81. Moreno-Moral A, Bagnati M, Koturan S, Ko JH, Fonseca C, Harmston N, et al. Changes in macrophage transcriptome associate with systemic sclerosis and mediate GSDMA contribution to disease risk. *Ann Rheum Dis*. (2018) 77:596–601. doi: 10.1136/annrheumdis-2017-212454

82. Lescoat A, Jégo P, Lecureur V. M-CSF and GM-CSF monocyte-derived macrophages in systemic sclerosis: the two sides of the same coin? *Ann Rheum Dis*. (2019) 78:e19. doi: 10.1136/annrheumdis-2018-213112

83. Stifano G, Christmann RB. Macrophage involvement in systemic sclerosis: do we need more evidence? *Curr Rheumatol Rep*. (2016) 18:2. doi: 10.1007/s11926-015-0554-8

84. Prasse A, Pechkovsky DV, Toews GB, Schäfer M, Eggeling S, Ludwig C, et al. CCL18 as an indicator of pulmonary fibrotic activity in idiopathic interstitial pneumonias and systemic sclerosis. *Arthritis Rheum*. (2007) 56:1685–93. doi: 10.1002/art.22559

85. Tiev KP, Hua-Huy T, Kettaneh A, Gain M, Duong-Quy S, Tolédano C, et al. Serum CC chemokine ligand-18 predicts lung disease worsening in systemic sclerosis. *Eur Respir J*. (2011) 38:1355–60. doi: 10.1183/09031936.00004711

86. Trombetta AC, Soldano S, Contini P, Tomatis V, Ruaro B, Paolino S, et al. A circulating cell population showing both M1 and M2 monocyte/macrophage surface markers characterizes systemic sclerosis patients with lung involvement. *Respir Res*. (2018) 19:186. doi: 10.1186/s12931-018-0891-z

87. McCubbrey AL, Barthel L, Mohning MP, Redente EF, Mould KJ, Thomas SM, et al. Deletion of c-FLIP from CD11b(hi) macrophages prevents development of bleomycin-induced lung fibrosis. *Am J Respir Cell Mol Biol*. (2018) 58:66–78. doi: 10.1165/rcmb.2017-0154OC

88. Nicolosi PA, Tombetti E, Giovenzana A, Donè E, Pulcinelli E, Meneveri R, et al. Macrophages guard endothelial lineage by hindering endothelial-to-mesenchymal transition: implications for the pathogenesis of systemic sclerosis. *J Immunol*. (2019) 203:247–58. doi: 10.4049/jimmunol.1800883

89. Sun C, Chen SY. RGC32 promotes bleomycin-induced systemic sclerosis in a murine disease model by modulating classically activated macrophage function. *J Immunol*. (2018) 200:2777–85. doi: 10.4049/jimmunol.1701542

90. Yaku A, Inagaki T, Asano R, Okazawa M, Mori H, Sato A, et al. Regnase-1 prevents pulmonary arterial hypertension through mRNA degradation of interleukin-6 and platelet-derived growth factor in alveolar macrophages. *Circulation*. (2022) 146:1006–22. doi: 10.1161/CIRCULATIONAHA.122.059435

91. Kang I, Bucala R. The immunobiology of MIF: function, genetics and prospects for precision medicine. *Nat Rev Rheumatol*. (2019) 15:427–37. doi: 10.1038/s41584-019-0238-2

92. Huang H, Chen D, Pu J, Yuan A, Fu Q, Li J, et al. The small molecule macrophage migration inhibitory factor antagonist MIF098, inhibits pulmonary hypertension associated with murine SLE. *Int Immunopharmacol*. (2019) 76:105874. doi: 10.1016/j.intimp.2019.105874

93. Ribatti D, Crivellato E. Immune cells and angiogenesis. *J Cell Mol Med*. (2009) 13:2822–33. doi: 10.1111/j.1582-4934.2009.00810.x

94. Huertas A, Tu L, Gambaryan N, Girerd B, Perros F, Montani D, et al. Leptin and regulatory T-lymphocytes in idiopathic pulmonary arterial hypertension. *Eur Respir J*. (2012) 40:895–904. doi: 10.1183/09031936.00159911

95. Iannone F, Riccardi MT, Guiducci S, Bizzoca R, Cinelli M, Matucci-Cerinic M, et al. Bosentan regulates the expression of adhesion molecules on circulating T cells and serum soluble adhesion molecules in systemic sclerosis-associated pulmonary arterial hypertension. *Ann Rheum Dis*. (2008) 67:1121–6. doi: 10.1136/ard.2007.080424

96. Xing Y, Zhao J, Zhou M, Jing S, Zhao X, Mao P, et al. The LPS induced pyroptosis exacerbates BMPR2 signaling deficiency to potentiate SLE-PAH. *FASEB J*. (2021) 35:e22044. doi: 10.1096/fj.202100851RR

97. Bhattacharyya S, Wei J, Varga J. Understanding fibrosis in systemic sclerosis: shifting paradigms, emerging opportunities. *Nat Rev Rheumatol*. (2011) 8:42–54. doi: 10.1038/nrrheum.2011.149

98. Sun Z, Gong X, Zhu H, Wang C, Xu X, Cui D, et al. Inhibition of Wnt/β-catenin signaling promotes engraftment of mesenchymal stem cells to repair lung injury. *J Cell Physiol*. (2014) 229:213–24. doi: 10.1002/jcp.24436

99. Lafyatis R. Transforming growth factor β–at the centre of systemic sclerosis. *Nat Rev Rheumatol*. (2014) 10:706–19. doi: 10.1038/nrrheum.2014.137

100. Gilbane AJ, Derrett-Smith E, Trinder SL, Good RB, Pearce A, Denton CP, et al. Impaired bone morphogenetic protein receptor II signaling in a transforming growth factor-β-dependent mouse model of pulmonary hypertension and in systemic sclerosis. *Am J Respir Crit Care Med*. (2015) 191:665–77. doi: 10.1164/rccm.201408-1464OC

101. Denton C, Pope J, Peter H-H, Gabrielli A, Boonstra A, Hoogen F, et al. Long-term effects of bosentan on quality of life, survival, safety and tolerability in pulmonary arterial hypertension related to connective tissue diseases. *Ann rheumatic Dis*. (2007) 67:1222–8. doi: 10.1136/ard.2007.079921

102. Preston IR, Lewis D, Gomberg-Maitland M. Using sotatercept in the care of patients with pulmonary arterial hypertension. *Chest*. (2024) 24:04611–7. doi: 10.1016/j.chest.2024.06.3801

103. Zamanian RT, Badesch D, Chung L, Domsic RT, Medsger T, Pinckney A, et al. Safety and efficacy of B-cell depletion with rituximab for the treatment of systemic sclerosis-associated pulmonary arterial hypertension: A multicenter, double-blind, randomized, placebo-controlled trial. *Am J Respir Crit Care Med*. (2021) 204:209–21. doi: 10.1164/rccm.202009-3481OC

104. Hennigan S, Channick RN, Silverman GJ. Rituximab treatment of pulmonary arterial hypertension associated with systemic lupus erythematosus: a case report. *Lupus*. (2008) 17:754–6. doi: 10.1177/0961203307087610

105. Braun-Moscovici Y, Butbul-Aviel Y, Guralnik L, Toledano K, Markovits D, Rozin A, et al. Rituximab: rescue therapy in life-threatening complications or refractory autoimmune diseases: a single center experience. *Rheumatol Int*. (2013) 33:1495–504. doi: 10.1007/s00296-012-2587-x

106. Kusaka K, Nakano K, Iwata S, Kubo S, Nishida T, Tanaka Y. Two patients with mixed connective tissue disease complicated by pulmonary arterial hypertension showing contrasting responses to pulmonary vasodilators. *Mod Rheumatol Case Rep*. (2020) 4:253–61. doi: 10.1080/24725625.2020.1758388

107. Li C, Liu P, Yao H, Zhu H, Zhang S, Meng F, et al. Regulatory B cells protect against chronic hypoxia-induced pulmonary hypertension by modulating the Tfh/Tfr immune balance. *Immunology*. (2023) 168:580–96. doi: 10.1111/imm.13589

108. Breitling S, Hui Z, Zabini D, Hu Y, Hoffmann J, Goldenberg NM, et al. The mast cell-B cell axis in lung vascular remodeling and pulmonary hypertension. *Am J Physiol Lung Cell Mol Physiol*. (2017) 312:L710–l721. doi: 10.1152/ajplung.00311.2016

109. Yu M, Wu X, Peng L, Yang M, Zhou H, Xu J, et al. Inhibition of bruton's tyrosine kinase alleviates monocrotaline-induced pulmonary arterial hypertension by modulating macrophage polarization. *Oxid Med Cell Longev*. (2022) 2022:6526036. doi: 10.1155/2022/6526036

110. Einhaus J, Pecher AC, Asteriti E, Schmid H, Secker KA, Duerr-Stoerzer S, et al. Inhibition of effector B cells by ibrutinib in systemic sclerosis. *Arthritis Res Ther*. (2020) 22:66. doi: 10.1186/s13075-020-02153-8

frontiers | Frontiers in Immunology

TYPE Review
PUBLISHED 25 September 2024
DOI 10.3389/fimmu.2024.1474688

OPEN ACCESS

EDITED BY
Ping Yuan,
Tongji University, China

REVIEWED BY
Hongxiang Wang,
Changhai Hospital, China
Jin-Ming Liu,
Tongji University, China

*CORRESPONDENCE
Zhaoyi Xia
birbirfly166@163.com

†These authors have contributed equally to this work and share first authorship

RECEIVED 02 August 2024
ACCEPTED 06 September 2024
PUBLISHED 25 September 2024

CITATION
Li X, Liu Y, Tang Y and Xia Z (2024) Transformation of macrophages into myofibroblasts in fibrosis-related diseases: emerging biological concepts and potential mechanism. *Front. Immunol.* 15:1474688. doi: 10.3389/fimmu.2024.1474688

Transformation of macrophages into myofibroblasts in fibrosis-related diseases: emerging biological concepts and potential mechanism

Xiujun Li[1†], Yuyan Liu[2†], Yongjun Tang[3] and Zhaoyi Xia[4,5*]

[1]Health Science Center, Chifeng University, Chifeng, China, [2]Rehabilitation Medicine College, Shandong Second Medical University, Jinan, China, [3]Department of Emergency, Affiliated Hospital of Chifeng University, Chifeng, China, [4]Department of Library, Children's Hospital Affiliated to Shandong University, Jinan, China, [5]Department of Library, Jinan Children's Hospital, Jinan, China

Macrophage-myofibroblast transformation (MMT) transforms macrophages into myofibroblasts in a specific inflammation or injury microenvironment. MMT is an essential biological process in fibrosis-related diseases involving the lung, heart, kidney, liver, skeletal muscle, and other organs and tissues. This process consists of interacting with various cells and molecules and activating different signal transduction pathways. This review deeply discussed the molecular mechanism of MMT, clarified crucial signal pathways, multiple cytokines, and growth factors, and formed a complex regulatory network. Significantly, the critical role of transforming growth factor-β (TGF-β) and its downstream signaling pathways in this process were clarified. Furthermore, we discussed the significance of MMT in physiological and pathological conditions, such as pulmonary fibrosis and cardiac fibrosis. This review provides a new perspective for understanding the interaction between macrophages and myofibroblasts and new strategies and targets for the prevention and treatment of MMT in fibrotic diseases.

KEYWORDS

macrophages, myofibroblasts, macrophage-to-myofibroblast transformation (MMT), TGF-β signaling pathway, fibrosis

1 Introduction

Macrophage-myofibroblast transformation (MMT) describes how macrophages from circulating monocytes originating in the bone marrow transform into myofibroblasts and contribute to fibrosis (1, 2). The term was coined by Nikolic-Paterson et al. In 2014 (3). MMT is a newly discovered mechanism that occurs in damaged tissues undergoing fibrosis; the study of MMT relies on the detection of intermediate cells that co-express macrophage markers, such as CD68, and myofibroblast markers, such as α-smooth muscle actin (SMA)

(4, 5). Hematopoietic stem cells (HSC) can differentiate into monocytes in the bone marrow. Blood monocytes entering the injured tissue can differentiate into an M2 pro-fibrotic phenotype, either directly or via an M1 pro-inflammatory phenotype. TGF-β/Smad3 signaling drives macrophage transition into collagen-producing α-SMA myofibroblasts via MMT (6) (Figure 1).

MMT is considered one of the essential mechanisms for the origin of myofibroblasts in solid organs (7–11). Experimental models of fibrosis, including lung fibrosis, renal fibrosis following transplantation or ureteric obstruction, and post-myocardial infarction fibrosis, have demonstrated MMT as an additional source of myofibroblasts (2, 3, 6, 12, 13). Wang et al. (1) also observed the occurrence of MMT, which contributes to interstitial fibrosis in case of human chronic active renal allograft injury. This was identified through the co-expression of macrophage markers (CD68 or F4/80) and myofibroblast markers (α-SMA). Similarly, Little et al. (14) demonstrated the presence of MMT in the subretinal fibrotic lesions, which ultimately led to subretinal fibrosis. Increasing evidence supports the role of macrophages in promoting fibrosis through their transformation into myofibroblasts, a process known as the MMT (15). Several signaling pathways, including TGF-β1/Smad, Notch, and Wnt signaling pathways, including are involved in MMT (3). It is worth noting that several studies have specifically highlighted the promotion of MMT by the TGF-β1/Smad2/β-catenin signaling pathway (3, 16–19).

This review provides an update on current advancements in MMT and summarizes recent evidence and mechanisms of MMT in fibrosis. Furthermore, we discussed the significance of MMT in physiological and pathological conditions. Under physiological conditions, MMT may participate in tissue repair and wound healing, which helps restore the structure and function of tissues. Under pathological conditions, excessive transformation may lead to the occurrence and development of fibrotic diseases, such as pulmonary fibrosis (PF) and cardiac fibrosis. Understanding this phenomenon and its underlying signal pathway would be beneficial in finding therapeutic targets for fibrosis disease.

2 Overview of macrophage

Macrophages were first described by Elie Metchnikoff in 1893 when he observed phagocytes attacking and engulfing microbes in starfish challenged by a rose thorn (20). Another significant milestone came in 1924 when Aschoff defined macrophages as a part of the reticulo-endothelial system (21). However, in 1968, Van Furth et al. (22) proposed the mononuclear phagocyte system, challenging the previous definition. According to this system, all macrophages were believed to originate from the terminal differentiation of circulating monocytes. This theory was further supported by other researchers around the world at that time (23–25). However, more recent studies have identified a dual origin of tissue macrophages. It has been found that macrophages can differentiate from circulating monocytes derived from bone marrow stem cells, as well as primitive macrophages derived from the embryonic yolk sac and fetal liver (26, 27). The mononuclear

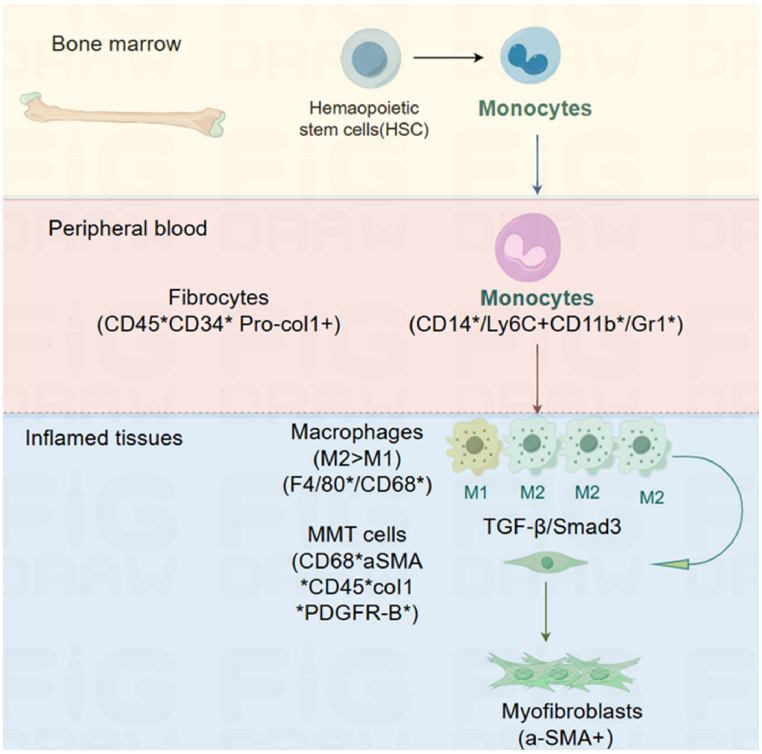

FIGURE 1
MMT in tissue fibrosis.

phagocyte system consists of three parts, including monocytes, macrophages, and dendritic cells, with macrophages playing a crucial role within this system (28).

Macrophages are strategically located throughout body tissues, ingesting and processing foreign bodies, dead cells, and debris while recruiting additional macrophages in response to inflammatory signals. These cells are highly heterogeneous cells and have the ability to rapidly change their function in response to local microenvironment signals (29). Macrophages are categorized into subsets based on their anatomical location and functional phenotype (30). Some examples of specialized tissue-resident macrophages include osteoclasts (bone), alveolar macrophages (lung), histiocytes (interstitial connective tissue), and Kupffer cells (liver). It is important to note that there is considerable overlap in the expression of surface markers between different subsets of macrophages (31).

Rather than being discrete and stable subsets, macrophages represent a spectrum of activated phenotypes (32). Classically activated macrophages, also known as M1 macrophages, are involved in host defense against various bacteria, protozoa, and viruses, and they also play a role in anti-tumor immunity. On the other hand, alternatively activated macrophages, or M2 macrophages, possess anti-inflammatory properties and contribute to wound healing. There are also "regulatory" macrophages that can secrete high levels of interleukin-10 (IL-10) upon binding to Fc receptors gamma (33, 34). Macrophages found in the lung (both interstitial and alveoli), peritoneum, liver (Kupffer cells), and brain (microglia) are generally considered to be distinct lineage of macrophages with unique functions (35, 36).

2.1 The classification and phenotype of macrophages

Monocytes are regarded as precursor cells of the mononuclear phagocytic system, with macrophages being one of the key members of this cellular system. Within the macrophage population, there exist various subpopulations of macrophages, each with its characteristics and functions.

2.1.1 Classification of organizational sources

The specialization of macrophages in particular microenvironments explains their heterogeneity. Macrophages take different names according to their tissue location, such as osteoclasts (bone), alveolar macrophages (lung), microglial cells (central nervous system), histiocytes (connective tissue), Kupffer cells (liver), and LC (skin). These populations have such highly different transcriptional profiles that they could be considered as many different and unique classes of macrophages (37).

2.1.2 General functional classification

Macrophages can be defined and classified based on their functions, such as phagocytosis and immunity, as well as specific markers like F4/80 and CD68 (38). This classification divides them into:

2.1.2.1 Classically activated macrophages

Classically activated macrophages, or M1 macrophages, are induced *in vitro* by interferon (IFN)-γ and lipopolysaccharide (LPS). They drive a pro-inflammatory response and aid in the elimination of infection. Mainly through the secretion of pro-inflammatory cytokines (such as IL-1, IL-6, TNF-α, etc.) and chemokines, they promote the occurrence and development of inflammatory reactions. They can devour and eliminate foreign pathogens, activate the immune response of T cells, and regulate and promote the Th1 immune response.

2.1.2.2 Selectively activated macrophages

Selectively activated macrophages, known as M2 macrophages, play a role in controlling the immune response and tissue remodeling (39). M2 macrophages encompass a variety of phenotypes that further subdivided into M2a (exposure to IL-4 or IL-13), M2b (induced by immune complexes in combination with IL-1β or LPS), M2c cells (after exposure to IL-10, TGF-β or glucocorticoids) and M2d cells (IL-6, angiogenic adenosineA2A) (40, 41). M2 macrophages inhibit inflammatory reactions and promote tissue repair and wound healing mainly by secreting anti-inflammatory cytokines (such as IL-10) and growth factors (such as vascular endothelial growth factor (VEGF) and TGF-β). They also regulate the Th2 immune response, which is beneficial for disease recovery in the late stage of inflammation.

Stimulated by GM-CSF, IFN-γ, and LPS, M0 macrophages polarize into M1 macrophages. Alternatively, M-CSF, IL-4, IL-13, and immune complexes (IC) stimulation cause the polarization of M0 macrophages to M2 macrophages. Various cytokines further induce M2 macrophages to differentiate into M2a, M2b, M2c, and M2d phenotypes. M1 macrophages are usually associated with inflammation and represent a prototypic subset of pro-inflammatory macrophages (39). In contrast, M2 macrophages are polarized by Th2 cytokines IL-4 and IL-13, among other factors. They are characterized by high levels of anti-inflammatory cytokines and pro-fibrotic factors (39, 42), contributing to matrix deposition and tissue remodeling (43). M2 macrophages are the primary source of TGF-β1, which is widely recognized as a critical cytokine associated with fibrosis (39, 44, 45). M2 macrophages have been found to affect pathological fibrosis (46) and play a role in the process of fibrosis, such as in PF (47–50), renal fibrosis (51, 52), ischemic cardiac fibrosis (53, 54), and neovascularization (55).

Therefore, on one end of the extreme, M1 pro-inflammatory cells facilitate the eradication of infections, albeit with the potential to inflict damage. On the other extreme, M2 anti-inflammatory cells have a repair phenotype that promotes a regression phase of the injury response (51). In response to various signals, macrophages may undergo classical M1 activation (stimulated by TLR ligands and IFN-γ) or alternative M2 activation (stimulated by IL-4/IL-13). These states reflect Th1-Th2 polarization in T cells (56, 57). The M1 phenotype is characterized by high levels of pro-inflammatory cytokine expression, high production of reactive nitrogen and oxygen intermediates, promotion of the Th1 response, and potent bactericidal and tumoricidal activity (58). M1 macrophages are also

believed to be involved in various chronic inflammatory and autoimmune diseases (59). M2 macrophages are considered to be involved in the control of parasites, promoting tissue remodeling and tumor progression, and have immunomodulatory functions. They exhibit effective phagocytic activity and high expression of scavenging molecules, among others (60).

2.1.3 Function classification of homeostatic activities

Mosser and Edwards proposed a classification of macrophages based on three primary functions that these cells perform to maintain homeostasis in the body: host defense (classically activated), wound healing, and immune regulation (32).

2.1.3.1 Host defense macrophages

The role of classically activated macrophages in host defense against intracellular pathogens has been well documented. Classically activated macrophages, as mentioned earlier, are crucial for host defense. However, their activation needs to be tightly regulated due to the potential for cytokines and mediators they produce to cause host-tissue damage. For instance, classically activated macrophages produce IL-1, IL-6, and IL-23, which have been associated with the development and expansion of TH17 cells (61). These cells produce IL-17, a cytokine involved in recruiting polymorphonuclear leukocytes (PMNs) to tissues, potentially contributing to inflammatory autoimmune pathologies. On the other hand, macrophages can inhibit inflammation by clearing apoptotic PMNs during inflammation, partly due to the production of TGF-β (62–64).

2.1.3.2 Wound-healing macrophages

Macrophages play a vital role in wound repair (11, 65). Alternatively, activated macrophages have anti-inflammatory functions and are involved in regulating wound healing. They contribute to dampening inflammation, clearing cell debris, and coordinating tissue repair, making them essential for the wound healing process (66). Wound-healing macrophages can develop in response to innate or adaptive signals. IL-4, released during tissue damage, is one of the initial innate signals that rapidly convert resident macrophages into a population of cells programmed to promote wound healing (67). IL-4 stimulates arginase activity in macrophages, allowing them to convert arginine to ornithine, a precursor of polyamines and collagen that contributes to extracellular matrix (ECM) production (68). When the inflammatory stimulus or pathogen is eliminated, M1 cell activation diminishes. Alarmins and Th2-type cytokines drive the immune response toward a wound-healing response characterized by the accumulation of M2 macrophages. These M2 macrophages promote wound healing and fibrosis by producing matrix metalloproteinases (MMPs), including MMP12, tissue inhibitor of metalloproteinases 1 (TIMP1), growth factors (including platelet-derived growth factor (PDGF)) and cytokines (such as TGF-β1) (29).

2.1.3.3 Regulatory macrophage

Regulatory macrophages have a key role in regulating the inflammatory immune response to limit tissue damage. Their primary physiological function is to dampen inflammatory immune responses and prevent the immunopathology associated with prolonged activation of classically activated macrophages (66). They are characterized by the production of high levels of IL-10 (69). Regulatory macrophages can secrete large amounts of this cytokine in response to Fc receptor γ -binding (34, 70). They represent a relatively broad category of macrophages that play a crucial role in inhibiting inflammatory immune responses and preventing the immunopathology associated with prolonged activation of classically activated macrophage (71). They are distinct from classically activated macrophages and differ from macrophages treated with Th2 cytokines, such as IL-4 or IL-13, known as alternatively activated macrophages (72).

2.1.4 Other classifications

Apart from M1 and M2 macrophages, there are additional subpopulations of macrophages, including tumor-associated macrophages (TAMs), CD169 macrophages, and T cell receptor-positive (TCR) macrophages (73).

2.1.4.1 TAM

Macrophages display plasticity, with their phenotype determined by their location and the physiological or pathological context. Classically activated macrophages (M1) and alternatively activated macrophages (M2) represent two ends of the macrophage phenotype spectrum (74). TAMs closely resemble M2 macrophages and are associated with the inhibition of anti-tumor immunity (75). Myeloid-derived suppressor cells (MDSC) are often associated with TAM and may serve as their precursors (32, 76). TAMs promote tumorigenesis, tumor growth, invasion, metastasis, and affect tumor metabolism through various mechanisms (77). Recent study indicated that TAMs have protumoral functions, indicating that they play a direct or indirect role in promoting tumor progression (78).

2.1.4.2 CD169 macrophages

As a specific subpopulation of macrophages, CD169 macrophages have been recently studied in malignant tumors (79). Current research suggests that CD169 macrophages have inhibitory effect on tumors. CD169/Siglec1/sialoadhesin, a sialic acid-binding immunoglobulin-like lectin, is primarily expressed in metallophilic macrophages in the marginal zone of the spleen and macrophages in the subcapsular sinus and medulla of lymph nodes. In addition to their role in anti-infectious immunity, recent study has demonstrated the involvement of CD169 macrophages in tumor immunity and their association with a favorable prognosis (79).

2.1.4.3 T cell receptor

The T cell receptor (TCR) is a molecule essential for antigen recognition and forms a complex with CD3 (80). Previous studies have reported the presence of TCR macrophages in both human and murine populations. TCR-αβ has been observed in peripheral blood monocytes and *in vitro* in activated monocyte-derived macrophages. TCR macrophages can release CCL2 and exhibit a high phagocytosis capacity (81). Recently, Fuchs et al. (82) reported that TCR-αβ macrophages are present in murine and human

atherosclerotic lesions, indicating their potential as a novel molecular target for diagnosing and treating diseases where cholesterol plays a central role in the pathophysiology.

2.2 Macrophage function

Macrophages have highly diverse roles in maintaining the body's integrity, including direct participation in pathogen elimination and tissue repair during aseptic inflammatory conditions. Their functions vary across different tissues, playing crucial roles in tissue development, immune response to pathogens, surveillance and monitoring of tissue changes, and maintenance of tissue homeostasis.

2.2.1 Phagocytosis and elimination of pathogenic microorganisms

Macrophages are specialized phagocytes that, often with a long lifespan, are present in all organs to maintain tissue integrity, remove debris, and respond rapidly to initiate repair in the event of innate immunity after injury or infection (30, 83). Plasticity and functional polarization are the hallmarks of the mononuclear phagocyte system (41). Their phagocytic activity is crucial for fibrogenesis, with the type of engulfed dead cells influencing fibrosis progression (84). Macrophages also act as heterologous phagocytes, detecting pathogen-related molecular patterns and injury-related molecular patterns through pattern recognition receptors (85, 86). TAMs demonstrate bidirectional transformation between anti-inflammatory and immunosuppressive phenotypes (57, 87). Furthermore, macrophages play a vital role in wound repair (65).

2.2.2 Antigen presentation, immunomodulation, and anti-inflammatory function

Macrophages have the capacity to take up and present antigens, bridging innate and adaptive immunity (88). They can act as antigen-presenting cells (APCs) and influence adaptive immune responses (89). Monocytes that enter the tissue during inflammation can carry antigens to lymph nodes and present them to naive T-cells (90). Regulatory macrophages have been shown to efficiently present antigens and induce antigen-specific T-cell responses dominated by the production of Th2 cytokines (89). Macrophages also play a crucial role in cellular immunity by secreting cytokines and chemokines, regulating the activities of other immune cells, and balancing the body's immune response. They can secrete both pro-inflammatory cytokines, such as IL-1 and IL-6, to promote inflammatory reactions, and anti-inflammatory cytokines, such as IL-10, to inhibit excessive inflammation.

2.2.3 Regulation function regulating fibrosis

Macrophages are considered to be the critical cell types in the development of fibrotic diseases (17). Recent studies have also revealed that their role as regulators of fibrosis. Like myofibroblasts, these cells are derived from resident tissue populations such as Kupffer cells or bone marrow migrants (91–95). Current studies have shown that the pathogenesis of fibrosis is tightly regulated by different populations of macrophages, which exert unique functional activities in the initiation, maintenance, and regression stages of fibrosis (96, 97). Activated hepatic stellate cells (HSCs) attract and stimulate macrophages, which produce profibrotic mediators like TGF-β1 and PDGF, directly activating fibroblasts (94, 98). Several studies have identified macrophages as a major source of TGF-β1 and PDGF in fibrosis (71, 99). While macrophages contribute to fibrosis progression, they may also mediate its regression (11). Given the multifunctional capacity and heterogeneous phenotype of macrophages, it is not surprising that they can enhance and limit fibrosis (100). M2 macrophages may be a promising potential target for future anti-fibrosis therapies.

3 Overview of myofibroblast

3.1 Source and characteristics of myofibroblasts

In 1971, Gabbiani and his colleagues discovered and characterized myofibroblasts, which are fibroblasts modified to exhibit active contraction in rat wound granulation tissue. This was the first time it had been shown that myofibroblasts promote dermal wound contraction (101). Myofibroblasts are a subset of activated fibroblasts that express molecular markers such as α-SMA and the fibronectin (FN) splice variant extracellular domain (ED)-A FN (102). Hyperactive myofibroblasts, marked by the expression of α-SMA, are primarily responsible for the production of pathogenic collagen tissue fibrosis (7, 103). One of the defining features of myofibroblasts is the development of *in vivo* stress fibers and contractile force (104). They exhibit morphological and structural characteristics similar to smooth muscle cells, including a flat and irregular morphology, developed cell-ECM interactions, and intercellular space junctions (105). The activation of myofibroblasts is crucial for physiological and pathological tissue repair. Myofibroblasts are the main ECM secretory cells in wound healing and fibrosis and are mainly responsible for the contractility of scar tissue when it matures (106). Myofibroblasts combine the ECM synthesis characteristics of fibroblasts with the cytoskeletal characteristics of contractile smooth muscle cells, regulating connective tissue remodeling (107).

Defining characteristics of myofibroblasts include abundant rough endoplasmic reticulum, moderately developed peripheral myofilaments with focal density, fibronectin, and α-SMA immunostaining (108). In wound granulation tissue, myofibroblasts coexist with prominent endoplasmic reticulum and contractile microfilaments (109). The transformation of myofibroblasts is triggered by integrating neurohumoral, cytokine, growth factor, and mechanical signals from the extracellular environment (110). Myofibroblast differentiation is a critical event for wound healing, tissue repair, and chronic fibrosis (104, 107, 111). At least three local events are required for the differentiation of α-SMA-positive myofibroblasts: accumulation of biologically active TGF-β1, the presence of specialized ECM proteins like ED-A splice variants of fibronectin, and high extracellular stress are caused by the mechanical properties of ECM and cellular remodeling activity

(104). The mechanical resistance of the ECM, combined with the action of fibrotic TGF-β1, is the primary stimulus for the differentiation and persistence of myofibroblasts (104).

3.2 Distribution of myofibroblasts

Myofibroblasts can originate from various sources, including epithelial-mesenchymal transition (EMT) (7), endothelial-mesenchymal transition (112, 113), resident fibroblast or pericyte proliferation (114), and the newly discovered phenomenon of MMT (115). Experimental evidence demonstrates that about 50% of myofibroblast accumulation comes from local proliferation of resident tissue fibroblasts, while approximately 35% comes from bone marrow-derived cells (116). Bone marrow transplantation studies have demonstrated the ability of bone marrow-derived cells to populate distal tissue sites (115, 117, 118).

3.3 The hazards of myofibroblasts

Myofibroblasts pose hazards in various ways. They are the primary cells responsible for collagen production in tissue fibrosis, and their contraction and ECM remodeling activity play a crucial role in fibrotic diseases (119–121). The fate of myofibroblasts in injured tissues, regardless of their origin, may ultimately determine whether healing occurs normally or progress to end-stage fibrosis (107). Persistent myofibroblast activity leads to progressive tissue fibrosis and distortion of the typical tissue architecture, resulting in organ failure and, ultimately, death (89). While the high contractile force generated by myofibroblasts is beneficial for physiological tissue remodeling, excessive force can be detrimental to tissue function, as seen in hypertrophic scars, fibrotic diseases, and stromal reactions to tumors (111).

Myofibroblasts are also critical components of the matrix reaction around hepatocellular carcinoma, contributing to the extracellular matrix component (122, 123). Activated hepatic stellate cells, portal vein fibroblasts, and bone marrow-derived myofibroblasts have been identified as central collagen-producing cells in the damaged liver (91). They play significant roles in renal fibrosis and are implicated in its pathogenesis (124). Additionally, myofibroblasts contribute to chronic cardiac fibrosis (110). Experimental and clinical observations suggest that myofibroblasts produce pro-invasive signals that may be associated with cancer progression and pain (125). Myofibroblasts present in the matrix reaction of epithelial tumors may contribute to the progression of cancer invasion (126, 127).

4 The contribution of MMT to the pathogenesis of PF

4.1 Introduction of PF

PF is a chronic and progressive irreversible pulmonary interstitial disease that poses a significant public threat health (128). It is a characteristic feature of a large class of interstitial lung diseases (ILD) (129, 130). Symptoms of PF typically include shortness of breath, unproductive cough, weight loss, and fatigue due to hypoxia (131). It is characterized by thickened fibrotic alveolar walls leading to impaired gas transfer, restricted ventilatory patterns, and, as a result, respiratory failure (132, 133).

Pre-existing inflammation is a key factor in PF development. Acute lung injury (ALI) and its more severe manifestation, acute respiratory distress syndrome (ARDS), are specific forms of lung inflammation characterized by diffuse alteration of the alveoli, non-cardiogenic lung edema, and local and systemic inflammation (134–137). Inflammatory cascades contribute to the pathogenesis of ALI, resulting in increased permeability of lung capillary vessels and diffuse alveolar damage (138–140). The pathomorphological changes in the lungs during ALI/ARDS include neutrophilic inflammatory infiltration, diffuse alveolar damage, alveolar and interstitial edema, hyalin membrane formation in the exudative phase, and ECM deposition in the proliferative phase (139, 141, 142).

PF is a heterogeneous disease characterized by a distinct pattern of tissue pathology and comprises a large number of chronic respiratory pathologies accompanied by connective tissue growth in various lung compartments, among which interstitial lung disease (ILD) and idiopathic PF (IPF) are the most severe and irreversible ones with progressive fibrosing of the lung parenchyma (130, 143–145). IPF, specifically, is a significant type of pulmonary fibrosis, predominantly affecting the elderly, with high mortality and poor prognosis (146). It can cause dyspnea, cough, impaired lung function, and death (147–149). The prevalence of IPF is around 10 cases per 100,000 population, while ILDs have a prevalence of 19.4 cases per 100,000 population (150, 151). In 2014, two drugs, pirfenidone and nintedanib, were approved by the FDA for the treatment of PF (152). However, effective therapeutic options for PF are still lacking, and current treatments only delay disease progression without providing a complete cure. Moreover, these drugs have undesirable side effects, such as gastric and intestinal bleeding and severe diarrhea. Lung transplantation is the last resort for patients, offering some extension of lifespan, but it is not accessible to most individuals. Therefore, studying the molecular mechanisms underlying the transition from acute lung inflammation to PF and identifying new molecular markers and promising therapeutic targets for preventing PF development remain important objectives.

4.2 Role of macrophages in pulmonary fibrosis

Macrophages, as innate immune cells with antibacterial and phagocytic activity, play a significant role in PF. They are the most abundant immune cell population, accounting for about 70% (153). They are widely distributed in the lung and alveolar tissue and are involved in almost all the physiological and pathological processes of the lung (154). They are the host lung defense, indispensable paramount sentry (155, 156), and also play a vital role in the pathogenesis of PF. Macrophage infiltration is observed in PF (157). Macrophages are involved in all stages of lung injury and repair and can both promote and inhibit fibrosis. They play an essential role in

the removal of lung pathogens clearance and maintaining homeostasis (157, 158). The pathogenic role of macrophages in PF has been investigated in multiple studies, involving reactive oxygen species generation (159–161), stimulation of proteinase-activated receptors (162, 163), and secretion of pro-fibrotic cytokines (164, 165).

There are three main types of pulmonary macrophages: alveolar macrophages (AM), interstitial macrophages (IM), and bronchial macrophages (BM), with AM accounting for more than 90% (166). Different subtypes of macrophages play distinct roles in lung injury, repair, and fibrosis (167). Single-cell sequencing of lung tissue from patients with PF have confirmed that alveolar macrophages play an essential role in PF (168–170). Alveolar macrophages are the first cells to come into contact with external pathogens and irritants, initiating and later resolving lung immune responses. Additionally, macrophages have other organ-specific functions, such as surfactant utilization and absorption of apoptosing and destroying cells (171–174). Monocyte-derived macrophages are key drivers of PF and supplement alveolar macrophages that are lost immediately upon injury (175, 176).

The effect of macrophages on PF is mainly related to their polarization, which occurs during the repeated damage and abnormal repair of alveolar epithelial cells (177, 178). Epithelial apoptosis is a critical component of fibrotic disease in many organs, including the lung (179, 180). Down-regulating the pro-fibrosis activity of alveolar macrophages or depleting this group of cells can effectively treat experimental PF (181–183). Macrophages can polarize into either a pro-inflammatory M1 phenotype or an alternatively activated M2 phenotype, depending on the microenvironment in which they reside (184). In response to lung injury, macrophages undergo a transition into pro-inflammatory M1 phenotypes and begin to secrete pro-inflammatory cytokines (TNF-α, IL-6, IL-1) and chemokines (IL-8, CCL7, CCL2), which leads to the increased chemotaxis and progressive enrichment of alveolar spaces by monocytes and neutrophils (185), which aggravate the pulmonary inflammatory response. On the other hand, M2 polarization releases various cytokines, such as TGF-β1 and IL-10, promoting the generation of myofibroblasts and the deposition of extracellular matrix, ultimately leading to PF.

During tissue damage and early inflammation stages, the activation of M1 macrophages promotes inflammation through extracellular matrix-degrading MMP and pro-inflammatory cytokines. An active cytokine environment, including Th1 cytokines, IL2, IFN-γ, and TNF-α, drives M1 macrophage activation. In contrast, other types of interstitial lung diseases (ILDs), including PF, often have a higher proportion of anti-inflammatory M2 macrophages (186) (Figure 2).

In the progression of PF, M1, and M2, macrophages are recruited to the site of the lung tissue injury site to regulate the fibrotic process after basement membrane destruction. M1 macrophages play a crucial role in matrix degradation by directly and indirectly producing MMP and various anti-fibrotic cytokines, essential for ECM remodeling and help reduce the pathological fibrous proliferation observed in late ALI (187). In contrast, M2 macrophages promote fibrous proliferation and ECM deposition in lung tissue (188, 189). Therefore, the degree of PF depends on the balance between M1 and M2 macrophages in the local microenvironment of lung tissue injury. Studies have shown that macrophages, predominantly M2 macrophages, contribute to the pathogenesis of PF (155, 190). M2 macrophages are the primary source of TGF-β1 and platelet-derived growth factors that induce fibroblast differentiation into myofibroblasts, initiating PF (191). Macrophage subsets may regulate fibrosis by differentiating into myofibroblasts, acting as sources of cytokines and growth factors with fibrotic properties, and secreting proteases involved in matrix remodeling (192). Therefore, the number and phenotype of macrophages are considered essential for the pathological process of PF (193, 194). While macrophages are essential for lung defense, they can also lead to tissue damage (195). Different subtypes of macrophages play distinct roles in lung injury, repair, and fibrosis (196).

4.3 Role of myofibroblasts in PF

The main morphological characteristics of PF, such as ECM deposition and remodeling of lung architecture, are consequences of a disbalance between two physiological processes in the lungs: (1) proliferation/apoptosis of fibroblasts and myofibroblasts; (2) synthesis/degradation of ECM components (197). These processes are closely interconnected, and the disruption of fibroblast and myofibroblast functioning is the primary driver behind the imbalance of ECM homeostasis and the development of PF. The fibroblastic phenotype present in that diseased lung primarily by the production of several soluble factors, such as TGF-β, PDGF, VEGF, and thrombospondin 1, which can differentiate resident fibroblast into myofibroblasts (170, 181, 195). Regardless of the source of lung fibroblasts, myofibroblasts, which resemble smooth muscle cells in terms of their contractile ability and expression of α-SMA, are considered the key cells in PF development.

Myofibroblasts are the primary effectors responsible for the excessive production of collagen and other extracellular matrix proteins in fibrotic lungs (104, 198). These contractile fibroblasts express α-SMA and abnormally proliferate in PF. They play a significant role in the occurrence and progression of PF by synthesizing and secreting large amounts of ECM components, such as collagen (I, III, IV, V, and VI), fibronectin, and laminin (199–201), making them critical in regulating the progression of PF. Myofibroblasts have also been found to secrete or release various proteins, lipids, and nucleic acid molecules that contribute to the pathological characteristics of other cell types in fibrotic lungs (129).

The accumulation of myofibroblasts is considered a marker of PF (202). Current research indicates that myofibroblasts involved in PF originate from several sources, including the proliferation and differentiation of resident fibroblasts, the recruitment of circulating fibroblasts to injury sites in organs, endothelial-mesenchymal transformation, and epithelial-mesenchymal transformation (203–205). The synthesis of pathogenic collagen by myofibroblasts, as the main effector of tissue fibrosis, and the process of MMT are essential regardless of the etiology of fibrosis (3, 206–208). Myofibroblast transdifferentiation is a marker of the fibrotic response. Evidence suggests that macrophages are involved in regulating fibrotic responses, with pulmonary myofibroblasts being the primary target for the development of new therapies for IPF (104, 198).

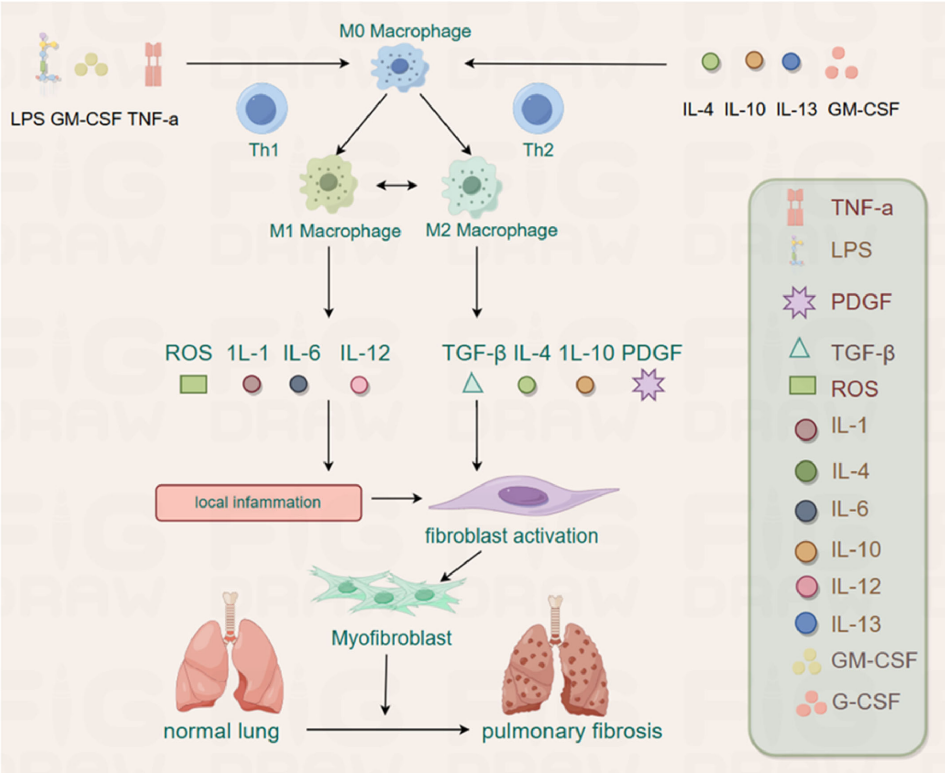

FIGURE 2
The M0 can be polarized into M1 and M2 by different stimuli. The M1 plays an inflammatory role by releasing ROS, IL-1, IL-6 and IL-12, whereas M2 has the potential to promote fibrosis by releasing TGF-β, IL-4, IL-10 and PDGF in PF.

4.4 MMT related signaling pathways in the development of PF

As described earlier, fibrosis is defined by the excessive accumulation of fibrous connective tissue in and around inflamed or damaged tissue, which can lead to permanent scarring, organ malfunction, and, ultimately, death, as seen in end-stage liver disease, kidney disease, IPF, and heart failure (91, 209). The development of PF involves genes and molecular pathways that primarily participate in pre- and postnatal lung development (210, 211). The key pathophysiological events of IPF include repetitive alveolar epithelial cell injury, the presence or absence of local inflammation, impaired epithelial-mesenchymal crosstalk, and subsequent fibroblast-to-myofibroblast activation (212–214). These mechanisms are mediated by abnormally activated signaling molecules that drive the process of fibrosis, such as TGF-β, Wnt/β-catenin, hedgehog, Notch, and fibroblast growth factor signaling pathways, with the TGF-β signaling pathway being the most critical (215, 216). While most of these pathways are inactive in the adult organism, they become active during tissue regeneration, and the chronic pathological activation of these signaling pathways is associated with injury restoration processes in all organs, including the lungs (210, 217, 218). Furthermore, a recent study demonstrated that nintedanib, one of the FDA-approved anti-fibrotic drugs, modulates TGF-β, VEGF, and Wnt/β-catenin signaling pathways, further supporting the central role of these pathways in PF development (219) (Figure 3).

4.4.1 TGF-β pathway

4.4.1.1 TGF-β biology

TGF-β is a member of a large polypeptide family, modulating several biological processes, including proliferation, differentiation, and cell apoptosis in internal organs (219). Initially isolated from platelets, TGF-β is a multifunctional cytokine that plays a crucial role in regulating fibrosis both at physiological and pathological levels (220, 221). The TGF-β signaling pathway is activated during the development of fibrosis in different tissues and regardless of the underlying cause. It leads to increased *de novo* synthesis of TGF-β by multiple cell types, including macrophages, platelets, and T-cells, as well as increased release from the extracellular matrix (222–225). Among the three identified members of the TGF-β family in mammals (TGF-β1, TGF-β2, and TGF-β3), TGF-β1 is the predominant form expressed in the immune system, and it is the most abundant subtype in most tissues, including the skin. TGF-β1 is a pro-fibrotic cytokine and a key initiator of organ inflammation and fibrosis (226–228). It can induce the differentiation of epithelial or endothelial cells into myofibroblasts *in vitro* (229–231).

4.4.1.2 TGF-β/Smad pathway

The TGF-β/Smad pathway is the primary signaling cascade through which the TGF-β signal is transduced into various cellular responses. Smad proteins, a family of cytoplasmic signal transduction proteins, mediate the signals from activated TGF-β receptors and interact with TGF-β responsive promoters. Smad2 and Smad3 are the key mediators of signals from activated TGF-β

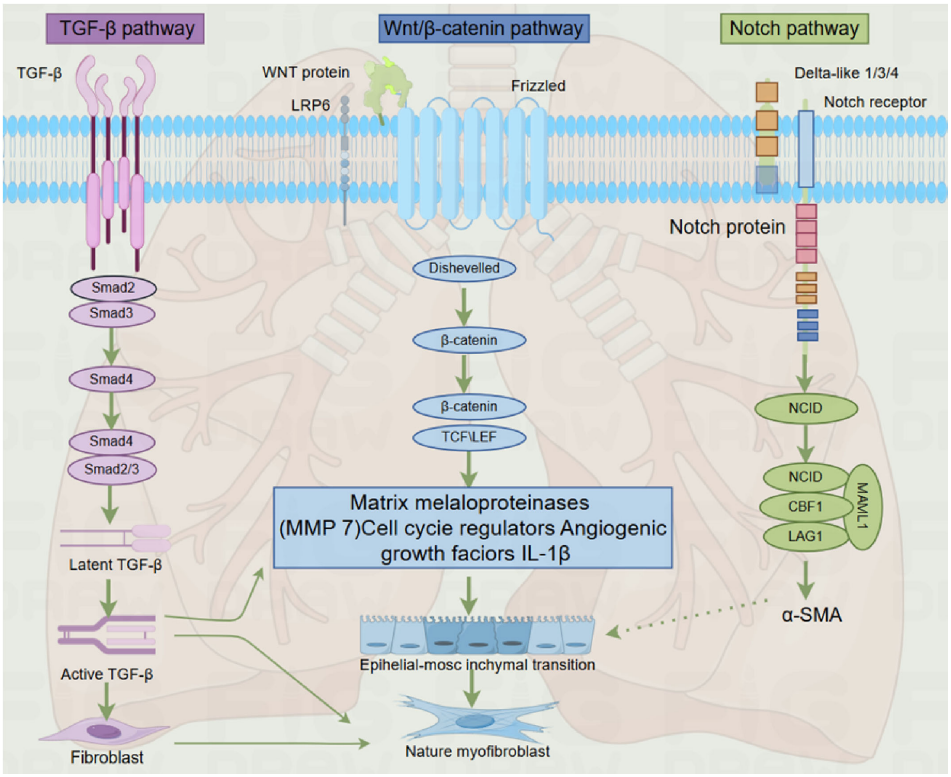

FIGURE 3
Overview of particular signaling pathways regulating pulmonary fibrosis development.

receptors, and they form complexes with other transcription factors to bind to DNA and regulate gene expression (232). Classical TGF-β1 signal transduction operates through TGF-β receptors and Smad2/3/4 transcription factors (230). In the tissue fibrosis models, the protective effects observed in Smad3 gene knockout mice indicate that TGF-β/Smad3 signaling is pro-fibrotic, while conditional Smad2 deficiency promotes fibrosis, indicating the opposite effects of Smad2 and Smad3 (233–235). It has been demonstrated that Smad3 is a key signaling pathway for fibrosis both *in vivo* and *in vitro* (131, 236, 237). The key role of Smad3 in the development of fibrosis has also been reported in many disease models, including bleomycin-induced PF (234). The TGF-β signaling cascade involves the binding of TGF-β to its receptors (TGF-βRII and TGF-βRI), leading to the activation of Smad2 and Smad3, their translocation into the nucleus, and the transcription of target genes (238).

4.4.1.3 Pathogenic effect of TGF-β in fibrosis

Macrophages are the primary source of the main effector molecule TGF-β in fibrosis. TGF-β is the primary effector molecule in fibrosis, promoting the proliferation of fibroblasts and collagen synthesis by producing growth factors, thereby promoting fibrosis (239). It accelerates the progression of PF by recruiting and activating monocytes and fibroblasts and inducing ECM production at the site of injury (240). Macrophages are one of the most important regulators of the fibrotic response, secreting cytokines, growth factors, and ECM-regulating proteins (43). They promote PF by releasing pro-fibrotic mediators (such as TGF-β), chemokines, and matrix metalloproteinases. TGF-β stimulates lung fibroblasts, circulating fibroblasts, and small airway epithelial cells to transdifferentiate into myofibroblasts (199).

TGF-β promotes fibrosis through various mechanisms, including the induction of myofibroblasts, increased synthesis of ECM components, and inhibition of collagen degradation (241). It plays a central role in the pathogenesis of PF by promoting the activation, proliferation, and differentiation of epithelial cells and collagen-producing myofibroblasts (242). TGF-β signaling is one of the most potent inducers of fibroblast activation, stimulating the synthesis of ECM components and inhibiting their degradation by matrix metalloproteinases (243, 244). It also regulates the differentiation of fibroblasts into myofibroblasts (245). TGF-β1, β2, and β3 are all involved in embryonic lung development, the maintenance of organ homeostasis, and responses to tissue damage. Increasing evidence suggests that the TGF-β pathway is activated in chronic lung diseases, including IPF (246). IPF and interstitial PF are particularly serious lung diseases, with TGF-β signaling pathway playing a significant role in fibrosis (247, 248).

4.4.2 Wnt/β- catenin signaling pathway

The Wnt gene family consists of 19 secreted glycoproteins and is involved in the regulation of mammalian embryonic development and tissue regeneration, making up the Wnt signaling pathway (249). Classical Wnt signal transduction inhibits the phosphorylation of β -catenin in the cytoplasm and subsequent

translocation into the nucleus and activation of the transcription factor TCF/LEF (250). The Wnt signaling pathway plays a vital role in the development and maintenance of multiple organ systems, including the brain, intestine, hematopoietic system, skin, and lung (251–253). Increasing evidence shows that the Wnt family of secreted glycoproteins and their associated signaling pathways are involved in the development and play an active role in wound repair and regeneration events, including PF, cancer, heart valve formation, and aortic valve calcification (217, 254–257).

Classical Wnt signal transduction regulates the expression of multiple gene families, including MMPs and angiogenic growth factors, which play a role in PF development (258, 259). Activation of the classical Wnt pathway is a common feature observed in fibrotic disorders, occurring in systemic fibrotic conditions like SSc and isolated organ fibrosis in the lung, kidney, or liver (19, 260–265). The data suggest that inhibition of the classical Wnt pathway may be an effective way to target TGF-β signaling in fibrotic diseases (266). Several Wnt genes, including Wnt2, Wnt5a, Wnt7b, Wnt11, and Wnt13, are expressed in developing and adult lungs (251). In the adult lung, the Wnt pathway maintains balance by regulating stem and precursor cells in both healthy conditions and during the response to injury (267).

Wnt/β-catenin signal transduction induces an anti-apoptotic and pro-fibrotic phenotype in lung fibroblasts, leading to fibroblast proliferation and differentiation into myofibroblasts, exacerbating lung tissue fibrosis (268). Activation of AEC II by Wnt/β-catenin increases the production of IL-1β, stimulating inflammatory and pro-fibrotic responses (269). Atypical activation of Wnt also stimulates fibroblast proliferation and increases the synthesis of ECM components (270). In adult lungs, the Wnt pathway maintains homeostasis by regulating stem and precursor cells, both in healthy conditions and during response to injury (267, 271). Additionally, Wnt signaling is involved in epithelial cell proliferation, EMT, myofibroblast differentiation, and collagen synthesis (217). In the epithelial cells of the lungs, Wnt stimulates the production of surfactant and AEC II into AEC I differentiation (272). In contrast, in lung fibroblasts, Wnt increases proliferation and fibronectin expression and inhibits apoptosis (270). Recent studies have also demonstrated the activation of Wnt signaling in IPF, suggesting that this pathway plays a role in the pathogenesis of human PF (19, 217). Inhibition of Wnt/β-catenin signaling leads to the neutralizing of bleomycin-induced PF (273). The Wnt pathway takes part in PF pathogenesis through multiple mechanisms, including: (1) Wnt/β-catenin signaling pathway induces the anti-apoptotic and pro-fibrotic phenotype in lung fibroblasts, leading to fibroblast proliferation and their differentiation into myofibroblasts, exacerbating lung tissue fibrosis (268). (2) Activation of AEC II by Wnt/β-catenin increases IL-1β production, stimulating inflammatory and pro-fibrotic responses (269). (3) Atypical activation of Wnt also stimulates fibroblast proliferation and increases the synthesis of ECM components (270).

Additionally, cooperative signaling pathways of Wnt/β-catenin and TGF-β play an essential role in the development of PF: TGF-β was shown to induce EMT synergistically with Wnt/β-catenin (274). These findings suggest that targeting the interplay between TGF-β and Wnt/β-catenin may be a promising therapeutic approach for PF. By inhibiting or modulating the cross-talks between these pathways, it may be possible to intervene in the pathogenesis of PF and potentially mitigate its progression.

4.4.3 Notch signaling pathway

The Notch signaling pathway is composed of four members in mammalian cells (275). With the exception of Notch4, all genes have been shown to regulate myofibroblast differentiation (276–279). Notch1 and Notch3 are known to stimulate lung fibroblasts (280). Moreover, Notch2 inhibit TGF-β induced α-SMA and collagen I gene expression by down-regulating Notch3 in myoblasts in hepatic stellate cells (278, 281), while in alveolar epithelial cells, Notch1 induces phosphorylation of Smad3 and activates α-SMA gene transcription in a manner dependent on SRF binding sites and TGF-β control elements (282). Other experiments have also shown that Notch1 inhibits fibroblast proliferation dependent on Wnt11-dependent WISP-1 expression (283). Notch signal transduction in fibrosis (including scleroderma (284)), may be due to the activation of this signaling pathway for myofibroblast differentiation, including through EMT)and endothelial-mesenchymal transformation.

The Notch signaling pathway is highly conserved and plays a crucial role in embryonic development and the homeostasis of various organs, including the lungs (285). It functions through paracrine signaling and one-way transmembrane receptors, regulating cell development during organogenesis. In adult lungs, along with other signaling pathways, the Notch pathway regulates stem cell functions and wound healing (285, 286). Enhanced Notch signaling has been observed during the development of PF (287), and the suppression of JAG1, Notch1, NICD, and Hes-1 has been shown to mitigate bleomycin-induced PF (288).

4.5 Effects of MMT on PF

MMT has been shown to contribute to interstitial fibrosis in patients with chronic renal allograft injury, a mouse model of unilateral ureteral obstruction (UUO), and progressive chronic kidney disease (1). Macrophages expressing CD68+ and α-SMA+ markers play a significant role in collagen production, particularly collagen I, and are associated with lung injury and interstitial fibrosis (12, 196, 289). MMT cells with M2 phenotype have been found to contribute to PF in animal models, including the lungs of rats with unilateral ureteral obstruction (UUO) (1, 196, 289). Eplerenone reduced the accumulation of MMT cells in the lung. In UUO rat lung fibrosis, UUO-induced lung injury, and fibrosis, MMT cells were found to account for the myofibroblast group, confirming that MMT plays a role in PF. These MMT cells in the lung exhibited an apparent M2 phenotype, indicating that the MMT process may be an important pathway leading to PF (12).

MMT plays a crucial role in the progression of chronic inflammation to pathological fibrosis, and the severity of interstitial fibrosis is closely related to the number of MMT cells (1, 51, 196, 289). MMT contributes to an increase in the population of myofibroblasts in the lungs, which have a strong proliferative capacity and further promote the proliferation of fibroblasts. Myofibroblasts, a subset of

activated fibroblasts, are primarily responsible for organ deformation by inducing the deposition of fibrous collagen during tissue fibrosis (290). Upon transdifferentiation, myofibroblasts secrete various components of the extracellular matrix, including collagen, leading to excessive deposition of extracellular matrix in the lungs, a key pathological characteristic of PF. This excessive deposition disrupts the normal alveolar structure, resulting in alveolar collapse and reduced lung function.

The pro-fibrotic cytokine TGF-β1 is an essential initiator of organ inflammation and fibrosis by activating the downstream Smad signaling cascade, especially the Smad3 signaling cascade (6). Smad3 is a crucial transcription factor for classical TGF-β1 signal transduction (234, 291). The inhibition of MMT by targeting cytokines such as TGF-β1 or blocking the Smad3 signal pathway can slow down the process of PF. Moreover, the non-receptor tyrosine kinase Src, which can be activated by TGF-β1, has been closely associated with tissue fibrosis. Inhibition of Src has been shown to block MMT in animal models and reduce the severity of PF induced by bleomycin (292–294). However, further research is needed to fully understand the role of MMT in Src-mediated PF and explore the potential of Src-targeted therapy for blocking MMT and treating PF.

In summary, MMT plays an essential role in the process of PF, which accelerates the process of PF by promoting the transdifferentiation of macrophages into myofibroblasts. Inhibiting the MMT process represents a potential therapeutic target for anti-fibrotic treatment. Future studies should focus on elucidating the regulatory mechanisms of MMT and its specific role in PF to provide novel insights and treatment strategies for PF. A comprehensive treatment approach considering various factors, including inflammation control, inhibition of the fibrotic process, and improvement of lung function, is essential for effectively managing PF.

4.6 Effects of MMT on lung cancer

Lung cancer is the leading cause of death worldwide. For decades, it has remained the second most common cancer and the leading cause of cancer deaths, accounting for about 11.4% of new cancer cases and 18% of cancer deaths globally in 2020. Cancer-associated fibroblasts (CAFs) are essential in tumor microenvironment (TME) driven cancer progression. CAFs are the most prominent stromal components (295). CAFs, a subtype of myofibroblasts, contribute to the malignancy and advancement of cancer (296). Cancer cells possess heterogeneity, versatility, and adaptability, resulting in primary and secondary drug resistance (297). The degree of macrophage-myofibroblast transition (MMT) has been found to be closely associated with the prognosis of certain cancers (297). MMT is an essential source of CAFs in non-small cell lung cancer (NSCLC). The hematopoietic transcription factor Runx1 has been identified as a critical regulator of MMT in cancer patients. Inhibition of Runx1, macrophage-specific and systemic, effectively blocks MMT-driven tumor formation *in vivo*, making it a potential therapeutic target for eliminating pro-tumor CAFs in patients with NSCLC (298).

Myofibroblasts can secrete various growth factors and cytokines, such as TGF-β and PDGF, which can stimulate the proliferation and migration of tumor cells and promote the progress of cancer. The TGF-β/Smad3 signal pathway is a critical regulatory factor promoting tumor microenvironment (299–301). It is essential to initiate MMT in chronic inflammatory diseases, including cancer. The MMT process and tumor growth in lung cancer are tightly regulated by Smad3 (302). TGF-β/Smad3 signal transduction is a key regulatory factor in the tumorigenic microenvironment. Recent evidence indicates that TGF-β can trigger the M1/M2 polarization of TAMs by activating Smad2/3 and PI3K/AKT pathways, thus enhancing the transcription of tumorigenic effectors such as IL-10, VEGFA, and CXCR4 (303). However, targeting Smad3 also inhibits T cell anti-cancer immunity, highlighting the complexity of potential therapeutic strategies (5, 207, 293, 304).

MMT is a critical pathophysiological process within the tumor microenvironment, leading to the generation of myofibroblasts that secrete inflammatory factors and fibrosis-related proteins in tumor tissues, promoting inflammation and fibrosis changes in the tumor microenvironment (305). Co-expression of TAM markers (CD68) and CAF markers (α-SMA) has been observed in lung, renal, and prostate cancers, indicating the presence of MMT in these types of cancer (1, 2, 196, 301). An interesting phenomenon in MMT is the further differentiation of TAMs into CAFs. Silencing Smad3 specifically in macrophages effectively inhibits MMT and consequently impedes CAF-mediated cancer progression. These findings highlight the significance of macrophage Smad3 in regulating CAFs through MMT, providing a specific therapeutic target for cancer immunotherapy (5). Given the critical role of MMT in cancer progression, inhibiting MMT may become a new target for cancer treatment. By blocking the process of MMT, the support of the tumor microenvironment can be weakened, the proliferation and migration of cancer cells can be inhibited, and the prognosis of cancer can be improved. Therefore, it is significant to study the mechanism and intervention strategy of MMT for developing new cancer treatment methods and improving cancer prognosis.

5 Summary and prospect

Organ fibrosis is a common pathway by which various chronic diseases progress to an end-stage state. The conversion of MMT is a process where bone marrow-derived macrophages differentiate into myofibroblasts, promoting organ fibrosis during injury. This paper reviews the origin, distribution, and characteristics of macrophages and myofibroblasts in organ fibrosis, along with their pathological effects on diseases caused by organ fibrosis. The purpose is to further understand MMT and its signaling pathway and to determine a new target for organ fibrosis treatment.

Current research on MMT primarily focuses on renal fibrosis, with limited studies on fibrotic diseases in other organs. The mechanisms and influencing factors of the conversion of MMT still require deeper exploration. Under specific conditions, MMT provides new ideas and possibilities for treating kidney, lung, and

liver diseases. Future studies need to focus on the crucial role of the TGF-β/Smad3 signaling pathway in the progression of MMT and organ fibrosis. Targeting the TGF-β/Smad3 signaling pathway for MMT treatment is expected to become a viable strategy for the prevention and treatment of progressive fibrosis.

The discovery of the MMT process also provides a new direction for studying the possible mechanisms by which macrophages promote fibrosis and offers a basis for intervening in myofibroblast activity through multiple pathways. MMT not only serves as a new therapeutic target for the prevention of fibrotic diseases but also acts as a key checkpoint for the development of chronic inflammation into pathogenic fibrosis. Understanding and elucidating the phenomenon of MMT and its potential signaling pathways will aid in identifying therapeutic targets for fibrosis.

Author contributions

XL: Writing – original draft. YL: Resources, Writing – original draft. YT: Writing – original draft. ZX: Investigation, Resources, Writing – review & editing.

Funding

The author(s) declare that no financial support was received for the research, authorship, and/or publication of this article.

Conflict of interest

The authors declare that the research was conducted in the absence of any commercial or financial relationships that could be construed as a potential conflict of interest.

Publisher's note

References

1. Wang YY, Jiang H, Pan J, Huang XR, Wang YC, Huang HF, et al. Macrophage-to-myofibroblast transition contributes to interstitial fibrosis in chronic renal allograft injury. *J Am Soc Nephrol*. (2017) 28:2053–67. doi: 10.1681/asn.2016050573

2. Haider N, Boscá L, Zandbergen HR, Kovacic JC, Narula N, González-Ramos S, et al. Transition of macrophages to fibroblast-like cells in healing myocardial infarction. *J Am Coll Cardiol*. (2019) 74:3124–35. doi: 10.1016/j.jacc.2019.10.036

3. Torres Á, Muñoz K, Nahuelpán Y, AP RS, Mendoza P, Jara C, et al. Intraglomerular monocyte/macrophage infiltration and macrophage-myofibroblast transition during diabetic nephropathy is regulated by the A(2B) adenosine receptor. *Cells*. (2020) 9:1051. doi: 10.3390/cells9041051

4. Xiong Y, Chang Y, Hao J, Zhang C, Yang F, Wang Z, et al. Eplerenone attenuates fibrosis in the contralateral kidney of UUO rats by preventing macrophage-to-myofibroblast transition. *Front Pharmacol*. (2021) 12:620433. doi: 10.3389/fphar.2021.620433

5. Tang PC, Chung JY, Xue VW, Xiao J, Meng XM, Huang XR, et al. Smad3 promotes cancer-associated fibroblasts generation via macrophage-myofibroblast transition. *Adv Sci (Weinh)*. (2022) 9:e2101235. doi: 10.1002/advs.202101235

6. Wang S, Meng XM, Ng YY, Ma FY, Zhou S, Zhang Y, et al. TGF-β/Smad3 signalling regulates the transition of bone marrow-derived macrophages into myofibroblasts during tissue fibrosis. *Oncotarget*. (2016) 7:8809–22. doi: 10.18632/oncotarget.6604

7. Klingberg F, Hinz B, White ES. The myofibroblast matrix: implications for tissue repair and fibrosis. *J Pathol*. (2013) 229:298–309. doi: 10.1002/path.4104

8. Hams E, Bermingham R, Fallon PG. Macrophage and innate lymphoid cell interplay in the genesis of fibrosis. *Front Immunol*. (2015) 6:597. doi: 10.3389/fimmu.2015.00597

9. Kryczka J, Boncela J. Leukocytes: the double-edged sword in fibrosis. *Mediators Inflamm*. (2015) 2015:652035. doi: 10.1155/2015/652035

10. Kurose H, Mangmool S. Myofibroblasts and inflammatory cells as players of cardiac fibrosis. *Arch Pharm Res*. (2016) 39:1100–13. doi: 10.1007/s12272-016-0809-6

11. Wynn TA, Barron L. Macrophages: master regulators of inflammation and fibrosis. *Semin Liver Dis*. (2010) 30:245–57. doi: 10.1055/s-0030-1255354

12. Yang F, Chang Y, Zhang C, Xiong Y, Wang X, Ma X, et al. UUO induces lung fibrosis with macrophage-myofibroblast transition in rats. *Int Immunopharmacol*. (2021) 93:107396. doi: 10.1016/j.intimp.2021.107396

13. Vierhout M, Ayoub A, Naiel S, Yazdanshenas P, Revill SD, Reihani A, et al. Monocyte and macrophage derived myofibroblasts: Is it fate? A review of the current evidence. *Wound Repair Regen*. (2021) 29:548–62. doi: 10.1111/wrr.12946

14. Little K, Llorián-Salvador M, Tang M, Du X, Marry S, Chen M, et al. Macrophage to myofibroblast transition contributes to subretinal fibrosis secondary to neovascular age-related macular degeneration. *J Neuroinflammation*. (2020) 17:355. doi: 10.1186/s12974-020-02033-7

15. Meng XM, Mak TS, Lan HY. Macrophages in renal fibrosis. *Adv Exp Med Biol*. (2019) 1165:285–303. doi: 10.1007/978-981-13-8871-2_13

16. Cheng P, Li S, Chen H. Macrophages in lung injury, repair, and fibrosis. *Cells*. (2021) 10:436. doi: 10.3390/cells10020436

17. Wang X, Chen J, Xu J, Xie J, Harris DCH, Zheng G. The role of macrophages in kidney fibrosis. *Front Physiol*. (2021) 12:705838. doi: 10.3389/fphys.2021.705838

18. Braga TT, Agudelo JS, Camara NO. Macrophages during the fibrotic process: M2 as friend and foe. *Front Immunol*. (2015) 6:602. doi: 10.3389/fimmu.2015.00602

19. Chilosi M, Poletti V, Zamò A, Lestani M, Montagna L, Piccoli P, et al. Aberrant Wnt/beta-catenin pathway activation in idiopathic pulmonary fibrosis. *Am J Pathol*. (2003) 162:1495–502. doi: 10.1016/s0002-9440(10)64282-4

20. Gordon S. Elie Metchnikoff: father of natural immunity. *Eur J Immunol*. (2008) 38:3257–64. doi: 10.1002/eji.200838855

21. Normann SJ. Function of the reticuloendothelial system IV. Evidence for two types of particle-induced reticuloendothelial paralysis. *Infect Immun*. (1970) 1:327–33. doi: 10.1128/iai.1.4.327-333.1970

22. van Furth R, Cohn ZA, Hirsch JG, Humphrey JH, Spector WG, Langevoort HL. The mononuclear phagocyte system: a new classification of macrophages, monocytes, and their precursor cells. *Bull World Health Organ*. (1972) 46:845–52.

23. Carrel A, Ebeling AH. THE FUNDAMENTAL PROPERTIES OF THE FIBROBLAST AND THE MACROPHAGE: I. THE FIBROBLAST. *J Exp Med*. (1926) 44:261–84. doi: 10.1084/jem.44.2.261

24. Marchesi VT, Florey HW. Electron micrographic observations on the emigration of leucocytes. *Q J Exp Physiol Cognit Med Sci*. (1960) 45:343–8. doi: 10.1113/expphysiol.1960.sp001489

25. Volkman A, Gowans JL. THE ORIGIN OF MACROPHAGES FROM BONE MARROW IN THE RAT. *Br J Exp Pathol*. (1965) 46:62–70.

26. Yona S, Kim KW, Wolf Y, Mildner A, Varol D, Breker M, et al. Fate mapping reveals origins and dynamics of monocytes and tissue macrophages under homeostasis. *Immunity*. (2013) 38:79–91. doi: 10.1016/j.immuni.2012.12.001

27. Ginhoux F, Guilliams M. Tissue-resident macrophage ontogeny and homeostasis. *Immunity*. (2016) 44:43949. doi: 10.1016/j.immuni.2016.02.024

28. Viehmann SF, Böhner AMC, Kurts C, Brähler S. The multifaceted role of the renal mononuclear phagocyte system. *Cell Immunol*. (2018) 330:97–104. doi: 10.1016/j.cellimm.2018.04.009

29. Murray PJ, Wynn TA. Protective and pathogenic functions of macrophage subsets. *Nat Rev Immunol*. (2011) 11:723–37. doi: 10.1038/nri3073

30. Gordon S, Taylor PR. Monocyte and macrophage heterogeneity. *Nat Rev Immunol*. (2005) 5:953–64. doi: 10.1038/nri1733

31. Geissmann F, Gordon S, Hume DA, Mowat AM, Randolph GJ. Unravelling mononuclear phagocyte heterogeneity. *Nat Rev Immunol*. (2010) 10:453–60. doi: 10.1038/nri2784

32. Mosser DM, Edwards JP. Exploring the full spectrum of macrophage activation. *Nat Rev Immunol*. (2008) 8:958–69. doi: 10.1038/nri2448

33. Sutterwala FS, Noel GJ, Clynes R, Mosser DM. Selective suppression of interleukin-12 induction after macrophage receptor ligation. *J Exp Med*. (1997) 185:1977–85. doi: 10.1084/jem.185.11.1977

34. Sutterwala FS, Noel GJ, Salgame P, Mosser DM. Reversal of proinflammatory responses by ligating the macrophage Fcgamma receptor type I. *J Exp Med*. (1998) 188:217–22. doi: 10.1084/jem.188.1.217

35. Laskin DL, Weinberger B, Laskin JD. Functional heterogeneity in liver and lung macrophages. *J Leukoc Biol*. (2001) 70:163–70. doi: 10.1189/jlb.70.2.163

36. Guillemin GJ, Brew BJ. Microglia, macrophages, perivascular macrophages, and pericytes: a review of function and identification. *J Leukoc Biol*. (2004) 75:388–97. doi: 10.1189/jlb.0303114

37. Gautier EL, Shay T, Miller J, Greter M, Jakubzick C, Ivanov S, et al. Gene-expression profiles and transcriptional regulatory pathways that underlie the identity and diversity of mouse tissue macrophages. *Nat Immunol*. (2012) 13:1118–28. doi: 10.1038/ni.2419

38. Wang W, Liang M, Wang L, Bei W, Rong X, Xu J, et al. Role of prostaglandin E2 in macrophage polarization: Insights into atherosclerosis. *Biochem Pharmacol*. (2023) 207:115357. doi: 10.1016/j.bcp.2022.115357

39. Murray PJ. Macrophage polarization. *Annu Rev Physiol*. (2017) 79:541–66. doi: 10.1146/annurev-physiol-022516-034339

40. Martinez FO, Sica A, Mantovani A, Locati M. Macrophage activation and polarization. *Front Biosci*. (2008) 13:453–61. doi: 10.2741/2692

41. Mantovani A, Sica A, Sozzani S, Allavena P, Vecchi A, Locati M. The chemokine system in diverse forms of macrophage activation and polarization. *Trends Immunol*. (2004) 25:677–86. doi: 10.1016/j.it.2004.09.015

42. Gieseck RL 3rd, Wilson MS, Wynn TA. Type 2 immunity in tissue repair and fibrosis. *Nat Rev Immunol*. (2018) 18:62–76. doi: 10.1038/nri.2017.90

43. Wynn TA, Vannella KM. Macrophages in tissue repair, regeneration, and fibrosis. *Immunity*. (2016) 44:450–62. doi: 10.1016/j.immuni.2016.02.015

44. Smigiel KS, Parks WC. Macrophages, wound healing, and fibrosis: recent insights. *Curr Rheumatol Rep*. (2018) 20:17. doi: 10.1007/s11926-018-0725-5

45. Murray PJ, Allen JE, Biswas SK, Fisher EA, Gilroy DW, Goerdt S, et al. Macrophage activation and polarization: nomenclature and experimental guidelines. *Immunity*. (2014) 41:14–20. doi: 10.1016/j.immuni.2014.06.008

46. Abu El-Asrar AM, De Hertogh G, Allegaert E, Nawaz MI, Abouelasrar Salama S, Gikandi PW, et al. Macrophage-myofibroblast transition contributes to myofibroblast formation in proliferative vitreoretinal disorders. *Int J Mol Sci*. (2023) 24:13510. doi: 10.3390/ijms241713510

47. Wang Y, Zhang L, Wu GR, Zhou Q, Yue H, Rao LZ, et al. MBD2 serves as a viable target against pulmonary fibrosis by inhibiting macrophage M2 program. *Sci Adv*. (2021) 7:6075. doi: 10.1126/sciadv.abb6075

48. Chen B, Yang Y, Yang C, Duan J, Chen L, Lu K, et al. M2 macrophage accumulation contributes to pulmonary fibrosis, vascular dilatation, and hypoxemia in rat hepatopulmonary syndrome. *J Cell Physiol*. (2021) 236:7682–97. doi: 10.1002/jcp.30420

49. Wang J, Xu L, Xiang Z, Ren Y, Zheng X, Zhao Q, et al. Microcystin-LR ameliorates pulmonary fibrosis via modulating CD206(+) M2-like macrophage polarization. *Cell Death Dis*. (2020) 11:136. doi: 10.1038/s41419-020-2329-z

50. Yang G, Yang Y, Liu Y, Liu X. Regulation of alveolar macrophage death in pulmonary fibrosis: a review. *Apoptosis*. (2023) 28:1505–19. doi: 10.1007/s10495-023-01888-4

51. Tang PM, Nikolic-Paterson DJ, Lan HY. Macrophages: versatile players in renal inflammation and fibrosis. *Nat Rev Nephrol*. (2019) 15:144–58. doi: 10.1038/s41581-019-0110-2

52. Kim MG, Kim SC, Ko YS, Lee HY, Jo SK, Cho W. The role of M2 macrophages in the progression of chronic kidney disease following acute kidney injury. *PloS One*. (2015) 10:e0143961. doi: 10.1371/journal.pone.0143961

53. Peet C, Ivetic A, Bromage DI, Shah AM. Cardiac monocytes and macrophages after myocardial infarction. *Cardiovasc Res*. (2020) 116:1101–12. doi: 10.1093/cvr/cvz336

54. Kim Y, Nurakhayev S, Nurkesh A, Zharkinbekov Z, Saparov A. Macrophage polarization in cardiac tissue repair following myocardial infarction. *Int J Mol Sci*. (2021) 22:2715. doi: 10.3390/ijms22052715

55. Cao X, Shen D, Patel MM, Tuo J, Johnson TM, Olsen TW, et al. Macrophage polarization in the maculae of age-related macular degeneration: a pilot study. *Pathol Int*. (2011) 61:528–35. doi: 10.1111/j.1440-1827.2011.02695.x

56. Biswas SK, Mantovani A. Macrophage plasticity and interaction with lymphocyte subsets: cancer as a paradigm. *Nat Immunol*. (2010) 11:889–96. doi: 10.1038/ni.1937

57. Mantovani A, Sozzani S, Locati M, Allavena P, Sica A. Macrophage polarization: tumor-associated macrophages as a paradigm for polarized M2 mononuclear phagocytes. *Trends Immunol*. (2002) 23:549–55. doi: 10.1016/s1471-4906(02)02302-5

58. O'Shea JJ, Murray PJ. Cytokine signaling modules in inflammatory responses. *Immunity*. (2008) 28:477–87. doi: 10.1016/j.immuni.2008.03.002

59. Sindrilaru A, Peters T, Wieschalka S, Baican C, Baican A, Peter H, et al. An unrestrained proinflammatory M1 macrophage population induced by iron impairs wound healing in humans and mice. *J Clin Invest*. (2011) 121:985–97. doi: 10.1172/jci44490

60. Sica A, Mantovani A. Macrophage plasticity and polarization: in *vivo* veritas. *J Clin Invest*. (2012) 122:787–95. doi: 10.1172/jci59643

61. Langrish CL, Chen Y, Blumenschein WM, Mattson J, Basham B, Sedgwick JD, et al. IL-23 drives a pathogenic T cell population that induces autoimmune inflammation. *J Exp Med*. (2005) 201:233–40. doi: 10.1084/jem.20041257

62. Fadok VA, Bratton DL, Konowal A, Freed PW, Westcott JY, Henson PM. Macrophages that have ingested apoptotic cells in *vitro* inhibit proinflammatory cytokine production through autocrine/paracrine mechanisms involving TGF-beta, PGE2, and PAF. *J Clin Invest*. (1998) 101:890–8. doi: 10.1172/jci1112

63. Nathan C. Metchnikoff's legacy in 2008. *Nat Immunol*. (2008) 9:695–8. doi: 10.1038/ni0708-695

64. Dale DC, Boxer L, Liles WC. The phagocytes: neutrophils and monocytes. *Blood*. (2008) 112:935–45. doi: 10.1182/blood-2007-12-077917

65. Ricardo SD, van Goor H, Eddy AA. Macrophage diversity in renal injury and repair. *J Clin Invest*. (2008) 118:3522–30. doi: 10.1172/jci36150

66. Kim SY, Nair MG. Macrophages in wound healing: activation and plasticity. *Immunol Cell Biol*. (2019) 97:258–67. doi: 10.1111/imcb.12236

67. Brandt E, Woerly G, Younes AB, Loiseau S, Capron M. IL-4 production by human polymorphonuclear neutrophils. *J Leukoc Biol*. (2000) 68:125–30. doi: 10.1189/jlb.68.1.125

68. Kreider T, Anthony RM, Urban JF Jr., Gause WC. Alternatively activated macrophages in helminth infections. *Curr Opin Immunol*. (2007) 19:448–53. doi: 10.1016/j.coi.2007.07.002

69. Saraiva M, O'Garra A. The regulation of IL-10 production by immune cells. *Nat Rev Immunol*. (2010) 10:170–81. doi: 10.1038/nri2711

70. Iannacone M, Moseman EA, Tonti E, Bosurgi L, Junt T, Henrickson SE, et al. Subcapsular sinus macrophages prevent CNS invasion on peripheral infection with a neurotropic virus. *Nature*. (2010) 465:1079–83. doi: 10.1038/nature09118

71. Bonner JC, Osornio-Vargas AR, Badgett A, Brody AR. Differential proliferation of rat lung fibroblasts induced by the platelet-derived growth factor-AA, -AB, and -BB isoforms secreted by rat alveolar macrophages. *Am J Respir Cell Mol Biol*. (1991) 5:539–47. doi: 10.1165/ajrcmb/5.6.539

72. Edwards JP, Zhang X, Frauwirth KA, Mosser DM. Biochemical and functional characterization of three activated macrophage populations. *J Leukoc Biol*. (2006) 80:1298–307. doi: 10.1189/jlb.0406249

73. Chávez-Galán L, Olleros ML, Vesin D, Garcia I. Much More than M1 and M2 Macrophages, There are also CD169(+) and TCR(+) Macrophages. *Front Immunol*. (2015) 6:263. doi: 10.3389/fimmu.2015.00263

74. Gordon S. Alternative activation of macrophages. *Nat Rev Immunol*. (2003) 3:23–35. doi: 10.1038/nri978

75. Balkwill F, Charles KA, Mantovani A. Smoldering and polarized inflammation in the initiation and promotion of Malignant disease. *Cancer Cell*. (2005) 7:211–7. doi: 10.1016/j.ccr.2005.02.013

76. Fleming BD, Mosser DM. Regulatory macrophages: setting the threshold for therapy. *Eur J Immunol*. (2011) 41:2498–502. doi: 10.1002/eji.201141717

77. Komohara Y, Jinushi M, Takeya M. Clinical significance of macrophage heterogeneity in human Malignant tumors. *Cancer Sci*. (2014) 105:1–8. doi: 10.1111/cas.12314

78. Tagliabue A, Mantovani A, Kilgallen M, Herberman RB, McCoy JL. Natural cytotoxicity of mouse monocytes and macrophages. *J Immunol*. (1979) 122:2363–70. doi: 10.4049/jimmunol.122.6.2363

79. Hou X, Chen G, Zhao Y. Research progress on CD169-positive macrophages in tumors. *Am J Transl Res*. (2021) 13:8589–97.

80. Puellmann K, Kaminski WE, Vogel M, Nebe CT, Schroeder J, Wolf H, et al. A variable immunoreceptor in a subpopulation of human neutrophils. *Proc Natl Acad Sci U S A*. (2006) 103:14441–6. doi: 10.1073/pnas.0603406103

81. Beham AW, Puellmann K, Laird R, Fuchs T, Streich R, Breysach C, et al. A TNF-regulated recombinatorial macrophage immune receptor implicated in granuloma formation in tuberculosis. *PloS Pathog*. (2011) 7:e1002375. doi: 10.1371/journal.ppat.1002375

82. Fuchs T, Puellmann K, Emmert A, Fleig J, Oniga S, Laird R, et al. The macrophage-TCRαβ is a cholesterol-responsive combinatorial immune receptor and implicated in atherosclerosis. *Biochem Biophys Res Commun*. (2015) 456:59–65. doi: 10.1016/j.bbrc.2014.11.034

83. Hume DA. Differentiation and heterogeneity in the mononuclear phagocyte system. *Mucosal Immunol*. (2008) 1:432–41. doi: 10.1038/mi.2008.36

84. Atabai K, Jame S, Azhar N, Kuo A, Lam M, McKleroy W, et al. Mfge8 diminishes the severity of tissue fibrosis in mice by binding and targeting collagen for uptake by macrophages. *J Clin Invest*. (2009) 119:3713–22. doi: 10.1172/jci40053

85. Di Gioia M, Spreafico R, Springstead JR, Mendelson MM, Joehanes R, Levy D, et al. Endogenous oxidized phospholipids reprogram cellular metabolism and boost hyperinflammation. *Nat Immunol*. (2020) 21:42–53. doi: 10.1038/s41590-019-0539-2

86. Kumar V. Pulmonary innate immune response determines the outcome of inflammation during pneumonia and sepsis-associated acute lung injury. *Front Immunol*. (2020) 11:1722. doi: 10.3389/fimmu.2020.01722

87. Watkins SK, Egilmez NK, Suttles J, Stout RD. IL-12 rapidly alters the functional profile of tumor-associated and tumor-infiltrating macrophages in *vitro* and in vivo. *J Immunol*. (2007) 178:1357–62. doi: 10.4049/jimmunol.178.3.1357

88. Ley K. The second touch hypothesis: T cell activation, homing and polarization. *F1000Res*. (2014) 3:37. doi: 10.12688/f1000research.3-37.v2

89. Anderson CF, Mosser DM. A novel phenotype for an activated macrophage: the type 2 activated macrophage. *J Leukoc Biol*. (2002) 72:101–6. doi: 10.1189/jlb.72.1.101

90. Jakubzick C, Gautier EL, Gibbings SL, Sojka DK, Schlitzer A, Johnson TE, et al. Minimal differentiation of classical monocytes as they survey steady-state tissues and transport antigen to lymph nodes. *Immunity*. (2013) 39:599–610. doi: 10.1016/j.immuni.2013.08.007

91. Bataller R, Brenner DA. Liver fibrosis. *J Clin Invest*. (2005) 115:209–18. doi: 10.1172/jci24282

92. Iredale JP. Models of liver fibrosis: exploring the dynamic nature of inflammation and repair in a solid organ. *J Clin Invest*. (2007) 117:539–48. doi: 10.1172/jci30542

93. Friedman SL. Mechanisms of hepatic fibrogenesis. *Gastroenterology*. (2008) 134:1655–69. doi: 10.1053/j.gastro.2008.03.003

94. Friedman SL. Hepatic stellate cells: protean, multifunctional, and enigmatic cells of the liver. *Physiol Rev*. (2008) 88:125–72. doi: 10.1152/physrev.00013.2007

95. Wallace K, Burt AD, Wright MC. Liver fibrosis. *Biochem J*. (2008) 411:1–18. doi: 10.1042/bj20071570

96. Luckey SW, Petersen DR. Activation of Kupffer cells during the course of carbon tetrachloride-induced liver injury and fibrosis in rats. *Exp Mol Pathol*. (2001) 71:226–40. doi: 10.1006/exmp.2001.2399

97. Ramadori G, Armbrust T. Cytokines in the liver. *Eur J Gastroenterol Hepatol*. (2001) 13:777–84. doi: 10.1097/00042737-200107000-00004

98. Friedman SL, Arthur MJ. Activation of cultured rat hepatic lipocytes by Kupffer cell conditioned medium. Direct enhancement of matrix synthesis and stimulation of cell proliferation via induction of platelet-derived growth factor receptors. *J Clin Invest*. (1989) 84:1780–5. doi: 10.1172/jci114362

99. Wahl SM, McCartney-Francis N, Allen JB, Dougherty EB, Dougherty SF. Macrophage production of TGF-beta and regulation by TGF-beta. *Ann N Y Acad Sci*. (1990) 593:188–96. doi: 10.1111/j.1749-6632.1990.tb16111.x

100. Duffield JS, Forbes SJ, Constandinou CM, Clay S, Partolina M, Vuthoori S, et al. Selective depletion of macrophages reveals distinct, opposing roles during liver injury and repair. *J Clin Invest*. (2005) 115:56–65. doi: 10.1172/jci22675

101. Hinz B. The myofibroblast: paradigm for a mechanically active cell. *J Biomech*. (2010) 43:146–55. doi: 10.1016/j.jbiomech.2009.09.020

102. Tomasek JJ, Gabbiani G, Hinz B, Chaponnier C, Brown RA. Myofibroblasts and mechano-regulation of connective tissue remodelling. *Nat Rev Mol Cell Biol*. (2002) 3:349–63. doi: 10.1038/nrm809

103. Hewitson TD. Renal tubulointerstitial fibrosis: common but never simple. *Am J Physiol Renal Physiol*. (2009) 296:F1239–44. doi: 10.1152/ajprenal.90521.2008

104. Hinz B, Phan SH, Thannickal VJ, Galli A, Bochaton-Piallat ML, Gabbiani G. The myofibroblast: one function, multiple origins. *Am J Pathol*. (2007) 170:1807–16. doi: 10.2353/ajpath.2007.070112

105. Vaughan MB, Howard EW, Tomasek JJ. Transforming growth factor-beta1 promotes the morphological and functional differentiation of the myofibroblast. *Exp Cell Res*. (2000) 257:180–9. doi: 10.1006/excr.2000.4869

106. Wynn TA. Cellular and molecular mechanisms of fibrosis. *J Pathol*. (2008) 214:199–210. doi: 10.1002/path.2277

107. Hinz B, Phan SH, Thannickal VJ, Prunotto M, Desmoulière A, Varga J, et al. Recent developments in myofibroblast biology: paradigms for connective tissue remodeling. *Am J Pathol*. (2012) 180:1340–55. doi: 10.1016/j.ajpath.2012.02.004

108. Eyden B. The myofibroblast: an assessment of controversial issues and a definition useful in diagnosis and research. *Ultrastruct Pathol*. (2001) 25:39–50. doi: 10.1080/019131201300004672

109. Gabbiani G, Ryan GB, Majne G. Presence of modified fibroblasts in granulation tissue and their possible role in wound contraction. *Experientia*. (1971) 27:549–50. doi: 10.1007/bf02147594

110. Davis J, Molkentin JD. Myofibroblasts: trust your heart and let fate decide. *J Mol Cell Cardiol*. (2014) 70:9–18. doi: 10.1016/j.yjmcc.2013.10.019

111. Hinz B. Formation and function of the myofibroblast during tissue repair. *J Invest Dermatol*. (2007) 127:526–37. doi: 10.1038/sj.jid.5700613

112. Jinde K, Nikolic-Paterson DJ, Huang XR, Sakai H, Kurokawa K, Atkins RC, et al. Tubular phenotypic change in progressive tubulointerstitial fibrosis in human glomerulonephritis. *Am J Kidney Dis*. (2001) 38:761–9. doi: 10.1053/ajkd.2001.27693

113. Ng YY, Huang TP, Yang WC, Chen ZP, Yang AH, Mu W, et al. Tubular epithelial-myofibroblast transdifferentiation in progressive tubulointerstitial fibrosis in 5/6 nephrectomized rats. *Kidney Int*. (1998) 54:864–76. doi: 10.1046/j.1523-1755.1998.00076.x

114. Zeisberg EM, Tarnavski O, Zeisberg M, Dorfman AL, McMullen JR, Gustafsson E, et al. Endothelial-to-mesenchymal transition contributes to cardiac fibrosis. *Nat Med*. (2007) 13:952–61. doi: 10.1038/nm1613

115. Humphreys BD, Lin SL, Kobayashi A, Hudson TE, Nowlin BT, Bonventre JV, et al. Fate tracing reveals the pericyte and not epithelial origin of myofibroblasts in kidney fibrosis. *Am J Pathol*. (2010) 176:85–97. doi: 10.2353/ajpath.2010.090517

116. LeBleu VS, Taduri G, O'Connell J, Teng Y, Cooke VG, Woda C, et al. Origin and function of myofibroblasts in kidney fibrosis. *Nat Med*. (2013) 19:1047–53. doi: 10.1038/nm.3218

117. Hashimoto N, Jin H, Liu T, Chensue SW, Phan SH. Bone marrow-derived progenitor cells in pulmonary fibrosis. *J Clin Invest*. (2004) 113:243–52. doi: 10.1172/jci18847

118. Kisseleva T, UChinami H, Feirt N, Quintana-Bustamante O, Segovia JC, Schwabe RF, et al. Bone marrow-derived fibrocytes participate in pathogenesis of liver fibrosis. *J Hepatol*. (2006) 45:429–38. doi: 10.1016/j.jhep.2006.04.014

119. Gabbiani G. The myofibroblast in wound healing and fibrocontractive diseases. *J Pathol*. (2003) 200:500–3. doi: 10.1002/path.1427

120. Sugimoto H, Mundel TM, Kieran MW, Kalluri R. Identification of fibroblast heterogeneity in the tumor microenvironment. *Cancer Biol Ther*. (2006) 5:1640–6. doi: 10.4161/cbt.5.12.3354

121. Meran S, Steadman R. Fibroblasts and myofibroblasts in renal fibrosis. *Int J Exp Pathol*. (2011) 92:158–67. doi: 10.1111/j.1365-2613.2011.00764.x

122. Faouzi S, Le Bail B, Neaud V, Boussarie L, Saric J, Bioulac-Sage P, et al. Myofibroblasts are responsible for collagen synthesis in the stroma of human hepatocellular carcinoma: an in *vivo* and in *vitro* study. *J Hepatol*. (1999) 30:275–84. doi: 10.1016/s0168-8278(99)80074-9

123. Le Bail B, Faouzi S, Boussarie L, Guirouilh J, Blanc JF, Carles J, et al. Osteonectin/SPARC is overexpressed in human hepatocellular carcinoma. *J Pathol*. (1999) 189:46–52. doi: 10.1002/(sici)1096-9896.(199909)189:1<46::Aid-path392>3.0.Co;2-x

124. Liu Y. Cellular and molecular mechanisms of renal fibrosis. *Nat Rev Nephrol*. (2011) 7:684–96. doi: 10.1038/nrneph.2011.149

125. De Wever O, Mareel M. Role of tissue stroma in cancer cell invasion. *J Pathol*. (2003) 200:429–47. doi: 10.1002/path.1398

126. Brown RD, Ambler SK, Mitchell MD, Long CS. The cardiac fibroblast: therapeutic target in myocardial remodeling and failure. *Annu Rev Pharmacol Toxicol*. (2005) 45:657–87. doi: 10.1146/annurev.pharmtox.45.120403.095802

127. Desmoulière A, Darby IA, Gabbiani G. Normal and pathologic soft tissue remodeling: role of the myofibroblast, with special emphasis on liver and kidney fibrosis. *Lab Invest*. (2003) 83:1689–707. doi: 10.1097/01.lab.0000101911.53973.90

128. Schafer MJ, White TA, Iijima K, Haak AJ, Ligresti G, Atkinson EJ, et al. Cellular senescence mediates fibrotic pulmonary disease. *Nat Commun*. (2017) 8:14532. doi: 10.1038/ncomms14532

129. Fernandez IE, Eickelberg O. New cellular and molecular mechanisms of lung injury and fibrosis in idiopathic pulmonary fibrosis. *Lancet*. (2012) 380:680–8. doi: 10.1016/s0140-6736(12)61144-1

130. Noble PW, Barkauskas CE, Jiang D. Pulmonary fibrosis: patterns and perpetrators. *J Clin Invest*. (2012) 122:2756–62. doi: 10.1172/jci60323

131. King TE Jr., Pardo A, Selman M. Idiopathic pulmonary fibrosis. *Lancet*. (2011) 378:1949–61. doi: 10.1016/s0140-6736(11)60052-4

132. Li N, Lin Z, Zhou Q, Chang M, Wang Y, Guan Y, et al. Metformin alleviates crystalline silica-induced pulmonary fibrosis by remodeling endothelial cells to mesenchymal transition via autophagy signaling. *Ecotoxicol Environ Saf*. (2022) 245:114100. doi: 10.1016/j.ecoenv.2022.114100

133. Zhang C, Zhao H, Li BL, Fu G, Liu H, Cai JM, et al. CpG-oligodeoxynucleotides may be effective for preventing ionizing radiation induced pulmonary fibrosis. *Toxicol Lett*. (2018) 292:181–9. doi: 10.1016/j.toxlet.2018.04.009

134. Feng X, Jia A. Protective effect of carvacrol on acute lung injury induced by lipopolysaccharide in mice. *Inflammation*. (2014) 37:1091–101. doi: 10.1007/s10753-014-9833-1

135. Lee JW, Chun W, Kwon OK, Park HA, Lim Y, Lee JH, et al. 3,4,5-Trihydroxycinnamic acid attenuates lipopolysaccharide (LPS)-induced acute lung injury via downregulating inflammatory molecules and upregulating HO-1/AMPK activation. *Int Immunopharmacol*. (2018) 64:123–30. doi: 10.1016/j.intimp.2018.08.015

136. Zhang H, Chen S, Zeng M, Lin D, Wang Y, Wen X, et al. Apelin-13 administration protects against LPS-induced acute lung injury by inhibiting NF-κB pathway and NLRP3 inflammasome activation. *Cell Physiol Biochem*. (2018) 49:1918–32. doi: 10.1159/000493653

137. Yang J, Li S, Wang L, Du F, Zhou X, Song Q, et al. Ginsenoside rg3 attenuates lipopolysaccharide-induced acute lung injury via merTK-dependent activation of the

PI3K/AKT/mTOR pathway. *Front Pharmacol*. (2018) 9:850. doi: 10.3389/fphar.2018.00850

138. He YQ, Zhou CC, Yu LY, Wang L, Deng JL, Tao YL, et al. Natural product derived phytochemicals in managing acute lung injury by multiple mechanisms. *Pharmacol Res*. (2021) 163:105224. doi: 10.1016/j.phrs.2020.105224

139. Blázquez-Prieto J, López-Alonso I, Huidobro C, Albaiceta GM. The emerging role of neutrophils in repair after acute lung injury. *Am J Respir Cell Mol Biol*. (2018) 59:289–94. doi: 10.1165/rcmb.2018-0101PS

140. Chen T, Zhu G, Meng X, Zhang X. Recent developments of small molecules with anti-inflammatory activities for the treatment of acute lung injury. *Eur J Med Chem*. (2020) 207:112660. doi: 10.1016/j.ejmech.2020.112660

141. Zarrilli G, Angerilli V, Businello G, Sbaraglia M, Traverso G, Fortarezza F, et al. The immunopathological and histological landscape of COVID-19-mediated lung injury. *Int J Mol Sci*. (2021) 22:974. doi: 10.3390/ijms22020974

142. Gouda MM, Shaikh SB, Bhandary YP. Inflammatory and fibrinolytic system in acute respiratory distress syndrome. *Lung*. (2018) 196:609–16. doi: 10.1007/s00408-018-0150-6

143. Piotrowski WJ, Martusewicz-Boros MM, Białas AJ, Barczyk A, Batko B, Błasińska K, et al. Guidelines of the polish respiratory society on the diagnosis and treatment of progressive fibrosing interstitial lung diseases other than idiopathic pulmonary fibrosis. *Adv Respir Med*. (2022) 90:425–50. doi: 10.3390/arm90050052

144. De Matteis S, Murgia N. Work-related interstitial lung disease: what is the true burden? *Int J Tuberc Lung Dis*. (2022) 26:1001–5. doi: 10.5588/ijtld.22.0212

145. Andreikos D, Karampitsakos T, Tzouvelekis A, Stratakos G. Statins' still controversial role in pulmonary fibrosis: What does the evidence show? *Pulm Pharmacol Ther*. (2022) 77:102168. doi: 10.1016/j.pupt.2022.102168

146. Lederer DJ, Martinez FJ. Idiopathic pulmonary fibrosis. *N Engl J Med*. (2018) 378:1811–23. doi: 10.1056/NEJMra1705751

147. Raghu G, Weycker D, Edelsberg J, Bradford WZ, Oster G. Incidence and prevalence of idiopathic pulmonary fibrosis. *Am J Respir Crit Care Med*. (2006) 174:810–6. doi: 10.1164/rccm.200602-163OC

148. Wolters PJ, Collard HR, Jones KD. Pathogenesis of idiopathic pulmonary fibrosis. *Annu Rev Pathol*. (2014) 9:157–79. doi: 10.1146/annurev-pathol-012513-104706

149. Raghu G, Collard HR, Egan JJ, Martinez FJ, Behr J, Brown KK, et al. An official ATS/ERS/JRS/ALAT statement: idiopathic pulmonary fibrosis: evidence-based guidelines for diagnosis and management. *Am J Respir Crit Care Med*. (2011) 183:788–824. doi: 10.1164/rccm.2009-040GL

150. Maher TM, Bendstrup E, Dron L, Langley J, Smith G, Khalid JM, et al. Global incidence and prevalence of idiopathic pulmonary fibrosis. *Respir Res*. (2021) 22:197. doi: 10.1186/s12931-021-01791-z

151. Duchemann B, Annesi-Maesano I, Jacobe de Naurois C, Sanyal S, Brillet PY, Brauner M, et al. Prevalence and incidence of interstitial lung diseases in a multi-ethnic county of Greater Paris. *Eur Respir J*. (2017) 50:1602419. doi: 10.1183/13993003.02419-2016

152. Raghu G, Selman M. Nintedanib and pirfenidone. New antifibrotic treatments indicated for idiopathic pulmonary fibrosis offer hopes and raises questions. *Am J Respir Crit Care Med*. (2015) 191:252–4. doi: 10.1164/rccm.201411-2044ED

153. Cai Y, Sugimoto C, Arainga M, Alvarez X, Didier ES, Kuroda MJ. *In vivo* characterization of alveolar and interstitial lung macrophages in rhesus macaques: implications for understanding lung disease in humans. *J Immunol*. (2014) 192:2821–9. doi: 10.4049/jimmunol.1302269

154. Yamasaki K, Eeden SFV. Lung macrophage phenotypes and functional responses: role in the pathogenesis of COPD. *Int J Mol Sci*. (2018) 19:582. doi: 10.3390/ijms19020582

155. Larson-Casey JL, Deshane JS, Ryan AJ, Thannickal VJ, Carter AB. Macrophage akt1 kinase-mediated mitophagy modulates apoptosis resistance and pulmonary fibrosis. *Immunity*. (2016) 44:582–96. doi: 10.1016/j.immuni.2016.01.001

156. Mesureur J, Feliciano JR, Wagner N, Gomes MC, Zhang L, Blanco-Gonzalez M, et al. Macrophages, but not neutrophils, are critical for proliferation of Burkholderia cenocepacia and ensuing host-damaging inflammation. *PloS Pathog*. (2017) 13:e1006437. doi: 10.1371/journal.ppat.1006437

157. Liu G, Zhai H, Zhang T, Li S, Li N, Chen J, et al. New therapeutic strategies for IPF: Based on the "phagocytosis-secretion-immunization" network regulation mechanism of pulmonary macrophages. *BioMed Pharmacother*. (2019) 118:109230. doi: 10.1016/j.biopha.2019.109230

158. Goda C, Balli D, Black M, Milewski D, Le T, Ustiyan V, et al. Loss of FOXM1 in macrophages promotes pulmonary fibrosis by activating p38 MAPK signaling pathway. *PloS Genet*. (2020) 16:e1008692. doi: 10.1371/journal.pgen.1008692

159. Bocchino M, Agnese S, Fagone E, Svegliati S, Grieco D, Vancheri C, et al. Reactive oxygen species are required for maintenance and differentiation of primary lung fibroblasts in idiopathic pulmonary fibrosis. *PloS One*. (2010) 5:e14003. doi: 10.1371/journal.pone.0014003

160. Schaberg T, Rau M, Stephan H, Lode H. Increased number of alveolar macrophages expressing surface molecules of the CD11/CD18 family in sarcoidosis and idiopathic pulmonary fibrosis is related to the production of superoxide anions by these cells. *Am Rev Respir Dis*. (1993) 147:1507–13. doi: 10.1164/ajrccm/147.6_Pt_1.1507

161. Ye Q, Dalavanga Y, Poulakis N, Sixt SU, Guzman J, Costabel U. Decreased expression of haem oxygenase-1 by alveolar macrophages in idiopathic pulmonary fibrosis. *Eur Respir J*. (2008) 31:1030–6. doi: 10.1183/09031936.00125407

162. Scotton CJ, Krupiczojc MA, Königshoff M, Mercer PF, Lee YC, Kaminski N, et al. Increased local expression of coagulation factor X contributes to the fibrotic response in human and murine lung injury. *J Clin Invest*. (2009) 119:2550–63. doi: 10.1172/jci33288

163. Howell DC, Johns RH, Lasky JA, Shan B, Scotton CJ, Laurent GJ, et al. Absence of proteinase-activated receptor-1 signaling affords protection from bleomycin-induced lung inflammation and fibrosis. *Am J Pathol*. (2005) 166:1353–65. doi: 10.1016/s0002-9440(10)62354-1

164. Martinet Y, Rom WN, Grotendorst GR, Martin GR, Crystal RG. Exaggerated spontaneous release of platelet-derived growth factor by alveolar macrophages from patients with idiopathic pulmonary fibrosis. *N Engl J Med*. (1987) 317:202–9. doi: 10.1056/nejm198707233170404

165. Prasse A, Pechkovsky DV, Toews GB, Jungraithmayr W, Kollert F, Goldmann T, et al. A vicious circle of alveolar macrophages and fibroblasts perpetuates pulmonary fibrosis via CCL18. *Am J Respir Crit Care Med*. (2006) 173:781–92. doi: 10.1164/rccm.200509-1518OC

166. Balhara J, Gounni AS. The alveolar macrophages in asthma: a double-edged sword. *Mucosal Immunol*. (2012) 5:605–9. doi: 10.1038/mi.2012.74

167. Burman A, Tanjore H, Blackwell TS. Endoplasmic reticulum stress in pulmonary fibrosis. *Matrix Biol*. (2018) 68-69:355–65. doi: 10.1016/j.matbio.2018.03.015

168. Reyfman PA, Walter JM, Joshi N, Anekalla KR, McQuattie-Pimentel AC, Chiu S, et al. Single-cell transcriptomic analysis of human lung provides insights into the pathobiology of pulmonary fibrosis. *Am J Respir Crit Care Med*. (2019) 199:1517–36. doi: 10.1164/rccm.201712-2410OC

169. Philip K, Mills TW, Davies J, Chen NY, Karmouty-Quintana H, Luo F, et al. HIF1A up-regulates the ADORA2B receptor on alternatively activated macrophages and contributes to pulmonary fibrosis. *FASEB J*. (2017) 31:4745–58. doi: 10.1096/fj.201700219R

170. Okabe Y, Medzhitov R. Tissue biology perspective on macrophages. *Nat Immunol*. (2016) 17:9–17. doi: 10.1038/ni.3320

171. Hussell T, Bell TJ. Alveolar macrophages: plasticity in a tissue-specific context. *Nat Rev Immunol*. (2014) 14:81–93. doi: 10.1038/nri3600

172. Gwyer Findlay E, Hussell T. Macrophage-mediated inflammation and disease: a focus on the lung. *Mediators Inflamm*. (2012) 2012:140937. doi: 10.1155/2012/140937

173. Byrne AJ, Mathie SA, Gregory LG, Lloyd CM. Pulmonary macrophages: key players in the innate defence of the airways. *Thorax*. (2015) 70:1189–96. doi: 10.1136/thoraxjnl-2015-207020

174. Garbi N, Lambrecht BN. Location, function, and ontogeny of pulmonary macrophages during the steady state. *Pflugers Arch*. (2017) 469:561–72. doi: 10.1007/s00424-017-1965-3

175. Satoh T, Nakagawa K, Sugihara F, Kuwahara R, Ashihara M, Yamane F, et al. Identification of an atypical monocyte and committed progenitor involved in fibrosis. *Nature*. (2017) 541:96–101. doi: 10.1038/nature20611

176. Misharin AV, Morales-Nebreda L, Reyfman PA, Cuda CM, Walter JM, McQuattie-Pimentel AC, et al. Monocyte-derived alveolar macrophages drive lung fibrosis and persist in the lung over the life span. *J Exp Med*. (2017) 214:2387–404. doi: 10.1084/jem.20162152

177. Michalski JE, Kurche JS, Schwartz DA. From ARDS to pulmonary fibrosis: the next phase of the COVID-19 pandemic? *Transl Res*. (2022) 241:13–24. doi: 10.1016/j.trsl.2021.09.001

178. Huang WJ, Tang XX. Virus infection induced pulmonary fibrosis. *J Transl Med*. (2021) 19:496. doi: 10.1186/s12967-021-03159-9

179. Selman M, Pardo A. Role of epithelial cells in idiopathic pulmonary fibrosis: from innocent targets to serial killers. *Proc Am Thorac Soc*. (2006) 3:364–72. doi: 10.1513/pats.200601-003TK

180. Tanjore H, Blackwell TS, Lawson WE. Emerging evidence for endoplasmic reticulum stress in the pathogenesis of idiopathic pulmonary fibrosis. *Am J Physiol Lung Cell Mol Physiol*. (2012) 302:L721–9. doi: 10.1152/ajplung.00410.2011

181. Byrne AJ, Maher TM, Lloyd CM. Pulmonary macrophages: A new therapeutic pathway in fibrosing lung disease? *Trends Mol Med*. (2016) 22:303–16. doi: 10.1016/j.molmed.2016.02.004

182. Ucero AC, Bakiri L, Roediger B, Suzuki M, Jimenez M, Mandal P, et al. Fra-2-expressing macrophages promote lung fibrosis in mice. *J Clin Invest*. (2019) 129:3293–309. doi: 10.1172/jci125366

183. McCubbrey AL, Barthel L, Mohning MP, Redente EF, Mould KJ, Thomas SM, et al. Deletion of c-FLIP from CD11b(hi) macrophages prevents development of bleomycin-induced lung fibrosis. *Am J Respir Cell Mol Biol*. (2018) 58:66–78. doi: 10.1165/rcmb.2017-0154OC

184. Kimura T, Nada S, Takegahara N, Okuno T, Nojima S, Kang S, et al. Polarization of M2 macrophages requires Lamtor1 that integrates cytokine and amino-acid signals. *Nat Commun*. (2016) 7:13130. doi: 10.1038/ncomms13130

185. Meyer NJ, Gattinoni L, Calfee CS. Acute respiratory distress syndrome. *Lancet*. (2021) 398:622–37. doi: 10.1016/s0140-6736(21)00439-6

186. Wojtan P, Mierzejewski M, Osińska I, Domagała-Kulawik J. Macrophage polarization in interstitial lung diseases. *Cent Eur J Immunol*. (2016) 41:159–64. doi: 10.5114/ceji.2016.60990

187. Strieter RM. What differentiates normal lung repair and fibrosis? Inflammation, resolution of repair, and fibrosis. *Proc Am Thorac Soc*. (2008) 5:305–10. doi: 10.1513/pats.200710-160DR

188. Tsoutsou PG, Gourgoulianis KI, Petinaki E, Germenis A, Tsoutsou AG, Mpaka M, et al. Cytokine levels in the sera of patients with idiopathic pulmonary fibrosis. *Respir Med*. (2006) 100:938–45. doi: 10.1016/j.rmed.2005.06.016

189. Chen X, Tang J, Shuai W, Meng J, Feng J, Han Z. Macrophage polarization and its role in the pathogenesis of acute lung injury/acute respiratory distress syndrome. *Inflammation Res*. (2020) 69:883–95. doi: 10.1007/s00011-020-01378-2

190. Yao Y, Wang Y, Zhang Z, He L, Zhu J, Zhang M, et al. Chop deficiency protects mice against bleomycin-induced pulmonary fibrosis by attenuating M2 macrophage production. *Mol Ther*. (2016) 24:915–25. doi: 10.1038/mt.2016.36

191. Su S, Zhao Q, He C, Huang D, Liu J, Chen F, et al. miR-142-5p and miR-130a-3p are regulated by IL-4 and IL-13 and control profibrogenic macrophage program. *Nat Commun*. (2015) 6:8523. doi: 10.1038/ncomms9523

192. Kong P, Christia P, Frangogiannis NG. The pathogenesis of cardiac fibrosis. *Cell Mol Life Sci*. (2014) 71:549–74. doi: 10.1007/s00018-013-1349-6

193. Froese AR, Shimbori C, Bellaye PS, Inman M, Obex S, Fatima S, et al. Stretch-induced activation of transforming growth factor-β1 in pulmonary fibrosis. *Am J Respir Crit Care Med*. (2016) 194:84–96. doi: 10.1164/rccm.201508-1638OC

194. Pechkovsky DV, Prasse A, Kollert F, Engel KM, Dentler J, Luttmann W, et al. Alternatively activated alveolar macrophages in pulmonary fibrosis-mediator production and intracellular signal transduction. *Clin Immunol*. (2010) 137:89–101. doi: 10.1016/j.clim.2010.06.017

195. Vannella KM, Wynn TA. Mechanisms of organ injury and repair by macrophages. *Annu Rev Physiol*. (2017) 79:593–617. doi: 10.1146/annurev-physiol-022516-034356

196. Meng XM, Wang S, Huang XR, Yang C, Xiao J, Zhang Y, et al. Inflammatory macrophages can transdifferentiate into myofibroblasts during renal fibrosis. *Cell Death Dis*. (2016) 7:e2495. doi: 10.1038/cddis.2016.402

197. Upagupta C, Shimbori C, Alsilmi R, Kolb M. Matrix abnormalities in pulmonary fibrosis. *Eur Respir Rev*. (2018) 27:18033. doi: 10.1183/16000617.0033-2018

198. Hu B, Phan SH. Myofibroblasts. *Curr Opin Rheumatol*. (2013) 25:71–7. doi: 10.1097/BOR.0b013e32835b1352

199. Walsh SM, Worrell JC, Fabre A, Hinz B, Kane R, Keane MP. Novel differences in gene expression and functional capabilities of myofibroblast populations in idiopathic pulmonary fibrosis. *Am J Physiol Lung Cell Mol Physiol*. (2018) 315:L697–l710. doi: 10.1152/ajplung.00543.2017

200. Sieber P, Schäfer A, Lieberherr R, Le Goff F, Stritt M, Welford RWD, et al. Novel high-throughput myofibroblast assays identify agonists with therapeutic potential in pulmonary fibrosis that act via EP2 and EP4 receptors. *PloS One*. (2018) 13:e0207872. doi: 10.1371/journal.pone.0207872

201. Bindu S, Pillai VB, Kanwal A, Samant S, Mutlu GM, Verdin E, et al. SIRT3 blocks myofibroblast differentiation and pulmonary fibrosis by preventing mitochondrial DNA damage. *Am J Physiol Lung Cell Mol Physiol*. (2017) 312:L68–l78. doi: 10.1152/ajplung.00188.2016

202. Yu QY, Tang XX. Irreversibility of pulmonary fibrosis. *Aging Dis*. (2022) 13:73–86. doi: 10.14336/ad.2021.0730

203. Lomas NJ, Watts KL, Akram KM, Forsyth NR, Spiteri MA. Idiopathic pulmonary fibrosis: immunohistochemical analysis provides fresh insights into lung tissue remodelling with implications for novel prognostic markers. *Int J Clin Exp Pathol*. (2012) 5:58–71.

204. Holm Nielsen S, Willumsen N, Leeming DJ, Daniels SJ, Brix S, Karsdal MA, et al. Serological assessment of activated fibroblasts by alpha-smooth muscle actin (α-SMA): A noninvasive biomarker of activated fibroblasts in lung disorders. *Transl Oncol*. (2019) 12:368–74. doi: 10.1016/j.tranon.2018.11.004

205. El Agha E, Moiseenko A, Kheirollahi V, De Langhe S, Crnkovic S, Kwapiszewska G, et al. Two-way conversion between lipogenic and myogenic fibroblastic phenotypes marks the progression and resolution of lung fibrosis. *Cell Stem Cell*. (2017) 20:261–73.e3. doi: 10.1016/j.stem.2016.10.004

206. Glasser SW, Hagood JS, Wong S, Taype CA, Madala SK, Hardie WD. Mechanisms of lung fibrosis resolution. *Am J Pathol*. (2016) 186:1066–77. doi: 10.1016/j.ajpath.2016.01.018

207. Tang PM, Zhang YY, Xiao J, Tang PC, Chung JY, Li J, et al. Neural transcription factor Pou4f1 promotes renal fibrosis via macrophage-myofibroblast transition. *Proc Natl Acad Sci U S A*. (2020) 117:20741–52. doi: 10.1073/pnas.1917663117

208. Bayes-Genis A, Campbell JH, Carlson PJ, Holmes DR Jr., Schwartz RS. Macrophages, myofibroblasts and neointimal hyperplasia after coronary artery injury and repair. *Atherosclerosis*. (2002) 163:89–98. doi: 10.1016/s0021-9150(01)00771-7

209. Wynn TA. Integrating mechanisms of pulmonary fibrosis. *J Exp Med*. (2011) 208:1339–50. doi: 10.1084/jem.20110551

210. Chanda D, Kurundkar A, Rangarajan S, Locy M, Bernard K, Sharma NS, et al. Developmental reprogramming in mesenchymal stromal cells of human subjects with idiopathic pulmonary fibrosis. *Sci Rep*. (2016) 6:37445. doi: 10.1038/srep37445

211. Lehmann M, Baarsma HA, Königshoff M. WNT signaling in lung aging and disease. *Ann Am Thorac Soc*. (2016) 13 Suppl 5:S411–s6. doi: 10.1513/AnnalsATS.201608-586AW

212. Selman M, King TE, Pardo A. Idiopathic pulmonary fibrosis: prevailing and evolving hypotheses about its pathogenesis and implications for therapy. *Ann Intern Med*. (2001) 134:136–51. doi: 10.7326/0003-4819-134-2-200101160-00015

213. White ES, Lazar MH, Thannickal VJ. Pathogenetic mechanisms in usual interstitial pneumonia/idiopathic pulmonary fibrosis. *J Pathol*. (2003) 201:343–54. doi: 10.1002/path.1446

214. Scotton CJ, Chambers RC. Molecular targets in pulmonary fibrosis: the myofibroblast in focus. *Chest*. (2007) 132:1311–21. doi: 10.1378/chest.06-2568

215. Herriges M, Morrisey EE. Lung development: orchestrating the generation and regeneration of a complex organ. *Development*. (2014) 141:502–13. doi: 10.1242/dev.098186

216. Morrisey EE, Hogan BL. Preparing for the first breath: genetic and cellular mechanisms in lung development. *Dev Cell*. (2010) 18:8–23. doi: 10.1016/j.devcel.2009.12.010

217. Königshoff M, Balsara N, Pfaff EM, Kramer M, Chrobak I, Seeger W, et al. Functional Wnt signaling is increased in idiopathic pulmonary fibrosis. *PloS One*. (2008) 3:e2142. doi: 10.1371/journal.pone.0002142

218. Selman M, Pardo A, Kaminski N. Idiopathic pulmonary fibrosis: aberrant recapitulation of developmental programs? *PloS Med*. (2008) 5:e62. doi: 10.1371/journal.pmed.0050062

219. Aschner Y, Downey GP. Transforming growth factor-β: master regulator of the respiratory system in health and disease. *Am J Respir Cell Mol Biol*. (2016) 54:647–55. doi: 10.1165/rcmb.2015-0391TR

220. Sporn MB, Roberts AB. The transforming growth factor-betas: past, present, and future. *Ann N Y Acad Sci*. (1990) 593:1–6. doi: 10.1111/j.1749-6632.1990.tb16095.x

221. Meng XM, Nikolic-Paterson DJ, Lan HY. TGF-β: the master regulator of fibrosis. *Nat Rev Nephrol*. (2016) 12:325–38. doi: 10.1038/nrneph.2016.48

222. Juban G, Saclier M, Yacoub-Youssef H, Kernou A, Arnold L, Boisson C, et al. AMPK activation regulates LTBP4-dependent TGF-β1 secretion by pro-inflammatory macrophages and controls fibrosis in duchenne muscular dystrophy. *Cell Rep*. (2018) 25:2163–76.e6. doi: 10.1016/j.celrep.2018.10.077

223. Meyer A, Wang W, Qu J, Croft L, Degen JL, Coller BS, et al. Platelet TGF-β1 contributions to plasma TGF-β1, cardiac fibrosis, and systolic dysfunction in a mouse model of pressure overload. *Blood*. (2012) 119:1064–74. doi: 10.1182/blood-2011-09-377648

224. Celada LJ, Kropski JA, Herazo-Maya JD, Luo W, Creecy A, Abad AT, et al. PD-1 up-regulation on CD4(+) T cells promotes pulmonary fibrosis through STAT3-mediated IL-17A and TGF-β1 production. *Sci Transl Med*. (2018) 10:eaar8356. doi: 10.1126/scitranslmed.aar8356

225. Falcone DJ, McCaffrey TA, Haimovitz-Friedman A, Vergilio JA, Nicholson AC. Macrophage and foam cell release of matrix-bound growth factors. Role of plasminogen activation. *J Biol Chem*. (1993) 268:11951–8. doi: 10.1016/S0021-9258(19)50292-7

226. Branton MH, Kopp JB. TGF-beta and fibrosis. *Microbes Infect*. (1999) 1:1349–65. doi: 10.1016/s1286-4579(99)00250-6

227. Li MO, Wan YY, Sanjabi S, Robertson AK, Flavell RA. Transforming growth factor-beta regulation of immune responses. *Annu Rev Immunol*. (2006) 24:99–146. doi: 10.1146/annurev.immunol.24.021605.090737

228. Han G, Li F, Singh TP, Wolf P, Wang XJ. The pro-inflammatory role of TGFβ1: a paradox? *Int J Biol Sci*. (2012) 8:228–35. doi: 10.7150/ijbs.8.228

229. Li J, Qu X, Yao J, Caruana G, Ricardo SD, Yamamoto Y, et al. Blockade of endothelial-mesenchymal transition by a Smad3 inhibitor delays the early development of streptozotocin-induced diabetic nephropathy. *Diabetes*. (2010) 59:2612–24. doi: 10.2337/db09-1631

230. Meng XM, Chung AC, Lan HY. Role of the TGF-β/BMP-7/Smad pathways in renal diseases. *Clin Sci (Lond)*. (2013) 124:243–54. doi: 10.1042/cs20120252

231. Huang XR, Chung AC, Yang F, Yue W, Deng C, Lau CP, et al. Smad3 mediates cardiac inflammation and fibrosis in angiotensin II-induced hypertensive cardiac remodeling. *Hypertension*. (2010) 55:1165–71. doi: 10.1161/hypertensionaha.109.147611

232. Massagué J, Gomis RR. The logic of TGFbeta signaling. *FEBS Lett*. (2006) 580:2811–20. doi: 10.1016/j.febslet.2006.04.033

233. Sato M, Muragaki Y, Saika S, Roberts AB, Ooshima A. Targeted disruption of TGF-beta1/Smad3 signaling protects against renal tubulointerstitial fibrosis induced by unilateral ureteral obstruction. *J Clin Invest*. (2003) 112:1486–94. doi: 10.1172/jci19270

234. Meng XM, Huang XR, Chung AC, Qin W, Shao X, Igarashi P, et al. Smad2 protects against TGF-beta/Smad3-mediated renal fibrosis. *J Am Soc Nephrol*. (2010) 21:1477–87. doi: 10.1681/asn.2009121244

235. Wang W, Huang XR, Canlas E, Oka K, Truong LD, Deng C, et al. Essential role of Smad3 in angiotensin II-induced vascular fibrosis. *Circ Res*. (2006) 98:1032–9. doi: 10.1161/01.RES.0000218782.52610.dc

236. du Bois RM. Strategies for treating idiopathic pulmonary fibrosis. *Nat Rev Drug Discovery*. (2010) 9:129–40. doi: 10.1038/nrd2958

237. Roberts AB, Russo A, Felici A, Flanders KC. Smad3: a key player in pathogenetic mechanisms dependent on TGF-beta. *Ann N Y Acad Sci*. (2003) 995:1–10. doi: 10.1111/j.1749-6632.2003.tb03205.x

238. Derynck R, Zhang YE. Smad-dependent and Smad-independent pathways in TGF-beta family signalling. *Nature*. (2003) 425:577–84. doi: 10.1038/nature02006

239. Ogawa T, Shichino S, Ueha S, Matsushima K. Macrophages in lung fibrosis. *Int Immunol*. (2021) 33:665–71. doi: 10.1093/intimm/dxab040

240. Chanda D, Otoupalova E, Smith SR, Volckaert T, De Langhe SP, Thannickal VJ. Developmental pathways in the pathogenesis of lung fibrosis. *Mol Aspects Med*. (2019) 65:56–69. doi: 10.1016/j.mam.2018.08.004

241. Bonniaud P, Margetts PJ, Ask K, Flanders K, Gauldie J, Kolb M. TGF-beta and Smad3 signaling link inflammation to chronic fibrogenesis. *J Immunol*. (2005) 175:5390–5. doi: 10.4049/jimmunol.175.8.5390

242. Border WA, Noble NA. Transforming growth factor beta in tissue fibrosis. *N Engl J Med*. (1994) 331:1286–92. doi: 10.1056/nejm199411103311907

243. Russo I, Cavalera M, Huang S, Su Y, Hanna A, Chen B, et al. Protective effects of activated myofibroblasts in the pressure-overloaded myocardium are mediated through smad-dependent activation of a matrix-preserving program. *Circ Res*. (2019) 124:1214–27. doi: 10.1161/circresaha.118.314438

244. Krafts KP. Tissue repair: The hidden drama. *Organogenesis*. (2010) 6:225–33. doi: 10.4161/org.6.4.12555

245. Fernandez IE, Eickelberg O. The impact of TGF-β on lung fibrosis: from targeting to biomarkers. *Proc Am Thorac Soc*. (2012) 9:111–6. doi: 10.1513/pats.201203-023AW

246. Bartram U, Speer CP. The role of transforming growth factor beta in lung development and disease. *Chest*. (2004) 125:754–65. doi: 10.1378/chest.125.2.754

247. Kalchiem-Dekel O, Galvin JR, Burke AP, Atamas SP, Todd NW. Interstitial lung disease and pulmonary fibrosis: A practical approach for general medicine physicians with focus on the medical history. *J Clin Med*. (2018) 7:476. doi: 10.3390/jcm7120476

248. Flanders KC. Smad3 as a mediator of the fibrotic response. *Int J Exp Pathol*. (2004) 85:47–64. doi: 10.1111/j.0959-9673.2004.00377.x

249. Logan CY, Nusse R. The Wnt signaling pathway in development and disease. *Annu Rev Cell Dev Biol*. (2004) 20:781–810. doi: 10.1146/annurev.cellbio.20.010403.113126

250. Nusse R, Clevers H. Wnt/β-catenin signaling, disease, and emerging therapeutic modalities. *Cell*. (2017) 169:985–99. doi: 10.1016/j.cell.2017.05.016

251. Morrisey EE. Wnt signaling and pulmonary fibrosis. *Am J Pathol*. (2003) 162:1393–7. doi: 10.1016/s0002-9440(10)64271-x

252. Moon RT, Kohn AD, De Ferrari GV, Kaykas A. WNT and beta-catenin signalling: diseases and therapies. *Nat Rev Genet*. (2004) 5:691–701. doi: 10.1038/nrg1427

253. Staal FJ, Clevers HC. WNT signalling and haematopoiesis: a WNT-WNT situation. *Nat Rev Immunol*. (2005) 5:21–30. doi: 10.1038/nri1529

254. Polakis P. Wnt signaling and cancer. *Genes Dev*. (2000) 14:1837–51. doi: 10.1101/gad.14.15.1837

255. Reya T, Clevers H. Wnt signalling in stem cells and cancer. *Nature*. (2005) 434:843–50. doi: 10.1038/nature03319

256. Hurlstone AF, Haramis AP, Wienholds E, Begthel H, Korving J, Van Eeden F, et al. The Wnt/beta-catenin pathway regulates cardiac valve formation. *Nature*. (2003) 425:633–7. doi: 10.1038/nature02028

257. Johnson ML, Rajamannan N. Diseases of wnt signaling. *Rev Endocr Metab Disord*. (2006) 7:41–9. doi: 10.1007/s11154-006-9003-3

258. Wu B, Crampton SP, Hughes CC. Wnt signaling induces matrix metalloproteinase expression and regulates T cell transmigration. *Immunity*. (2007) 26:227–39. doi: 10.1016/j.immuni.2006.12.007

259. Qu B, Liu BR, Du YJ, Chen J, Cheng YQ, Xu W, et al. Wnt/β-catenin signaling pathway may regulate the expression of angiogenic growth factors in hepatocellular carcinoma. *Oncol Lett*. (2014) 7:1175–8. doi: 10.3892/ol.2014.1828

260. He W, Dai C, Li Y, Zeng G, Monga SP, Liu Y. Wnt/beta-catenin signaling promotes renal interstitial fibrosis. *J Am Soc Nephrol*. (2009) 20:765–76. doi: 10.1681/asn.2008060566

261. He W, Zhang L, Ni A, Zhang Z, Mirotsou M, Mao L, et al. Exogenously administered secreted frizzled related protein 2 (Sfrp2) reduces fibrosis and improves cardiac function in a rat model of myocardial infarction. *Proc Natl Acad Sci U S A*. (2010) 107:21110–5. doi: 10.1073/pnas.1004708107

262. Henderson WRJr., Chi EY, Ye X, Nguyen C, Tien YT, Zhou B, et al. Inhibition of Wnt/beta-catenin/CREB binding protein (CBP) signaling reverses pulmonary fibrosis. *Proc Natl Acad Sci U S A*. (2010) 107:14309–14. doi: 10.1073/pnas.1001520107

263. Liu L, Carron B, Yee HT, Yie TA, Hajjou M, Rom W. Wnt pathway in pulmonary fibrosis in the bleomycin mouse model. *J Environ Pathol Toxicol Oncol*. (2009) 28:99–108. doi: 10.1615/jenvironpatholtoxicoloncol.v28.i2.20

264. Wei J, Melichian D, Komura K, Hinchcliff M, Lam AP, Lafyatis R, et al. Canonical Wnt signaling induces skin fibrosis and subcutaneous lipoatrophy: a novel mouse model for scleroderma? *Arthritis Rheum*. (2011) 63:1707–17. doi: 10.1002/art.30312

265. Trensz F, Haroun S, Cloutier A, Richter MV, Grenier G. A muscle resident cell population promotes fibrosis in hindlimb skeletal muscles of mdx mice through the Wnt canonical pathway. *Am J Physiol Cell Physiol*. (2010) 299:C939–47. doi: 10.1152/ajpcell.00253.2010

266. Akhmetshina A, Palumbo K, Dees C, Bergmann C, Venalis P, Zerr P, et al. Activation of canonical Wnt signalling is required for TGF-β-mediated fibrosis. *Nat Commun*. (2012) 3:735. doi: 10.1038/ncomms1734

267. Flozak AS, Lam AP, Russell S, Jain M, Peled ON, Sheppard KA, et al. Beta-catenin/T-cell factor signaling is activated during lung injury and promotes the survival and migration of alveolar epithelial cells. *J Biol Chem*. (2010) 285:3157–67. doi: 10.1074/jbc.M109.070326

268. Hamburg-Shields E, DiNuoscio GJ, Mullin NK, Lafyatis R, Atit RP. Sustained β-catenin activity in dermal fibroblasts promotes fibrosis by up-regulating expression of extracellular matrix protein-coding genes. *J Pathol*. (2015) 235:686–97. doi: 10.1002/path.4481

269. Aumiller V, Balsara N, Wilhelm J, Günther A, Königshoff M. WNT/β-catenin signaling induces IL-1β expression by alveolar epithelial cells in pulmonary fibrosis. *Am J Respir Cell Mol Biol*. (2013) 49:96–104. doi: 10.1165/rcmb.2012-0524OC

270. Vuga LJ, Ben-Yehudah A, Kovkarova-Naumovski E, Oriss T, Gibson KF, Feghali-Bostwick C, et al. WNT5A is a regulator of fibroblast proliferation and resistance to apoptosis. *Am J Respir Cell Mol Biol*. (2009) 41:583–9. doi: 10.1165/rcmb.2008-0201OC

271. Zhang Y, Goss AM, Cohen ED, Kadzik R, Lepore JJ, Muthukumaraswamy K, et al. A Gata6-Wnt pathway required for epithelial stem cell development and airway regeneration. *Nat Genet*. (2008) 40:862–70. doi: 10.1038/ng.157

272. Xu W, Xu B, Zhao Y, Yang N, Liu C, Wen G, et al. Wnt5a reverses the inhibitory effect of hyperoxia on transdifferentiation of alveolar epithelial type II cells to type I cells. *J Physiol Biochem*. (2015) 71:823–38. doi: 10.1007/s13105-015-0446-4

273. Kim TH, Kim SH, Seo JY, Chung H, Kwak HJ, Lee SK, et al. Blockade of the Wnt/β-catenin pathway attenuates bleomycin-induced pulmonary fibrosis. *Tohoku J Exp Med*. (2011) 223:45–54. doi: 10.1620/tjem.223.45

274. Zhou B, Liu Y, Kahn M, Ann DK, Han A, Wang H, et al. Interactions between β-catenin and transforming growth factor-β signaling pathways mediate epithelial-mesenchymal transition and are dependent on the transcriptional co-activator cAMP-response element-binding protein (CREB)-binding protein (CBP). *J Biol Chem*. (2012) 287:7026–38. doi: 10.1074/jbc.M111.276311

275. Hansson EM, Lendahl U, Chapman G. Notch signaling in development and disease. *Semin Cancer Biol*. (2004) 14:320–8. doi: 10.1016/j.semcancer.2004.04.011

276. Chen S, Xu L, Lin N, Pan W, Hu K, Xu R. Activation of Notch1 signaling by marrow-derived mesenchymal stem cells through cell-cell contact inhibits proliferation of hepatic stellate cells. *Life Sci*. (2011) 89:975–81. doi: 10.1016/j.lfs.2011.10.012

277. Chen YX, Weng ZH, Zhang SL. Notch3 regulates the activation of hepatic stellate cells. *World J Gastroenterol*. (2012) 18:1397–403. doi: 10.3748/wjg.v18.i12.1397

278. Ono Y, Sensui H, Okutsu S, Nagatomi R. Notch2 negatively regulates myofibroblastic differentiation of myoblasts. *J Cell Physiol*. (2007) 210:358–69. doi: 10.1002/jcp.20838

279. Kennard S, Liu H, Lilly B. Transforming growth factor-beta (TGF- 1) down-regulates Notch3 in fibroblasts to promote smooth muscle gene expression. *J Biol Chem*. (2008) 283:1324–33. doi: 10.1074/jbc.M706651200

280. Liu T, Hu B, Choi YY, Chung M, Ullenbruch M, Yu H, et al. Notch1 signaling in FIZZ1 induction of myofibroblast differentiation. *Am J Pathol*. (2009) 174:1745–55. doi: 10.2353/ajpath.2009.080618

281. Carthy JM, Garmaroudi FS, Luo Z, McManus BM. Wnt3a induces myofibroblast differentiation by upregulating TGF-β signaling through SMAD2 in a β-catenin-dependent manner. *PloS One*. (2011) 6:e19809. doi: 10.1371/journal.pone.0019809

282. Aoyagi-Ikeda K, Maeno T, Matsui H, Ueno M, Hara K, Aoki Y, et al. Notch induces myofibroblast differentiation of alveolar epithelial cells via transforming growth factor-{beta}-Smad3 pathway. *Am J Respir Cell Mol Biol*. (2011) 45:136–44. doi: 10.1165/rcmb.2010-0140oc

283. Liu ZJ, Li Y, Tan Y, Xiao M, Zhang J, Radtke F, et al. Inhibition of fibroblast growth by Notch1 signaling is mediated by induction of Wnt11-dependent WISP-1. *PloS One*. (2012) 7:e38811. doi: 10.1371/journal.pone.0038811

284. Kavian N, Servettaz A, Weill B, Batteux F. New insights into the mechanism of notch signalling in fibrosis. *Open Rheumatol J*. (2012) 6:96–102. doi: 10.2174/1874312901206010096

285. Xu K, Moghal N, Egan SE. Notch signaling in lung development and disease. *Adv Exp Med Biol*. (2012) 727:89–98. doi: 10.1007/978-1-4614-0899-4_7

286. Noseda M, Fu Y, Niessen K, Wong F, Chang L, McLean G, et al. Smooth Muscle alpha-actin is a direct target of Notch/CSL. *Circ Res*. (2006) 98:1468–70. doi: 10.1161/01.Res.0000229683.81357.26

287. Hu B, Wu Z, Bai D, Liu T, Ullenbruch MR, Phan SH. Mesenchymal deficiency of Notch1 attenuates bleomycin-induced pulmonary fibrosis. *Am J Pathol*. (2015) 185:3066–75. doi: 10.1016/j.ajpath.2015.07.014

288. Liu Y, Huang G, Mo B, Wang C. Artesunate ameliorates lung fibrosis via inhibiting the Notch signaling pathway. *Exp Ther Med*. (2017) 14:561–6. doi: 10.3892/etm.2017.4573

289. Nikolic-Paterson DJ, Wang S, Lan HY. Macrophages promote renal fibrosis through direct and indirect mechanisms. *Kidney Int Suppl*. (2011) 4:34–8. doi: 10.1038/kisup.2014.7

290. Rockey DC, Bell PD, Hill JA. Fibrosis–a common pathway to organ injury and failure. *N Engl J Med*. (2015) 372:1138–49. doi: 10.1056/NEJMra1300575

291. Lan HY, Chung AC. TGF-β/Smad signaling in kidney disease. *Semin Nephrol*. (2012) 32:236–43. doi: 10.1016/j.semnephrol.2012.04.002

292. Tanaka Y, Kobayashi H, Suzuki M, Kanayama N, Terao T. Transforming growth factor-beta1-dependent urokinase up-regulation and promotion of invasion are involved in Src-MAPK-dependent signaling in human ovarian cancer cells. *J Biol Chem*. (2004) 279:8567–76. doi: 10.1074/jbc.M309131200

293. Tang PM, Zhou S, Li CJ, Liao J, Xiao J, Wang QM, et al. The proto-oncogene tyrosine protein kinase Src is essential for macrophage-myofibroblast transition during renal scarring. *Kidney Int*. (2018) 93:173–87. doi: 10.1016/j.kint.2017.07.026

294. Zheng G, Zhang J, Zhao H, Wang H, Pang M, Qiao X, et al. [amp]]alpha;3 integrin of cell-cell contact mediates kidney fibrosis by integrin-linked kinase in proximal tubular E-cadherin deficient mice. *Am J Pathol*. (2016) 186:1847–60. doi: 10.1016/j.ajpath.2016.03.015

295. Costa A, Kieffer Y, Scholer-Dahirel A, Pelon F, Bourachot B, Cardon M, et al. Fibroblast heterogeneity and immunosuppressive environment in human breast cancer. *Cancer Cell*. (2018) 33:463–79.e10. doi: 10.1016/j.ccell.2018.01.011

296. Sakai T, Aokage K, Neri S, Nakamura H, Nomura S, Tane K, et al. Link between tumor-promoting fibrous microenvironment and an immunosuppressive microenvironment in stage I lung adenocarcinoma. *Lung Cancer*. (2018) 126:64–71. doi: 10.1016/j.lungcan.2018.10.021

297. Calaf GM, Zepeda AB, Castillo RL, Figueroa CA, Arias C, Figueroa E, et al. Molecular aspects of breast cancer resistance to drugs (Review). *Int J Oncol*. (2015) 47:437–45. doi: 10.3892/ijo.2015.3055

298. Tang PC, Chan MK, Chung JY, Chan AS, Zhang D, Li C, et al. Hematopoietic transcription factor RUNX1 is essential for promoting macrophage-myofibroblast transition in non-small-cell lung carcinoma. *Adv Sci (Weinh)*. (2024) 11:e2302203. doi: 10.1002/advs.202302203

299. Tang PC, Chung JY, Liao J, Chan MK, Chan AS, Cheng G, et al. Single-cell RNA sequencing uncovers a neuron-like macrophage subset associated with cancer pain. *Sci Adv*. (2022) 8:eabn5535. doi: 10.1126/sciadv.abn5535

300. Wang QM, Tang PM, Lian GY, Li C, Li J, Huang XR, et al. Enhanced cancer immunotherapy with smad3-silenced NK-92 cells. *Cancer Immunol Res*. (2018) 6:965–77. doi: 10.1158/2326-6066.Cir-17-0491

301. Tang PM, Zhou S, Meng XM, Wang QM, Li CJ, Lian GY, et al. Smad3 promotes cancer progression by inhibiting E4BP4-mediated NK cell development. *Nat Commun*. (2017) 8:14677. doi: 10.1038/ncomms14677

302. Li HY, McSharry M, Bullock B, Nguyen TT, Kwak J, Poczobutt JM, et al. The tumor microenvironment regulates sensitivity of murine lung tumors to PD-1/PD-L1 antibody blockade. *Cancer Immunol Res*. (2017) 5:767–77. doi: 10.1158/2326-6066.Cir-16-0365

303. Zhang F, Wang H, Wang X, Jiang G, Liu H, Zhang G, et al. TGF-β induces M2-like macrophage polarization via SNAIL-mediated suppression of a pro-inflammatory phenotype. *Oncotarget*. (2016) 7:52294–306. doi: 10.18632/oncotarget.10561

304. Chen J, Tang Y, Zhong Y, Wei B, Huang XR, Tang PM, et al. P2Y12 inhibitor clopidogrel inhibits renal fibrosis by blocking macrophage-to-myofibroblast transition. *Mol Ther*. (2022) 30:3017–33. doi: 10.1016/j.ymthe.2022.06.019

305. Ishii G, Ochiai A, Neri S. Phenotypic and functional heterogeneity of cancer-associated fibroblast within the tumor microenvironment. *Adv Drug Delivery Rev*. (2016) 99:186–96. doi: 10.1016/j.addr.2015.07.007

frontiers | Frontiers in Immunology

TYPE Original Research
PUBLISHED 17 December 2024
DOI 10.3389/fimmu.2024.1495581

OPEN ACCESS

EDITED BY
Yi Yan,
Shanghai Jiaotong University School of Medicine, China

REVIEWED BY
Arzu Ulu,
University of California, Riverside, United States
Hong Yong Peh,
National University of Singapore, Singapore

*CORRESPONDENCE
Tara M. Nordgren
Tara.Nordgren@colostate.edu
Julie A. Moreno
Julie.Moreno@colostate.edu

RECEIVED 12 September 2024
ACCEPTED 19 November 2024
PUBLISHED 17 December 2024

CITATION
Threatt AN, White J, Klepper N, Brier Z, Dean LS, Ibarra A, Harris M, Jones K, Wahl MJL, Barahona M, Oyewole EO, Pauly M, Moreno JA and Nordgren TM (2024) Aspirin-triggered resolvin D1 modulates pulmonary and neurological inflammation in an IL-22 knock-out organic dust exposure mouse model. *Front. Immunol.* 15:1495581. doi: 10.3389/fimmu.2024.1495581

Aspirin-triggered resolvin D1 modulates pulmonary and neurological inflammation in an IL-22 knock-out organic dust exposure mouse model

Alissa N. Threatt[1], Jade White[1,2], Nathan Klepper[1,3], Zachary Brier[1,4], Logan S. Dean[1,5], Ash Ibarra[6], Macallister Harris[7], Kaylee Jones[1], Maëlis J. L. Wahl[8], Melea Barahona[1,5], Emmanuel O. Oyewole[1], Morgan Pauly[8], Julie A. Moreno[1,9]* and Tara M. Nordgren[1]*

[1]Department of Environmental and Radiological Health Sciences, College of Veterinary Medicine and Biomedical Sciences, Colorado State University, Fort Collins, CO, United States, [2]Department of Biology, College of Natural Sciences, Colorado State University, Fort Collins, CO, United States, [3]Department of Animal Sciences, College of Agricultural Sciences, Colorado State University, Fort Collins, CO, United States, [4]Department of Biomedical Sciences, College of Veterinary Medicine and Biomedical Sciences, Colorado State University, Fort Collins, CO, United States, [5]Cell and Molecular Biology Graduate Program, Colorado State University, Fort Collins, CO, United States, [6]Department of Chemistry, College of Natural Sciences, Colorado State University, Fort Collins, CO, United States, [7]Experimental Pathology Facility, Department of Microbiology, Immunology, and Pathology, College of Veterinary Medicine and Biomedical Sciences, Colorado State University, Fort Collins, CO, United States, [8]Department of Biochemistry and Molecular Biology, College of Natural Sciences, Colorado State University, Fort Collins, CO, United States, [9]Brain Research Center, Colorado State University, Fort Collins, CO, United States

Agriculture dust contains many organic immunogenic compounds, and organic dust exposure is strongly associated with the development of immune-mediated chronic pulmonary diseases such as chronic obstructive pulmonary disease (COPD). Chronic organic dust exposure from agriculture sources induces chronic lung inflammatory diseases and organic dust exposure has recently been linked to an increased risk of developing dementia. The cytokine interleukin-22 (IL-22) has been established as an important mediator in the resolution and repair of lung tissues. The omega-3 fatty acid metabolite aspirin-triggered Resolvin D1 (AT-RvD1) has shown efficacy in modulating the immune response in both pulmonary and neurological inflammation but has not been explored as a therapeutic in organic dust exposure-induced neuroinflammation. Investigating the link between IL-22 and AT-RvD1 may help in developing effective therapies for these immune-mediated diseases. We aimed to investigate the link between organic dust exposure and neuroinflammation, the role of IL-22 in the pulmonary and neurological immune response to organic dust exposure, and the immune-modulating therapeutic applications of AT-RvD1 in an IL-22 knock-out mouse model of organic dust exposure. C57BL/6J (WT) and IL-22 knock-out (KO) mice were repetitively exposed to aqueous agriculture organic dust extract (DE) 5 days per week for 3 weeks (15 total instillations) and treated with AT-RvD1 either once per week (3 total injections) or 5 times per week (15 total injections) for 3 weeks and allowed to recover for 3 days. We observed a significant pulmonary and neurological

immune response to DE characterized by the development of inducible bronchus associated lymphoid tissue in the lung and gliosis in the frontal areas of the brain. We also observed that IL-22 knock-out increased pulmonary and neurological inflammation severity. Animals exposed to DE and treated with AT-RvD1 displayed reduced lung pathology severity and gliosis. Our data demonstrate that DE exposure contributes to neurological inflammation and that IL-22 is crucial to effective tissue repair processes. Our data further suggest that AT-RvD1 may have potential as a novel therapeutic for organic dust exposure-induced, immune-mediated pulmonary and neurological inflammation, improving outcomes of those with these diseases.

KEYWORDS

agriculture dust, lung inflammation, neuroinflammation, omega-3 fatty acids, SPM, aspirin-triggered resolvin D1, AT-RvD1

Introduction

The Centers for Disease Control and Prevention ranked chronic lower respiratory diseases (CLRD) as a leading cause of death in the United States (US) with 147,367 deaths in 2023 (1). Chronic inflammatory lung diseases have also been linked to neuroinflammation and the development of neurodegenerative diseases such as Alzheimer's (2–5). In 2023, 6.7 million people were reported as diagnosed and living with Alzheimer's disease in the US, and estimates project that number to increase to 14 million people by 2060 (1, 6). CLRDs include chronic obstructive pulmonary disease (COPD), asthma, and allergies (7–9). Particulate matter (PM) exposure is a significant occupational hazard for agriculture workers, with organic dust exposure strongly linked to occupational-associated CLRDs (10–13). Organic dusts contain a variety of particulate matter (PM) sizes from 2.5 µm to 0.25 µm, microbes, and many immunogenic compounds such as microbial components, endotoxins, and metals that contribute to the pulmonary immune response (14, 15).

Our laboratory has extensively characterized the pulmonary immunological and pathological effects of organic dust exposure in a murine model of repetitive dust exposure, but the secondary neuroinflammatory effects of inhaled organic dust exposure have not been explored (10, 16–19). Inhaled PM exposure has been recently linked to an increased risk of developing dementia, with the greatest risk being associated with agricultural organic dust exposure over all other PM exposures (20). COPD patients have documented increases in depressive symptoms, confusion, memory loss, and mental functional decline as their disease progresses (21, 22). A study conducted by the CDC analyzed comorbidities of 8,094 patients in resident care facilities diagnosed with CLRDs including chronic bronchitis, emphysema, and COPD (23). This study found that 51.4% of patients with one more CLRD also presented with Alzheimer's disease or dementia ($p < 0.001$), 27.4% were diagnosed with depression ($p=0.012$), 7.7% were diagnosed with multiple sclerosis, Parkinson's disease, or epilepsy ($p= 0.020$), and 11.7% presented with other mental disorders ($p=0.007$) (23). Overall, the authors found that 64.9% of patients with more CLRD experienced a mental or behavioral health disorder, and 11.6% experienced a nervous system disorder (23). Agriculture workers often experience high levels of mental disorders including anxiety (males: 22% females: 39%, total: 31%) and depression (males: 35%, females: 42%, total: 39%) (24). Additionally, air pollution exposure has been linked to neurological inflammation in murine models but has not been assessed in the specific context of agricultural organic dust exposure (3, 25, 26).

Both COPD and Alzheimer's are incurable, progressive, and ultimately fatal diseases with severe symptoms that reduce patients' quality of life during the progression of disease (25, 27–29). The search for therapies that combat these diseases is thus at the forefront of immunotoxicological research. Omega-3 fatty acid metabolites termed specialized pro-resolving mediators (SPMs), have been proposed as exogenous therapies for a variety of inflammatory diseases, suggesting they may be effective in reducing inflammation in a repetitive organic dust exposure model of pulmonary and neurological inflammation (30, 31). Aspirin-Triggered Resolvin D1 (AT-RvD1), a SPM, has demonstrated restorative functions in pulmonary and neuroinflammation models (32–35). Specifically, the aspirin-triggered 17(R)-RvD1 epimer has shown increased stability and pharmacological efficacy compared to its 17(S)-RvD1 epimer in murine models of acute lung injury and a chronic organic dust exposure-mediated pulmonary inflammation murine model (32, 36–38).

Interleukin-22 (IL-22), an interleukin-10 (IL-10)-family cytokine has been implicated in inflammation modulation, tissue repair, and antimicrobial defense (39). Murine models investigating the inflammatory consequence of IL-22 knock-out in infection, allergy, and organic dust exposure models have demonstrated increased disease severity in animals lacking IL-22 (40–45). We recently demonstrated that whole-body IL-22 knock-out mice exhibit increased pathology severity, cellular infiltrate counts, pro-

inflammatory cytokine production, and altered tissue pathology following repetitive organic dust exposure (45). We aimed to investigate the link between attenuation of IL-22 and the tissue repair functions of AT-RvD1 in an IL-22 knock-out mouse model repetitively exposed to organic dust exposure.

We explored the link between inhaled organic dust exposure-induced pulmonary and neurological inflammation via a mouse model repetitively exposed to aqueous agriculture organic dust extract (DE). We also aimed to investigate the SPM AT-RvD1 as an exogenous therapy for pulmonary and neurological inflammation utilizing an IL-22 knock-out transgenic mouse model of severe pulmonary inflammation to explore its role in modulating lung-brain axis inflammation. To investigate our hypotheses, we evaluated the inflammatory response to organic dust exposure and the immune modulation of AT-RvD1 in an IL-22 knock-out model repetitively exposed to DE through evaluation of lung immune cell infiltrates, bronchoalveolar lavage fluid (BALF) and lung tissue cytokines, lung pathology, brain microglia quantification, and transcript evaluation in lung and brain tissue via RNAscope technology.

Materials and methods

Dust extract preparation

Dust was collected from hog confinement facilities in the Midwest, United States from surfaces at least 1 meter off the ground to represent the respirable fraction. Dust aliquots were stored at -20°C until use. Dust extracts were prepared as previously described (18, 46). Briefly, whole dust was combined with Hank's balanced saline solution (HBSS) (HyClone Laboratories) at a ratio of 1 g dust to 10 mL HBSS on a magnetic stir plate for 1 hour at room temperature. The resulting mixture was centrifuged at 2500 rpm for 20 minutes at 4°C. The supernate was collected, while the pellet was discarded. Supernate was transferred to a new tube and centrifuged again at 2500 rpm for 20 minutes at 4°C. Supernate was collected and filtered through 0.22 µm syringe filters to produce 100% dust extract (DE) and stored at -20°C. The resulting extract contains predominantly gram-positive bacterial components, endotoxins, and trace metals (15). Complete analysis of dust extract can be found at Online Repository Methods at www.jacionline.org (15).

Animal husbandry and care

All animal protocols were reviewed and approved by the Institutional Animal Care and Use Committee (Protocol Number 2887). C57BL/6J (WT) and whole-body IL-22 knock-out [C57BL/6-*Il22*$^{tm1.1(icre)Stck}$/J] (KO) (Jackson Labs) mice aged 8-12 weeks were housed in the Colorado State University Painter Facility in a specific pathogen-free environment with free access to standard mouse feed and water. Three pairs of KO animals were purchased to establish a breeding colony of IL-22cre x IL-22cre that produced all experimental animals. Animals from the original breeding pairs and all offspring were genotyped through TransnetYX (Memphis, TN) genotyping PCR service to ensure accurate genotypes. WT mice were purchased directly from Jackson Laboratories, age and sex matched to KO mice. Purchased mice were acclimated for at least 7 days before performing any procedures.

In vivo repetitive DE exposure and AT-RvD1 treatment model

Mice were intranasally (i.n.) instilled with 50 µl 12.5% DE or sterile saline 5 days/week for 3 weeks under light isoflurane sedation. The concentration of DE was previously determined by a dose-response study, which was found to elicit a strong pulmonary inflammatory response without the risk of mortality (47). Sedation for instillations was achieved using a SomnoSuite Small Animal Anesthesia System (Kent Scientific Corporation) fitted with a small animal anesthesia box. Animals were placed into the box with a flow rate of 100 mL/minute at 2.0-3.0% anesthesia. Animals were removed for instillations once breathing appeared slowed and even. Animals were held in a supine position and 50 µl of the appropriate exposure was loaded into a pipette tip and deposited at the tip of the animal's nose one drop at a time to allow natural inhalation. Afterwards, animals were returned to their enclosures in a supine position to encourage recovery and monitored for several minutes to ensure return of normal behaviors. AT-RvD1 treated mice were administered intraperitoneal (i.p) injections of 50 µl of 250 ng AT-RvD1 or 5% ethanol (EtOH) (AT-RvD1 vehicle) in sterile saline either once per week after the 5th DE instillation (weekly, for a total of 3 injections) or 5 times per week (daily, for a total of 15 injections) (Figures 1A, B). Dosages and controls were determined based on previously published data and a dose-response pilot study (data not shown) (32, 33, 48, 49). Animals were allowed to recover for 72 hours past-last DE instillation and AT-RvD1 injection before sacrifice.

Animal sacrifice and sample collection

Animals were euthanized in accordance with the American Veterinary Medical Association guidelines by isoflurane overdose immediately followed by cervical dislocation, 72 hours following the final DE instillation and AT-RvD1 injection. Bronchoalveolar lavage fluid (BALF) was obtained by inserting a 25G catheter into the trachea, tying it off with suture, and lavaging the lungs three times with 1 mL of ice-cold phosphate-buffered saline (PBS) (HyClone Laboratories) for each wash. The first wash was collected in one 5 mL FACS tube while washes two and three were collected in a second 5 mL FACS tube. Both tubes were centrifuged at 300 x g for 8 minutes to pellet the cells. The supernatant fraction from wash 1 was aliquoted into a separate tube and stored at -80°C for cytokine analysis by enzyme-linked immunosorbent assay (ELISA). The supernates from washes two and three were discarded, and cell pellets from both tubes were combined with 400 µl of red blood cell lysis buffer (Life Technologies

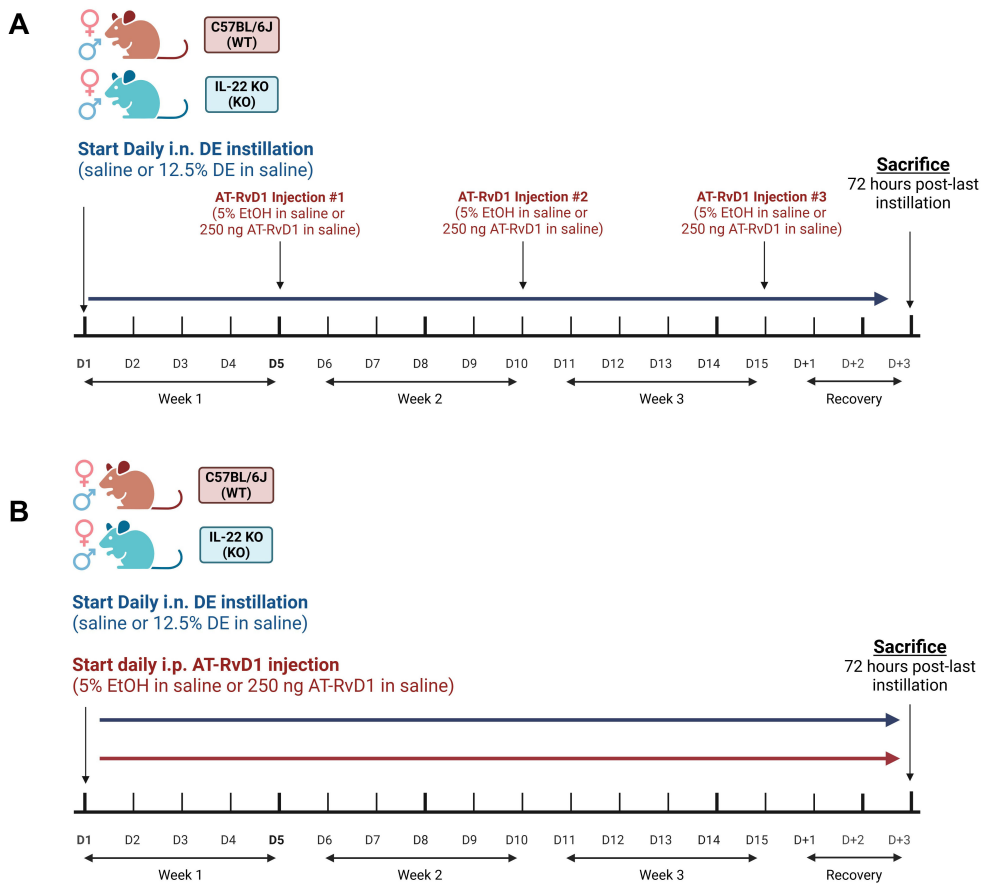

FIGURE 1
AT-RvD1 dosing strategies in WT and IL-22 KO mice. **(A)** once weekly AT-RvD1 dosing strategy timeline; WT and KO animals were instilled i.n. with 12.5% DE 5 days/week for 3 weeks and treated with 250 ng AT-RvD1 i.p. once/week for 3 weeks, **(B)** Once daily AT-RvD1 dosing strategy timeline; WT and KO animals were instilled i.n. with 12.5% DE 5 days/week for 3 weeks and treated with 250 ng AT-RvD1 i.p. 5 days/week for 3 weeks. Created with BioRender.com.

Corporation), placed on ice for 5 minutes, then centrifuged at 300 x g for 8 minutes at 4°C. The supernatant fraction was discarded, and the cell pellets were resuspended with 200 µL of PBS. A 10 µl aliquot of the cell suspension was then collected for counting using a Countess 3 FL automatic cell counter to generate total cell infiltrate values. The cell suspensions were diluted with PBS to achieve a concentration of $1x10^6$ cells/mL. 200 µl of the final cell suspension was then added to a Thermo Cytospin 4 cytocentrifuge and centrifuged at 600 rpm for 5 minutes. Slides were dried overnight for further staining and analysis. The left lobes of the lungs were tied off with suture, removed, placed in 800 µl of RNAlater (Invitrogen), and stored at -80°C until use. The right lung lobes were extracted along with the heart and tracheal tissue, then inflated with 10% neutral-buffered formalin (NBF) (Cancer Diagnostics Inc.) before hanging under 20 cm of pressure and submerged in 10% NBF overnight. They were then transferred to cassettes and stored in 10% NBF for at least 48 hours before further processing. Brains were extracted *en bloc* and immediately fixed whole in tissue cassettes in 10% NBF for at least 48 hours before further processing. All tissues were submitted to the Colorado State University Veterinary Diagnostic Laboratory Experimental Pathology Facility (EPF) for paraffin embedding and sectioning at 5 µm.

Cellular infiltrate analysis

Staining was performed on dried slides using a Volu-Sol dip-stain kit, with methanol as the fixative, and eosin and methylene blue (Volu-Sol) as the differential stains. Slides were imaged at 20X magnification using an Olympus BX35 microscope and cellSense software version 4.1. Differential counts were performed by counting 300 cells on each image to evaluate macrophages, neutrophils, eosinophils, and lymphocytes, assisted by QuPath version 0.5.1.

Cytokine quantification

Bronchoalveolar lavage fluid (BALF) was collected, processed, and stored as previously described above. Left lung lobes in RNAlater were homogenized with lysis buffer containing PBS, 1X RIPA lysis buffer (Thermo Scientific, Cat#: J62524.AE), and 1X proteinase inhibitor cocktail (Thermo Scientific, Cat#: 1861279) at a ratio of 50 mg tissue to 1 mL buffer. A Bead Mill 24 bead homogenizer was used to break up the tissues (speed: 5.00, time:

0:05, cycles: 3, duration: 0:03). The samples were then incubated on ice for 30 minutes, with agitation every 10 minutes. Homogenate aliquots were stored at -80°C until use. Cytokine protein concentrations in BALF and lung tissue were quantified using sandwich ELISAs. Kits were purchased from DuoSet (R&D Systems) and used according to the manufacturer's recommendations with the modification of capture antibody diluted in BupH Carbonate-Bicarbonate Buffer (Voller's Coating Buffer, Thermo Scientific). High-binding half-well 96-well plates (Greiner Biotech) were coated with manufacturer-specified capture antibody concentrations and incubated overnight at room temperature before progression of assay. All washes were performed using a Tecan HydroFlex™ plate washer. After completion of the assay, plates were read on a FLUOstar Omega spectrophotometer at 450 nm using Omega software version 5.7. Concentration values were calculated from standards using a four-parameter fit model in Omega MARS Software Version 4.00.

Lung histopathology

Whole right lung coronal sections, collected as previously described above, were stained with hematoxylin and eosin (H&E) following deparaffinization and rehydration with xylene and graded EtOH solutions (xylene, 100% EtOH, 95% EtOH, 80% EtOH, 50% EtOH, and finally 1X PBS). Slides were scanned at 40X on a Vectra Polaris scanning microscope. Images of lungs from animals administered weekly AT-RvD1 injections were blinded and manually scored using a well-established semiquantitative scoring method (19, 32, 45, 46, 50). Images from animals administered daily AT-RvD1 injections were imported into VisioPharm version 2023.09.3.15043 x64 and processed through an artificial intelligence (AI) workflow for quantitative assessment of alveolar space, alveolar septa thickness, peribronchiolar inflammation, perivascular inflammation, total alveolar septa nuclei, and percentage of inducible bronchus-associated lymphoid tissue (iBALT) formations relative to tissue area. AI quantification was performed on the whole lung tissue with output measurements including area, percentages of parameters to total tissue area or total parameter counts. VisioPharm is one of the leading AI histopathology analysis software available. Our workflow and applications were designed, annotated, trained, and verified by a board-certified veterinary anatomic pathologist to identify our desired readouts and ensure accurate results. The workflow is then trained through a large set of sample images by a board-certified veterinary anatomic pathologist where structures are identified by the software and confirmed by the pathologist, allowing the software to "learn" how structures are organized and are identified in the experimental images. Briefly, the workflow consisted of multiple stepwise applications of increasing specificity, starting with identification of the lung tissue, followed by identification of airways and vessels, then inflammation and iBALT, and finally identification of airway epithelial cells and alveolar nuclei. During each step of the workflow, the results are confirmed manually to ensure accurate detection of structures. All parameters are normalized to tissue area to mitigate size and artifact skewing.

Immunofluorescence

Whole brain sagittal paraffin embedded tissue sections, as previously described above, were deparaffinized by baking slides at 60°C for 20 minutes, followed by rehydration through an EtOH gradient (xylene, 50% xylene/50% EtOH, 100% EtOH, 95% EtOH, 70% EtOH), and then incubated in 1.0 M Tris buffered saline (TBS). Antigen retrieval was achieved using 1 nM EDTA buffer with 0.05% Tween20, pH 8.0 at 95°C for 20 minutes in a Biocare Medical Decloaking Chamber™ NxGen (Biocare Medical). Tissues were washed three times for 10 minutes each with 0.05M TBS and blocked using 2% donkey serum in 0.2% Triton-X in 1.0 M TBS for 1 hour at room temperature. Microglia were identified using rabbit anti-ionized calcium binding adaptor molecule 1 (Iba1) (1:1000; Abcam, Cat #: ab178846) diluted in 1.0 M TBS and incubated overnight at 4°C. Tissues were then washed four times for 10 minutes each with 0.05 M TBS. A goat anti-rabbit Alexa Fluor 647 secondary antibody (Invitrogen, Cat#: A21244) diluted 1:500 in 2% donkey serum in 1.0 M TBS, was applied and incubated for 1 hour at room temperature. Sections were washed three times for 10 minutes each with 0.05 M TBS. Nuclear staining was achieved by incubation with Hoechst 33342, diluted 1:2000 in PBS (Invitrogen, Cat #: H3570), for three minutes, then washed three times for 10 minutes each with 0.05 M M TBS. ProLong Diamond Antifade Mountant (Fisher Scientific, Cat #: P36970) was then applied before mounting with glass coverslips. Slides were kept at room temperature, protected from light, for 24 – 48 hours to cure mounting medium, then stored at 4°C in the dark prior to imaging. Stained sections were scanned at 40X using a Vectra Polaris microscope, and the number of microglia per area of each brain region of interest were quantified using QuPath Version 0.5.1. All sections were imaged on the same day with the same exposure settings for each channel.

RNAscope

RNAscope® assays were performed according to the formalin-fixed, paraffin-embedded (FFPE) tissue protocol provided in the RNAscope™ Multiplex Fluorescent Reagent Kit v2 Assay Manual (Document Number: UM 323100). Mouse lung and brain sections previously described above were utilized, with 3 animals per sex, per treatment condition, per genotype selected. Probes for IL-1β (Cat #: 316891-C3), CXCL10 (Cat #: 408921-C3), IL-10 (Cat #: 317261-C2), TGF-β (Cat #: 407751), and AREG (Cat #: 430501) were purchased from Advanced Cell Diagnostics, Inc. TSA Vivid Fluorophore dyes 570 (Cat #: 323272) and 650 (Cat #: 232273) were purchased from Advanced Cell Diagnostics, Inc. and diluted in TSA buffer 1:1500 (Cat #: 322809). Opal Polaris 780 Fluorophore Reagent Pack was purchased from Akoya Biosciences (Cat #: FP1501001KT). TSA-DIG was diluted 1:1500 in TSA buffer for lung sections and 1:750 for brain sections. Opal Polaris 780 Fluorophore was diluted 1:500 in Antibody Diluent/Block (Akoya Biosciences, Cat #: ARD1001EA) for lung sections and 1:200 for brain sections. Positive control slides using RNAscope™ 3-plex

positive control probes (CAT #: 320881) and negative control slides using RNAscope™ 3-plex negative control probes (Cat#: 320871) were utilized to validate the assay and results. After completion of the RNAscope® protocol, sections were incubated with RNAscope® DAPI (Advanced Cell Diagnostics, Inc.) for 30 seconds, then mounted on glass coverslips with ProLong Diamond Antifade mounting medium (Invitrogen). The mounted sections were kept at room temperature, protected from light, for 24–48 hours to cure mounting medium, before being stored at 4°C until imaging. Slides were scanned at 40X using a Vectra Polaris microscope, with all sections imaged on the same day using the same exposure settings for each channel. QuPath Version 0.5.1 was used according to manufacturer protocols to detect the cell nuclei and quantify subcellular dots per nucleus for the entirety of the lung tissue and for each of the brain regions of interest.

Statistical analysis

All statistical and graphical analyses were performed using GraphPad Prism Version 10. Outliers were tested for and removed from the datasets using ROUT analysis with Q=1%. Statistical significance was determined by performing 3-way ANOVA analyses with Benjamini, Krieger and Yekutieli *post-hoc* analysis for pairwise comparisons to reduce false discovery rate. A p-value of less than or equal to 0.05 was used to determine significance and a p-value of less than or equal to 0.1 was considered a trend. Individual animals are represented by a single symbol on figures, with filled shapes representing male animals and unfilled shapes representing female animals. On figures, significance is denoted by, * = $p \leq 0.05$; ** = $p \leq 0.01$; *** = $p \leq 0.001$; **** = $p \leq 0.0001$.

Results

IL-22 KO alters lung immune cell trafficking and weekly AT-RvD1 administration reduces cellular infiltration in IL-22 KO mice following repetitive organic dust exposure

We have previously demonstrated that DE exposure leads to increased infiltration of immune cells into the airways (19, 32, 51). One well-established mechanism of AT-RvD1 is its ability to modify immune cell recruitment to sites of infection and injury (49). We aimed to establish an effective dosing strategy to assess the therapeutic applications of AT-RvD1 in a model of repetitive ODE. WT and IL-22 KO mice were instilled i.n. with 50 µl of either 12.5% DE in sterile saline or sterile saline for 5 days per week for 3 weeks (15 total installations) and injected i.p. with 50 µl of either 250 ng AT-RvD1 in sterile saline or 5% EtOH (AT-RvD1 carrier) in sterile saline once per week following the 5th DE instillation each week (3 total injections) (Figure 1A). To determine the impact of AT-RvD1 treatment on immune cell recruitment following DE, we examined cellular infiltration into the airway via BALF cellular analysis (Figures 2A–E) and lung histopathology (Figures 3A–D).

Upon analysis of BALF cellular infiltrates, we observed an increase in the total number of cellular infiltrates in both WT (p=0.0011) and KO (p<0.0001) mice exposed to DE compared to saline controls (Figure 2A). Additionally, we observed a trend of increased total cells in KO mice exposed to DE compared to WT mice exposed to DE (p=0.0702) (Figure 2A). KO mice exposed to DE and treated with AT-RvD1 exhibited reduced total cell counts compared to KO mice exposed to DE and treated with saline (p=0.0265) (Figure 2A). Macrophage differential counts revealed increased influx in WT (p=0.0162) and KO (p=0.0015) mice exposed to DE compared to WT and KO mice exposed to saline, respectively (Figure 2B). We also observed a trend between KO mice exposed to DE and WT mice exposed to DE (p=0.0966) (Figure 2B). KO mice exposed to DE and treated with AT-RvD1 demonstrated significantly reduced macrophage differential counts compared to KO mice exposed to DE and treated with AT-RvD1 (p=0.0457) (Figure 2B). We did not observe any significant differences or trends in the number of neutrophils, regardless of exposure or treatment condition (Figure 2C). Eosinophil differential counts revealed a decrease in the number of eosinophil influx in KO mice exposed to DE and treated with AT-RvD1 compared to KO mice exposed to DE and treated with saline (p=0.0180) (Figure 2D). We also observed elevated trafficking of lymphocytes in WT (p=0.0013) and KO (p<0.0001) mice exposed to DE compared to saline exposed controls as well as significantly increased lymphocyte counts in KO mice exposed to DE compared to WT mice exposed to DE (p=0.0454) (Figure 2E).

We also examined lung pathology of mice injected with 250 ng AT-RvD1 once per week to assess the effectiveness of AT-RvD1 at reducing DE-induced lung pathology. We evaluated inducible bronchus associated lymphoid tissue (iBALT), peribronchiolar inflammation, and alveolar inflammation using a semiquantitative scoring method previously utilized in our laboratory (19, 32, 50, 52, 53). Statistical analysis revealed a significant main effect of DE exposure in all three parameters evaluated: iBALT (p=0.0002), peribronchiolar inflammation (p<0.0001) and alveolar inflammation (p<0.0001) (Figures 3B–D). However, on *post-hoc* analysis, we observed no statistically significant differences or trends between AT-RvD1 i.p. and saline i.p. treatment groups (Figures 3B–D). Interestingly, we observed a similar pattern in all parameters evaluated. We found a significant increase in the mean inflammatory score of iBALT in both WT (p=0.0446) and KO (p=0.0025) animals exposed to DE compared to saline-exposure controls (Figure 3B). Additionally, we observed a significantly increased peribronchiolar inflammation in WT (p=0.0064) and KO (p=0.0005) animals exposed to DE compared to saline-exposed controls (Figure 3C), as well as a significant increase in the mean score for alveolar inflammation in KO animals exposed to DE compared to saline-exposure controls (p=0.0004) and a trend in WT animals exposed to DE compared to saline-exposure controls (p=0.0596) (Figure 3D). We also did not observe any significant changes in mean pathological scores of WT compared to KO animals regardless of exposure or treatment group.

Following our observations of no statistically significant changes in animals exposed to DE and treated with AT-RvD1 once weekly (Figures 3A–D), we developed a 5 day/week AT-RvD1

10.3389/fimmu.2024.1495581

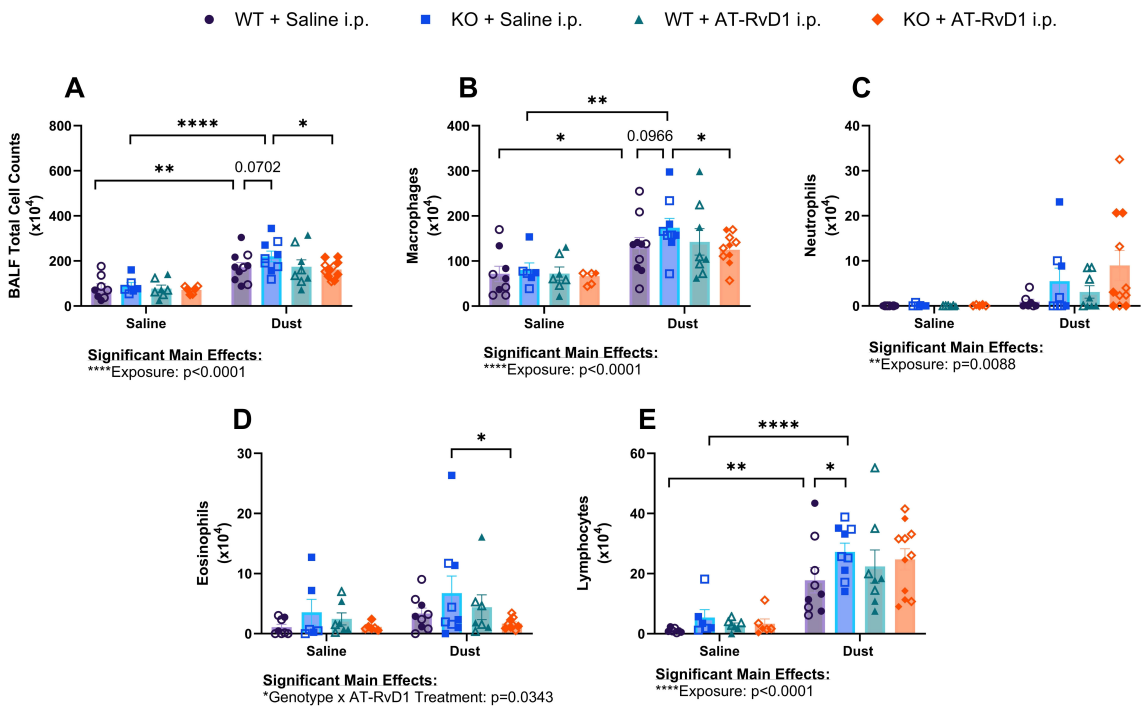

FIGURE 2
Impacts of DE and AT-RvD1 on BALF immune cellular infiltrates in WT and IL-22 KO animals. WT and KO animals were instilled i.n. with 12.5% DE 5 days/week for 3 weeks and treated with 250 ng AT-RvD1 i.p. once/week for 3 weeks. **(A)** total cell counts, **(B)** macrophages, **(C)** neutrophils, **(D)** eosinophils, **(E)** lymphocytes. 3 way ANOVA with Benjamini, Krieger and Yekutieli *post-hoc* analysis, error bars = SEM; * = $p \leq 0.05$; ** = $p \leq 0.01$; **** = $p \leq 0.0001$. Sample sizes: WT Saline i.n. + Saline i.p (3 female/3 male), WT Saline i.n. + AT-RvD1 i.p (3 female/3 male), WT Dust i.n. + Saline i.p (5 female/5 male), WT Dust i.n. + AT-RvD1 i.p (4 female/4 male), KO Saline i.n. + Saline i.p (3 female/3 male), KO Saline i.n. + AT-RvD1 i.p (3 female/3 male), KO Dust i.n. + Saline i.p (5 female/4 male), KO Dust i.n. + AT-RvD1 i.p (6 female/5 male).

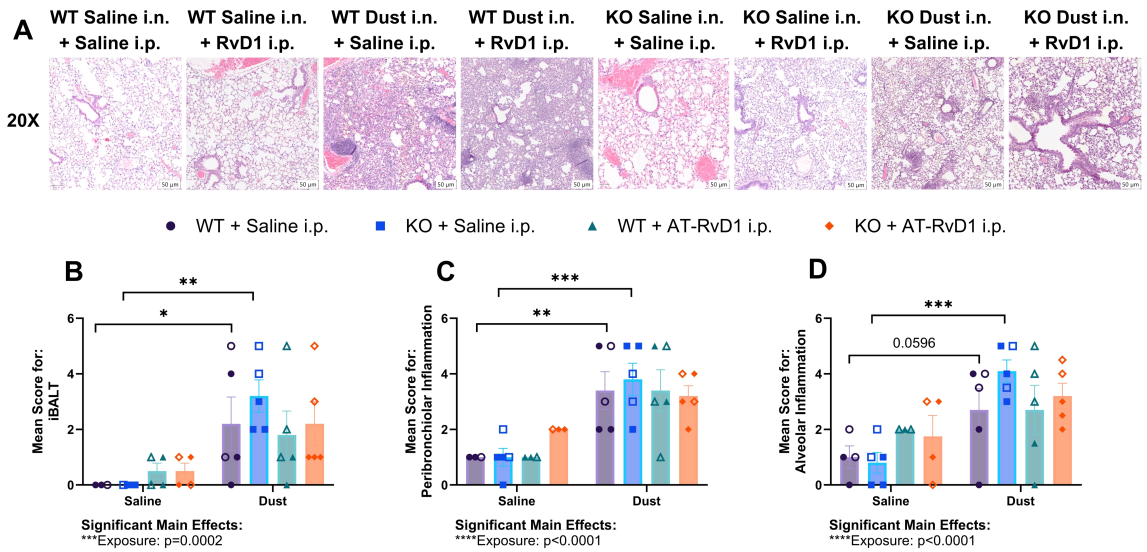

FIGURE 3
AT-RvD1 administration once weekly does not improve lung pathology. WT and KO animals were instilled i.n. with 12.5% DE 5 days/week for 3 weeks and treated with 250 ng AT-RvD1 i.p. once/week for 3 weeks. **(A)** representative images at 20X magnification, **(B)** mean inflammatory score for iBALT, **(C)** mean inflammatory score for peribronchiolar inflammation, **(D)** mean inflammatory score for alveolar inflammation. Scale bar = 50 µm. 3 way ANOVA with Benjamini, Krieger and Yekutieli *post-hoc* analysis, error bars = SEM; * = $p \leq 0.05$; ** = $p \leq 0.01$; *** = $p \leq 0.001$. Sample sizes: WT Saline i.n. + Saline i.p (2 female/2 male), WT Saline i.n. + AT-RvD1 i.p (2 female/2 male), WT Dust i.n. + Saline i.p (2 female/3 male), WT Dust i.n. + AT-RvD1 i.p (3 female/3 male), KO Saline i.n. + Saline i.p (3 female/3 male), KO Saline i.n. + AT-RvD1 i.p (2 female/2 male), KO Dust i.n. + Saline i.p (3 female/3 male), KO Dust i.n. + AT-RvD1 i.p (3 female/3 male).

10.3389/fimmu.2024.1495581

injection regimen, which we found yielded more significant therapeutic efficacy, through histopathology resolution, and was thus employed as our model for further analysis of the pulmonary and neurological inflammatory response to DE. Briefly, WT and IL-22 KO mice were instilled i.n. with 50 µl of either 12.5% DE in sterile saline or sterile saline for 5 days per week for 3 weeks, and then injected i.p. with 50 µl of either 250 ng AT-RvD1 in sterile saline or 5% EtOH (AT-RvD1 carrier) in sterile saline 5 days per week for 3 weeks (Figure 1B).

Our analysis of lung histopathology via VisioPharm AI applications revealed an increase in the percentage of iBALT relative to lung tissue area in both WT (p=0.0014) and KO mice (p<0.0001) exposed to DE (Figure 4B). Interestingly, we also observed a significant increase in iBALT percentage in KO mice compared to WT mice exposed to DE (p=0.0002) (Figure 4B). Additionally, KO mice exposed to DE and treated with AT-RvD1 displayed a significant decrease in iBALT percent of lung tissue compared to KO mice exposed to DE and treated with saline (p<0.0001) (Figure 4B). Furthermore, we discovered significant sex differences in the iBALT percentages displayed by both WT and KO animals. We found that female animals exposed to DE and treated with saline exhibited a significantly higher iBALT percentage than male animals exposed to DE and treated with saline in both WT (p<0.0001) and KO (p<0.0001) animals (Figures 4C, D). Additionally, both WT (p=0.0021) and KO (p<0.0001) female animals exposed to dust and treated with AT-RvD1 displayed significantly reduced iBALT

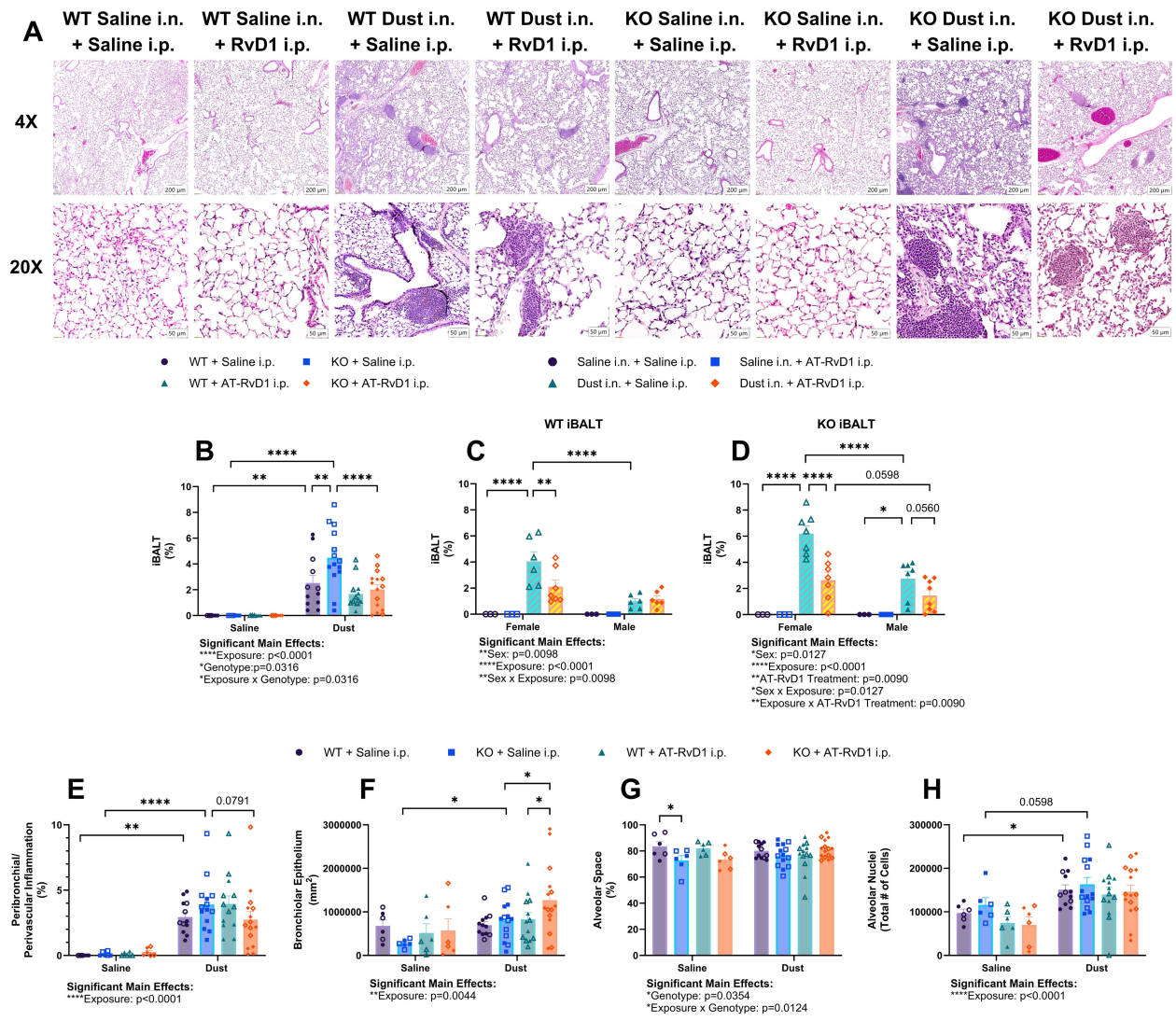

FIGURE 4
AT-RvD1 treatment daily reduces iBALT in animals exposed to DE. WT and KO animals were instilled i.n. with 12.5% DE 5 days/week for 3 weeks and treated with 250 ng AT-RvD1 i.p. 5 days/week for 3 weeks. **(A)** representative images at 4X and 10X magnification, **(B)** iBALT percentage in all animals, **(C)** iBALT percentage in WT animals by sex, **(D)** iBALT percentage in KO animals by sex, **(E)** combined peribronchiolar and perivascular inflammation percentage in all animals, **(F)** bronchiolar epithelium area, **(G)** alveolar space percentage, **(H)** total alveolar nuceli. Scale bar = 50 µm. 3 way ANOVA with Benjamini, Krieger and Yekutieli *post-hoc* analysis, error bars = SEM; * = $p \leq 0.05$; ** = $p \leq 0.01$; **** = $p \leq 0.0001$. Sample sizes: WT Saline i.n. + Saline i.p (3 female/3 male), WT Saline i.n. + AT-RvD1 i.p (3 female/3 male), WT Dust i.n. + Saline i.p (6 female/6 male), WT Dust i.n. + AT-RvD1 i.p (6 female/6 male), KO Saline i.n. + Saline i.p (3 female/3 male), KO Saline i.n. + AT-RvD1 i.p (3 female/3 male), KO Dust i.n. + Saline i.p (7 female/7 male), KO Dust i.n. + AT-RvD1 i.p (7 female/8 male).

compared to saline treated female animals (Figures 4C, D). Evaluation of peribronchiolar and perivascular inflammation percentage revealed a significant increase in both WT (p=0.0013) and KO (p<0.0001) mice exposed to DE (Figure 4E). We observed a trend of reduced peribronchiolar and perivascular inflammation in KO animals exposed to DE and treated with saline and KO mice exposed to DE and treated with AT-RvD1 (p=0.0791) (Figure 4E). Bronchiolar epithelium area in KO mice exposed to DE was significantly increased compared to KO mice exposed to saline (p=0.0474) and was further increased in KO mice exposed to DE and treated with AT-RvD1 compared to KO mice exposed to DE and treated with saline (p=0.0233) (Figure 4F). Bronchiolar epithelium area was also decreased in WT mice exposed to DE and treated with AT-RvD1 compared to KO mice exposed to DE and treated with AT-RvD1 (p=0.0353) (Figure 4F). We observed a significant decrease in alveolar air space in KO mice exposed to saline compared to WT mice exposed to saline (p=0.0301) (Figure 4G). Total alveolar nuclear counts were observed to be elevated in WT mice exposed to DE compared to WT mice exposed to saline (p=0.0377), with an observed trend of increased nuclei in KO mice exposed to DE compared to KO mice exposed to saline (p=0.0598) (Figure 4H).

Impacts of AT-RvD1 on lung inflammatory mediator production in WT and IL-22 KO mice during recovery following repetitive DE exposure

We have previously demonstrated that ODE in mice increases both pro- and anti-inflammatory cytokine production (32, 45, 47). In our recovery model, we found that after 15 DE instillations, mice displayed altered cytokine and inflammatory mediator production in the airway and pulmonary tissue compartments at the protein level (Figures 5A–F).

Evaluation of amphiregulin (AREG) concentrations in BALF showed that KO mice exposed to DE exhibited decreased concentrations compared to saline controls (p=0.0130) and that KO mice exposed to DE displayed a trend of decreased AREG concentrations compared to WT mice exposed to DE (p=0.0887) (Figure 5A). Concentrations of interleukin-10 (IL-10), a classic anti-inflammatory, pro-resolution cytokine was decreased in the BALF of WT mice exposed to DE compared to saline controls (p=0.0009) and a trend of decreased concentrations in KO mice exposed to DE compared to saline controls (p=0.0535) was also observed (Figure 5B). Transforming growth factor-β (TGF-β) concentrations in BALF did not yield any significant differences regardless of genotype or treatment groups, however we did observe a significant main effect of DE exposure (p=0.0021) (Figure 5C). In the tissue compartment, IL-10 was observed to be elevated in KO mice exposed to saline compared to WT mice exposed to saline (p=0.0003) and in KO mice exposed to DE compared to WT mice exposed to DE (p=0.0002). WT mice exposed to DE and treated with AT-RvD1 exhibited increased tissue IL-10 concentrations compared to WT mice exposed to DE and treated with saline (p=0.0070) (Figure 5D). AREG quantification in lung tissues of WT mice exposed to DE displayed increased concentrations compared to WT saline controls (p=0.0005) and were observed to be decreased in KO mice exposed to DE compared to WT mice exposed to DE (p=0.0051) (Figure 5E). We also observed a significant decrease in AREG concentrations in KO mice exposed to DE and treated with AT-RvD1 compared to WT mice exposed to DE and treated with AT-RvD1 (p<0.0001). Lung tissue TGF-β concentrations demonstrated a trend of increased concentrations in KO mice exposed to saline compared to WT mice exposed to saline (p=0.0533) and a significant increase in KO mice exposed to DE and treated with AT-RvD1 compared to WT mice exposed to DE and treated with AT-RvD1 (p<0.0003) (Figure 5F).

To evaluate mRNA transcript expression in animals exposed to DE and treated with AT-RvD1, we utilized RNAscope technology to visualize and quantify mRNA transcripts in whole lung tissue sections. We evaluated *areg*, *il10*, and C-X-C motif chemokine ligand 10 (*cxcl10*) transcripts in the alveolar and airway compartments to assess the recovery of IL-22 KO mice and the therapeutic impacts of AT-RvD1 and to assess the differences between alveolar and airway inflammatory markers (Figures 6A–E). In the alveolar compartment, we observed a significant increase in *areg* expression in KO mice exposed to saline and treated with AT-RvD1 compared to KO mice exposed to saline and treated with saline (p=0.0051) (Figure 6B). Assessment of *il10* expression in the alveolar compartment yielded no significant differences or trends of, regardless of DE exposure or AT-RvD1 treatment or genotype (Figure 6C). Expression of *cxcl10* in the alveolar compartments of KO mice exposed to DE displayed a trend of increased expression compared to saline-exposed KO controls (p=0.0559) (Figure 6D). In the airway compartment, we again observed a significant increase in *areg* expression in KO mice exposed to saline and treated with AT-RvD1 compared to KO mice exposed to saline and treated with saline (p=0.0187) (Figure 6F). We again observed no significant differences or trends of *il10* expression in the airway compartment (Figure 6G). Interestingly, we did observe significantly elevated *cxcl10* expression in WT mice exposed to DE compared to saline-exposed WT controls (p=0.0156), which was then revealed to be decreased in WT animals exposed to DE and treated with AT-RvD1 (p=0.0107) (Figure 6H).

Agriculture dust exposure is associated with gliosis and AT-RvD1 administration reduces neuroinflammation

Brains of WT and IL-22 KO animals exposed to DE and treated with AT-RvD1 were assessed for microglia proliferation via immunofluorescence for Iba1$^+$ cells. Cells were counted and represented as a function of the area of each brain region of interest: olfactory bulb, frontal cortex, isocortex, hippocampus, cerebellum, and hindbrain. The olfactory bulb was chosen due to its close proximity to the nasal passages and based upon previous investigations that have shown that intranasal instillations of other particulate matter sources result in gliosis in this region (54). The frontal cortex, isocortex, and hippocampus regions of interest were evaluated due to their functions involving memory and cognition, the decline of which is a hallmark of neurodegenerative disease. The cerebellum was chosen as it controls motor function, and changes in

10.3389/fimmu.2024.1495581

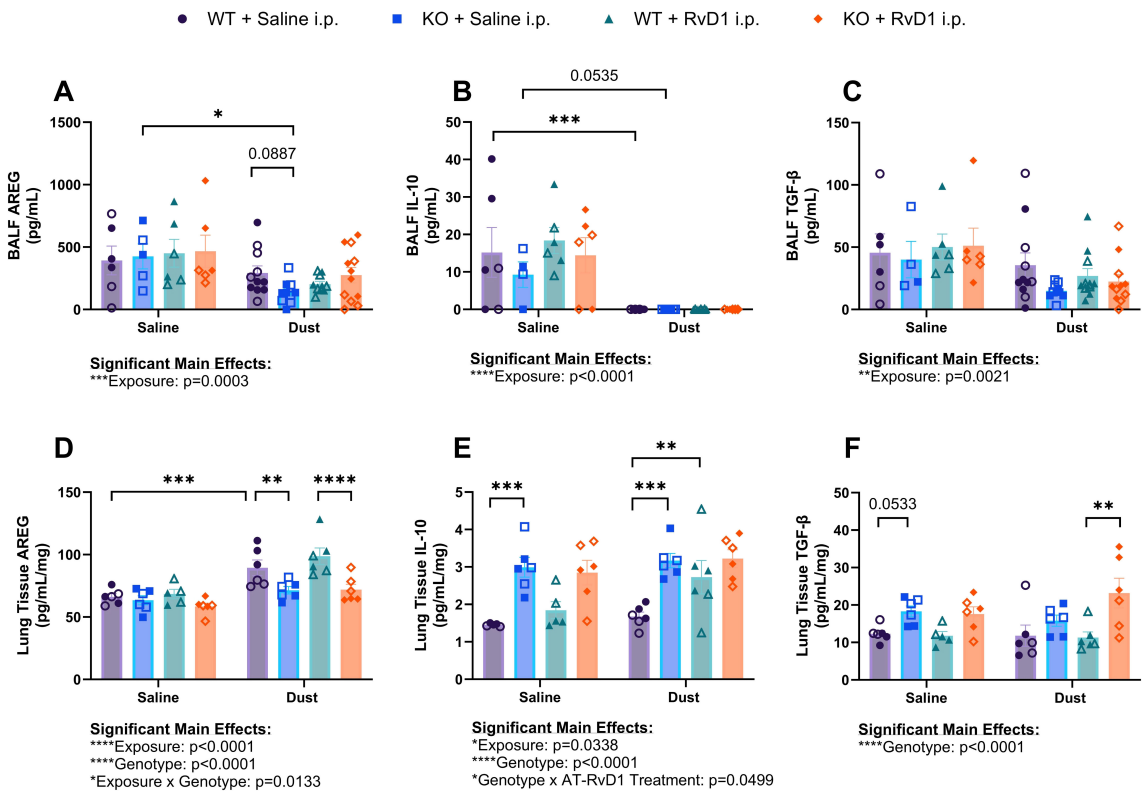

FIGURE 5
Effects of repetitive dust exposure and RvD1 treatment on bronchoalveolar lavage fluid (BALF) and lung tissue homogenate cytokines. WT and KO animals were instilled i.n. with 12.5% DE 5 days/week for 3 weeks and treated with 250 ng AT-RvD1 i.p. 5 days/week for 3 weeks. **(A)** amphiregulin (AREG) concentrations in BALF, **(B)** interleukin-10 (IL-10) concentrations in BALF, **(C)** transforming growth factor-β (TGF-β) concentrations in BALF, **(D)** AREG concentrations in lung tissue, **(E)** IL-10 concentrations in lung tissue, and **(F)** TGFβ concentrations in lung tissue. 3 way ANOVA with Benjamini, Krieger and Yekutieli *post-hoc* analysis, error bars = SEM; * = $p \leq 0.05$; ** = $p \leq 0.01$; *** = $p \leq 0.001$; **** = $p \leq 0.0001$. BALF sample sizes: WT Saline i.n. + Saline i.p (3 female/3 male), WT Saline i.n. + AT-RvD1 i.p (3 female/3 male), WT Dust i.n. + Saline i.p (6 female/6 male), WT Dust i.n. + AT-RvD1 i.p (6 female/6 male), KO Saline i.n. + Saline i.p (3 female/3 male), KO Saline i.n. + AT-RvD1 i.p (3 female/3 male), KO Dust i.n. + Saline i.p (7 female/7 male), KO Dust i.n. + AT-RvD1 i.p (7 female/8 male). Lung tissue sample sizes: WT Saline i.n. + Saline i.p (3 female/3 male), WT Saline i.n. + AT-RvD1 i.p (3 female/3 male), WT Dust i.n. + Saline i.p (3 female/3 male), WT Dust i.n. + AT-RvD1 i.p (3 female/3 male), KO Saline i.n. + Saline i.p (3 female/3 male), KO Saline i.n. + AT-RvD1 i.p (3 female/3 male), KO Dust i.n. + Saline i.p (3 female/3 male), KO Dust i.n. + AT-RvD1 i.p (3 female/3 male).

motor function can also be a pathological marker seen in neurodegenerative disease. The hindbrain region of the brain stem is the innervation site for the vagus nerve, which has been implicated in neuroinflammatory models of chronic lung inflammation (2). Increased numbers of Iba1$^+$ microglia were detected in areas involved in olfactory sensing and cognition including the olfactory bulb, frontal cortex, and isocortex in WT and KO mice (Figures 7A–F). KO mice displayed increased Iba1$^+$ microglia in the cerebellum, which is associated with motor function (Figures 7I, J). These data indicate that KO mice have altered responses to DE compared to WT controls, but that all mice regardless of genotype, experienced microgliosis in their brains following DE exposure. The increased number of microglia cells detected in brain tissue, is a hallmark sign of neuroinflammation and is a reliable marker for detecting neuroinflammatory processes (55–57).

Evaluation of the olfactory bulbs of animals exposed to DE revealed significant increases in the number of microglia in both WT ($p<0.0001$) and KO ($p=0.0109$) animals. We also observed an increase in the number of microglia in mice exposed to saline and treated with AT-RvD1 compared to with saline-exposed, saline-treated controls in both WT ($p=0.0002$) and KO ($p=0.0223$) genotypes (Figure 7B). Additionally, in the olfactory bulbs we observed a trend of increased microglia numbers in KO mice exposed to saline and treated with saline compared to their WT saline-exposed, saline-treated controls (0.0645) (Figure 7B). Animals exposed to DE and treated with AT-RvD1 displayed decreased numbers of Iba1+ cells compared to DE-exposed, saline-treated controls in both WT ($p=0.0090$) and KO ($p=0.0027$) genotypes (Figure 7B). In the frontal cortex, both WT ($p=0.0094$) and KO ($p=0.0009$) animals exposed to DE displayed increased microglia numbers (Figure 7D). Saline-exposed, AT-RvD1-treated KO animals also displayed increased numbers compared to saline-exposed, saline-treated KO animals ($p=0.0030$) (Figure 7D). DE-exposed, AT-RvD1-treated WT animals displayed a trend of decreased numbers compared to WT DE-exposed, saline-treated animals ($p=0.0633$) (Figure 7D). Microglia numbers in the isocortex revealed a similar pattern as the olfactory bulb, with both WT ($p=0.0051$) and KO ($p=0.0052$) animals exposed to DE and treated with saline demonstrating increased microglia numbers compared to their saline controls (Figure 7F). We did not observe any significant

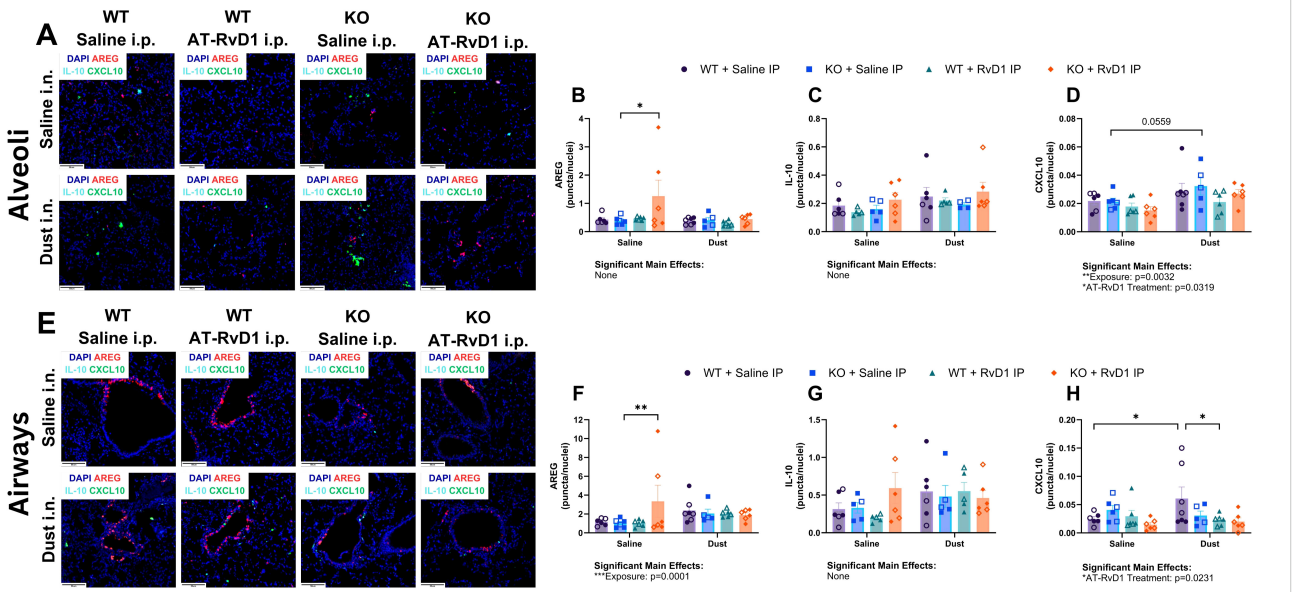

FIGURE 6
AT-RvD1 treatment reduces cxcl10 mRNA expression in WT animals exposed to DE. WT and KO animals were instilled i.n. with 12.5% DE 5 days/week for 3 weeks and treated with 250 ng AT-RvD1 i.p. 5 days/week for 3 weeks. **(A)** representative images of the alveolar compartment at 40X magnification, **(B)** areg expression, **(C)** il10 expression, **(D)** cxcl10 expression, **(E)** representative images of the airway compartment at 40X magnification, **(F)** areg expression, **(G)** il10 expression, **(H)** cxcl10 expression. Scale bar = 50 µm. 3 way ANOVA with Benjamini, Krieger and Yekutieli *post-hoc* analysis, error bars = SEM; * = $p \leq 0.05$; ** = $p \leq 0.01$. Sample sizes: WT Saline i.n. + Saline i.p (3 female/3 male), WT Saline i.n. + AT-RvD1 i.p (3 female/3 male), WT Dust i.n. + Saline i.p (4 female/3 male), WT Dust i.n. + AT-RvD1 i.p (3 female/3 male), KO Saline i.n. + Saline i.p (3 female/3 male), KO Saline i.n. + AT-RvD1 i.p (3 female/3 male), KO Dust i.n. + Saline i.p (3 female/3 male), KO Dust i.n. + AT-RvD1 i.p (3 female/3 male).

differences in the number of microglia in the hippocampus, regardless of exposure or treatment condition (Figures 7G, H). Additionally, animals treated with AT-RvD1 exhibited decreased microglia numbers compared to their saline-treated controls for both WT (p=0.0247) and KO (p=0.0117) animals (Figure 7F). Saline-exposed KO animals displayed increased microglia counts in their cerebellums compared to WT saline-exposed animals (p=0.0093) and increased counts in DE-exposed, saline treated KO animals compared to saline-exposed controls (p=0.0313) (Figures 7I, J). WT animals exposed to saline and treated with AT-RvD1 displayed increased microglia numbers compared to saline-exposed, saline-treated WT animals in the hindbrain (p=0.0253) (Figures 7K, L).

AT-RvD1 treatment alters brain transcript expression in animals exposed to DE

We again utilized RNAscope technology to visualize and quantify mRNA transcript expression in WT and KO animals exposed to DE and treated with AT-RvD1 using whole brain tissue sections to evaluate individual regions of interest. We evaluated *tgfb*, *il10*, and *il1β* transcripts in the olfactory bulb, frontal cortex, isocortex, hippocampus, cerebellum, and hindbrain (Figures 8A–X).

Transcript quantification in the olfactory bulb revealed a trend of increased *tgfb* expression between WT saline-exposed mice and KO saline-exposed mice (p=0.0929) (Figure 8B). Additionally, a trend was observed for increased *il10* transcription in KO mice exposed to DE and treated with AT-RvD1 compared to WT mice exposed to DE and treated with AT-RvD1 (p=0.0669) (Figure 8C). Finally, *il1b* was significantly increased in WT DE-exposed, AT-RvD1-treated mice compared to KO DE-exposed, AT-RvD1-treated mice (p=0.0228) (Figure 8D). In the frontal cortex, tgfb displayed a trend of increased transcription between WT and KO mice exposed to saline (p=0.0600), and a trend of reduced transcription between KO mice exposed to DE and KO mice exposed to saline (p=0.0560) (Figure 8F). Evaluation of the isocortex revealed significantly increased *tgfb* transcription between WT and KO saline-exposed mice (p=0. 0355), as well as significantly increased *tgfb* expression in KO mice exposed to DE compared to KO saline-exposed controls (p=0.0355) (Figure 8J). We also found that *il1b* expression was significantly reduced in WT DE-exposed, AT-RvD1 treated mice compared to KO DE-exposed, AT-RvD1 treated mice (p=0.0245) (Figure 8L). Transcript evaluation of the hippocampus revealed significantly increased *tgfb* expression in KO saline-exposed, saline-treated mice compared to WT saline-exposed, saline-treated mice (p=0.0049) (Figure 8N) and a significant decrease in *tgfb* expression in KO DE-exposed, saline-treated mice compared to KO saline-exposed, saline-treated controls (p=0.0198) (Figure 8N). We did not observe any significant differences or trends in the cerebellum. We did observe a change in the hindbrain, with *il1b* transcripts significantly decreased in WT saline-exposed and AT-RvD1 treated mice compared to WT saline-exposed, saline-treated (p=0.0252) (Figure 8X).

10.3389/fimmu.2024.1495581

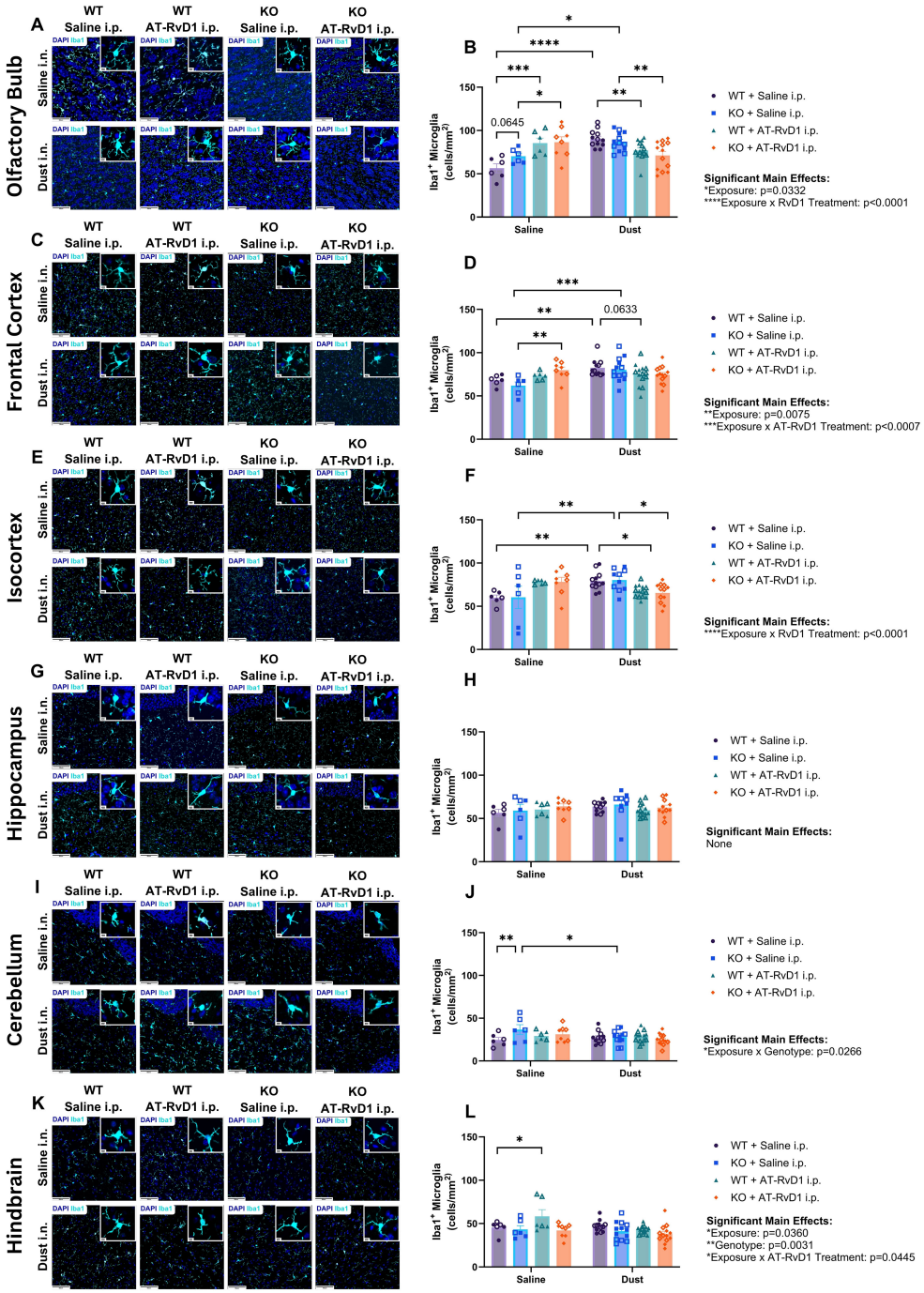

FIGURE 7
Gliosis is associated with agriculture dust exposure. WT and KO animals were instilled i.n. with 12.5% DE 5 days/week for 3 weeks and treated with 250 ng AT-RvD1 i.p. 5 days/week for 3 weeks. **(A)** representative images of the olfactory bulb at 40X magnification, **(B)** microglia counts in the olfactory bulb, **(C)** representative images of the frontal cortex at 40X magnification, **(D)** microglia counts in the frontal cortex, **(E)** representative images of the isocortex at 40X magnification, **(F)** microglia counts in the isocortex, **(G)** representative images of the hippocampus at 40X magnification, **(H)** microglia counts in the hippocampus, **(I)** representative images of the cerebellum at 40X magnification, **(J)** microglia counts in the cerebellum, **(K)** representative images of the hindbrain at 40X magnification, **(L)** microglia counts in the hindbrain. Scale bar = 50 µm and 5 µm. 3 way ANOVA with Benjamini, Krieger and Yekutieli *post-hoc* analysis, error bars = SEM; * = $p \leq 0.05$; ** = $p \leq 0.01$; *** = $p \leq 0.001$; **** = $p \leq 0.0001$. WT Saline i.n. + Saline i.p (3 female/3 male), WT Saline i.n. + AT-RvD1 i.p (3 female/3 male), WT Dust i.n. + Saline i.p (6 female/6 male), WT Dust i.n. + AT-RvD1 i.p (8 female/6 male), KO Saline i.n. + Saline i.p (3 female/3 male), KO Saline i.n. + AT-RvD1 i.p (4 female/4 male), KO Dust i.n. + Saline i.p (7 female/6 male), KO Dust i.n. + AT-RvD1 i.p (6 female/7 male).

10.3389/fimmu.2024.1495581

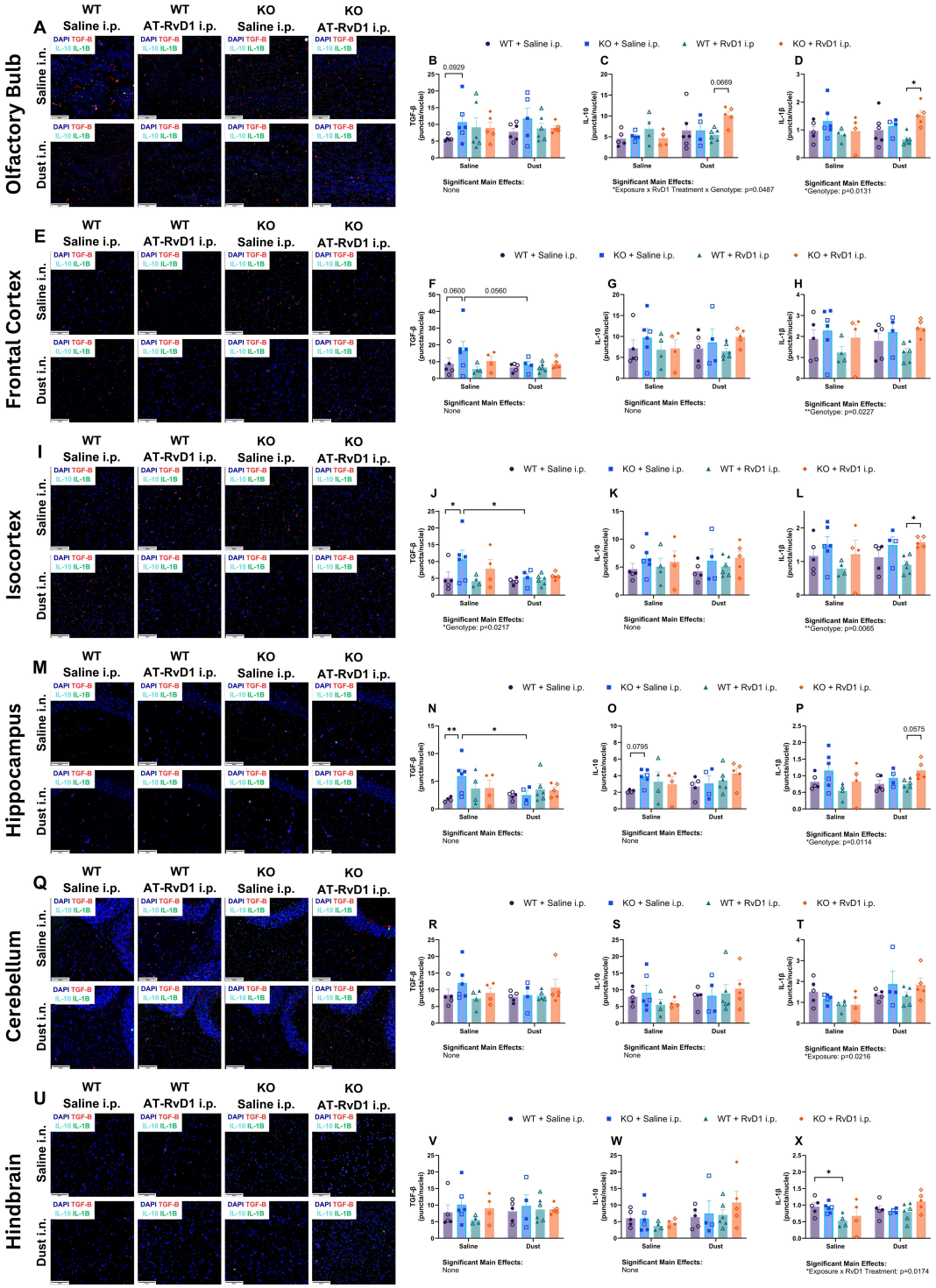

FIGURE 8
IL-22 knock-out alters brain mRNA transcripts in the presence of AT-RvD1 and DE. WT and KO animals were instilled i.n. with 12.5% DE 5 days/week for 3 weeks and treated with 250 ng AT-RvD1 i.p. 5 days/week for 3 weeks. **(A)** representative images of the olfactory bulb at 40X magnification, **(B)** tgfb expression in the olfactory bulb, **(C)** il10 expression in the olfactory bulb, **(D)** il1b expression in the olfactory bulb, **(E)** representative images of the frontal cortex at 40X magnification, **(F)** tgfb expression in the frontal cortex, **(G)** il10 expression in the frontal cortex, **(H)** il1b expression in the frontal cortex, **(I)** representative images of the isocortex at 40X magnification, **(J)** tgfb expression in the isocortex, **(K)** il10 expression in the isocortex, **(L)** il1b expression in the isocortex, **(M)** representative images of the hippocampus at 40X magnification, **(N)** tgfb expression in the hippocampus, **(O)** il10 expression in the hippocampus, **(P)** il1b expression in the hippocampus, **(Q)** representative images of the cerebellum at 40X magnification, **(R)** tgfb expression in the cerebellum, **(S)** il10 expression in the cerebellum, **(T)** il1b expression in the cerebellum, **(U)** representative images of the hindbrain at 40X magnification, **(V)** tgfb expression in the hindbrain, **(W)** il10 expression in the hindbrain, **(X)** il1b expression in the hindbrain. Scale bar = 50 µm. 3 way ANOVA with Benjamini, Krieger and Yekutieli *post-hoc* analysis, error bars = SEM; * = $p \leq 0.05$; ** = $p \leq 0.01$. Sample sizes: WT Saline i.n. + Saline i.p (3 female/3 male), WT Saline i.n. + AT-RvD1 i.p (2 female/2 male), WT Dust i.n. + Saline i.p (3 female/3 male), WT Dust i.n. + AT-RvD1 i.p (3 female/3 male), KO Saline i.n. + Saline i.p (3 female/3 male), KO Saline i.n. + AT-RvD1 i.p (2 female/2 male), KO Dust i.n. + Saline i.p (2 female/2 male), KO Dust i.n. + AT-RvD1 i.p. (3 female/3 male).

Discussion

The pulmonary inflammatory response to ODE has been well established, however the neuroinflammatory effects of this environmental and occupational exposure are not clear (10, 16, 47). Other models of environmental exposures examining neuroinflammation have demonstrated that inhalant exposures can be associated with neuroinflammation and can ultimately lead to neurodegenerative disease (3, 22, 25, 58). In addition, a pulmonary infection model *of Mycobacterium tuberculosis* demonstrated severe pulmonary bacterial infection without microbial dissemination to the brain that produced gliosis, neuroinflammation, and misfolded proteins, pathologies of animals developing neurodegenerative disease (2). Epidemiological studies have also linked pulmonary inflammation and infection in patients with COPD and *Mycobacterium tuberculosis* to neurological disease and early signs of neurodegenerative disease including cognitive decline, depression and anxiety, reduced social interaction, and ultimately reduced quality of life (27, 28, 59). To assess whether ODE contributes to neurological inflammation, microglia cell numbers were evaluated as an indicator of inflammation (2, 60, 61). Glial cells such as microglia are the primary mediators of the neuroinflammatory response and have been evaluated as markers of neuroinflammation in other peripheral inflammation models (2, 59). Proliferation and migration of microglia in different brain regions have been implicated in neurodegenerative disease and impaired neuron functionality. Increases in the number of microglia indicate inflammation or inflammatory processes, while reduction of these cells indicates resolution of inflammation (55–57). AT-RvD1 has shown efficacy in reducing neuroinflammation, suggesting that it may be an effective treatment to restore microglia homeostasis in deficient models, and our data demonstrates that AT-RvD1 may be effective in reducing microglia numbers in a mouse model of ODE (15, 62).

We found that proliferation of microglia primarily occurred in the rostral brain areas assessed: the olfactory bulb, frontal cortex, and isocortex. This may be attributed to the route of DE exposure, intranasal instillation, and the proximity of these brain regions to the olfactory system. One study found that two intranasal instillations of carbon nanoparticles were disseminated into the olfactory bulbs, which may be a mechanism of the observed gliosis, given the localization of the gliosis (54). Another possible mechanism is that peripheral inflammation can contribute to gliosis without translocation of the inflammatory substances to the brain, as observed in a study examining gliosis in a guinea pig model of *Mycobacterium tuberculosis* infection observed gliosis without dissemination of bacteria to the brain (2). It is also possible that the components of the DE used in this study, such as lipopolysaccharides (LPS) could be transported to the brain through transport proteins and be directly activating microglia via TLR4 pathways (63). We however did not observe an increase in IL-1β transcripts in brains of mice exposed to DE, so further evaluation of the cytokines profile and signaling is needed. We hypothesize that the inflammatory response observed in the brain of animals exposed to DE is TLR-mediated by microglia, however more information is required to decern the pathways and mechanisms that contribute to neuroinflammation in organic dust exposure. Our study is limited by the intranasal instillation of DE technique that is an effectively sterile, non-live infection model that may not be directly translatable to occupation exposure to ODE, which contains larger particles and live microbes (14, 47, 62). In addition, our mice are also only exposed a total of 15 times, which may not provide a sufficient exposure duration to elicit a robust neurological inflammatory response in all brain regions. Our laboratory has previously explored the role of IL-22 in the pulmonary immune response to ODE, but we have not examined the role of this cytokine in a neurological inflammatory model or in a recovery model of repetitive ODE (45). We previously explored this knock-out model in a 15-intstillation repetitive exposure model, however this study examining tissues 5 hours post-last DE instillation, but we have not yet explored the recovery period in the days following cessation of DE exposure (45). We have also previously examined the therapeutic actions of AT-RvD1 in a chronic dust exposure model but have not explored its applications in an ODE-induced neuroinflammatory model (32). We investigated the neuroinflammatory response to agriculture dust, the role of IL-22 in pulmonary and neurological inflammation, and the therapeutic applications of AT-RvD1 in a pulmonary and neurological IL-22 knock-out mouse model repetitively exposed to agriculture dust extract and treated with AT-RvD1. We found that in many of our parameters, IL-22 KO mice displayed increased disease severity via increased iBALT percentage (Figure 4B), increased microglia numbers in the olfactory bulb and cerebellum of saline-exposed animals (Figures 7B, J), and many of the differences in expression of cytokines and mediators evaluated at the protein (Figures 5D, E) and transcript (Figures 6B, F, 8B, D, F, J, L, N, P) levels were genotype-driven. We observed a significant increase in the total cells collected and lymphocyte differential counts in both WT and KO animals following DE exposure and a significant influx of macrophages in KO animals. This is consistent with our previous findings that IL-22 KO is associated with increased total and differential cell counts after DE exposure (Figure 2A) (45). However, we did find that the differential cell counts differed in our 72-hour recovery model. This is likely due to a shift in the immune response from an innate response characterized by high neutrophil counts to a more adaptive response dominated by lymphocytes (Figures 2A–E) (45, 64). KO animals treated with 250 ng AT-RvD1 once per week displayed decreased total cells and lymphocytes. KO animals also displayed a trend of increased total cell counts and significantly increased lymphocytes compared to WT animals. These data suggest that IL-22 knock-out may modulate cell recruitment to sites of injury and that AT-RvD1 also regulates immune cell recruitment, a well-known action of this SPM (34, 38, 43, 45, 65). In addition, KO animals displayed increased pathology severity including increased iBALT percentage in DE-exposed animals compared to WT DE-exposed animals (Figure 4B). This may also be due to altered lymphocytic recruitment as iBALT is largely composed of organized B and T cells (66–68).One inflammatory mediator, AREG is involved in modulating repair and remodeling in the lung after injury and has previously been evaluated in a repetitive 15-instillation ODE model where mice were allowed to recover for 1, 2, 3, or 4 weeks post-last DE instillation (50). However, the modulation of AREG has not been examined in a repetitive ODE model with a shorter, 72-hour recovery period or in an IL-22 knock-out model treated with AT-RvD1 (50). In our previous study, we observed that AREG concentrations in BALF increased as the recovery timepoints lengthened following

cessation of DE exposure (50). Interestingly, we did not find that AREG was upregulated in WT animals exposed to DE, but we did observe that KO mice exposed to DE and recovered for 72 hours displayed significantly decreased AREG tissue concentrations compared to WT mice exposed to DE. Interestingly, KO mice administered AT-RvD1 also displayed a significant decrease in AREG lung tissue concentrations compared to WT mice exposed to DE and treated with AT-RvD1. This may suggest that IL-22 may play an important role in effective tissue repair and resolution response after DE exposure as other models have found that IL-22 knock-out results in reduced skin wound healing, however the specific mechanisms warrant further investigation (69, 70).

We previously explored the use of AT-RvD1 treatment in a chronic 24-week ODE mouse model and observed significantly reduced pathology severity in mice injected with 500 ng AT-RvD1 via intravenous tail injection once weekly for 20 weeks (32). We found that this dose was effective in reducing lung inflammation and cellular infiltration in this model and aimed to evaluate the efficacy of AT-RvD1 in reducing ODE-induced pulmonary and neurological inflammation in a repetitive 15-instillation exposure model (32). We evaluated the neurological immune response via microglia counts and mRNA transcript evaluation using RNAscope in several brain regions. We utilized two dosing regimen models to determine which strategy was most effective. We first examined cellular infiltrates and histopathology in animals treated with 250 ng AT-RvD1 once-weekly (Figures 1A, 2A–E, 3A–D) and found limited efficacy in immune cell influx, and no therapeutic efficacy in lung histopathology (Figures 3A–D). We then evaluated lung histopathology outcomes in a once-daily AT-RvD1 injection schedule and found that animals treated with 250 ng AT-RvD1 daily displayed significant inflammation resolution in histopathology evaluation (Figures 4A–H), therefore, our 5 day/week injection regimen was employed for further analysis of the pulmonary and neurological inflammatory response to DE. Our histopathological analysis of animals administered daily AT-RvD1 injections revealed that iBALT was the primary parameter improved in AT-RvD1-treated animals. iBALT is considered a pathological phenotype of COPD that is correlated with disease severity and its increased formation has been linked to increased severity of patient clinical signs (71–73). We have previously found that mice exposed to DE, whether repetitively or chronically, develop significant iBALT (32, 45, 50, 51). In this study, we observed that WT and KO mice exposed to DE revealed increased iBALT formation, with significantly increased iBALT percentage in female mice compared to male mice. This may be due to sex hormones contributing to adaptive immunity to varying degrees, however our study is limited by a lack of estrus cycling and sex hormone quantification data that would be needed to make more informed conclusions on the mechanisms of the observed sex-specific pathology (74). Furthermore, female animals treated with AT-RvD1 displayed significantly less iBALT formation, indicating its effectiveness in reducing immune cell aggregates in these animals, but more investigation into the mechanism of these sex differences is warranted. This pattern of increased lung pathology severity in females has been documented in human patients with COPD, where female patients tend to experience more severe symptoms and have higher mortality rates (54, 59). Together, these data demonstrate that attenuation of IL-22 alters the pulmonary immune response to agriculture dust and increases the severity of lung pathology and that the efficacy of AT-RvD1 attenuation of lung pathology is IL-22- and sex-dependent. Females have also demonstrated higher toll-like receptor production, present with more $CD4^+$ T cells and B cells compared to males and have a more robust antibody response than males (74). The increased T and B cell numbers may account for the reduced resolution of iBALT in females, but more investigation of the mechanisms of these sex differences in our dust exposure model is warranted.

mRNA transcript evaluation of whole lung tissue sections revealed significant differences in *cxcl10* expression in WT mice exposed to DE with a significant decrease in WT animals exposed to DE and treated with AT-RvD1. CXCL10 participates in monocyte, neutrophil, and lymphocyte recruitment and significantly contributes to the progression of COPD disease state, which may present as a therapeutic target of AT-RvD1 in dust-induced lung disease (21, 75, 76). mRNA transcript evaluation of brains revealed limited significant differences between treatment groups, with significantly reduced *il1b* expression in WT animals exposed to DE and treated with AT-RvD1 compared to KO animals exposed to DE and treated with AT-RvD1. The mechanism of this observation is unclear, but another study found that cultured microglia displayed reduced *il1b* expression after treatment with 17(S)-RvD1 (77). This is not directly comparable to our model of AT-RvD1 (17(R)-RvD1) treatment but may still be informative as we explore the therapeutic targets of AT-RvD1. A major limitation of this study is our restricted panel of mRNA transcripts in both the lung and brain tissues, with only one pro-inflammatory mediator included per tissue type. This has hindered our investigation of the therapeutic applications of AT-RvD1, and we may simply be missing those mediators that are affected by At-RvD1 treatment. Another limitation is our 72-hour post-last instillation timepoint, where the mice are primarily in the resolution phase and may not be producing high quantities of pro-inflammatory cytokines. Expansion of our investigation of mRNA transcripts to include a broader range of classic inflammatory mediators may assist our assessment of the contribution of ODE to neuroinflammation and the therapeutic actions of AT-RvD1 in our ODE model.

We aimed to determine whether agriculture dust exposure contributes to neurological inflammation in a repetitive ODE mouse model. Our data support the hypothesis that agriculture dust exposure contributes microgliosis in a mouse model of repetitive ODE. We also aimed to assess the regulation of the pulmonary and neurological inflammatory response to ODE in an IL-22 deficient mouse model and the immune-modulating and therapeutic applications of AT-RvD1. Our data show that ODE leads to pulmonary and neurological inflammation, and that IL-22 attenuation increases the severity of the pulmonary and neurological immune response to ODE. This study confirmed our previous findings and expanded upon our prior knowledge by demonstrating that IL-22 KO mice exhibit increased inflammatory markers in the recovery phase following cessation of DE exposure. We also demonstrate that AT-RvD1 treatment once per week was effective in reducing cellular infiltrates in BALF of KO animals, but did not produce a significant decrease in lung pathology outcomes.

We observed that a once daily regimen was more effective in increasing lung anti-inflammatory cytokine protein production, reducing lung pathology severity, reducing lung chemokine transcript expression, and decreasing microglia numbers in mice exposed to DE. These data indicate that AT-RvD1 may require more frequent administration to be effective, however more evidence and exploration is needed. We also demonstrated that AT-RvD1 treatment is more effective in IL-22 KO mice, in terms of reducing lung cellular infiltrates and pro-inflammatory cytokine protein concentrations, but that it is also effective in reducing lung pathology and microglia numbers in both WT and KO animals. We hypothesize that this is due to a dysregulation of the repair processes in KO mice, which is partially restored by AT-RvD1 treatment, but requires further investigation to determine the specific pathways and mechanisms involved in these observations.

Further investigation aims to identify the mechanisms by which ODE contributes to neurological inflammation through evaluation of various routes of escape from the pulmonary to the neurological systems and the specific cellular mechanisms that lead to neuroinflammation in a model of ODE. These data demonstrate that ODE leads to neurological inflammation and that AT-RvD1 may be an effective treatment for attenuating immune-mediated pulmonary and neurological disease caused by ODE, mitigating its severe health effects.

Data availability statement

The raw data supporting the conclusions of this article will be made available by the authors, without undue reservation.

Ethics statement

The animal study was approved by Colorado State University Institutional Animal Care and Use Committee (Protocol Number 2887). The study was conducted in accordance with the local legislation and institutional requirements.

Author contributions

AT: Conceptualization, Data curation, Formal analysis, Investigation, Methodology, Validation, Writing – original draft, Writing – review & editing, Visualization. JW: Data curation, Investigation, Writing – review & editing. NK: Data curation, Investigation, Writing – review & editing. ZB: Data curation, Writing – review & editing, Investigation. LD: Data curation, Writing – review & editing. AI: Data curation, Writing – review & editing. MH: Writing – review & editing, Methodology, Software, Writing – original draft. KJ: Data curation, Writing – review & editing. MW: Data curation, Writing – review & editing. MB: Data curation, Writing – review & editing. EO: Data curation, Writing – review & editing. MP: Writing – review & editing, Data curation. JM: Writing – review & editing. TN: Writing – review & editing.

Funding

The author(s) declare financial support was received for the research, authorship, and/or publication of this article. This work was supported by National Heart, Lung, and Blood Institute R01HL185926 to TN.

Acknowledgments

The authors would like to acknowledge the support of Colorado State University personnel and Core Facilities that were integral to the completion of this work. The technicians at the Laboratory Animal Resources were integral in the care and wellbeing of the animals used in this study. The Experimental Pathology Facility embedded and sliced tissues used for histological staining and developed the AI applications used for pathological analyses. The Gonzalez-Juarrero Laboratory assisted with histological imaging via the Vectra Polaris microscope to allow for acquisition of high-quality images of histological, immunofluorescence, and RNAscope sections (Funding provided by the Office of the Director of the NIH: 1310OD030263-01).

Conflict of interest

The authors declare that the research was conducted in the absence of any commercial or financial relationships that could be construed as a potential conflict of interest.

The reviewer AU declared a past co-authorship with the author TN to the handling editor.

Publisher's note

References

1. Centers for Disease Control and Prevention. *Mortality in the United States National center for health statistics* (2021). Available online at: https://www.cdc.gov/nchs/fastats/leading-causes-of-death.htm (Accessed September 4, 2024).

2. Latham AS, Geer CE, Ackart DF, Anderson IK, Vittoria KM, Podell BK, et al. Gliosis, misfolded protein aggregation, and neuronal loss in a Guinea pig model of pulmonary tuberculosis. *Front Neurosci*. (2023) 17. doi: 10.3389/fnins.2023.1157652

3. Li W, Lin G, Xiao Z, Zhang Y, Li B, Zhou Y, et al. A review of respirable fine particulate matter (PM2.5)-induced brain damage. *Front Mol Neurosci*. (2022) 7:15. doi: 10.3389/fnmol.2022.967174

4. Pryor JT, Cowley LO, Simonds SE. The physiological effects of air pollution: particulate matter, physiology and disease. *Front Public Health*. (2022) 10. doi: 10.3389/fpubh.2022.882569

5. You R, Ho YS, Chang RCC. The pathogenic effects of particulate matter on neurodegeneration: a review. *J Biomed Sci*. (2022) 29:15. doi: 10.1186/s12929-022-00799-x

6. Centers for Disease Control and Prevention. *About alzheimer's disease* (2023). Available online at: https://www.cdc.gov/aging/alzheimers-disease-dementia/about-alzheimers.html (Accessed September 4, 2024).

7. Von Essen S, Romberger D. The respiratory inflammatory response to the swine confinement building environment. *J Agric Saf Health*. (2003) 9:185–96. doi: 10.13031/2013.13684

8. Nordgren TM, Charavaryamath C. Agriculture occupational exposures and factors affecting health effects(2018) (Accessed 2023 Feb 26).

9. Sigsgaard T, Basinas I, Doekes G, de Blay F, Folletti I, Heederik D, et al. Respiratory diseases and allergy in farmers working with livestock: a EAACI position paper. *Clin Transl Allergy*. (2020) 10:29. doi: 10.1186/s13601-020-00334-x

10. Nordgren TM, Bailey KL. Pulmonary health effects of agriculture. *Curr Opin Pulmonary Med*. (2016) 22:144–9. doi: 10.1097/MCP.0000000000000247

11. Wunschel J, Poole JA. Occupational agriculture organic dust exposure and its relationship to asthma and airway inflammation in adults. *J Asthma*. (2016) 53:471–7. doi: 10.3109/02770903.2015.1116089

12. Bailey K, Meza J, Smith L, Von Essen S, Romberger D. *Agricultural exposures in patients with COPD in health systems serving rural areas* (2008). Available online at: https://doi.org/101080/10599240801887918.

13. Syamlal G, Kurth LM, Dodd KE, Blackley J, Hall NB, et al. *Morbidity and mortality weekly report chronic obstructive pulmonary disease mortality by industry and occupation-United States* (2020). Available online at: https://www.cdc.gov/nchs/data/dvs/Industry-and-Occupation-.

14. Boissy RJ, Romberger DJ, Roughead WA, Weissenburger-Moser L, Poole JA, LeVan TD. Shotgun pyrosequencing metagenomic analyses of dusts from swine confinement and grain facilities(2014) (Accessed 2023 Feb 20).

15. Poole JA, Alexis NE, Parks C, MacInnes AK, Gentry-Nielsen MJ, Fey PD, et al. Repetitive organic dust exposure *in vitro* impairs macrophage differentiation and function. *J Allergy Clin Immunol*. (2008) 122:375–82. doi: 10.1016/j.jaci.2008.05.023

16. Poole JA, Romberger DJ. Immunological and inflammatory responses to organic dust in agriculture(2012) (Accessed 2023 Apr 19).

17. Poole JA, Wyatt TA, Oldenburg PJ, Elliott MK, West WW, Sisson JH, et al. Intranasal organic dust exposure-induced airway adaptation response marked by persistent lung inflammation and pathology in mice. *Am J Physiology-Lung Cell Mol Physiol*. (2009) 296:L1085–95. doi: 10.1152/ajplung.90622.2008

18. Ulu A, Burr A, Heires AJ, Pavlik J, Larsen T, Perez PA, et al. A high docosahexaenoic acid diet alters lung inflammation and recovery following repetitive exposure to aqueous organic dust extracts. *J Nutr Biochem*. (2021) 97. doi: 10.1016/j.jnutbio.2021.108797

19. Ulu A, Velazquez JV, Burr A, Sveiven SN, Yang J, Bravo C, et al. Sex-specific differences in resolution of airway inflammation in fat-1 transgenic mice following repetitive agricultural dust exposure. *Front Pharmacol*. (2022) 12. doi: 10.3389/fphar.2021.785193

20. Zhang B, Weuve J, Langa KM, D'Souza J, Szpiro A, Faul J, et al. Comparison of particulate air pollution from different emission sources and incident dementia in the US. *JAMA Intern Med*. (2023) 183:1080–9. doi: 10.1001/jamainternmed.2023.3300

21. Chung KF, Adcock IM. Multifaceted mechanisms in COPD: Inflammation, immunity, and tissue repair and destruction. *Eur Respir J*. (2008) 31:1334–56. doi: 10.1183/09031936.00018908

22. Costa LG, Cole TB, Coburn J, Chang YC, Dao K, Roqué PJ. Neurotoxicity of traffic-related air pollution. *Neurotoxicology*. (2017) 59:133–9. doi: 10.1016/j.neuro.2015.11.008

23. Wheaton AG, Ford ES, Cunningham TJ, Croft JB. Chronic obstructive pulmonary disease, hospital visits, and comorbidities: National Survey of Residential Care Facilities, 2010. *J Aging Health*. (2015) 27:480–99. doi: 10.1177/0898264314552419

24. National Center for Farmworker Health. *Agricultural workers and mental health* (2021). Available online at: https://www.ncfh.org/mental-health-fact-sheet.html:~:text=Elevated%20levels%20of%20anxiety%20and,females)%20had%20elevated%20depressive%20symptoms (Accessed November 7, 2024).

25. Calderón-Garcidueñas L, Reed W, Maronpot RR, Henríquez-Roldán C, Delgado-Chavez R, Calderón-Garcidueñas A, et al. Brain inflammation and Alzheimer's-like pathology in individuals exposed to severe air pollution. *Toxicol Pathol*. (2004) 32:650–8. doi: 10.1080/01926230490520232

26. Schuller A, Montrose L. Influence of woodsmoke exposure on molecular mechanisms underlying alzheimer's disease: existing literature and gaps in our understanding. *Epigenet Insights*. (2020) 13:251686572095487. doi: 10.1177/2516865720954873

27. Greenlund KJ, Liu Y, Deokar AJ, Wheaton AG, Croft JB. Association of chronic obstructive pulmonary disease with increased confusion or memory loss and functional limitations among adults in 21 states, 2011 behavioral risk factor surveillance system. *Prev Chronic Dis*. (2016) 13. doi: 10.5888/pcd13.150428

28. Liu Y, Croft JB, Anderson LA, Wheaton AG, Presley-Cantrell LR, Ford ES. The association of chronic obstructive pulmonary disease, disability, engagement in social activities, and mortality among US adults aged 70 years or older, 1994-2006. *Int J COPD*. (2014) 9:75–83. doi: 10.2147/COPD.S53676

29. CDC. *National trends - chronic obstructive pulmonary disease (COPD)*. Centers for Disease Control and Prevention (2020). Available at: https://www.cdc.gov/copd/php/case-reporting/national-trends-in-copd.html (Accessed January 24, 2024).

30. Serhan CN. Novel pro-resolving lipid mediators in inflammation are leads for resolution physiology(2014) (Accessed 2023 Feb 28).

31. Serhan CN, Krishnamoorthy S, Recchiuti A, Chiang N. Novel anti-inflammatory – pro-resolving mediators and their receptors(2011) (Accessed 2023 Feb 25).

32. Dominguez EC, Phandthong R, Nguyen M, Ulu A, Guardado S, Sveiven S, et al. Aspirin-triggered resolvin D1 reduces chronic dust-induced lung pathology without altering susceptibility to dust-enhanced carcinogenesis. *Cancers (Basel)*. (2022) 14. doi: 10.3390/cancers14081900

33. Eickmeier O, Seki H, Haworth O, Hilberath JN, Gao F, Uddin M, et al. Aspirin-triggered resolvin D1 reduces mucosal inflammation and promotes resolution in a murine model of acute lung injury. *Mucosal Immunol*. (2013) 6:256–66. doi: 10.1038/mi.2012.66

34. Serhan CN, Levy BD. Resolvins in inflammation: Emergence of the pro-resolving superfamily of mediators. *Vol. 128 J Clin Invest Am Soc Clin Investigation;*. (2018) p:2657–69. doi: 10.1172/JCI97943

35. Tiberi M, Chiurchiù V. Specialized pro-resolving lipid mediators and glial cells: emerging candidates for brain homeostasis and repair. *Front Cell Neurosci*. (2021) 15. doi: 10.3389/fncel.2021.673549

36. Hu X, Shen H, Wang Y, Zhang L, Zhao M. Aspirin-triggered resolvin D1 alleviates paraquat-induced acute lung injury in mice. *Life Sci*. (2019) 218:38–46. doi: 10.1016/j.lfs.2018.12.028

37. Serhan CN, Arita M, Hong S, Gotlinger K. Resolvins, docosatrienes, and neuroprotectins, novel omega-3-derived mediators, and their endogenous aspirin-triggered epimers(2004) (Accessed 2023 Feb 25).

38. Sun YP, Oh SF, Uddin J, Yang R, Gotlinger K, Campbell E, et al. Resolvin D1 and its aspirin-triggered 17R epimer: Stereochemical assignments, anti-inflammatory properties, and enzymatic inactivation. *J Biol Chem*. (2007) 282:9323–34. doi: 10.1074/jbc.M609212200

39. Dudakov JA, Hanash AM, Van Den Brink MRM. Interleukin-22: immunobiology and pathology. *Annu Rev Immunol*. (2015) 33:747. doi: 10.1146/annurev-immunol-032414-112123

40. Ahlfors H, Morrison PJ, Duarte JH, Li Y, Biro J, Tolaini M, et al. IL-22 fate reporter reveals origin and control of IL-22 production in homeostasis and infection. *J Immunol*. (2014) 193:4602–13. doi: 10.4049/jimmunol.1401244

41. Alcorn JF. IL-22 plays a critical role in maintaining epithelial integrity during pulmonary infection. *Front Immunol*. (2020) 11. doi: 10.3389/fimmu.2020.01160

42. Broquet A, Jacqueline C, Davieau M, Besbes A, Roquilly A, Martin J, et al. Interleukin-22 level is negatively correlated with neutrophil recruitment in the lungs in a Pseudomonas aeruginosa pneumonia model(2017) (Accessed 2023 Feb 27).

43. Mcaleer JP, Kolls JK. Directing traffic: IL-17 and IL-22 coordinate pulmonary immune defense. *Immunol Rev*. (2014) 260:129–44. doi: 10.1111/imr.2014.260.issue-1

44. Pociask DA, Scheller EV, Mandalapu S, McHugh KJ, Enelow RI, Fattman CL, et al. IL-22 is essential for lung epithelial repair following influenza infection. *Am J Pathol*. (2013) 182:286–96. http://ajp.amjpathol.org/article/S0002944013000163/fulltext.

45. Ulu A, Sveiven S, Bilg A, Velazquez JV, Diaz M, Mukherjee M, et al. IL-22 regulates inflammatory responses to agricultural dust-induced airway inflammation. *Toxicol Appl Pharmacol*. (2022) 446. doi: 10.1016/j.taap.2022.116044

46. Nordgren TM, Bauer CD, Heires AJ, Poole JA, Wyatt TA, West WW, et al. Maresin-1 reduces airway inflammation associated with acute and repetitive exposures to organic dust. *Trans Res*. (2015) 166:57–69. doi: 10.1016/j.trsl.2015.01.001

47. Romberger DJ, Bodlak V, Von Essen SG, Mathisen T, Wyatt TA. Hog barn dust extract stimulates IL-8 and IL-6 release in human bronchial epithelial cells via PKC activation. *J Appl Physiol*. (2002) 93:289–96. doi: 10.1152/japplphysiol.00815.2001

48. McCaskill ML, Romberger DJ, DeVasure J, Boten J, Sisson JH, Bailey KL, et al. Alcohol exposure alters mouse lung inflammation in response to inhaled dust.

Nutrients. (2012) 4:695–710. https://pubmed.ncbi.nlm.nih.gov/22852058/. doi: 10.3390/nu4070695

49. McCaskill ML, Romberger DJ, DeVasure J, Boten J, Sisson JH, Bailey KL, et al. Alcohol exposure alters mouse lung inflammation in response to inhaled dust. *Nutrients*. (2012) 4:695–710. https://pubmed.ncbi.nlm.nih.gov/22852058/. doi: 10.3390/nu4070695

50. Warren KJ, Wyatt TA, Romberger DJ, Ailts I, West WW, Nelson AJ, et al. Post-injury and resolution response to repetitive inhalation exposure to agricultural organic dust in mice(2017) (Accessed 2024 Jun 26).

51. Poole JA, Wyatt TA, Oldenburg PJ, Elliott MK, West WW, Sisson JH, et al. Intranasal organic dust exposure-induced airway adaptation response marked by persistent lung inflammation and pathology in mice. *Am J Physiol Lung Cell Mol Physiol.* (2009) 296:1085–95. doi: 10.1152/ajplung.90622.2008

52. Dominguez EC, Heires AJ, Pavlik J, Larsen TD, Guardado S, Sisson JH, et al. A high docosahexaenoic acid diet alters the lung inflammatory response to acute dust exposure. *Nutrients.* (2020) 12:1–19. doi: 10.3390/nu12082334

53. Poole JA, Gleason A, Romberger DJ, Kielian T. Repetitive intranasal inhalation of organic dust induces A predominant th17-polarized airway inflammatory response. In: *American thoracic society international conference meetings abstracts* (2011) Denver, Colorado, p. A4802–2.

54. Oberdörster G, Sharp Z, Atudorei V, Elder A, Gelein R, Kreyling W, et al. Translocation of inhaled ultrafine particles to the brain. In: *Inhalation toxicology* (2004). p. 437–45.

55. Caetano-Silva ME, Rund L, Hutchinson NT, Woods JA, Steelman AJ, Johnson RW. Inhibition of inflammatory microglia by dietary fiber and short-chain fatty acids. *Sci Rep*. (2023) 13. doi: 10.1038/s41598-022-27086-x

56. Piano I, Votta A, Colucci P, Corsi F, Vitolo S, Cerri C, et al. Anti-inflammatory reprogramming of microglia cells by metabolic modulators to counteract neurodegeneration; a new role for Ranolazine. *Sci Rep*. (2023) 13. doi: 10.1038/s41598-023-47540-8

57. Risen SJ, Boland SW, Sharma S, Weisman GM, Shirley PM, Latham AS, et al. Targeting neuroinflammation by pharmacologic downregulation of inflammatory pathways is neuroprotective in protein misfolding disorders. *ACS Chem Neurosci*. (2024) 15:1533–47. doi: 10.1021/acschemneuro.3c00846

58. Terzano C, Di Stefano F, Conti V, Graziani E, Petroianni A, Terzano C. Air pollution ultrafine particles: toxicity beyond the lung. *Eur Rev Med Pharmacol Sci*. (2010) 14:809–21.

59. Peng YH, Chen CY, Su CH, Muo CH, Chen KF, Liao WC, et al. Increased risk of dementia among patients with pulmonary tuberculosis. *Am J Alzheimer's Dis Other Dementiasr*. (2015) 30:629–34. doi: 10.1177/1533317515577186

60. Gao C, Jiang J, Tan Y, Chen S. *Microglia in neurodegenerative diseases: mechanism and potential therapeutic targets*. Signal Transduction and Targeted Therapy. Springer Nature: Vol. 8 (2023).

61. Skaper SD, Facci L, Zusso M, Giusti P. An inflammation-centric view of neurological disease: Beyond the neuron. *Front Cell Neurosci*. (2018) 12. doi: 10.3389/fncel.2018.00072

62. Poole JA, Alexis NE, Parks C, MacInnes AK, Gentry-Nielsen MJ, Fey PD, et al. Repetitive organic dust exposure *in vitro* impairs macrophage differentiation and function. (2008) (Accessed 2023 Apr 19).

63. Vargas-Caraveo A, Sayd A, Maus SR, Caso JR, Madrigal JLM, García-Bueno B, et al. Lipopolysaccharide enters the rat brain by a lipoprotein-mediated transport mechanism in physiological conditions. *Sci Rep*. (2017) 7:5922–43. doi: 10.1038/s41598-017-13302-6

64. Netea MG, Schlitzer A, Placek K, Joosten LAB, Schultze JL. Innate and adaptive immune memory: an evolutionary continuum in the host's response to pathogens. *Cell Host Microbe Cell Press;*. (2019) 25:13–26. doi: 10.1016/j.chom.2018.12.006

65. Serhan CN, Petasis NA. Resolvins and protectins in inflammation-resolution (2011) (Accessed 2024 Jun 26).

66. Polverino F, Seys LJM, Bracke KR, Owen CA. B cells in chronic obstructive pulmonary disease: moving to center stage. *Am J Physiology-Lung Cell Mol Physiol*. (2016) 311:L687–95. doi: 10.1152/ajplung.00304.2016

67. Poole JA, Mikuls TR, Duryee MJ, Warren KJ, Wyatt TA, Nelson AJ, et al. A role for B cells in organic dust induced lung inflammation. *Respir Res*. (2017) 18. doi: 10.1186/s12931-017-0703-x

68. Silva-Sanchez A, Randall TD. Role of iBALT in respiratory immunity. *In: Curr Topics Microbiol Immunol Springer Sci Business Media Deutschland GmbH;*. (2020) p:21–43. doi: 10.1007/82_2019_191

69. Arshad T, Mansur F, Palek R, Manzoor S, Liska V. A double edged sword role of interleukin-22 in wound healing and tissue regeneration. *Front Immunol*. (2020) 11:112148. doi: 10.3389/fimmu.2020.02148

70. Nordgren TM, Heires AJ, Bailey KL, Katafiasz DM, Toews ML, Wichman CS, et al. Docosahexaenoic acid enhances amphiregulin-mediated bronchial epithelial cell repair processes following organic dust exposure. *Am J Physiol Lung Cell Mol Physiol*. (2018) 314:421–31. www.ajplung.org.

71. Briend E, Ferguson GJ, Mori M, Damera G, Stephenson K, Karp NA, et al. IL-18 associated with lung lymphoid aggregates drives IFNγ production in severe COPD. *Respir Res*. (2017) 18. doi: 10.1186/s12931-017-0641-7

72. Foo SY, Phipps S. Regulation of inducible BALT formation and contribution to immunity and pathology. Vol. 3. In: *Mucosal immunology*. Nature Publishing Group; (2010). p. 537–44.

73. Hogg JC, Chu F, Utokaparch S, Woods R, Mark Elliott W, Buzatu L, et al. The nature of small-airway obstruction in chronic obstructive pulmonary disease. *N Engl J Med*. (2004) 26:n engl j med. 2004. Available from: www.nejm.org.

74. Klein SL, Flanagan KL. Sex differences in immune responses. *Nat Rev Immunol*. (2016) 16:626–38. doi: 10.1038/nri.2016.90

75. Hardaker EL, Bacon AM, Carlson K, Roshak AK, Foley JJ, Schmidt DB, et al. Regulation of TNF-alpha- and IFN-gamma-induced CXCL10 expression: participation of the airway smooth muscle in the pulmonary inflammatory response in chronic obstructive pulmonary disease. *FASEB journal : Off Publ Fed Am Societies Exp Biol*. (2004) 18:191–3. doi: 10.1096/fj.03-0170fje

76. Jing H, Liu L, Zhou J, Yao H. Inhibition of C-X-C motif chemokine 10 (CXCL10) protects mice from cigarette smoke-induced chronic obstructive pulmonary disease. *Med Sci Monitor*. (2018) 24:5748–53. doi: 10.12659/MSM.909864

77. Rey C, Nadjar A, Buaud B, Vaysse C, Aubert A, Pallet V, et al. Resolvin D1 and E1 promote resolution of inflammation in microglial cells *in vitro*. *Brain Behav Immun*. (2016) 55:249–59. doi: 10.1016/j.bbi.2015.12.013

Frontiers in Immunology

Explores novel approaches and diagnoses to treat immune disorders.

The official journal of the International Union of Immunological Societies (IUIS) and the most cited in its field, leading the way for research across basic, translational and clinical immunology.

Discover the latest Research Topics

See more →

Frontiers

Avenue du Tribunal-Fédéral 34
1005 Lausanne, Switzerland
frontiersin.org

Contact us

+41 (0)21 510 17 00
frontiersin.org/about/contact